Channel Network Morphodynamics in the Lower Paraná Delta

Leon Brok

Modelling the Influence of Natural Processes and Anthropogenic Activities on Morphological Changes in the Lower Paraná Delta Channel Network

Channel Network Morphodynamics in the Lower Paraná Delta

by

Leon Brok

to obtain the degree of Master of Science
at the Delft University of Technology,
to be defended publicly on Friday September 9, 2022 at 14:00.

Student number:	4906764	
Project duration:	September 1, 2021 – September 9, 2022	
Thesis committee:	Dr. ir. A. Blom,	TU Delft, committee chair
	Dr. ir. C. J. Sloff,	TU Delft, daily supervisor
	Dr. ir. D. S. van Maren,	TU Delft
	Ir. M. Sabarots Gerbec,	Universidad de Buenos Aires

An electronic version of this thesis is available at http://repository.tudelft.nl/.
Frontpage picture from Sentinel-HUB / ESA

TU Delft

Preface

This thesis concludes an intense but fruitful period as a MSc student in Hydraulic Engineering at Delft University of Technology (TU Delft). The study was commissioned by the University of Buenos Aires, Faculty of Engineering (FIUBA), post-graduate school of Port Engineering (EGIP) and conducted as part of the Memorandum of Understanding between EGIP and TU Delft. The research started in September 2021, in the middle of the global Covid-19 pandemic. This lead to much uncertainty concerning the (im)possibilities on travelling to Argentina to conduct part of the research. Luckily, travel restrictions were loosened in February 2022, making it possible for me to live and work in Buenos Aires for a period of three months, starting in March 2022. During this period I interviewed Argentine professionals with thorough knowledge on the Paraná River system, collected useful data during several field trips and finally got to meet Pablo Arecco and Martín Sabarots Gerbec, two key figures in the initiation and execution of the research. I also gained an unforgettable personal experience by temporarily being part of the vibrant, authentic city of Buenos Aires. I am very grateful for the opportunity to work on a challenging project that fits my personal preferences so well, and for the option to personally travel to Argentine during such extraordinary and uncertain times.

I would first like to thank my Dutch committee members for their help and support. Thank you Astrid Blom for your clear advise on overall readability and presentability of the products of this research. Thank you Kees Sloff for your excellent role as daily supervisor. Thank you for alleviating the struggle of working on a difficult subject with little data and a variety of physical processes. Our conversations about your personal experience while working abroad have much inspired me. Thank you Bas van Maren for your help interpreting model results and offering your specialistic knowledge on fine sediment dynamics.

Thank you Pablo Arecco, for helping me initiate the research project, aiding in the various practical implications that came with travelling to Argentine, the contacts you provided whose knowledge enriched myself and the research, providing me with a workplace at your office in Buenos Aires and most of all, your personal attitude and involvement that made my arrival and stay in your country a wonderful experience. Thank you Martín Sabarots Gerbec for your extensive involvement in the contents of the research, from carrying out field surveys with me, to aiding in interpreting model results and providing me with a desk at Instituto Nacional del Agua (INA). I would like to thank Raúl Escalante and Sebastián García, for your valuable time, providing me with knowledge on the Paraná River system and feedback on my preliminary research results. Thank you Héctor Hugo Prendes, Carlos Ramonell, Ricardo Szupiany and other researchers and employees of the University of Littoral in Santa Fé, for taking the time to listen and respond to my presentation, providing me with information on the upstream behaviour of the Paraná River and analyzing the soil samples in your laboratory. Thank you Kate Happee, for helping me with the first phase of the research by providing me with your literature list knowledge of the river system. Thank you Erik de Goede from Deltares, for providing invaluable support in the use and application of Delft3D Flexible Mesh.

Lastly, I would like to thank my family, friends and girlfriend for their unconditional support. Without you, I would not have been able to bring my period as a student to a satisfactory conclusion.

Leon Brok, Delft, September 2022

Abstract

The La Plata Basin is the second largest drainage basin in South America. The Paraná River, the basin's main river, discharges into the Río de la Plata estuary. The Paraná River is the country's most important navigation route, with seagoing vessels sailing up to Rosario, 300 km upstream of the deltaic front. Both the Río de Plata and one of the river's main tributaries, the Paraná de las Palmas, are subject to high rates of sedimentation, leading to the necessity for continuous dredging efforts in order to maintain the minimum navigation depth. Significant increases in the supply of (fine) sediment and river discharge occurred during the second half of the twentieth century, caused by extensive land use change in the catchment and (climate change related) precipitation increases in the catchment. IPCC projections predict a likely 10 to 20% increase in river discharge by the end of this century, with a high likelihood of sediment loads to increase as well. Such historic and potential future increases in fluvial input are mostly manifested during El Niño years.

In the Lower Paraná delta, near the deltaic front, a complex system of mostly natural and some man-made channels redistribute a part of the river flow. Like the river and the estuary, the channel network has been subject to sediment deposition, limiting the navigability needed for the small-scale transport of goods, leading to hindrance to tourism and other economic activities in the Lower Delta. Compared to the river system on the large scale, not much is known about the characteristics and the morphodynamic behaviour of the channel network. The objective of this research is to set a first step in providing insight on the relevant processes and human activities that influence morphology changes in the Lower Delta channel network. The three main steps executed to achieve this goal are as follows:

- Analysis of literature and existing data, leading to the formulation of a first set of hypotheses regarding the natural processes and anthropogenic activities that influence channel morphodynamics;
- Execution of field surveys in order to obtain more location-specific sedimentary, morphological and hydrodynamic data. This data is used to complement the formulation of the hypotheses and serves as input and validation data for the numerical model;
- Setting up a 2DH Delft 3D Flexible Mesh model in order to test the hypotheses. The most south-eastern region of the Lower Paraná delta is included in the model domain, as the most frequently used navigation channels are located in this area.

Our analysis provided various insights in the behaviour of the Lower Delta channel network, and the influence of human activities and natural processes on this behaviour. The following list contains the most notable insights.

1. Deepening of the Paraná de Las Palmas by dredging its thalweg since 1990 has lead to a decrease in its water level, leading to a significant reduction in river flow entering channels supplied by the river branch and increased sedimentation rates in these channels. Channels located north of the Paraná de las Palmas that normally confluence with the river branch experienced a decrease in sedimentation due to the increase in hydraulic gradient caused by the lowering of the Paraná de las Palmas water level.
2. High and extreme discharges of the Paraná River lead to a relatively large increase of the Paraná de las Palmas water level. This leads to an increase in flow and sediment transport capacity in the channels supplied by the Paraná de las Palmas (located mainly south of the river branch) inducing erosive patterns in these channels. Channels located north of the Paraná de las Palmas experience little to no morphodynamic response to an increase in river discharge.
3. Changes in sediment input primarily influence the depositional patterns in channels located south of the Paraná de las Palmas, due to the relatively high transport capacities of the river branch. The

Paraná Mini's lower velocities can not carry high loads of sediment into the northern channels, leading to a lesser dependency of sediment input of the channels between the Paraná Mini and Paraná de las Palmas. Various (terminal) channels located near the deltaic front also show a minimal morphological response to sediment supply changes due to the relatively energetic tidal and fluvial flow conditions in these channels.

4. During the field surveys, convex-upward longitudinal bed level profiles were measured in various channels in the network. These profiles imply the presence and influence of tidal divides inside the channel network. Although tidal divides are not produced in the model, the hypothesis of tidal divides influencing channel morphologies is deemed reasonable due to the measurements results. If present, morphological tidal divides would have a limiting effect on the navigability of specific locations in channels where the morphological tidal divides occur.

This research has provided a first, global insight into the relevant processes governing channel morphodynamics. Insight 1, as given above, can serve as input for future dredging strategies, as it implies that the current strategy has lead to limitations to the navigability of an intensively navigated part of the channel network. Furthermore, the outcome of this research can serve as a starting point for research on one of the specific topics covered by the hypotheses, including but not limited to the influence of storm surges, the effect of a potential spatial heterogeneity in soil composition and the influence of tidal divides on morphological features in the channel network.

Contents

1 Introduction

1.1. The Lower Paraná River Delta

The lower Paraná river delta is located in The La Plata basin in South America, which is the continent's second largest river basin. The La Plata basin extends over parts of Brazil, Paraguay, Uruguay, Bolivia and Argentina. The main rivers of the La Plata basin are the Paraná River and the Uruguay River, both rivers flow into the Río de la Plata estuary. The Río de la Plata is one of the largest estuaries in the world and it forms a natural national border between Argentina and Uruguay. The Argentinian capital of Buenos Aires is located on the north-western part of the estuary and the capital of Uruguay, Montevideo, on the north-eastern part of the coast. The river system is displayed in Figure 1.1.

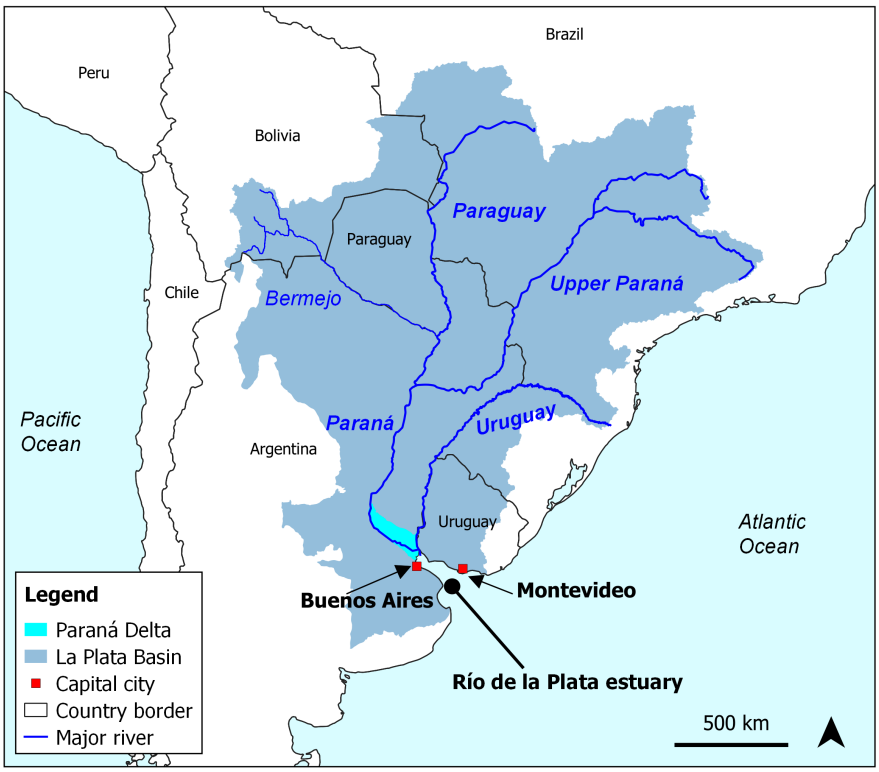

Figure 1.1: La Plata Basin

The delta of the Paraná River, located in Argentina, is a vast area of wetlands containing one of the country's largest freshwater reserves. The fluvial regime can be classified as braided with a meandering thalweg [Ramonell et al., 2002], with more meandering characteristics in the most downstream reach of

the river. The river forms a large network of natural streams and ponds, spreading over the entire delta. Large volumes of fine sediment, primarily originating from the Bermejo region in the Bolivian Andes, are transported into the delta throughout the year. This large annual supply of sediment enables growth of the delta, manifesting in a progradating coastline, an accreting subaquaes delta and sedimentation in the river tributaries.

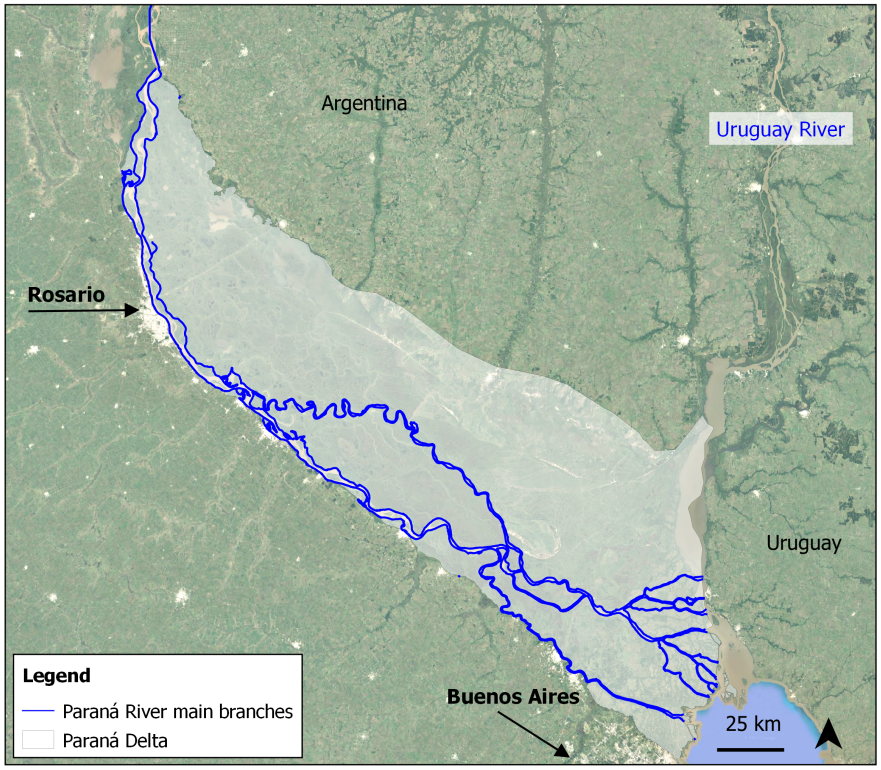

Figure 1.2: Paraná Delta

One of the two main river tributaries in the delta, the Paraná de las Palmas, is Argentina's most important navigational corridor, facilitating seagoing vessels to navigate from the Port of Buenos Aires to Rosario, located 300 km upstream. Due to the sedimentary regime of the Paraná River, long reaches of the Paraná River, both in and upstream of the delta, are subject to continuous dredging efforts in order to maintain the accessibility of the country's most important commercial transportation network. Due to the large economical interests associated with maintaining the navigability of the shipping route, conducting research and collecting data on the the hydraulic and sedimentological characteristics of the Paraná River and the estuarine system has been a priority for the involved governmental and educational institutions.

1.2. Channel accretion in the Lower Paraná delta

The Lower Paraná Delta (Figure 1.3) is the area located near the deltaic front. In the Lower Delta, activities related to apiculture (beekeeping), forestry, small-scale transportation of goods and tourism compose a large portion of the inhabitants' economic activity [Galperín et al., 2013]. For these purposes, the accessibility of the small waterways in this region is of importance to the local communities. Similarly to the main waterways and in the estuary, sediment deposition and rising bed levels have been a widely occurring phenomenon in the channel network. Reports from inhabitants indicating hindrance in navigability in the small waterways have been coming in for decades, however these reports have been poorly documented.

In addition to the main problem of channel accretion, various other elements endanger the quality of life for local communities. Conservation of ecological values and traditional societal structures in the Lower Delta have been under pressure during the last century [Zagare, 2014]. While commercially scaled

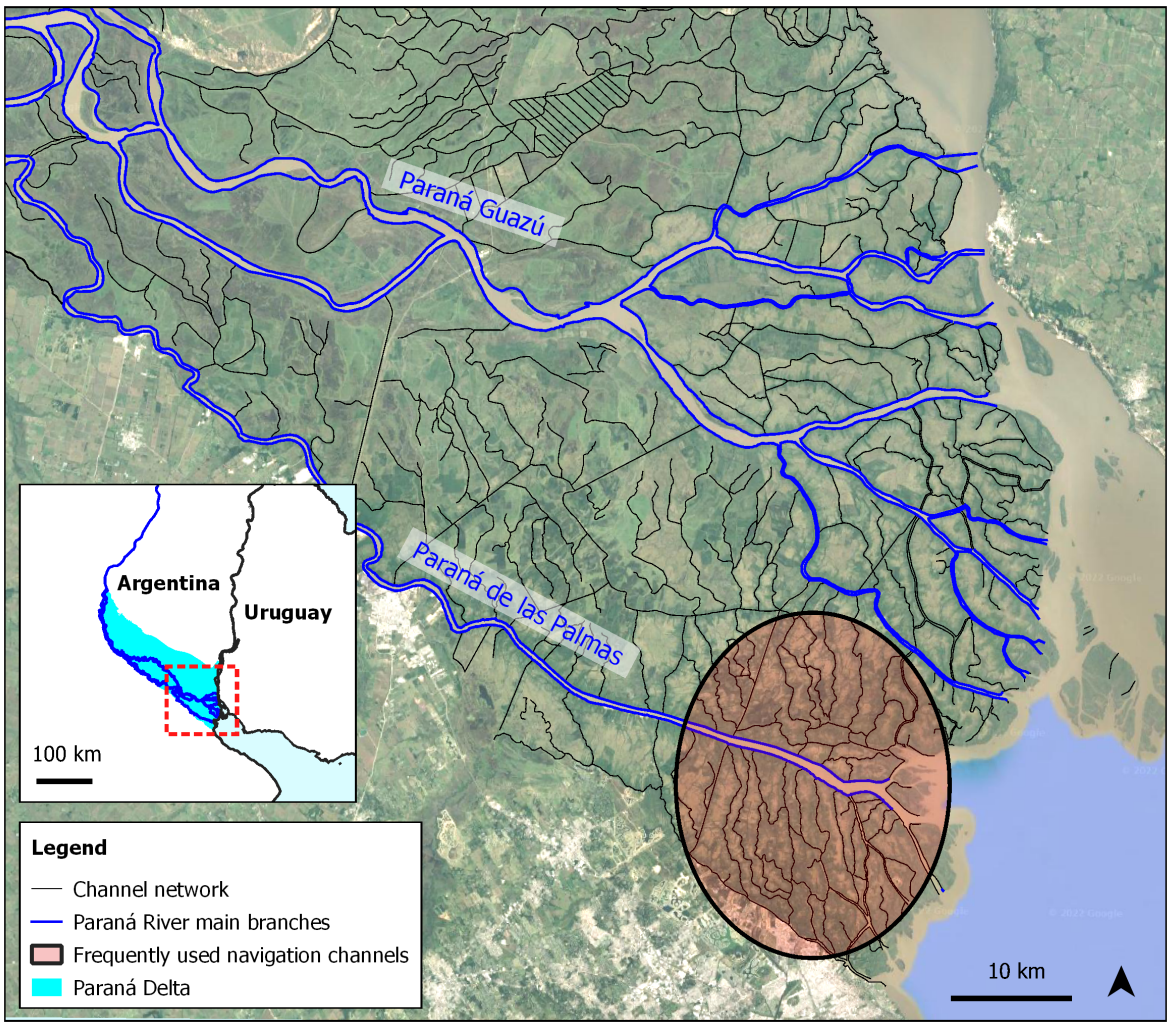

Figure 1.3: The Paraná Delta (small frame) and the Lower Delta

extraction of natural resources has been negatively influencing the ecological values and livelihoods of the local inhabitants, the effects of a changing global climate now poses another potential threat. Rising sea levels put the low-lying regions of the delta under pressure, while a possible increase in intensity of extreme meteorological events in the catchment can lead to a rise in flood occurrences. In addition to long-term climate related risks, inter-annual climatic variabilities associated with El Niño Southern Oscillation (ENSO) are strongly related to historic precipitation increases in the catchment [González et al., 2016] that have lead to a significant increase in streamflow and sediment supply into the delta and estuary [Happee, 2019]. In order to understand and quantify the (future) risks associated with living in the (Lower) Paraná Delta, a thorough understanding of the physical mechanisms that shape the system is needed.

The economical interests associated with the Lower Delta channel network are inferior to those of the main branches of the Paraná River, which serve as navigational corridors for seagoing vessels. For this reason, not much research or measurements campaigns have been carried out in the channel network compared to the main river branches. This has resulted in a knowledge gap on the hydro- and morphodynamic patterns in the Lower Delta, as well as in the geometrical and sedimentary characteristics of the channel network. For most streams in the delta, depth measurement campaigns have never been carried out. This scarcity in data, in combination with limited documentation on the (mainly orally) reported sedimentation patterns, results in large uncertainties regarding the time, locations and volumes of deposited sediment in the channel network.

1.3. Research objective & research questions

This research aims to contribute to understanding the morphodynamic behaviour of the Lower Paraná Delta's channel network. Obtaining knowledge on the mechanisms that cause sedimentation and erosion in the waterways will aid in designing measures or policy that contributes to the navigability and thus benefiting the accessibility to the region's economic actors. More generally, understanding the hydro- and morphodynamic behaviour can contribute to decision making in dredging strategies, navigation policy, spatial planning, environmental policies and flood safety. The main objective of this research is as follows:

Understanding the influence of natural processes and anthropogenic activities on the morphodynamic developments of the secondary channel network in the Lower Paraná Delta.

In order to achieve this objective, the following research questions are presented:

1. What are the occurring patterns of sedimentation and erosion in the Lower Delta's channel network?
   (a) What are the main sedimentary, morphological and hydraulic characteristics of the Lower Delta and its channel network?
   (b) How do local hydrodynamic processes influence the occurring morphodynamic patterns?
2. How do climatic and meteorological variability and anthropogenic activities influence the morphodynamic development of the Lower Delta's secondary channel network?
   (a) What is the influence of the El Niño Southern Oscillation phenomenon on the morphological development?
   (b) What is the influence of climate change scenarios on the future morphological development?
   (c) What is the influence of anthropogenic activities on the morphological development?
3. Which of the morphodynamic patterns are limiting the navigability of the channel network?

1.4. Research methodology

The core of this research consists of the formulation of hypotheses regarding the processes influencing morphological development in the channel network of the Lower Paraná Delta and testing these hypotheses by means of a Delft3D Flexible Mesh hydrodynamic and morphodynamic numerical model. The first step in formulating the hypotheses is done by analysing relevant literature and historically obtained hydrometric and sedimentological data. In order to gain field-specific knowledge on the Lower Delta channel network, various field surveys were carried out in December 2021 and March 2022. The obtained data was used to both improve qualitative insight in the system as well as serve as input for the numerical model. In order to formulate or substantiate the validity of the hypotheses, various analytical models or computations were carried out. After the definite formulation of the hypotheses, the hypotheses were tested by running various scenarios in which certain natural processes or human-induced influences were (de)activated, leading to a set of model output with which the (relative) influence of the said processes on the morphological development of the Lower Delta channel network can be estaablished. Figure 1.4 schematically depicts the research methodology and the relations between the phases.

1.5. Contents of this Thesis

Chapter 2 of this thesis introduces the physical characteristics of the Paraná river system and its delta, considering typical hydraulic, sedimentological and morphological characteristics of the (Lower) Paraná Delta. In the last sections of Chapter 2, physical natural processes that can influence the morphodynamic behaviour of the channel network are introduced. By means of the application of some theoretical principles, analytical models and the results of the field surveys, the expected influence of the natural processes such as fluvial deposition, tidal motion and storm surges are introduced and concretized in the form of several hypotheses.

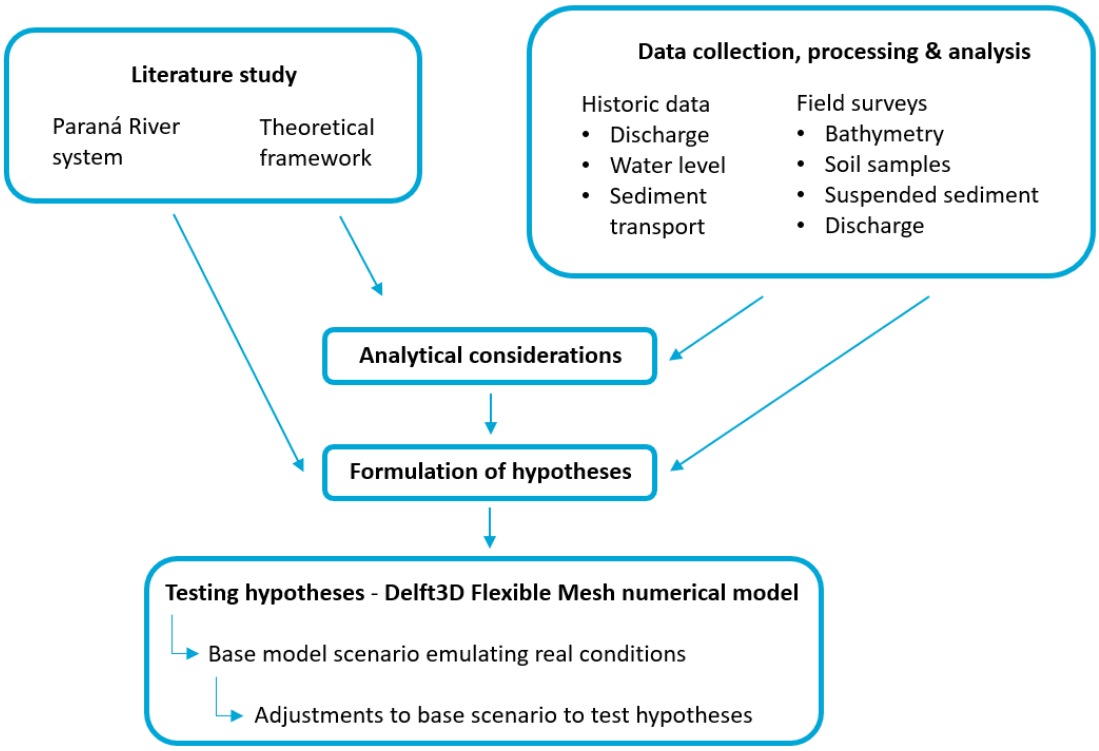

Figure 1.4: Research methodology

Chapter 3 describes some of the anthropogenic and natural impacts on flow patterns in the delta and the discharge and sediment input variability of the Paraná river into its delta. Background information is provided on the natural and anthropogenic influence that cause variation in fluvial forcing and sediment supply on a several temporal scales. The second part of Chapter 3 considers the dredging activities taking place in the (Lower) Paraná Delta and its potential influence on channel morphodynamics. Again, hypotheses are formulated concerning the influence on the Lower Delta channel network. Chapter 3 is concluded with a list of all formulated hypotheses that will be tested by the numerical model.

The set-up of the Delft 3D Flexible Mesh numerical model used to test the hypotheses is contained in Chapter 4. This chapter contains argumentation of the model choice, general settings of the model, validation results and a sensitivity analysis to explore the influence of uncertainties related to the sediment parameters. Boundary conditions and input data of the two base scenarios used to test the hypotheses are also described

Chapter 5 gives a brief description of the adjustments made to the base scenarios that lead to the model scenarios, each related to one or several hypotheses as defined in Chapter 2 and 3. The results are structured based on the physical processes related to the hypotheses and model scenario. This is done in order to avoid repetition.

Chapter 6 touches upon some practical implications of the research results and the recommendations concerning future research. Chapter 7 concludes this thesis by answering the research questions as formulated in Section 1.3.

2

The Lower Paraná Delta - Physical Characteristics and Processes

Sections 2.1 to 2.4 of this chapter describe the physical characteristics of the Paraná Delta and natural forcings that are imposed on the lower deltaic region and its channel network. The information presented in this chapter was collected both during the literature study and the analyses of pre-existing data and data obtained from the field surveys (see Appendix I for the field report).

The last section of this chapter (Section 2.5) touches upon the physical processes that potentially influence the morphological development of the Lower Delta channel network. Various hypotheses are formulated based on these processes, some of which are substantiated by the application of related theoretical principles. All hypotheses throughout this thesis are displayed in grey frames.

The reader without much time is advised to move to Section 2.5, more specifically the hypotheses, recognizable by the grey frames.

2.1. Geographic location of the research area

The extent of the Paraná Delta and (abbreviations of) cities located within the delta are indicated in Figure 2.1. Currently the delta exists as a vast area of floodplains and wetlands, reaching from the Río de la Plata estuary up to, considering the various definitions used for the extent of the delta, the city of Diamante, approximately 500 km upstream of the current mouth of the Paraná River.

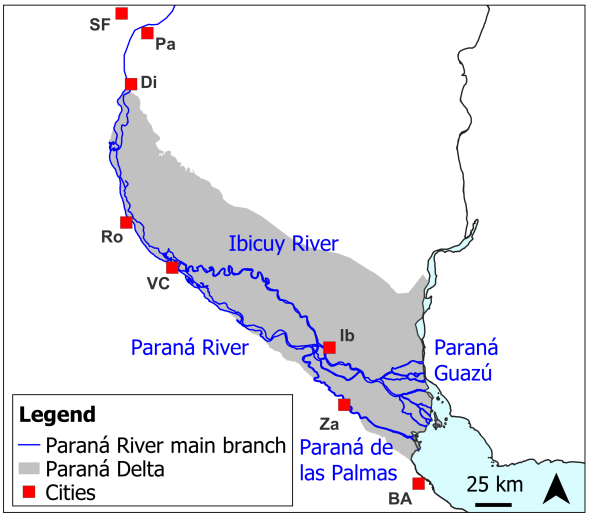

Figure 2.1: Main river branches and cities in the Paraná Delta

The Paraná River enters the delta near the city of Diamante (Di) and it passes the city of Rosarío (Ro) as it flows downstream. The river divides into a main branch and the Ibicuy River near the town of Villa Consitución (VC). At the height of the town Ibicuy (Ib), the main branch bifurcates into the Paraná de las Palmas and the Paraná Guazú, the latter of which confluences with the Ibicuy River and further downstream branches off into various tributaries as it approaches the estuary on the north side of the Lower Delta. The Paraná de las Palmas approaches the estuary in the southern part of the Lower Delta. The tributaries of the two main river branches, the Paraná de las Palmas and Guazú, form a complex network of many natural channels and some man-made canals. The construction of the artificial canals in the Lower Delta occurred between 1903 and 1906 [Barletti, 2021]. The Luján river is a small river originating approximately 100 km south-west of the delta, and it forms a natural border between the more elevated metropolitan region of Buenos Aires and the Deltaic area. The Lower Delta and its river network is depicted in Figure 2.2. Impressions obtained during the field survey (Appendix I) are displayed in Figure 2.3.

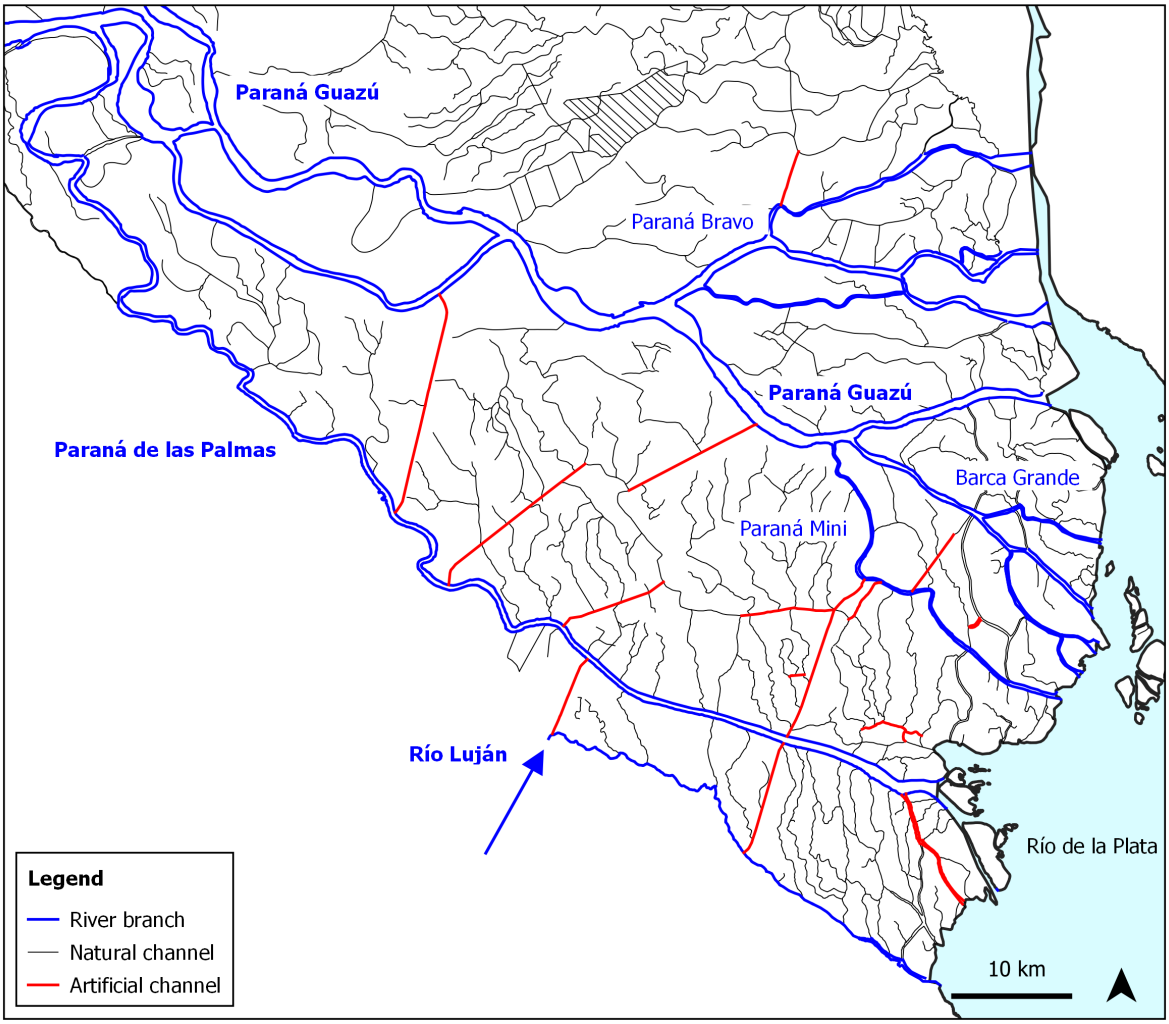

Figure 2.2: Lower Delta river network

2.2. Hydrodynamic characteristics

The hydrodyanmics in the Lower Delta are influenced by both fluvial and marine forcing and the complex interaction between them. The following sections describe some basic characteristics on the river discharge, tidal influence and non-tidal water level variations.

Figure 2.3: Channels in the Lower Paraná Delta

2.2.1. River Discharge

The average annual discharge of the Paraná River into the delta is in the order of 18,000 m^3/s. The average discharge increases to 22,000 m^3/s around February and reduces to 14,000 m^3/s around August [Sabarots Gerbec, 2014]. The Ibicuy River branch is of minor importance as it discharges around 1600 m^3/s [Happee, 2019], or about 5% of the Paraná River total.

Flow partitioning

Discharge partitioning of the Paraná River into the Guazú and Las Palmas branches was measured by Sarubbi and Menendez [2007] and the results are presented below. Figure 2.2 displays the Lower Delta channel network, including the names of the distributary channels of the Paraná Guazú.

- Paraná de las Palmas: 33%
- Paraná Guazú main channel: 67%, of which:
  - Paraná Guazú: 23%
  - Paraná Bravo: 37%
  - Barca Grande: 4.5 %
  - Paraná Mini: 2.5%

Based on data by INA, Sarubbi et al. [2004] reported that the flow distribution between the Paraná de las Palmas and Guazú branches are 21% and 79% respectively. Based on 5 measurements between 1920 and 1983, Re et al. [2009] approximated that the relative discharge in the Paraná Guazú increases from 70% during low discharge events (15,000 m^3/s) to 80% during high discharge events (40,000 m^3/s or higher, see Figure 2.4). This relation is presented in Figure 2.4 and Equation (2.1). The relation in equation form was approximated by graphic analysis of the graph presented in Sarubbi et al. [2004].

$$\frac{Q_G}{Q_T} \cdot 100\% = 66 + 33 \cdot 10^{-5} \cdot Q_T \tag{2.1}$$

The average discharge into the Río de la Plata estuary is rather constant throughout the year. This is due to the approximate negative correlation in seasonal variability between the Uruguay and Paraná river systems [Colombo et al., 2014]. The Uruguay River discharges roughly 25%, or 5,500 m^3/s into the estuary, the Paraná River thus discharges approximately 75% of the total La Plata catchment runoff.

The overall flow direction during regular conditions in the Lower Paraná Delta is from north-west to south-east [Personal communication with Martín Sabarots Gerbec]. Modelling efforts by Re et al. [2015] confirm this, as long term averaged water levels in the Paraná Guazú are higher than in the Palmas branch.

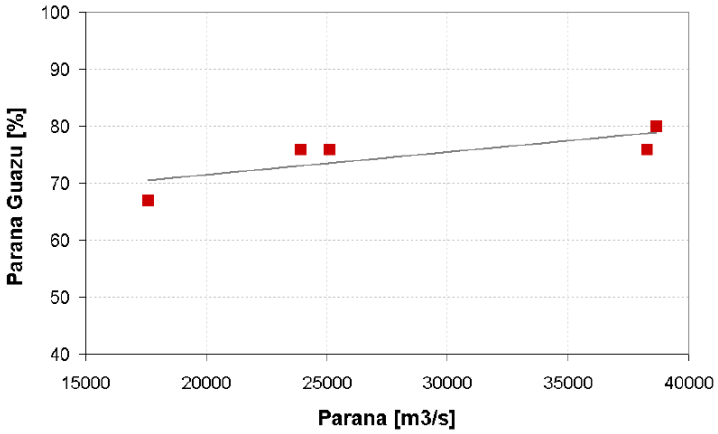

Figure 2.4: Discharge ratio Guazú branch (Q_G) and Paraná river total (Q_T)

Extreme discharges and river floods

Camilloni and Barros [2004] reported the 16 maximum discharge events in the twentieth century, during which maximum river discharge anomalies (with respect to the monthly mean between 1931 to 1980) at Corrientes range from 15,000 to 38,300 m^3/s. This implies extreme discharges to be in the order of 35,000 to 55,000 m^3/s. The most recent period with extremely high discharges was during the 2016 El Niño event (Chapter 3 elaborates on this phenomena), with discharges of the Paraná River exceeding 30,000 m^3/s. In more recent years, the discharge of the Paraná River has been extremely low. In 2021, the average discharge was around 6,000 m^3/s, the lowest in 77 years [Turcot, 2022]. The recent discharge extremes are evident in Figure 2.5, presenting discharge time series at Timbúes, 20 km upstream of Rosario. A description on the generation of the time series is given in Appendix F. The analysed time series end at September 2021, however the low discharge has continued at least until the moment of publication (summer 2022).

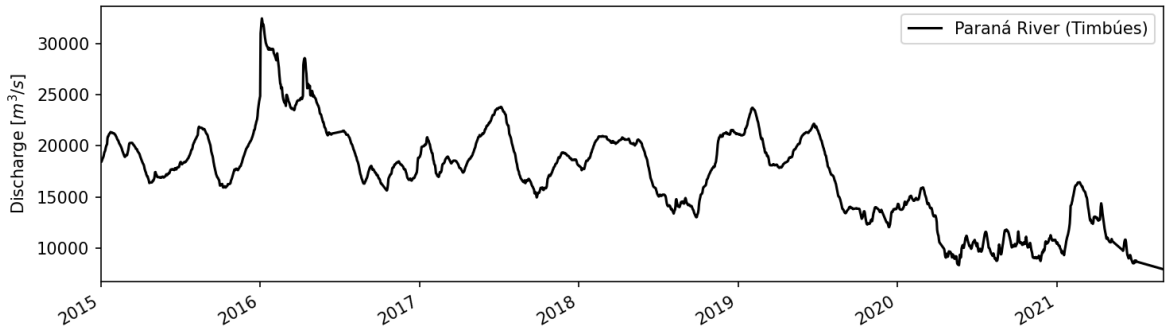

Figure 2.5: Discharge Paraná River at Timbués - El Niño took place in 2016

During high discharges, more upstream located deltaic plains around the Paraná River are flooded. The mechanism of flooding is such that the impact of moderately high floods is restricted to ponds and lagoons located in the vicinity of the main channel, and only extraordinary flooding events inundate the flood valley completely [Depetris, 2007]. Happee [2019] approximated that the minor flooding stage occurs at a river discharge of around 25,000 m^3/s, and more extreme events around 30,000 m^3/s. The effect of upstream flooding could be that a significant fraction of the sediment carried by the river is deposited in the floodplains, causing the downstream directed flow to be sediment poor and thus to be more likely to cause erosive patterns in the downstream reaches. However, the magnitude of this effect is unknown, and it could well be that high overall discharges induce sedimentation in the Lower Delta and the estuary, where this effect was clearly observed during the ENSO event in 2016, as deposited volumes in the Paraná de las Palmas were extraordinarily high. As will become clear in Section 2.3, peaks in sediment transport occur after heavy rain in the Bermejo region. If discharge

Table 2.1: Amplitude (A) and phase (ϕ) constituents of the astronomical tide and overtide M_4 at the Buenos Aires Port, obtained by harmonic analyses by Fossati and Piedra-Cueva [2013] (***FP13***) and Santamaria-Aguilar et al. [2017] (***SA17***)

	M_2	N_2	S_2	O_1	K_1	M_4
SA17						
A [m]	0.270	0.046	0.100	0.143	-	-
ϕ [◦]	298.8	40.3	253.0	262.2	-	-
FP13						
A [m]	0.275	-	0.044	0.15	0.096	0.03
ϕ [◦]	219	-	305	228	35	340

peaks of the Paraná River do not coincide with discharge peaks in the Bermejo River and subsequent sediment concentration peaks, the expected effect on Lower Delta channel morphology is erosion due to increased flow velocities.

2.2.2. Tidal characteristics

The tidal wave of the Atlantic ocean approaches the South-American coast from the south. Due to the shallowness of the Patagonian shelf the approaching Kelvin wave is significantly dissipated. The effect of the shallow bathymetry of the estuary is a decrease in wavelength. The result is a micro-tidal, co-oscillating tide with almost an entire wavelength in the Río de la Plata estuary, taking roughly 12 hours to travel through [Vieira and Lanfredi, 1996]. Predictions from the *Servicio de Hidrografia Naval, SHN* show a typical neap tidal range of 0.5 m and a spring tidal range of 1.1 m at the Port of Buenos Aires [SHN, 2021]. Fossati and Piedra-Cueva [2013] carried out a harmonic analysis for the astronomical tidal signal at the port of Buenos Aires, resulting in four main astronomical tidal constituents. Results of this analysis are depicted in Table 2.1. Regularly occurring sea surface amplitude anomalies associated with the meteorological tide are in the order of 0.5 meters at Buenos Aires [Santoro et al., 2013].

The shape of the tidal wave at the Buenos Aires port is flood dominated, as ebb phases have a longer duration than flood phases, with a difference between the two phase durations in the order of 30%. Another harmonic analysis on the tidal signal at the port of Buenos Aires was executed by Santamaria-Aguilar et al. [2017], including the constituent associated with this asymmetry. The computed amplitude and phase, as well as the other constituents from the analysis by Santamaria-Aguilar et al. are displayed in Table 2.1. The asymmetry has slightly increased over the twentieth century, while the tidal range has experienced a slight decrease of 0.5 mm/year. The low waters are rising at a higher rate than the high waters, this trend is significantly correlated with the increase in river runoff over the last century [Santamaria-Aguilar et al., 2017].

Even though the tidal amplitudes are considered small, the tide dominates the flow regime in the estuary. This is due to the large width of the estuary resulting in a large tidal prism [Fossati and Piedra-Cueva, 2008]. Measured maximum tidal current velocities during regular conditions are in the order of 20 cm/s at the bottom and 40 cm/s at the surface in the center of the Río de la Plata estuary [Fossati and Piedra-Cueva, 2013]. During regular conditions, tidal currents can exceed 0.5 m/s at the Argentinian coasts [Santoro et al., 2013], during storm surges, current magnitudes in the order of 1-1.5 m/s were observed in the outer regions of the estuary near Montevideo [Cueva et al., 2003].

During normal conditions the tidal wave propagates into the Paraná River up to the city of Villa Constitución, located 220 km upstream of the deltaic front. During storm surge conditions, the tidal influence reaches up to Rosario [Balay, 1958]. Although tides are present far upstream the river, salinity intrusion is practically non-existent in the Paraná Delta. The salinity front is normally located in the outer region of the Río de la Plata estuary [Berbery and Mechoso, 2001].

Water levels in the Lower Delta channel network are influenced by the tidal motion in the Río de la Plata. An analysis of water level data (Appendix E) indicates that the tidal wave propagates through the river and channel network, and that the tidal wave is significantly delayed and damped in relation to the phase and amplitude at San Fernando, at the deltaic front. Figure 2.6 display the approximate delay of the tidal wave in hours and the damping factor, as defined in Equation (2.2) (with A being the tidal amplitude). The analysis was executed by manually analysing the water level records over various periods with regular conditions, therefore the values are indicative and will vary during extreme

conditions.

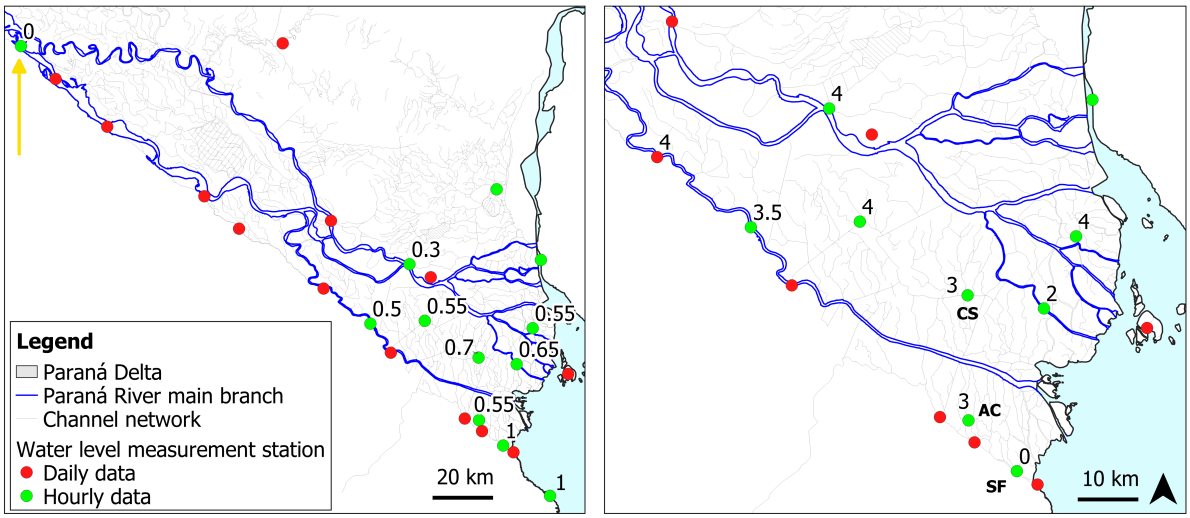

Figure 2.6: Tidal damping coefficient in relation to the amplitude in San Fernando (left figure, yellow arrow indicates the upstream limit of the tidal influence during regular conditions) and the delay of the tidal wave [hours] in the Lower Delta (right figure)

$$A_{Location} = \alpha \cdot A_{SanFernando} \tag{2.2}$$

2.2.3. Non-tidal nearshore water level variations

Apart from the water level variations associated with the astronomical and meteorological tide, the water level in the Lower Delta is influenced both by the magnitude of the river discharge and by meteorological conditions at sea. These effects are superimposed on the (daily) tidal variation.

Relation river discharge - downstream water level

Water levels at the deltaic front are not independent of the momentary river discharge. In Figure 2.7 it is visible that during high discharges in 2016 (associated with an El Niño event, see Chapter 3) the monthly averaged water level at San Fernando (near the deltaic front) exceeds the average level in sub- and preceding years. During the more recent period of low discharge, starting in 2020, the water level at San Fernando shows a slight negative trend. As these two trends in water level follow the relative magnitude of the river discharge it implies that the mean water level near the deltaic front is not only influenced by oceanic but also by fluvial forcing. This should be taken into account when determining appropriate downstream water level boundary conditions in the numerical modelling practices, as described in Chapter 4.

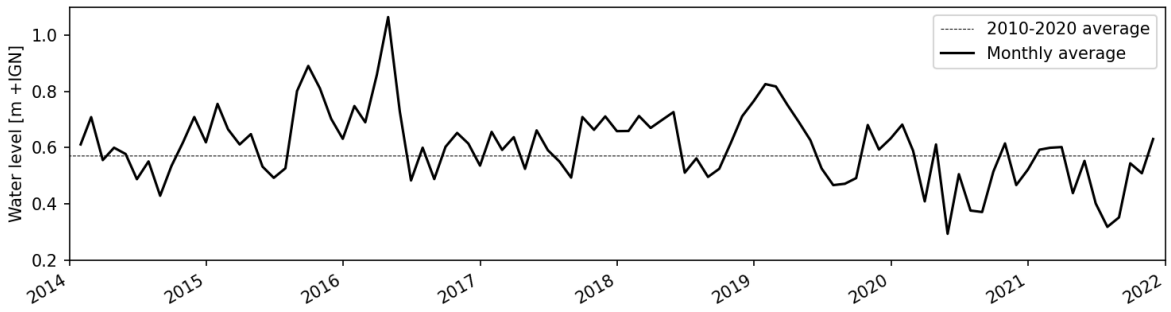

Figure 2.7: Water levels at San Fernando

Flood events due to storm surges

During stormy weather and strong south-eastern winds ('Sudestadas') in the Atlantic Ocean, the water level in the Río de la Plata can rise several meters. Maximum water levels of 2 m + IGN occur on a yearly basis, while water levels of 3 m + IGN and higher are rare. One-dimensional modelling practices by Bronstein and Menéndez [1995] give an indication of the flood heights (water level above the ground) in the Lower Delta. Figure 2.8 displays flood heights of the Paraná River and the Río de la Plata for return periods of 10 and 100 years. From these model results, it can be observed that floods in the Lower Delta will exclusively occur under the influence of a storm surge, and not due to high river discharge alone. Although the original research by Bronstein and Menéndez could not be obtained, it is likely that this is because the one-dimensional modelling by Bronstein and Menéndez did not consider a relation between high river discharge and increased water level in the Río de la Plata, but rather considered a fixed downstream boundary water level during high discharge conditions. An analysis (see 2.2.3) of the water level records during extremely high (2016 ENSO event) and low (2020 - 2022) rivers discharge indicates that there is a slight influence of the discharge on the downstream water level. However, this influence appears to be small, and it would therefore appear that flooding in the Lower Delta happens exclusively during Sudestada induced storm surge events. An analysis of water level series (Appendix E) shows that flooding in the Lower Delta channel 'Arroyo Carapachay' and more upstream in the Paraná de las Palmas (at Zarate) occur when the local water level exceeds 1.7 m and 2 m + IGN, respectively.

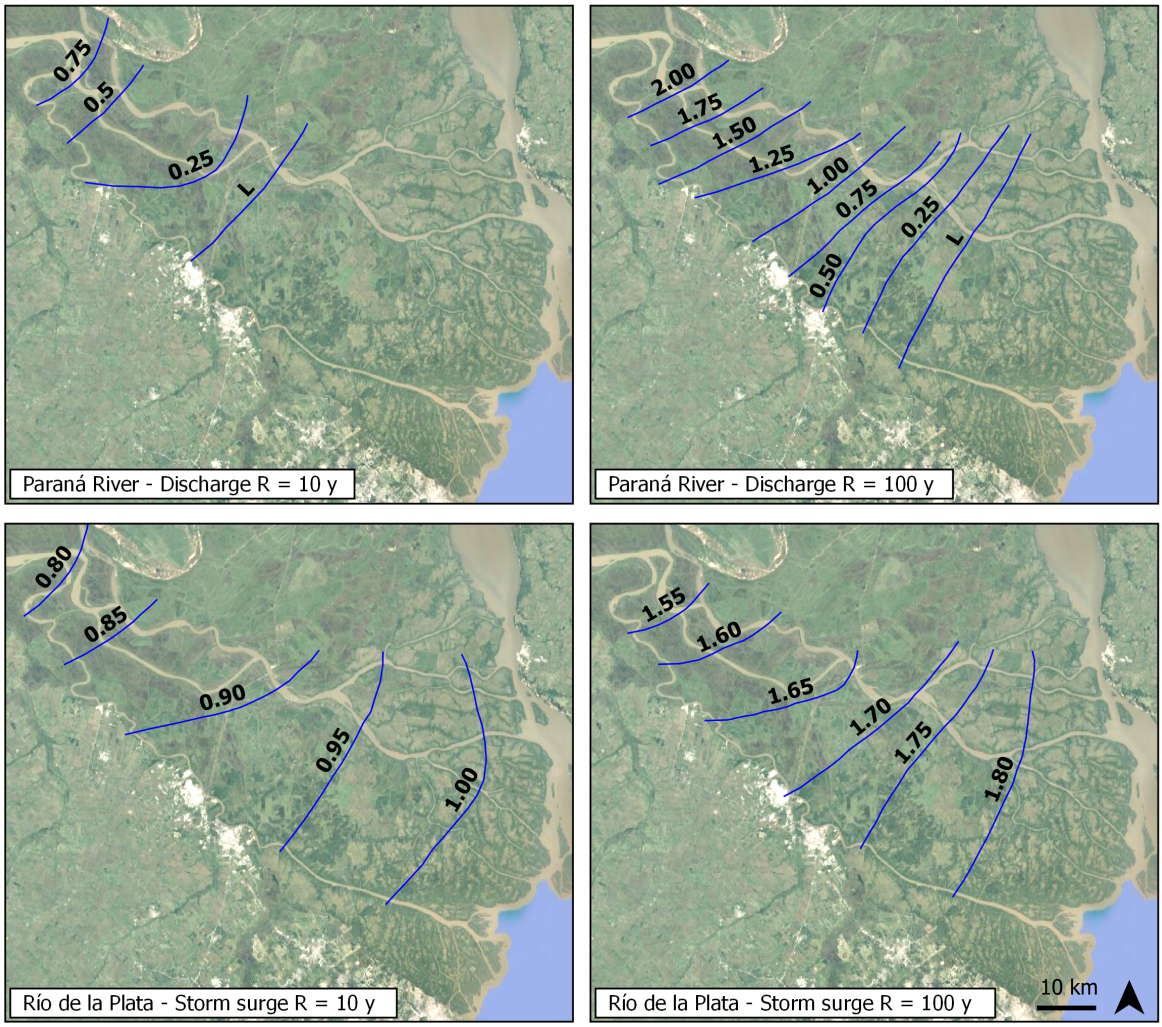

Figure 2.8: Flood heights due to high discharge and storm surge events for return periods R of 10 and 100 years [Bronstein and Menéndez, 1995]

2.3. Sedimentary characteristics

The following section summarizes the most important sedimentary and geomorphological characteristics of the (Lower) Paraná Delta. A thorough analysis on this subject is included in Appendix B. The information in this Appendix and section is based on literature and results from the December 2021 and March 2022 field survey (see Appendix I for field report).

The majority of the sediment that is carried into the delta by the Paraná River consists of fine sediment supplied from the upstream basin of the Bermejo river, a tributary of the Paraguay River in the Bolivian Andes. While constituting only 5% of the Paraná River's annual discharge, the Bermejo region is the source of almost 80% of the river's sediment load at city of Paraná, located just upstream of the delta entrance [Amsler et al., 2007].

The high sediment yield of the Paraná river contributes to the protrusion of the deltaic front into the Río de la plata estuary. The coastline progradates 25 m/year at the Guazú mouth and up to 100 m/year at the Las Palmas mouth [Menéndez et al., 2009]. This difference is due to the small bed slope of the Las Palmas, causing low flow velocities and high depositional volumes in the downstream river reach and at the deltaic front. Distinct flow corridors in the Río de la Plata make for little mixing between the outflows of the different rivers [Fossati and Piedra-Cueva, 2008], positively influencing the differential in protrusion rates of the coastline . Figures 2.9 and 2.10 display the deltaic growth and the flow corridors.

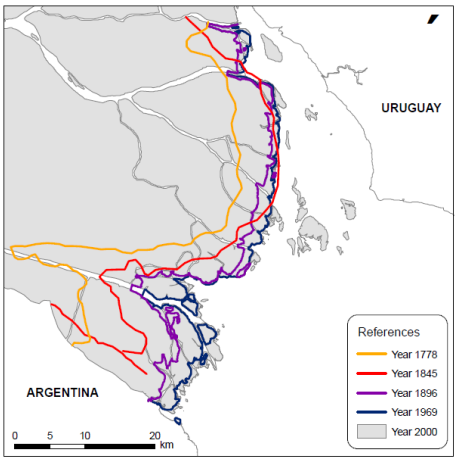

Figure 2.9: Advance of the deltaic front [Menéndez et al., 2009]

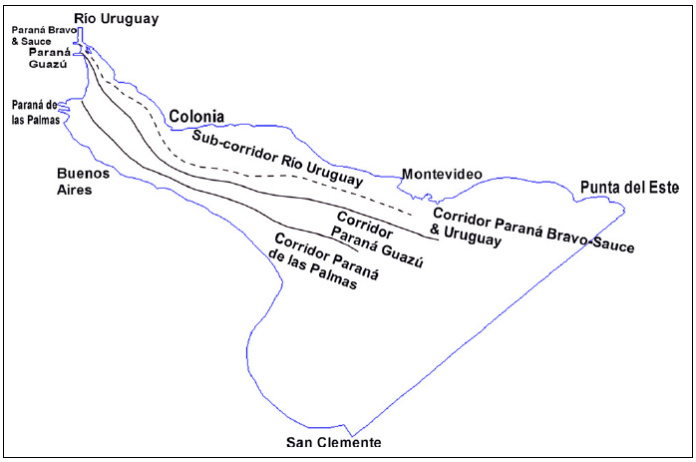

Figure 2.10: Flow corridors in the Río de la Plata [Fossati and Piedra-Cueva, 2008]

The total sediment yield of the Paraná River into the delta is in the order of 100 - 150 Mt/year. Due to anthropogenic and natural factors elaborated upon in Chapter 3, the sediment yield has increased significantly since 1960. Assuming that roughly 90% is transported in suspension (see next paragraph), and a sediment density of 2650 kg/m^3, above mentioned yearly sediment loads correspond with average concentrations of 160 - 240 mg/l.

Approximately 90% of the sediment entering the delta is transported as suspended load, almost all of which originates from the Bermejo sub-basin [Amsler et al., 2007]. Fine silt is the most abundant (50 to 60% of the total load) followed by clay (35%), with a small percentage of the total load (5 to 10%) being sand [Drago and Amsler, 1988]. Happee [2019] showed that high sediment concentrations in the Paraná River are always preceded by heavy precipitation events in the Bermejo region, which in the subtropical climate predominantly occur between February to March.

Typical suspended sediment concentrations of the Paraná River in the Lower Delta are in the order of 250 to 350 mg/l. van Rijn [2017] measured the suspended sediment concentrations composition and conceptualized the mixture into three representative fractions. His measurements were carried out at Campana (in the Paraná de Las Palmas) during regular conditions with depth-averaged flow velocities of 0.5 to 1 m/s. The representative fractions are presented in Table 2.2.

Table 2.2: Sediment fractions as determined by van Rijn [2017]. Concentrations are presented as depth averaged values (c_m) and values in the upper 5 m of the water column.

	c_m [mg/l]	c ($\zeta \in$ [-5,0 m]) [mg/l]	w_s [mm/s]	D_{50} [μm]
Clay	115	115	0.005	8
Silt	165	100	0.7	30
Fine sand	50	0	7	100

Bed soil samples taken during the December 2021 field survey in various channels in the Lower Delta indicate the following:

- The composition of the muddy beds in the Lower Delta channels is dominated by silt (roughly 50% of the total mass), with lower percentages fine sand and clay (30%) and fine sand (20%).
- Typical values of the median diameter D_{50} are in the order of 10 to 30 μm.
- No characteristic patterns (eg. downstream coarsening) in the spatial distribution of bed sediment size are observed. The bed composition of the channels is spatially uniform.

Suspended sediment samples taken in March 2022 in various channels in the Lower Delta indicate the following:

- Measured sediment concentrations are in the order of 100 to 300 mg/l, which is in accordance with estimates based on annual sediment fluxes and values from literature (see previous paragraphs).
- No significant differences in sediment concentrations between regular (17 March) and storm surge (18 March) conditions were measured.

The results of the sediment sampling and analysis are included in Appendix B.

2.4. Morphological characteristics

Various sources of morphological data in the (Lower) Delta of the Paraná river and the channel network from various dates were analysed and the results are described in detail in Appendix D. The following subsections summarize the morphological characteristics of the Paraná River in the Lower Delta and the channel network.

2.4.1. Morphology of the main Paraná River branches

From Timbúes/Rosario down to the bifurcation of the Paraná de las Palmas and the Paraná Guazú, the main channel of the Paraná River has a bed slope of approximately 10^{-5}. After the bifurcation, the Guazú branch continues downstream with a similar bed slope, however the many tributaries of the river have an effect on the bed levels located most downstream. The bed of the Paraná Mini is a good example of this; it has a bed level of approximately -7 m + IGN until its bifurcation with the artificial channel Gobernador La Serna, after which the bed level increases to approximately - 3 m + IGN. Thalweg and average bed bed levels are displayed in Figure 2.11. In Appendix D, these figures are repeated including top views of the system.

The most downstream part of the Paraná de las Palmas has a positive bottom slope, i.e. average bed levels rise as the estuary is approached. High sedimentation rates in this region lie at the basis of this characteristic, with dredging activities (see Chapter 3) counteracting the effects of sedimentation, but only in the approximately 150 m wide thalweg/navigation channel. At 40 km from the estuary, the bed level of the Paraná de las Palmas is rather uniform for approximately 50 km, after which it starts sloping upward with a slope in the order of 10^{-4}. Conveyance areas of the downstream reach of the Palmas are in the order of 6500 to 8500 m^2.

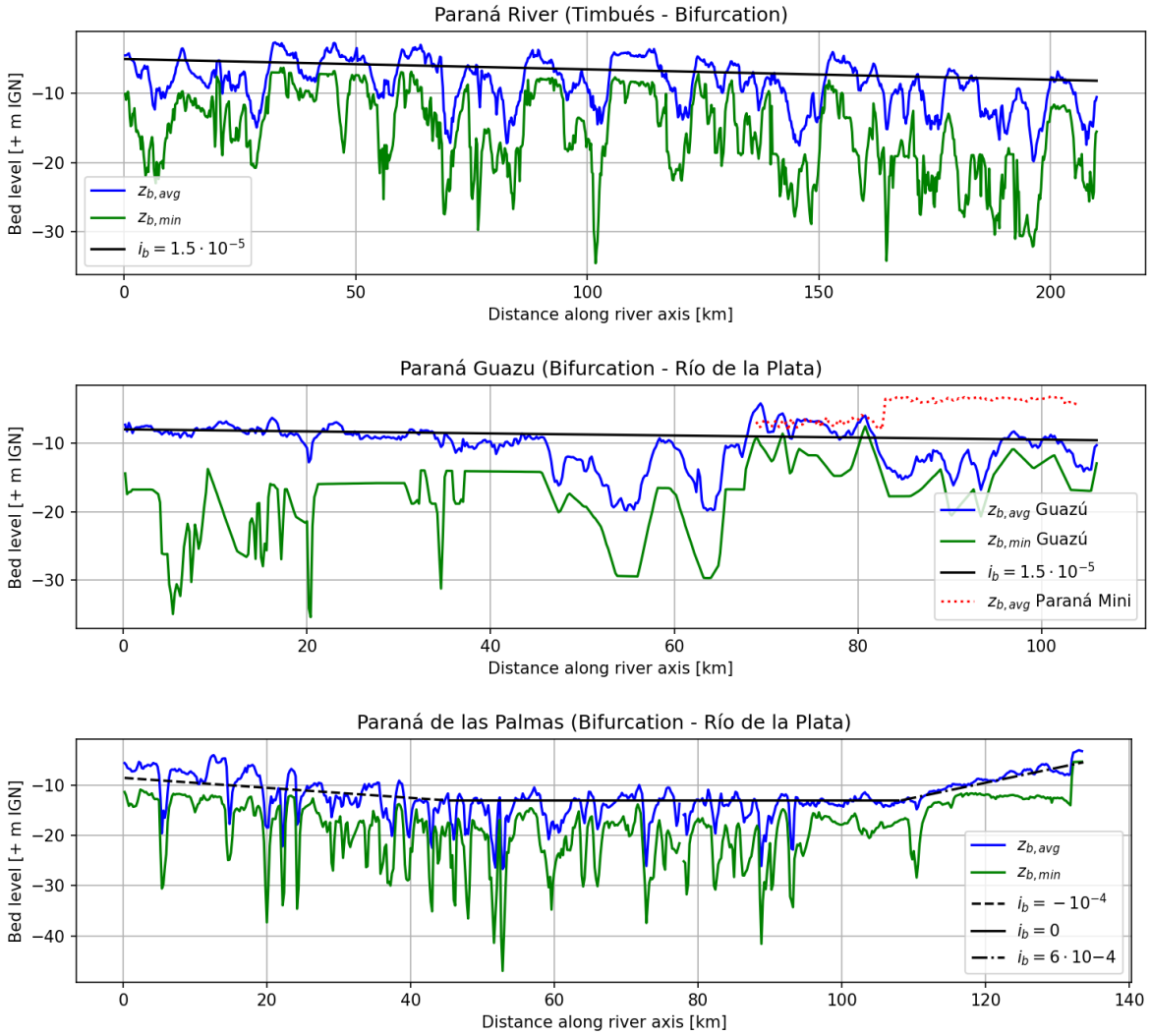

Figure 2.11: Paraná river, average ($z_{b,avg}$) and thalweg ($z_{b,min}$) bed levels

The small Luján River forms the natural border between the delta and the urbanized area. Downstream of its junction with the artificial canal Gobernador Arias, the average bed levels are around -3 to -5 m + IGN, with a thalweg slope of approximately 10^{-4}. Upstream of its junction with Gobernador Alias, the bed level is approximately 2 meters higher, and continues with a similar slope.

2.4.2. Morphology of the Lower Delta channel network

Measured bathymetries

Channel centerline and cross section measurements in the Lower Delta channel network were carried out during various measurement campaigns in 2021 and 2022. The following must be noted concerning the channel geometries:

- More upstream located channels (e.g. Arroyo Caraguata, Figure 2.12) display higher bed levels with increasing distance from the main river branch increases, resulting in a 'convex-upward' type longitudinal section.
- More downstream located channels (e.g. Río Capitan, Río Sarmiento, Figure 2.12) have a near-horizontal bed level. The terminal channels of the network have a slight tendency of increasing bed levels towards the downstream end.
- Upstream located channels are generally shallower than downstream located channels.

- More bathymetry results, including the geographical location of the displayed channels, is available in Appendix D.

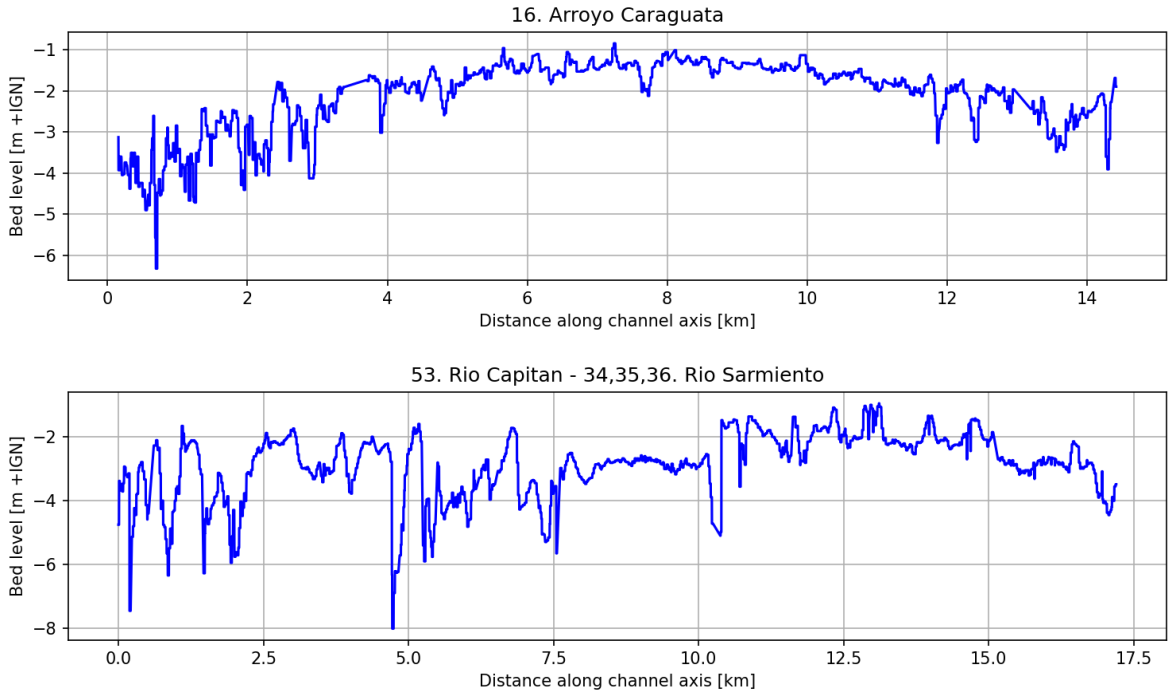

Figure 2.12: Measured thalweg bed levels of Arroyo Caraguata and Río Capitan / Sarmiento

A clear distinction between channel type based on channel dimensions was identified. Various (terminal) channels located near the deltaic front have relatively low bottom levels and large channel widths compared to channels located more upstream. These channels can be up to 8 meters deep and 100 meters wide, while more upstream located channels often have characteristic depths of 2 to 5 meters and widths of 30 to 50 m. The channels measured during the surveys and the characterization based on channel dimensions are displayed in Figure 2.13.

Spatial distribution of the channel network

A satellite imagery analysis was carried in order to obtain knowledge on the spatial characteristics of the channel network and the individual channels. The complete procedure and results are available in Appendix B. The results of the analysis show that a relatively large number of channels are concentrated in the south-eastern part of the Lower Delta. In these regions, the majority of the channels are conveying water (nearly) all year round. In the more northern and western regions of the Lower Delta, located higher up the deltaic plain, permanently inundated channels become less common and channels that are cut off or have dead ends are often present. Figure 2.13 displays the results of the analysis in which distinction is made between permanently inundated ('Regular') channels, dry channels and channels with a dead end.

2.5. Hypotheses on physical processes governing channel morphodynamics

In the following section, various physical processes related to deltaic hydro- and morphodynamic behaviour are presented, and their relevance to the morphodynamic behaviour of the Lower Delta channel network is argued using theoretical principles and/or simple analytical considerations. Several hypotheses on the influence of these processes Lower Delta channel morphodynamics are formulated and repeated in the last section of Chapter 3.

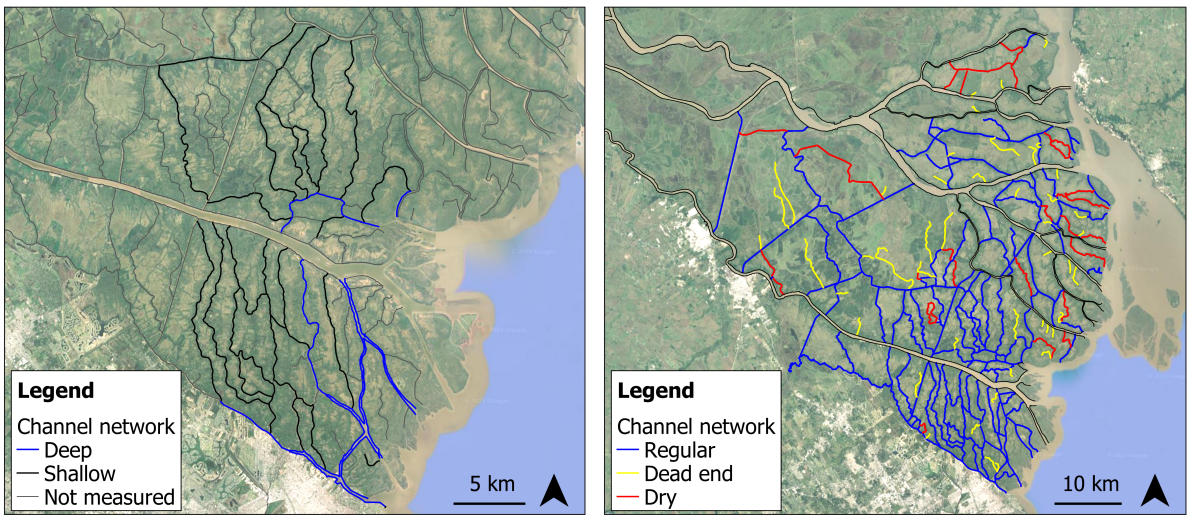

Figure 2.13: Lower delta channel characterization based on measured bed level (left) and conveyance permanence

2.5.1. Fluvial processes

The widespread sedimentation experienced in the Paraná de las Palmas and the Río de la Plata estuary are characteristics of system that is, on the large scale, incapable of transporting all the sediment supplied from upstream. When considering only fluvial processes, three physical concepts that can be at the basis of the direct deposition of fluvial sediment in the Lower Delta channel network are elaborated upon below.

M1 Backwater curve

A backwater curve occurs when a river system is not in equilibrium, i.e. the streamwise forcing caused by gravity on the water is not balanced by the anti-streamwise force caused by bed friction. The manifestation of this imbalance is a change in hydraulic gradient in streamwise direction, leading to flow acceleration and erosion (in the case of a M2 backwater curve) or deceleration and deposition (in the case of a M1 backwater curve, see Figure 2.14. Backwater curves can occur when human interventions or natural processes cause a change in the river geometry, hydraulic roughness, bed slope or hydraulic boundary conditions. A natural river is never in perfect equilibrium as (discharge) boundary conditions are never constant in time, making a river system dynamic, i.e. capable of changing bed slopes, river geometry, soil composition and layout. The theory behind the occurrence of backwater curves is more thoroughly elaborated upon in Appendix A.

The morphodynamic pattern associated with an M1 backwater curve is and displayed in Figure 2.14. More often than not, a delta is a depositional system, implying the presence of flow decelerations and the presence of a M1 backwater curve at least during regular (base flow) conditions. As presented in Section 2.3, high rates of deposition occur in the most downstream end of the Paraná de las Palmas and in the Río de la Plata, with dredging activities (see Chapter 3) counteracting this accretion. In general, the (high rates of) sedimentation in the Lower Delta and coastline progradation is the sign of a system that tries to approach a new equilibrium by sediment deposition, a process of which the M1 backwater curve is the hydraulic manifestation. Note that depositional patterns are only present in the Las Palmas branch and some side channels, while the Paraná Guazú does not experience significant sedimentation at all, implying a near-equilibrium state. The Paraná Guazú has a rather uniform bed slope, similar to the slope of the Paraná River upstream of the bifurcation. This is in accordance with the Paraná Guazú being defined as the true continuation of the fluvial regime (see Section 2.3) of the Paraná River. The potential occurrence of a M2 backwater curve during peak flow is touched upon in Section 2.5.3.

Mouth-bar deposits

Mouth bar deposits occur in the mouth of a river or channel, or on another location where the flow decelerates heavily due to sudden widening of the flow profile. Deposition takes place in the widened

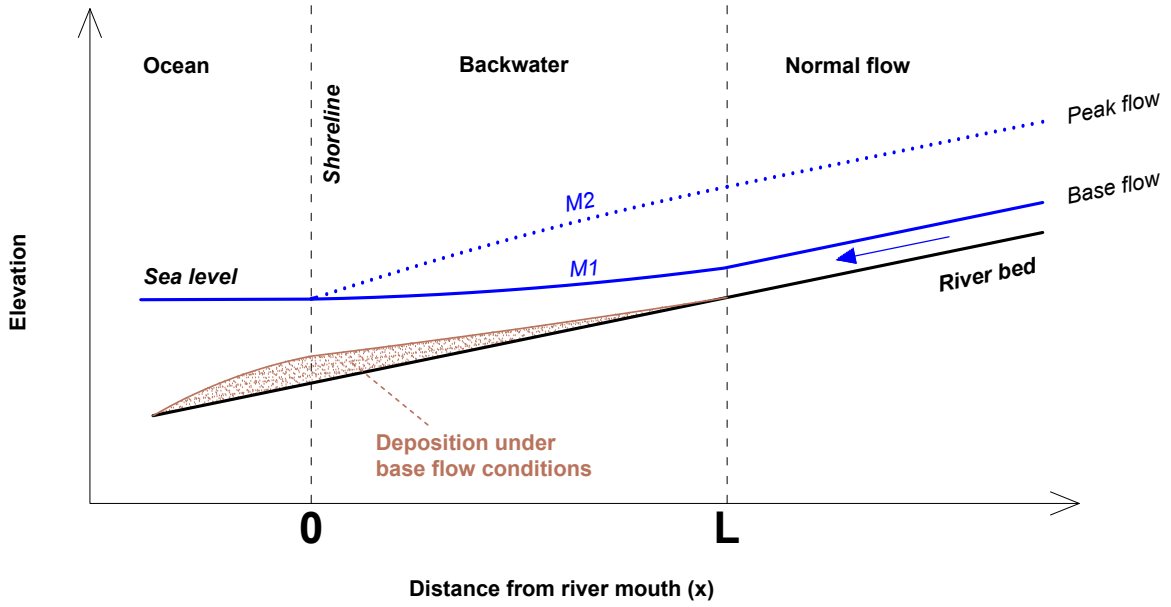

Figure 2.14: Backwater curves

region, often causing the flow to separate and potentially initiate the formation of a river bifurcation [Mikhailov, 1966]. The bed level of the Paraná de las Palmas and some of the more downstream located (terminal) channels (e.g. Canal Honda - Río San Antonio, see Appendix D) display slight positive slopes and increased bed levels towards the most downstream end of the reach or channel. Such patterns are related to mouth-bar deposits [Hoitink et al., 2017], indicating that this well-known concept in deltaic morphology is likely to occur in the Lower Paraná Delta terminal channels.

Flow decelerations in channel entrances

Flow velocities decrease significantly as water flows from the main river branches into the channel network, leading to a decrease in sediment transport capacity and subsequent depositional patterns. As elaborated upon in Appendix A, the rate of deposition or erosion for suspended sediments depends on the difference between the equilibrium suspended sediment concentration c_e, which is approximately proportional to the bed shear stress $\tau_b \propto u^2$, the actual sediment concentration c and the relaxation time T. For fine material (suspended non-equilibrium transport), the relaxation time is relevant as this timescale is at least as large as the time scale with which changes in the flow take place. The particle therefore takes enough time to settle so that it can be transported during the settling. For coarser material (bed load and suspended equilibrium transport), the relaxation time T is negligible as the transport reacts almost directly to the changes in flow.

In Appendix H, a highly simplified case demonstrating that a decrease in sediment transport capacity occurs when river discharge enters the Lower Delta channel network is presented. The following points summarize this approximation:

- Channel dimensions are based on the bathymetries of the Paraná de las Palmas and Arroyo Caraguata.
- Characteristic flow velocities are based on river equilibrium flow conditions.
- Flow deceleration in the channel entrances are likely to cause the equilibrium concentration c_e to decrease with a factor 9 to 16, implying that sediment deposition occurring after flow enters the channel network is likely.
- Channel deposits are likely to consist of predominantly (fine) sand and silt, as clay particles settle so slow that they are more likely to flow trough the channel, into the estuary.

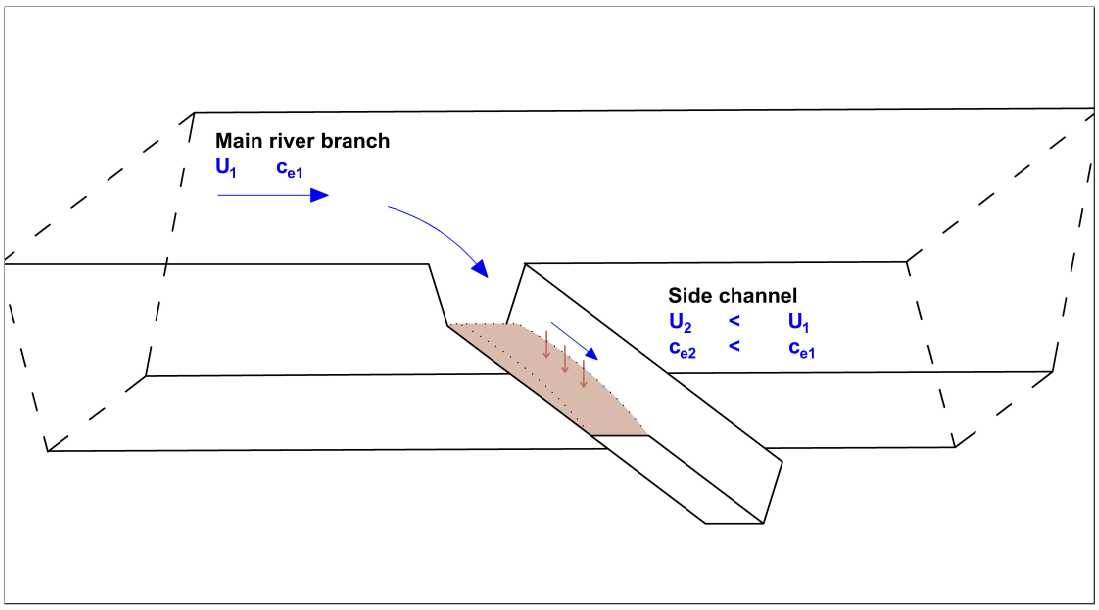

Figure 2.15: Deceleration and deposition in a side channel

Concerning the direct deposition of fluvial sediment, a first hypothesis is formulated:

1. **Tidal and fluvial processes** ***Hypothesis***

   (a) Channel sedimentation is mainly caused by the supply and deposition of fluvial sediment Three fluvial processes are expected to play a significant role in the morphological development of the channel network:

   - Flow of the Paraná de las Palmas decelerates in the downstream end due to the presence of a M1 backwater curve during regular conditions, leading to widespread sedimentation near the deltaic front;
   - Sediment carried by the Paraná River is directly deposited due to decelerations in flow velocity when entering the secondary channel network;
   - Sediment carried towards the deltaic front experiences decelerations due to widening of the channel, leading to the formation of mouth bar deposits in the downstream reaches of (terminal) channels.

2.5.2. Tidal processes

Stabilizing effect tides on delta morphology

The Paraná Delta is a system likely significantly influenced both by fluvial and tidal controls. Under the condition of equal sediment import (during low to regular flows) and export (during high flows), tides often act to stabilize delta morphology on the landscape scale. For example, tidally-influenced distributary channels often have relatively small migration rates. Another stabilizing mechanism of tides is the counteracting channel abandonment due to an asymmetry in river flow distribution. When a tidal river splits into a large and small distributary channel, the setup created by the interaction between mean flow and the tidal motion in the larger channel increases the water level gradient in the smaller channel, redistributing the river discharge [Hoitink et al., 2017].

When considering the (Lower) Paraná delta, a deltaic system that is (heavily) accreting and thus out of equilibrium, several tidal processes can amplify or lie at the root of such depositional behaviour. Net sediment transport by tidal forcing is induced by a kind of asymmetry of hydrodynamic forcing, either in space or in time. Two main asymmetries and related morphodynamic features applicable to the Lower Paraná Delta channel network are elaborated upon in the following sections. Note that most

literature cited concerns tidal basin morphology, however much of this literature is also applicable to tidally influenced river channels.

Peak-velocity asymmetry
Asymmetry in the tidal signal can lead to net sediment im- or export in a tidal basin. In Section 2.2.2 it was mentioned that the tidal signal near the deltaic front is asymmetric, i.e. flood velocities exceed ebb velocities. This type of asymmetry has been mainly investigated for coarse (bed-load) sediment fractions, as sediment transport S is dependent on instantaneous flow velocities U by the power law $S \propto U^n$ with $n = 3$ to 5. However, also in case of suspended transport, the concentration is proportional to the erosion flux, which is proportional to $\tau_b \propto U^2$, therefore peak-velocity asymmetry might also lead to net import of fines [Gatto et al., 2017].

Acceleration / deceleration asymmetry
Another type of asymmetry considers the difference in high and low slack water periods. This type of acceleration-deceleration (or: slack water) asymmetry originates from the dependency of the temporal gradient in velocity $\frac{\partial u}{\partial t}$ on the landward basin area and conveying cross section. In the case of little intertidal storage and shallow channels, high water slack duration is longer than low water slack. The inverse is true at a basin where vast storage-offering tidal flats and deep channels are present. Due to the time dependency of fine sediment dynamics, this type of asymmetry can be dominant in influencing net tidal im- or export of fine, suspended matter. In any case, net tidal transport into the flood direction will only occur if tidal velocities exceed the river flow velocities, allowing for flow velocities to be directed landward / against the residual river flow.

In Appendix H, some simple analytical considerations are made using only water level data, assessing the plausibility of above described asymmetries significantly influencing the Lower Delta channel network. The following points describe the essence of these calculations and the results:

- A velocity signal was approximated by assuming a friction dominated flow in a short basin ($u = \frac{\partial h}{\partial t}\frac{A_b}{A_s}$). The quantity $u = \frac{\partial h}{\partial t}$ was approximated by means of a first order central difference scheme. Using this approximation, peak flow velocities exceed peak ebb velocities by a factor 2.
- The difference in slack water duration was assessed by evaluating the number of extreme values in the quantity $\frac{\partial^2 h}{\partial t^2}$, approximated with a second order central difference scheme. The values of the maxima are in the same order as the minima, therefore a significant difference in slack water duration is not evident.
- Tidal velocities in different channels were approximated with the characteristic flow velocity of the elementary wave equation $\hat{U}_{tide} = \sqrt{\frac{g}{h}} \cdot \hat{\zeta}$ and compared to fluvial flow velocities determined with river equilibrium flow theory. The outcome is that at least during regular conditions, flow reversal and thus tidal import is only likely to occur in certain channels located close to the deltaic front, and less in the main river branches (Río Luján, Paraná de las Palmas).
- By comparing characteristics settling time scales of particle types, it is expected that clay particles do not have sufficient time to settle and that therefore mostly silt and sandy particles could be subject to processes of residual tidal transport acting on a diurnal timescale.

Regarding the import of sediment by tidal currents into the channel network, the following hypothesis is formulated:

1. **Tidal and fluvial processes** ***Hypothesis***

   (b) Due to the relative magnitude of the tidal velocities and the insignificance in slack water duration asymmetry, import of sediment is not expected to play a significant role in shaping the bathymetry of the Lower Delta channel network.

Tidal divides

As mentioned in Section 2.2.2, the tidal wave propagates through the deltaic channel network, and penetrates deep into the main branches of the Parana River. In the rising stage of the tide, tidal currents are in the direction of the propagation, and in the opposite direction during the falling stage. When the tidal wave enters a channel from both ends, the waves can coincide, creating a 'tidal divide'. The tidal wave is a special manifestation of spatial asymmetry in flow velocities, caused by the oppositely directed tidal currents.

A criterion for this mechanism to take place is that an oppositely directed propagating tidal wave must be present in a channel at the same time without too large of a phase difference [Vroom, 2011]. To assess this criterium, a simplified case of Arroyo Caraguata is considered. The tidal wave approaches from the south via the Lujan River and from the north via the Las Palmas river branch. The celerities of the tidal wave will is approximated with $\sqrt{gh}$. Assuming the tidal wave reaches the whole deltaic front simultaneously (as would be the case for a purely co-oscillating tidal wave), the tidal delay in hours at the entrances of Arroyo Caraguata is calculated and presented in Table 2.3. The principle of the tidal delay and tidal divide is schematically represented in Figure 2.16.

Table 2.3: Estimation of tidal delay into Arroyo Caraguata

	Río Luján	Paraná de las Palmas	
Tidal celerity $\sqrt{gh}$	7	10.9	m/s
Distance to deltaic front	13	23	km
Tidal delay to Arroyo Caraguata	t_1 = 31	t_2 = 35	minutes

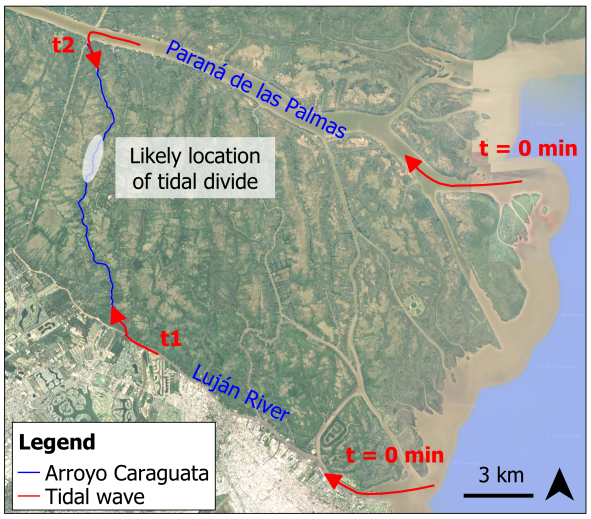

Figure 2.16: Schematic representation of the tidal divide in Arroyo Caraguata

The tidal delay between the entrances of Arroyo Caraguata is 4 minutes. The location of the tidal divide in Arroyo Caraguata is approximated and displayed in Figure 2.16. It must be stated that this calculation is based on characteristic values in which the non-steady character of water levels and bed levels are not taken into account. It is therefore likely that, depending on the conditions, the tidal divide occurs at varying locations along the channel.

A consequence of tidal divides occurring in a channel could be that around the location of the tidal divides, depositional patterns occur leading to higher bed levels than at the channel entrances. Depth measurements taken in December 2021 and March 2021 (see Appendix D and Figure 2.12) substantiate the hypothesis, as it clearly visible that water depths in multiple channels, including Arroyo Caraguata, decrease towards the middle of the channels. This observation is mainly valid for the channels located more upstream, rather than the channels with their mouths located in the estuary. Channels located more perpendicular to the main river branches are more likely to have oppositely travelling

tidal waves. The following hypothesis is formulated considering the influence of the tide propagating into the channel network:

1. **Tidal and fluvial processes** ***Hypothesis***

   (c) Deposition of sediment occurs at tidal divides inside the channel network

2.5.3. Extreme events

In previous Sections 2.2.1 and 2.2.3, the occurrence of extreme events was discussed. In the following section, the hypothesised influence of extreme forcings on the Lower Delta channel network are discussed. The two types of extreme events discussed are high discharge occurrences and floods due to storm surges induced by 'Sudestadas' (strong south-eastern winds).

Erosion during high river discharge

Generally, high river discharges induce high flow velocities, allowing the flow to carry more sediment out of the delta, into the estuary. Peak flow conditions can induce an M2 backwater curve in a delta, leading to flow acceleration and subsequent erosion (see Figure 2.14). However, as these notions implicitly assume that morphological changes only occur due to changes in hydraulic conditions (bed load and equilibrium sediment transport), the increase in downstream supply of (fine) sediment due to the high discharge is not considered. It seems that, at least in the Paraná de las Palmas, high discharge leads to increased sedimentation, as sedimentation rates in the downstream reach of the Paraná de las Palmas drastically increased during years of high discharge (see Chapter 3). By modelling practice, Happee [2019] reproduced the characteristic of the Río de la Plata estuarine system that increased discharge results in increased sedimentation in the estuary for the same sediment concentration input boundary condition.

It is not straightforward that this characteristic is also valid for the channel network. Whereas the supply of sediment into the channel network will undoubtedly increasing during high discharge years, the increased flow velocities and the susceptibility to erosion of the soft channel beds might lead to a erosive effect during high discharge. In addition, higher discharges might shift potential depositional features downstream or even into the Río de la Plata estuary. Due to above mentioned reasons, the expected effect of high discharge events on channel morphodynamics is erosive compared to regular flow conditions. The following hypothesis is formulated concerning the influence of high discharge events on the morphological development of the Lower Paraná Delta channel network:

2. **Extreme discharge events and storm surges** ***Hypothesis***

   (a) Extreme river discharges cause erosion or counteract deposition in the Lower Delta channel network compared to regular discharge conditions, due to increased flow velocities and sediment transport capacity.

Erosion due to return flow after storm surge flood

As described in the geomorphological analysis (Appendix B), the Lower Delta consists of islands with slight depressions in the center and natural embankments around the channels. These embankments, along with general vertical growth of the delta, are formed by sedimentary deposits during floods, leading to fining of sediment size with increasing distance from the channels [Medina and Codignotto, 2013]. As floods in the Lower Delta occur yearly and are predominantly instigated by Sudestadas (strong south-eastern winds), therefore this specific meteorological condition will likely influence channel morphodynamics. After the flood peak, the water on the floodplains return to the channels depleted of most sediment. The return flow can induce erosion in the channels as the sediment previously carried by the flow is deposited on the floodplains and discharges can be relatively high, depending on the magnitude of the storm surge and its retreat [Persona contact with Raúl Escalante]. The principle is displayed in Figure 2.17.

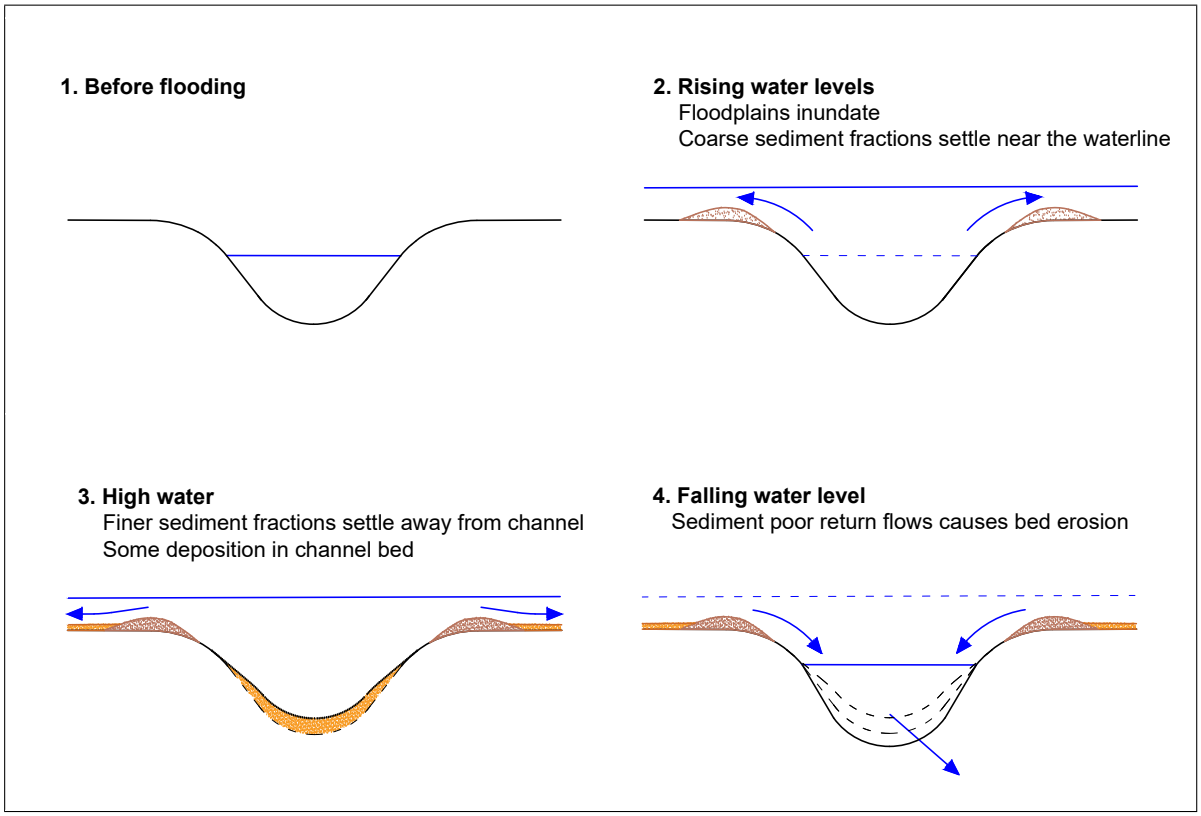

Figure 2.17: Natural levees and bed erosion after storm surge induced flood plain inundation

If the water entering the system during rising water levels is sediment laden, the net effect of the storm surge could be deposition due to higher volumes of sediment entering and settling inside the channel network. However, such net depositional patterns have not been observed after the occurrence of high water [Personal contact with Diego Moreira].

The following hypothesis is formulated concerning the influence of storm surges on the morphological development of the Lower Paraná Delta channel network:

2. **Extreme discharge events and storm surges** ***Hypothesis***

   (b) The sediment-depleted return flow after a flood instigated by a storm surge can pick up sediment from the channel beds, leading to a net erosive effect of the storm surge event and the flood.

2.5.4. Riparian vegetation

Vegetation on the banks of natural streams ('riparian vegetation') can have a significant effect on the flow velocity, effectively increasing the hydraulic roughness of the channel and inducing locally increased sedimentation rates. In addition, vegetation cover and the presence of roots can strengthen the superficial soil layer in a channel, making the bed more resistant against erosion [Vargas-Luna et al., 2015]. The invasion of riparian vegetation during periods of low flow can instigate a positive feedback mechanism, as the presence of the vegetation facilitates a depositional regime leading to lower water depths, benefiting the continuation of the invasion of the vegetation [Dean and Schmidt, 2011]. Figure 2.18 schematically depicts this mechanism.

During the field surveys, it was observed that riparian vegetation is abundant in especially the smaller channels in the Lower Delta (see Figure 2.19). The reed cover can reach large distances from the banks, indicating high bed levels and the possibility of the occurrence of the feedback process as

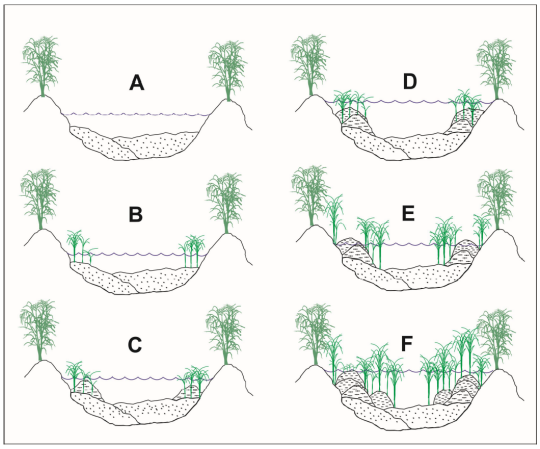

Figure 2.18: Vegetation feedback mechanism [Ramonell, 2021]

Figure 2.19: Reed in the Lower Delta channel network (Photo courtesy of M. Sabarots Gerbec)

depicted in Figure 2.18. The following hypothesis is formulated concerning the influence of riparian vegetation in the Lower Delta Channel network:

3. **Riparian vegetation** ***Hypothesis***

   The abundance of riparian vegetation in the Lower Delta Channel network facilitates local patterns of sediment deposition

3

Anthropogenic and Natural Impacts on Fluvial Forcing and Flow Patterns

This chapter describes the natural and anthropogenic factors that impact the hydraulics and morphodynamics in the Lower Delta. Sections 3.1 to 3.5 discuss the natural processes and anthropogenic activities that have lead and potentially will lead to trends in discharge and sediment input into the Paraná River system, including the formulation of hypotheses on the subject. Sections 3.6 and 3.7 cover the (potential influence of) dredging activities in the Lower Delta. The final Section 3.8, lists all the hypotheses formulated in Chapters 2 and 3.

The reader without much time is advised to move to Section 3.5 and 3.7, most specifically the hypotheses, recognizable by the grey frames. All hypotheses, including those introduced in Chapter 2, are listed in Section 3.8.

3.1. Interannual climatic variability: ENSO

El Niño Southern Oscillation (ENSO) is a major mechanism behind interannual variation in global meteorological patterns. ENSO occurs every 2 to 7 years and is caused by sea temperature anomalies in the pacific ocean. It influences weather patterns across the globe, the overall effects are displayed in Figure 3.1. The size and variability in physical characteristics of Argentina makes for a spatially inhomogeneous effect of ENSO. Warm phases (El Niño) are related to increased spring and autumn precipitation in Mesopothamia (northeastern Argentina) and the Central Andes [González et al., 2016]. Overall patterns of positive precipitation anomalies cause a statistically significant increase in the discharge of the Paraná River. This feature is most pronounced from December-February and in May-June. Streamflows during cold events (El Niña) and regular conditions are similar [García and Mechoso, 2005]. The highest monthly recorded positive discharge anomaly during El Niño in the twentieth century is as high as 38,000 m^3/s [Barros, 2005].

The measure of strength of ENSO events is described with the Oceanic Niño Index (ONI), which is based on the magnitude of sea surface temperature anomalies in the equatorial pacific ocean. An analysis by Happee [2019] showed that peaks in annual river discharge and sediment supply in the Paraná River are linked to strong and very strong El Niño events. Discharge anomalies during strong an very strong El Niño events are visualized in Figure 3.3. Yearly-averaged sediment deposition volumes in the Paraná de las Palmas and Canal Emilio Mitre (see Section 3.6) are multiples of the deposited volumes during non-ENSO years, indicating large positive sediment supply anomalies during El Niño events.

3.2. Long term climatic variability and trends

Global warming, the subsequent rising of sea levels and the changing variability in climatic and meteorological characteristics and events can pose serious consequences to fluvial and deltaic, urbanized regions. Without addressing the general causes, effects and uncertainties around the changing cli-

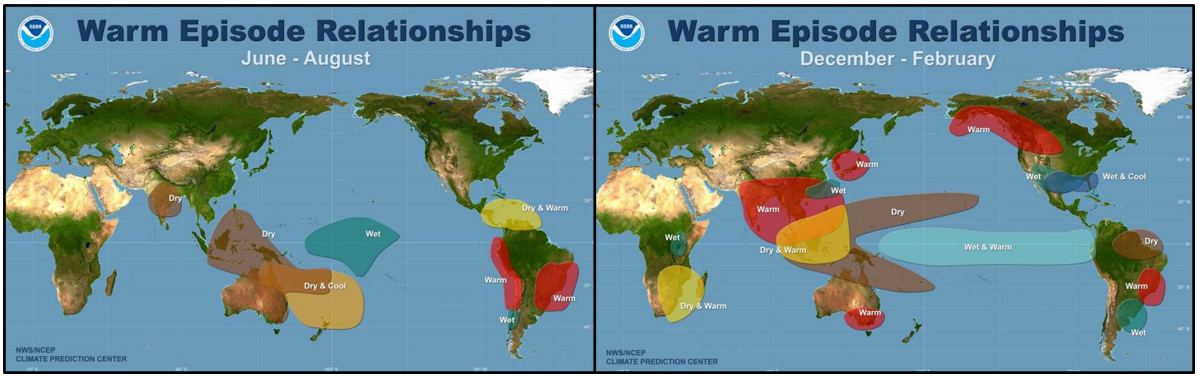

Figure 3.1: Global effects of warm (El Niño) and cold El Niña) ENSO episodes [NOAA, 2005]

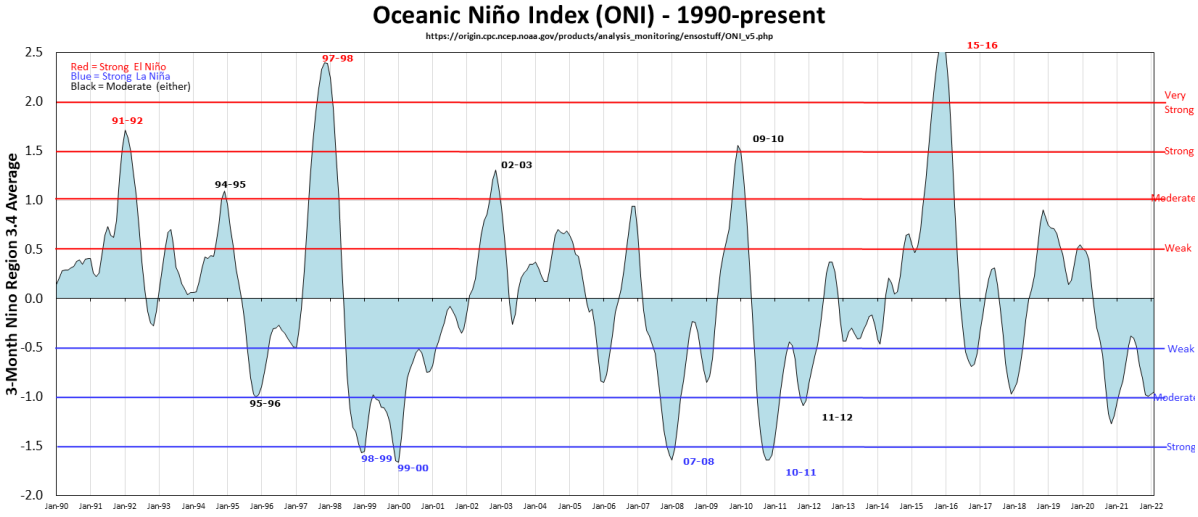

Figure 3.2: ONI index 1990-2022 (from Null [2022])

mate, the following notions are addressed regarding potential and observed consequences of climate change for the Paraná River system and the deltaic region.

Precipitation and discharge trends

Doyle et al. [2005] found that the observed trend on precipitation in the La Plata catchment from 1960 to 1999 has been positive and was approximately 5 mm/yr, or approximately 15%. According to Doyle et al., this trend can be attributed to an increase in precipitation in the majority of the catchment area (including the Bermejo subcatchment), with exceptions of negative trends in the north-eastern and north-western parts of the catchment (see Figure 3.4). The overall increase in precipitation has manifested mainly in the intensification of extreme rainfall events during El Niño years. Furthermore, Doyle et al. found that a general hydrological characteristic of the La Plata basin observed since 1960 is that the ratio between the relative increase of river discharge and precipitation is approximately a factor two. A 15% increase in precipitation would have thus lead to a 30% increase in river runoff. This sensitivity was found to be reasonably stable, both for two or more consecutive years, ENSO anomalies and multi-decadal changes [Berbery and Barros, 2002]. Another effect of increased precipitation was a higher occurrence and severity of flooding [Depetris, 2007].

Projected changes in precipitation patterns in Southeastern South America are spatially dependent due to the size of the catchment. Most models project a wetter climate near the Paraná Delta and drier conditions along much of the southern Andes. In the 2014 IPCC report [Magrin et al., 2014], various projections on precipitation patterns, based on different models and scenarios, are presented. In all of the projections of Southeastern South America overall precipitation increases in the order of 20 to 30% and 1 to 2 mm/day in the 21th century. Intensity of rainfall events and the frequency of occurrence of

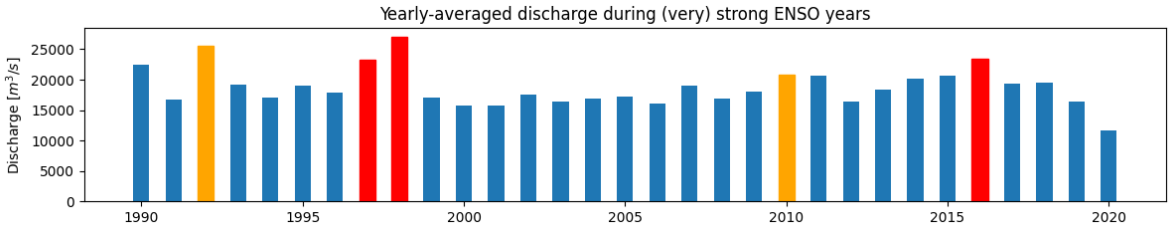

Figure 3.3: Discharge at Corrientes, orange and red bars indicating strong and very strong ENSO events, respectively

these events are likely to increase as well. The model by Cabré et al. [2010] projected a precipitation increase of 0.5 to 1.5 mm/day by 2050 for the La Plata basin specifically.

The IPCC 2014 report presents two ”robust” (indicating a certain expected level of validity) projections concerning future discharge trends in the Paraná River. Marengo et al. [2011] projected a 10 to 20 % increase from in 2100, Nakaegawa et al. [2013] projected an increase of 18.4% by the late twentieth century (2075-2010).

Sediment supply trends
The sediment yield of the Paraná river has increased significantly over the same period as the discharge increase. This is partly due to the increase in precipitation patterns, and partly due to increased soil degradation in the Bermejo Region, mostly due to agricultural activities (see Section 3.3). Amsler and Drago [2009] report an increase of 35% in the wash load discharge transported annualy by the Middle Paraná River. Figure 3.5 displays the increase of annual average sediment concentrations in various parts of the Paraguay River.

A model comparison study by Moreda et al. [2016] on the projection of future river discharges and sediment loads originating from the Bermejo region had varying results. Most models projected a decrease in river discharge from the Bermejo region in the order of 10 to 20% in 2014-2050 compared to the baseline period (1990-1998). Trends in sediment load vary from 6 to 20 % decreases to a 42% increase. This large variation is due to the manner in which the different models incorporate the influence of high intensity rainfall events on the sediment load. Moreda et al.’s study suggests the models with outcomes as increases in sediment load are more suitable for watershed management practices. In any case, as stated by Moreda et al., there is an important effect of peak discharges (on sediment load) during high flows that would potentially lead to an increment of the overall sediment transport load in the next decades.

Trends in marine forcing
The combination of sea level rise and increasing storm surge frequencies endanger the habitability of the low lying lands in the Paraná Delta. The ICPP’s RCP 4.5 scenario sea level forecast of the Mar del Plata, located approximately 200 km from the La Plata estuary’s centerline, predicts an approximate sea level rise of 4.8 mm/yr until 2100. Sudestada levels seem to follow the trend of the relative sea level rise, while the frequency and duration of the storm surges have increased throughout the twentieth century.

3.3. Land use change in the river catchment

The Bermejo region has a history of unregulated and exploitive agricultural activities, which have resulted in a decline in natural vegetation and wetlands. As natural vegetation slows down surface runoff and has a high evapotransporative capacity, the substitution of nature with agriculture has resulted in increased surface runoff and subsequent soil degradation in over half of the catchment area [OAS, 2005], leading to an increase in sediment loads in the Bermejo River. Sediment supply from the Bermejo region has increased with approximately 35% from 1970 to 2008 [Amsler and Drago, 2009]. Additional consequences of the land use change is a strong reduction in biodiversity and the impoverishment of natural resources, negatively influencing the quality of life of particularly the many small farmers and indigenous populations in the region [OAS, 2005].

Land use change and its effects are not limited to the (sediment load originating from the) Bermejo region. Since 1960, extensive agricultural activities (predominantly in Brazil) have increased the annual discharge of the Paraná River significantly [Doyle et al., 2005]. Between 2000 and 2014, agricultural land in the La Plata Basin increased with 23%, adding over 50,000 km^2 of new crop land. Most agricultural expansion came at the cost of loss of grass lands at both sides of the Uruguay River [Baeza and Paruelo, 2020]. Doyle et al. [2005] found that land use change during 1960 and 1999 in the Plata Basin caused a reduction in local evapotranspiration, resulting in a significant increase in river discharge [Doyle and Barros, 2011]. Whereas Doyle and Barros attribute the total increase in discharge predominantly to the increase in precipitation, Lee et al. [2018] argues that the discharge increase is mainly attributable to increased surface runoff cause by the land use change. In any case, the effect of precipitation patterns and land use change have had a significant influence on the discharge of the Paraná River

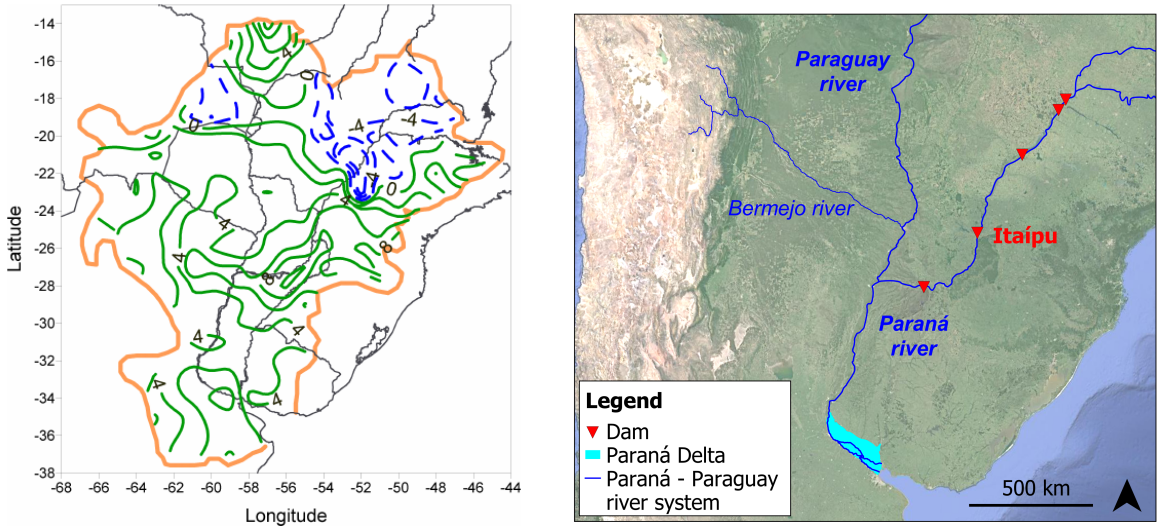

Figure 3.4: Precipitation trends [mm/year] in the La Plata Basin between 1960 - 1999 [Doyle and Barros, 2011] (left) and locations of dams in the Upper Paraná River

3.4. Dam construction

From 1967 to 2000, five dams have been constructed in the Paraná River for the purposes of generating hydroelectric power, flood control and navigation management. The Itaípu Dam is the second largest hydroelectric dam (by power production) in the world. Large-scale effects of dam construction have been a decrease in sediment supply and a reduction in the occurrence of discharge minima [Brea and Spalletti, 2010]. The Bermejo river, which is dominant in the supply of (fine) sediments to the delta, is located upstream of the Paraguay - Paraná rivers confluence. Dam construction has only taken place in the Upper Paraná River upstream of the confluence, therefore the sediment regime in the Paraná Delta has not changed drastically due to the damming. Figure 3.5 schematically displays the reduction in sediment concentration from the Upper Paraná River, counteracting the basin-wide effect of increased sediment concentrations caused by an intensification of precipitation patterns, increase in land use change and the subsequent surface runoff.

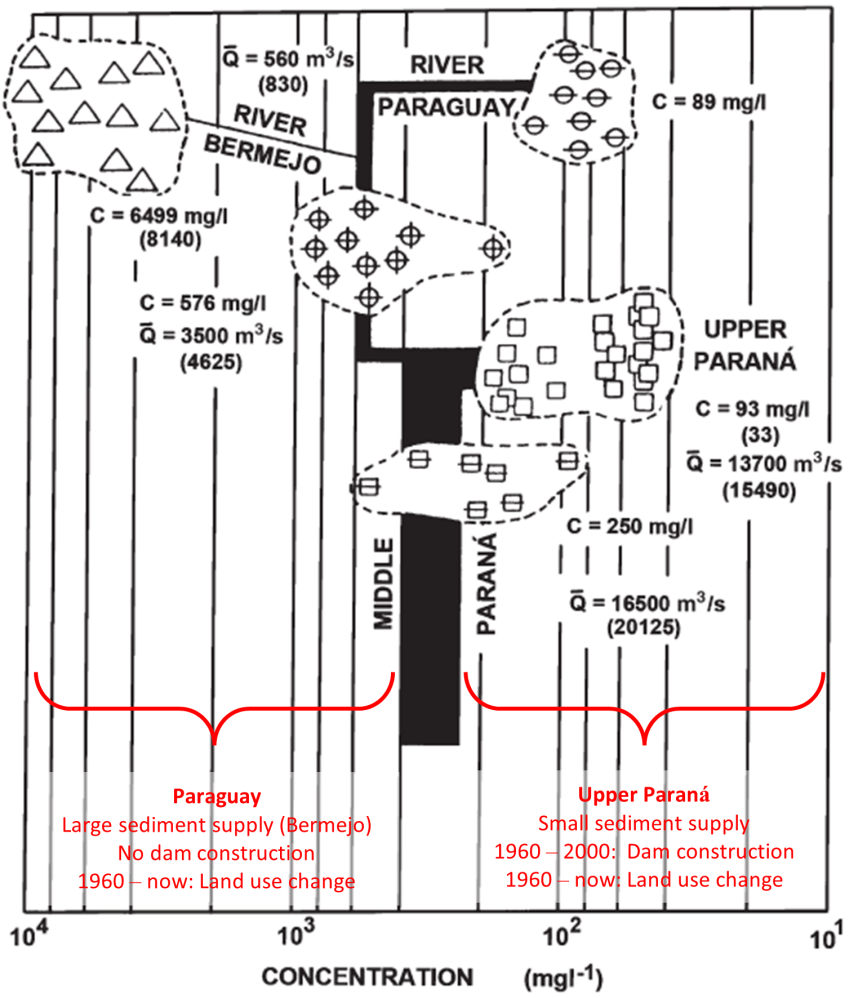

Figure 3.5: Schematic depicting mean values of sediment concentrations from the period 1970-1979 (C), 1993-2003 (in between brackets) and river discharge (Q), edited from Amsler and Drago [2009]

3.5. Hypotheses on the influence of discharge and sediment input variability and trends

The following hypotheses are formulated considering variability and trends in the La Plata catchment due to climatic and anthropogenic influences:

4. **Historic and future changes in sediment input and river discharge** ***Hypothesis***

   (a) The combination of an overall increased river discharge, manifesting mainly in increased discharge peaks, and increased sediment load from the Bermejo region between 1960 and 2000 caused by increased precipitation patterns and land use change have had a positive effect on the annually averaged sediment concentrations entering the delta, which subsequently lead to increased sedimentation rates in the Lower Delta channel network.

   (b) The projected increase in discharge peaks in the 21st century will counteract depositional patterns in the Lower Delta, essentially 'flushing' the channel system.

   (c) When considering the possibility of higher sediment loads during the discharge peak, the overall sediment concentrations in the Lower Delta will increase, leading to an increase of net sedimentation rates in the Lower Delta channel network.

3.6. Dredging activities in the Lower Paraná Delta

3.6.1. Deepening of the Paraná de las Palmas

Deepening of the Paraná River has been essential in maintaining the navigability of the river system. In the Lower Delta, the Paraná de las Palmas branch is used as the main waterway. Sea-going vessels can sail up to the Port of Rosario, approximately 300 km upstream of the Buenos Aires port. Extensive dredging is needed in the Río de la Plata estuary, connecting the river reaches to the port of Buenos Aires and the port to the open ocean. Canal Emilio Mitre is the channel connecting the Paraná de las Palmas to the Buenos Aires port, as can be seen in Figure 3.6.

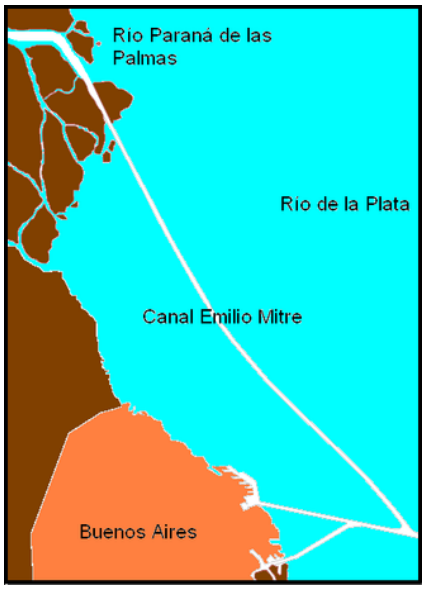

Figure 3.6: Canal Emilio Mitre [Image from Wikipedia]

Data from the governmental institution responsible for carrying out dredging activities (*Subsecretaria de Puertos Vías Navegalbes y Martina Mercante*, SSPYVN [2019]) containing dredged volumes, dates, locations and deposition sites in the Río de la Plata and the Paraná river were obtained and analysed. The timespan of the analysed data was 1995-2019, and existed of:

- The counter-streamwise coordinates of the dredged reaches in the Paraná de las Palmas river and the Canal Emitre in the Río de la Plata
- The width of the dredged reaches
- The total volumes of dredged material per year

With this information, the total and yearly dredged volumes and heights over the period 1995-2019 were approximated. Spatial variation within the dredged reaches was not taken into account. Figure 3.7 displays the reaches and the dredged heights over the period 1995 - 2019. It is clear that the largest volumes are dredged from Canal Emilio Mitre. It must be noted that Canal Emilio Mitre is not dredged continuously but rather sporadically. This is due to the strategy of using dredging pits, effectively trapping sediment and preventing sedimentation to occur in high quantities over the entire channel bed. This prevents the need for continues dredging in the waterway. The use of dredging pits cause annual dredged volumes to be not uniquely representative for sedimentation volumes in the same year [Happee, 2019]. Sedimentation occurs mainly in the seaward side of the Canal [Happee, 2019], the part of the channel connecting the river mouth with the Río de la Plata is a narrow, excavated, deep channel that stays at depth naturally due to the high discharges flowing through the narrow channel [Personal contact with Sebastian Garcia].

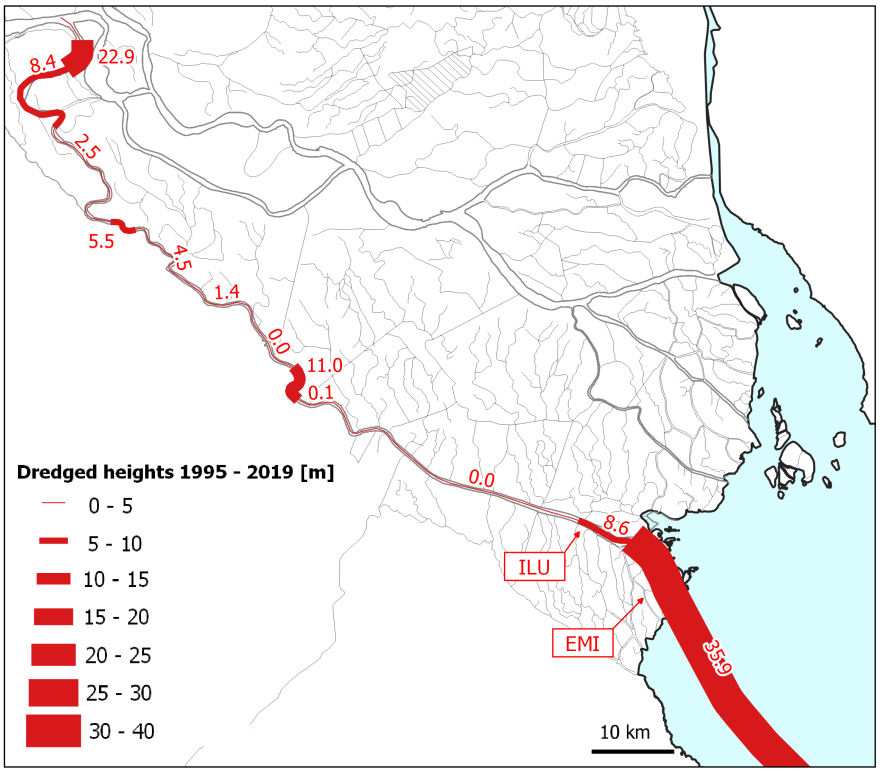

Figure 3.7: Dredged heights along the Paraná de las Palmas between 1995 - 2019

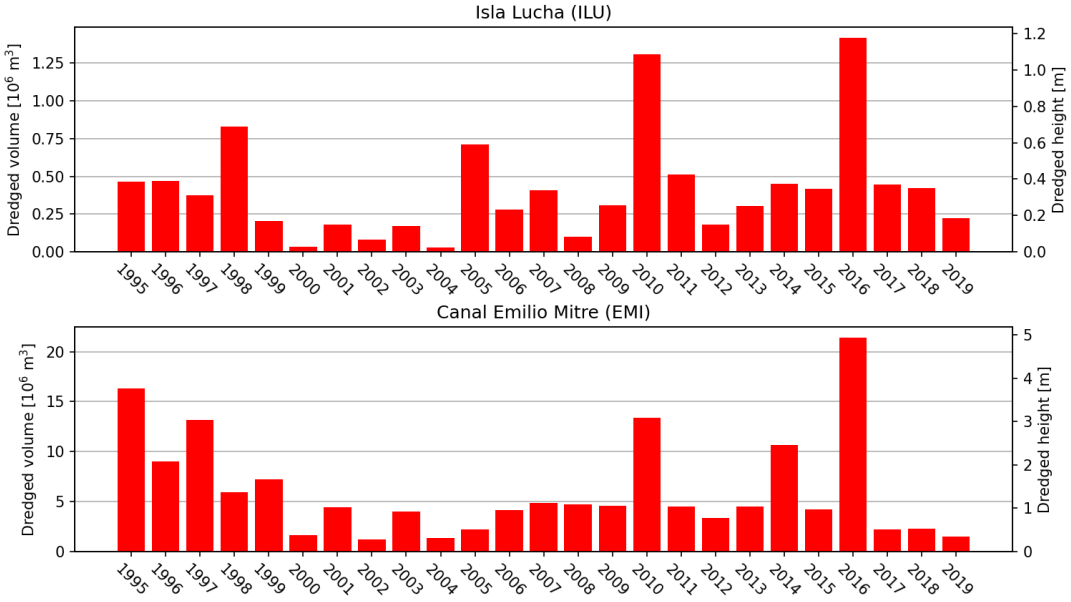

Figure 3.8: Dredged volumes and heights in the reaches Isla Lucha (ILU) and Canal Emilio Mitre (EMI)

The spatial heterogeneity of the dredged volumes over the Palmas is evident, especially the most downstream part of the Palmas is dredged heavily, and thus experiences higher sedimentation rates compared to other reaches. Total dredged volumes and heights over the analysed period are displayed in Figures and 3.8. Years during strong positive ENSO anomalies (1998, 2010, 2016) are undoubtedly linked to high rates of sedimentation.

3.6.2. Dredged-material disposal site

One of the dredged-sediment disposal sites locations is closely situated next to the channel network north of the Paraná de las Palmas (see Figure 3.9). Point data on the locations and depth after disposal on 03-08-2018 was analysed. Due to the lack of recent bathymetric information on the site and lack of exact time data of the moment of deposition (taking into account the tidal phase) it was not possible to quantify the material deposited.

Assuming the material was dredged and thus naturally deposited nearby (at the river mouth), it can be assumed that typical flow velocities at the deposition site could potentially carry sediment into the channel network, after which it could settle due to flow decelerations. This strongly depends on the flow conditions at the moment of deposition, as well as the tidal phase during disposal.

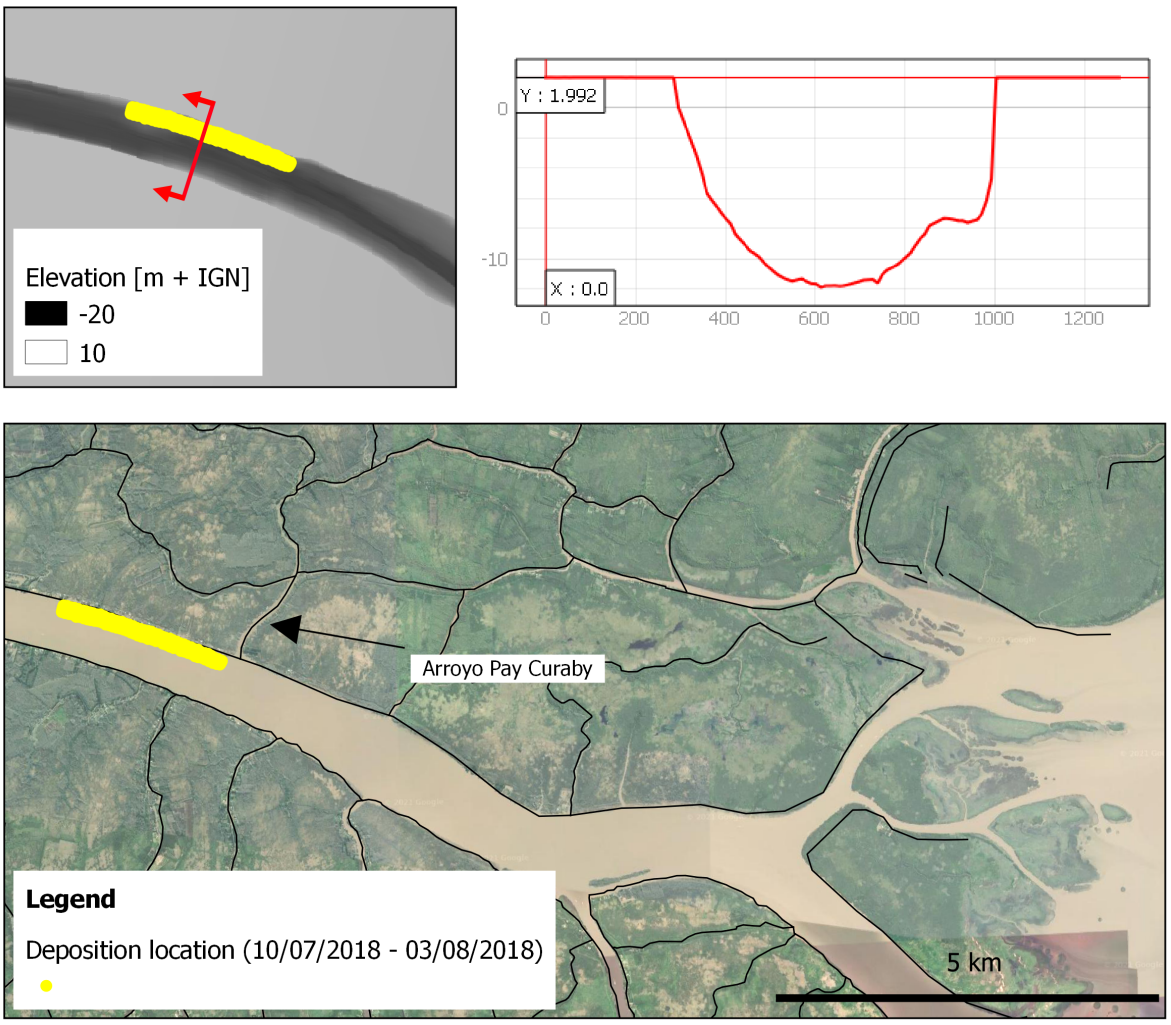

Figure 3.9: Disposal location Paraná de las Palmas

3.7. Hypotheses on the influence of dredging and channel excavation channel hydrodynamics

Two analytical models were used in order to asses the potential influence of deepening the Paraná de las Palmas on the hydrodynamics in the channel network. The following three subsections briefly describe the relevant processes, the analytical models and the associated hypotheses. The complete description of the analytical quantification is included in Appendix H.

3.7.1. Influence of deepening on tidal characteristics

Increasing the cross section of a flow profile by artificially deepening the river thalweg influences the celerity of the tidal wave, which is related to the depth via $\sqrt{gh}$. A calculation was done, assessing the influence of lowering the conveyance area of the Paraná de las Palmas with 0.5 meter (equivalent to 'undoing' several years of dredging activities). Using $\sqrt{gh}$, the tidal celerity only decreased slighthy in the reduced cross section, implying that the influence of deepening the Paraná de las Palmas on the tidal celerity is negligible, especially considering that the (non-)tidal variations in water level cause at least similar changes in water depth and tidal celerity.

As stated in the Theoretical Framework (Appendix A), tidal energy is damped due to friction when propagating through a channel. When the conveying cross section of the river does not decrease significantly upstream, the result is a reduction in tidal wave height and the eventual complete dissipation of tidal energy. Using the analytical formulation of the amplitude of a harmonic wave with linear friction in a straight channel, the difference in tidal amplitude between current characteristics of the Paraná de las Palmas and a reduction in conveyance area was approximated. The following bullets describe the outcome of the analytical model:

- When using a constant dimensionless friction factor c_f for both cases, the tidal damping factor does not change significantly when reducing the conveyance area of the Paraná de las Palmas.
- When increasing the friction factor from 0.0015 to 0.002 in the not-deepened case, the damping increases with approximately 5 percent, leading to a slight but significant decrease in tidal range in the Paraná de las Palmas. Figure 3.10 displays the results.

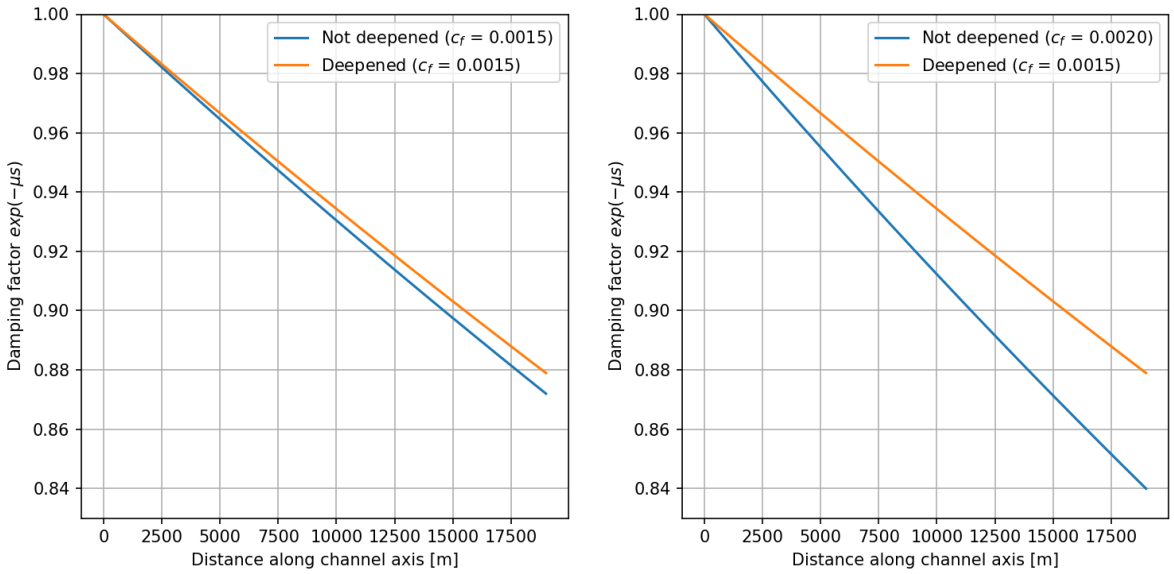

Figure 3.10: Damping coefficient with and without deepening of the Paraná de las Palmas

The analytical approximations yield a limited influence of dredging on tidal characteristics in the Paraná de las Palmas. However, various effects are not considered, such as the interaction between tides and river discharge and variability in hydraulic friction. The results of the analytical approximations must therefore not be interpreted as definite.

The following hypothesis is formulated concerning the effect of dredging the Paraná de las Palmas on the characteristics of the tidal wave:

5. **Dredging activities and channel excavation** ***Hypothesis***

(a) Deepening the main channel of a river can enhance tidal amplification or change the celerity of the tidal wave, altering the hydraulic conditions at the boundaries of a channel and changing the location of tidal divides.

3.7.2. Influence of deepening on flow partitioning

Deepening a river branch can alter the water levels at upstream channel bifurcations and can lead to reduced flow velocities in the side channels. A highly schematized case of the Paraná de las Palmas and a side channel is presented, demonstrating the effect that artificially deepening a main channel has on the discharge distribution, and associated changes of sediment transport capacity between the channels. The theoretical principles of the model are displayed in Figure 3.11. The complete description of the analytical quantification is included in Appendix H, and the most important points are listed below.

- It is assumed that before deepening the main river branch, both channels are in equilibrium state.
- The main channel is deepened by 0.5 m.
- The results of the analytical model indicate a significant change in transport capacity in the side channels after dredging. For a typical channel as present in the Lower Delta, bed shear stresses decrease with 20 to 30%.

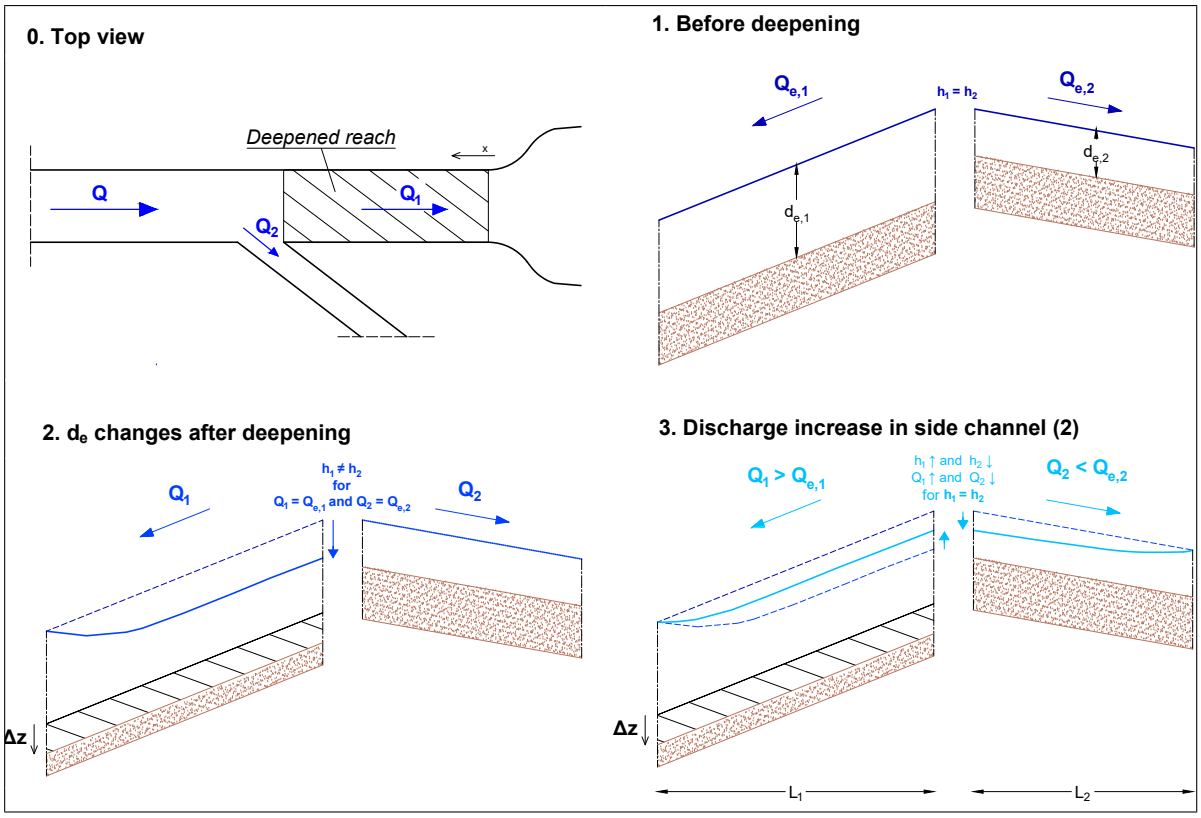

Figure 3.11: Top view and theoretical behaviour before and after deepening

The following hypothesis is formulated concerning the effect of deepening the Paraná de las Palmas on the sediment transport capacity in the channel network:

5. **Dredging activities and channel excavation** ***Hypothesis***

   (b) Deepening a river branch will attract flow, leading to a repulsion of flow in nearby channels, lowering the sediment transport capacity in these channels and thus inducing channel accretion.

3.7.3. Influence of newly excavated navigation channels

As described in Chapter 2, various navigation channels located in the Lower Delta were excavated in the early 20th century. The effect of excavation new channels can be similar to the deepening the main river branch. After the excavation of a channel, the discharge of the main river branch reduces, effectively lowering the equilibrium water depth downstream, leading to a decrease in flow and in the side channels. Regarding the influence on historically excavated navigation channels in the Lower Delta, the following hypothesis is formulated:

5. **Dredging activities and channel excavation** ***Hypothesis***

   (c) The excavation of artificial channels has decreased the river discharge through the existing, natural channels, and the subsequent reduction in sediment transport capacity has had positive effect on deposition in the channel network.

3.7.4. Channel feeding from dredged-sediment disposal site

By means of a highly simplified case, the possibility of disposed dredged material being transported into a side channel is considered. The situation at Arroyo Pay Curaby (section 3.6.2) is used as a reference case.

It is assumed that the dredged material originates from nearby, i.e. from the river mouth. Typical soil characteristics at the Paraná de las Palmas mouth were sampled and characterized by Drago and Amsler [1998], described in Chapter 2 and repeated in Table 3.1.

Table 3.1: Bed sediment at the Paraná de las Palmas [Drago and Amsler, 1998]

	D_n [mm]	Fraction in bed
Fine sand	0.125 - 0.250	24 %
Very fine sand	0.062 - 0.125	50 %
Silt	0.002 - 0.062	12 %
Clay	0.002	12 %

Typical flow conditions during regular conditions are assumed to be similar to those measured by INA (Morale et al. [2018]). The flow velocity, near the shore, around the location of deposition is approximately 0.5 m/s. For such conditions, the maximum particle diameter that can be transported is approximated by using the concept of the critical shields factor (see Appendix A). For a critical shields factor θ_{cr} of 0.04, a friction factor c_f of 0.0015 and a dry density of 2650 kg/m^3, the threshold sediment diameter D_{cr} becomes 0.57 mm, implying that the finer sand, silt and clay particles might be transported by the current. Flow decelerations in the channel network could cause the transported material to settle, however the extent of this process is highly dependent on local conditions.

$$\begin{aligned} \theta_{cr} &= \frac{\tau_{b,cr}}{(\rho_s - \rho)gD} \\ 0.04 &= \frac{0.0015 \cdot 0.5^2}{(1650 \cdot 9.81 \cdot D_{cr}} \\ D_{cr} &= 0.57mm \end{aligned} \tag{3.1}$$

The following hypothesis is formulated concerning the influence of the deposition of dredged material nearby channel entrances:

5. **Dredging activities and channel excavation** ***Hypothesis***

   (d) Deposition of dredged material nearby a channel entrance can lead to unwanted sediment supply into the channel network.

3.8. All hypotheses

The following list repeats and numbers all hypotheses formulated in Chapter 2 and 3. The hypotheses are structured as the sections in Chapters 2 and 3. The numbering will be used in the following chapters to indicate the link between a hypothesis and model scenario.

1. **Tidal and fluvial processes**

   (a) Channel sedimentation is mainly caused by the supply and deposition of fluvial sediment
   Three fluvial processes are expected to play a significant role in the morphological development of the channel network:
   - Flow of the Paraná de las Palmas decelerates in the downstream end due to the presence of a M1 backwater curve during regular conditions, leading to widespread sedimentation near the deltaic front;
   - Sediment carried by the Paraná River is directly deposited due to decelerations in flow velocity when entering the secondary channel network;
   - Sediment carried towards the deltaic front experiences decelerations due to widening of the channel, leading to the formation of mouth bar deposits in the downstream reaches of (terminal) channels.

   (b) Due to the relative magnitude of the tidal velocities and the insignificance in slack water duration asymmetry, import of sediment is not expected to play a significant role in shaping the bathymetry of the Lower Delta channel network.

   (c) Deposition of sediment occurs at tidal divides inside the channel network

2. **Extreme discharge events and storm surges**

   (a) Extreme river discharges cause erosion or counteract deposition in the Lower Delta channel network compared to regular discharge conditions, due to increased flow velocities and sediment transport capacity.

   (b) The sediment-depleted return flow after a flood instigated by a storm surge can pick up sediment from the channel beds, leading to a net erosive effect of the storm surge event and the flood.

3. **Riparian vegetation**

   The abundance of riparian vegetation in the Lower Delta Channel network facilitates local patterns of sediment deposition

4. **Historic and future changes in sediment input and river discharge**

   (a) The combination of an overall increased river discharge, manifesting mainly in increased discharge peaks, and increased sediment load from the Bermejo region between 1960 and 2000 caused by increased precipitation patterns and land use change have had a positive effect on the annually averaged sediment concentrations entering the delta, which subsequently lead to increased sedimentation rates in the Lower Delta channel network.

   (b) The projected increase in discharge peaks in the 21st century will counteract depositional patterns in the Lower Delta, essentially 'flushing' the channel system.

   (c) When considering the possibility of higher sediment loads during the discharge peak, the overall sediment concentrations in the Lower Delta will increase, leading to an increase of net sedimentation rates in the Lower Delta channel network.

5. **Dredging activities and channel excavation**

   (a) Deepening the main channel of a river can enhance tidal amplification or change the celerity of the tidal wave, altering the hydraulic conditions at the boundaries of a channel and changing the location of tidal divides.

   (b) Deepening a river branch will attract flow, leading to a repulsion of flow in nearby channels, lowering the sediment transport capacity in these channels and thus inducing channel accretion.

   (c) The excavation of artificial channels has decreased the river discharge through the existing, natural channels, and the subsequent reduction in sediment transport capacity has had positive effect on deposition in the channel network.

   (d) Deposition of dredged material nearby a channel entrance can lead to unwanted sediment supply into the channel network.

4

Numerical Experiments - Model Setup

4.1. Modelling approach

In order to test the hypotheses presented in the previous chapters, a 2DH Delft3D Flexible Mesh hydrodynamic model was constructed. As will become clear further in this section, a partly schematized approach to the model set-up was chosen in order to allow for the distinct identification of the physical processes related to testing the different hypotheses, under the circumstance of unavailability of validation data for morphological changes in the channel network. The schematic nature of the model also allowed for the exclusion or simplification of locations that are outside the area of interest, reducing the computational time. Two base scenarios (further elaborated upon in Section 4.4) including typical regular, non-ENSO and extreme, ENSO-associated forcing conditions were constructed and validated with in-field data as far as the data availability allowed for.

Step by step, model scenarios are constructed by altering the base scenario's input parameters and data step by step. Each of the model scenarios is made in order to test the validity of the hypotheses formulated in Chapters 2 and 3. Chapter 5 describes the model scenarios, the alterations to the base scenarios and the relation to the formulated hypotheses.

As the purpose of the model is not to as accurately as possible simulate deposition volumes, but rather to explore the (relative) influence of different physical processes, the various model runs with alterations to the base scenario will hereafter be referred to as *numerical experiments*. To explore the influence of uncertainties around input parameters, various sensitivity runs were carried out (see Section 4.7).

4.1.1. Physical processes included

The physical processes included in the numerical experiments are based on the expected relevant physical processes as described in the previous chapters. In order to test the hypotheses as defined in Chapter 2 and 3 and listed in the last section of Chapter 3, the following processes must be included:

- **River discharge** is included as it is an important forcer for the dynamics of any estuarine system;
- **Tidal motion** in the form of an harmonic downstream water level boundary condition was included as the morphodynamics of the downstream located river reaches, and in particular the secondary channel network, are expected to be influenced by tidal currents;
- **(Cohesive) sediment transport and morphological updating** is included. Processes related to Hypotheses 1, 2 and 5 could in principle be tested by assessing the change in sediment transport capacity (bed shear stress) only, but the past and projected changes in sediment supply associated with Hypotheses 4a, 4b and 4c require a full morphological model. Theoretical concepts for fine and cohesive sediment fractions have been used as it is evident that clay and silt particles play a dominant role in the sediment dynamics in the deltaic channel network;
- Tidal import is included by explicitly defining sediment concentrations in the downstream boundary conditions (Dirichlet boundary condition);

- Return in the channel network flow associated with flooding of the flood plains is schematized by means of the lateral discharge functionality in the software (Scenario A3).

4.2. Choice for the modelling software

Delft3D Flexible Mesh Suite (D3D FM) is hydrodynamic modelling software developed by Deltares. D3D FM is the successor of the Delft 3D 4 Suite (D3D), which is widely used for hydrodynamic simulation of environmental flows for a wide range of civil and environmental engineering applications. Delft3D can simulate 1D, 2D or 3D hydrodynamics and has various additional modules or applications for the simulation of (cohesive) sediment transport, water quality, wind waves and ecology. The most pronounced difference between D3D and D3D FM is that the latter includes the generation of non-structured grids, resulting in more freedom and possibilities in the representation of complex geometries such as estuarine coastlines and sharp corners in channel bifurcations [Deltares, 2022]. The following considerations were made regarding the choice of using D3DFM as the modelling software for the numerical experiments.

- D3D FM is directly available for MSc students at Delft University, and proper training is available for easy and straighforward usage.
- The application of unstructured grids is explicitly well applicable to the many sharp-angled bifurcations and confluences present in the Lower Delta channel network.
- A D3D FM model made by INA in collaboration with Deltares [Sabarots Gerbec and Pablo E. Garcia, 2018] was available to use as a starting point.
- The advanced options on cohesive sediment modelling of the D-Morphology are specifically well applicable to the silt dominated channel network.
- The option to spatially define hydraulic and sediment parameters allows for characterization of the two distinct systems; the channel network and the main river branches

4.3. Model domain

4.3.1. Area of interest

As the area of interest of this research is the Lower Delta channel network, and in particular the channels located around the Paraná de las Palmas, these are the channels included in the numerical experiments. The channels with the smallest dimensions in the area of interest are not included, as i) their applicability for navigation is limited and ii) the importance of the channels in the overall distribution of water and sediment in the channel network is expected to be small. Figure 4.1 displays exactly which channels are in- and excluded in the model domain.

The (main) river branches that are included in the domain are the Paraná de las Palmas and the Paraná Mini (tributary of the Guazú branch). Two additional minor natural streams, Río Luján and Canal Carabelas Grandes also supply discharge to the computational domain. It is assumed that these four river branches/channels supply the entire river discharge to the channel network included in the computation. In reality, there will undoubtedly be an exchange of river and tidal discharge through other channel connections. It is however expected that the dynamics of the system will be sufficiently captured when including the Paraná Mini and the Paraná de las Palmas as the main suppliers of river discharge and sediment. The boundary conditions associated with this input are described in Section 4.4.

4.3.2. Computational grid

An existing computational Delft3D Flexible Mesh irregular grid made by INA [Sabarots Gerbec and Pablo E. Garcia, 2018] was used as a starting point. The existing grid covered roughly half of the Paraná Delta, including the floodplains. The existing grid was clipped around the project area, and the resolution was increased. The channels connected to the main river branches are mostly one computational cell wide, effectively leading to a 1D channel network connected to the 2DH main river branches. The width and orientation of individual channels are mostly based on real characteristics,

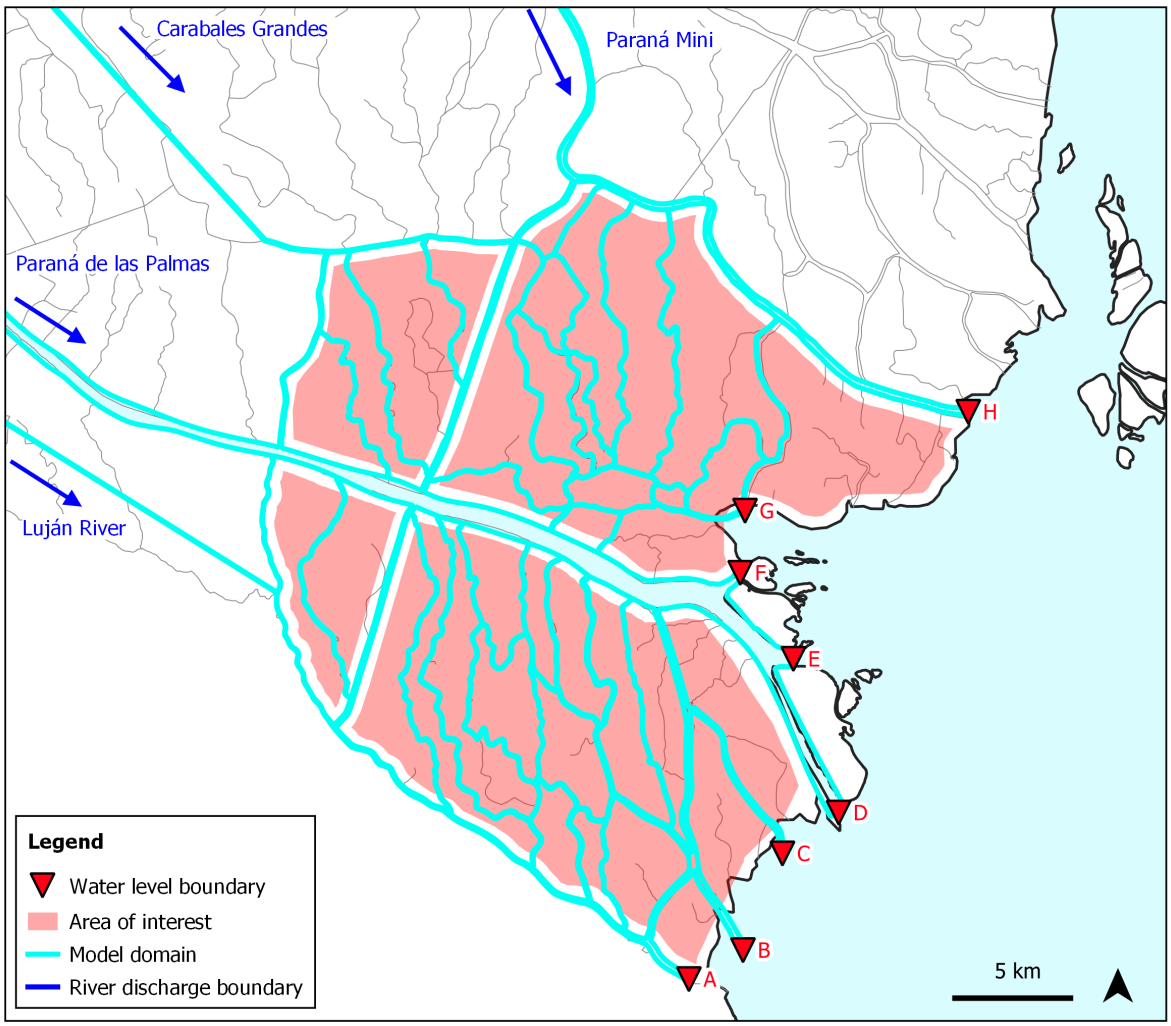

Figure 4.1: Model domain

however sharp angles in channel orientation are often simplified or cut off in order to more easily comply with grid orthogonality and smoothness restrictions. Upstream reaches of the river branches are schematized as (near) one-dimensional, straight reaches. These reaches are made sufficiently long in order to prevent reflection of of the tidal wave into the area of interest.

The grid was constructed with the smoothness and orthogonality limitations in mind, as described in the D-Flow FM manual. Grid orthogonality within the area of interest subceeds the prescribed value of 0.08 at all cells. The prescribed maximum value of smoothness (1.1) was harder to obtain at all cell borders due to the irregular angles and varying channel dimensions, both within one reach and at channel connections. However, the cases of exceedence of the smoothness parameter within the area of interest are rare and small in magnitude. Extreme deviations from the prescribed value are only present outside the area of interest, i.e. in the main river branches. Regarding the schematic nature of modelling practices in this research, it is not expected that numerical errors caused by smoothness exceedences will influence the outcome of this research significantly.

The total number of grid cells, including the upstream schematization of the main river branches, is approximately 27500, with typical grid dimensions varying from 20 to 100 meters. Figure 4.1 displays the entire grid domain (excluding the upstream schematized parts) and an example of the connection between the Paraná de las Palmas and a channel. Figure 4.2 gives an impression of the grid inside the modelling software, including some of the Las Palmas - channel network connections.

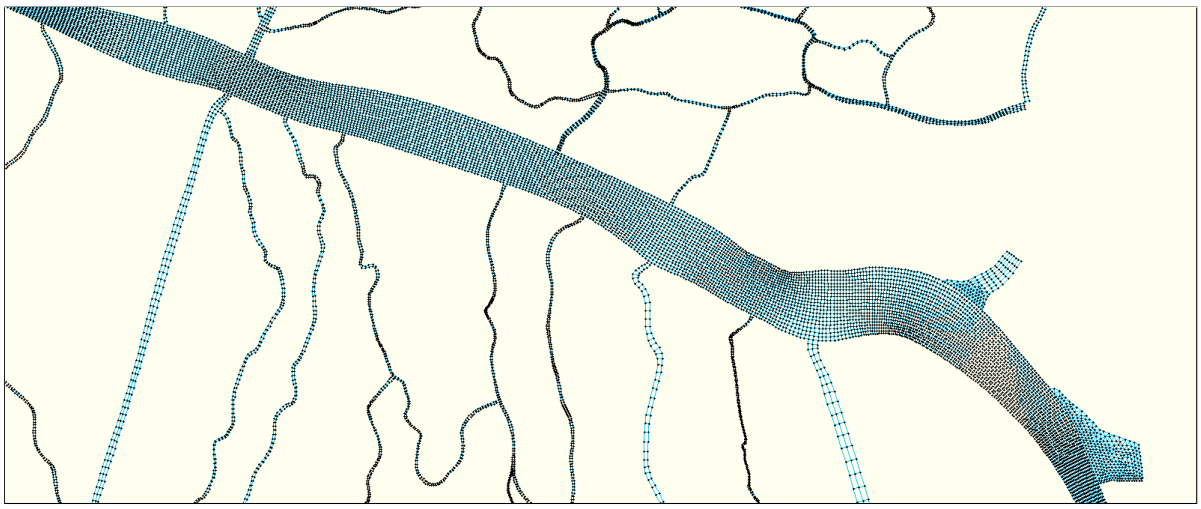

Figure 4.2: Snapshot of the grid

4.3.3. Topography input

Topography input for the model was based on the most recent data available, the collection and processing of which is thoroughly described in Appendices I (field surveys) and D (analysis bathymetrical data) and briefly described in the following points:

- Topography of the Paraná de las Palmas and the Paraná Mini was taken from the Digital Elevation Model prepared by INA, consisting of various data of different sources collected over different time periods between 2010 and 2020.
- Bathymetries of the Río Luján and Canal Gobernador Arias were based on a 2019 survey by INA.
- The upstream, one-dimensional schematizations of the Paraná de las Palmas, the Paraná Mini, Río Luján and Canal Carabelas Grandes are modelled with constant bed slopes, roughly based on the realistic upstream bed slopes of (see Appendix D). This resulted in a bed slope of 10^{-5} for the Paraná de las Palmas and Carabelas Grandes, $1.5 \cdot 10^{-5}$ for the Paraná Mini and 10^{-4} for Río Lujan.
- Bathymetry data of the channel network were collected during the December 2021 and March 2022 field surveys using an Echo Sounder device. A small number of channels were not measured due to time constraints. The depth of these channels were estimated based on nearby channels with the same dimensions.

4.4. Boundary conditions

Two model base scenarios were constructed with different time frames and boundary conditions, based on regular, non-ENSO conditions (base scenario A) and high-discharge, ENSO associated conditions (base scenario B). Both base scenarios have a running time of 6 months, which is enough time to obtain the initial morphological response to the conditions enforced on the model.

4.4.1. Discharge boundary conditions

Discharge boundary conditions of the Paraná de las Palmas and the Paraná Mini are based on the time series of the total discharge of the Paraná River at Timbués. The Paraná de las Palmas discharge was determined with the linear relationship between the discharge distribution as determined by Re et al. [2009], which was introduced in Chapter 2, and repeated in Table 4.1 for convenience (adjusted to equate Q_{Palmas}). The Paraná Mini was assumed to convey 2.5 % of the Paraná River discharge at Timbúes, as measured by [Sarubbi and Menendez, 2007] (see Chapter 2). Discharges of the Luján River and the Caraboles Grandes stream were set to 10 and 150 m^3/s respectively. These are based on estimates of the magnitude of the river discharge extracted from recent one-dimensional modelling

practices at INA [Personal contact with S. Guizzardi]. All discharge boundaries are displayed in Table 4.1.

Table 4.1: Discharge boundary conditions as a function of the total Paraná River discharge (Q_T)

Boundary	Discharge [m^3/s]	Source
Paraná de las Palmas	$Q_{Palmas} = Q_T(0.33 - 33 \cdot 10^{-7} \cdot Q_T)$	Re et al. [2009]
Paraná Mini	$Q_{ParanMini} = 0.025 \cdot Q_T$	[Sarubbi and Menendez, 2007]
Caraboles Grandes	150	INA
Río Luján	10	INA

4.4.2. Water level boundary conditions

Downstream water level boundary conditions are the astronomic constituents based on the harmonic analysis by Santamaria-Aguilar et al. [2017]. Direct measured time series were not used as a boundary condition for the following reason:
A specific procedure including the use the lateral discharge functionality is used to mimic the effect of flooding and return flow in the channel network in Scenario A3. As (mild) flooding occurs multiple times per year, the sources and sinks approach would have to be included in the base scenarios. By keeping the downstream water levels below flood levels in the base scenarios and adding a storm surge in Scenario A3, the relative effect of the storm surge and subsequent flooding can be isolated in a separate scenario run and therefore easily identified.
The A0 harmonic component (mean water level) is based on the weekly running average of timeseries at San Fernando. This way the daily variation associated with the tide is filtered out, while the variation associated with the spring-tidal cycle and the relation between high discharge and water level increases to some extent included. Figure 4.4 display the computed time series of the A0 component.

By visual comparison of measured water level time series and the harmonic components by Santamaria-Aguilar et al. [2017], it can be observed that the asymmetry in the measured signal is not fully captured my the artificial M4 component. In order to better mimic the asymmetry, the amplitude of the M4 component was increased from 0.03 to 0.07 m. The new signal has a better resemblance with the flood-dominant tidal signal at San Fernando, as can be seen in Figure 4.3.

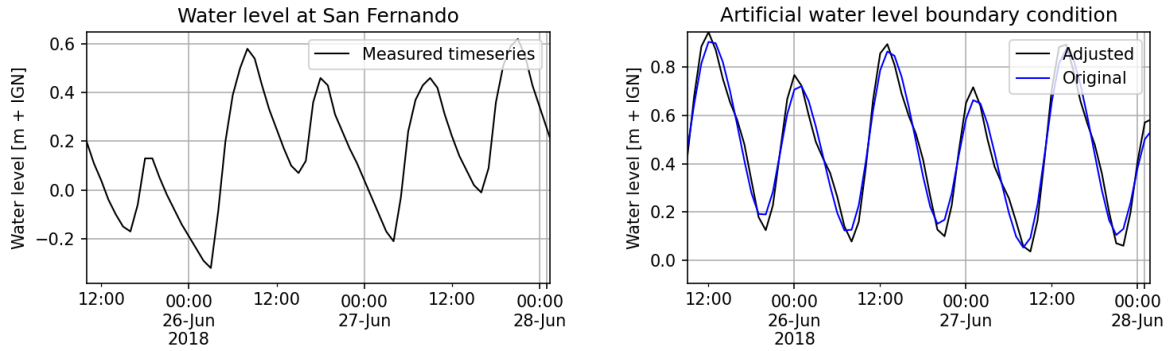

Figure 4.3: Comparison between the asymmetry of measured water level timeseries (left) and original and adjusted harmonic components

A northward-upward sloping water level was applied to the reference water level at San Fernando, as demonstrated in Sabarots Gerbec and Pablo E. Garcia [2018] and as advised by INA. Not much data is available on the instantaneous water level slope along the deltaic front, it is however known that there is a slight slope in water level due to the outflow of the Uruguay River in the north. The water level boundaries of outflow locations A to H (as displayed in Figure 4.1) are given in Table 4.2.

Table 4.2: Water level boundary conditions (**1*: Harmonic analysis by Santamaria-Aguilar et al. [2017])

	Outflow location	A_0	M_2 S_2 O_1 K_1	M_4
A	Río Luján - San Fernando	Monthly-averaged time series	**1*	Adjusted from **1*
B	Arroyo San Martin	”	”	”
C	Canal Del Este	”	”	”
D	Canal Emilio Mitre	”	”	”
E	Paraná de las Palmas 1	” + 0.06 m	”	”
F	Paraná de las Palmas 2	” + 0.09 m	”	”
G	Arroyo Chania	” + 0.06 m	”	”
H	Paraná Mini	” + 0.09 m	”	”

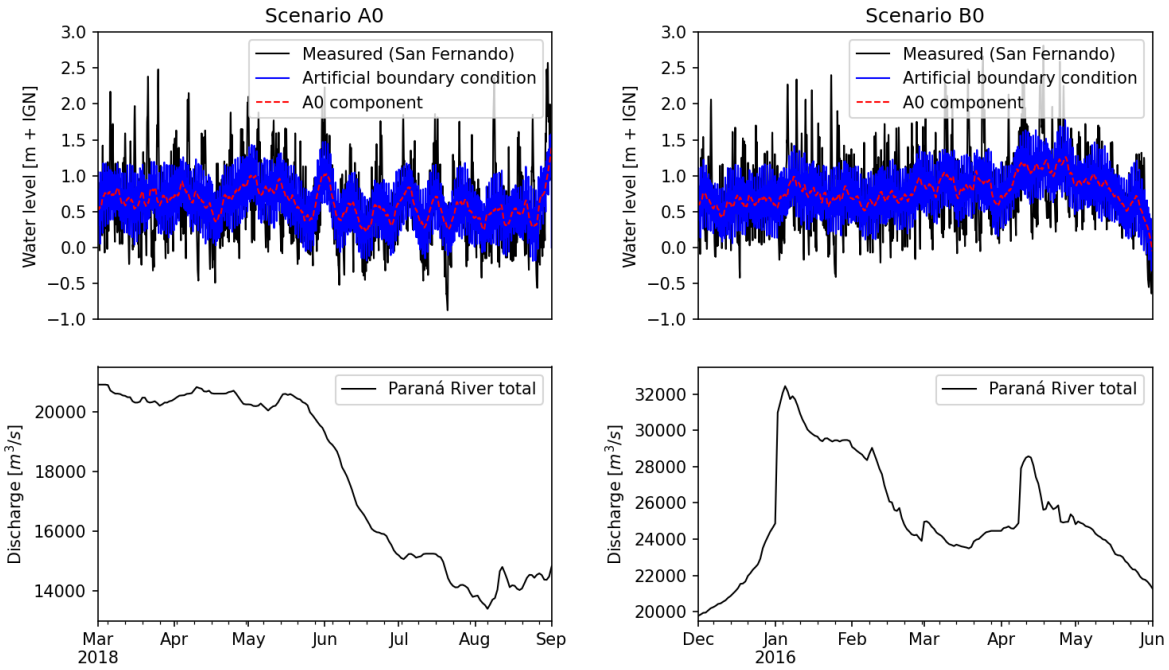

Figure 4.4: Discharge at Timbúes and measured and computed downstream water level at San Fernando

4.4.3. Sediment concentration boundary conditions

At an open or incoming boundary, conditions should be applied regarding the sediment concentrations. It is possible to explicitly assign a sediment concentration value or time series at a river inflow (Dirichlet) or a zero-gradient Neumann condition at an outflow. A Dirichlet condition may be combined with a Thatcher-Harleman return time, which may be applied to approximate the re-entry of material that was transported out of the model after the flow reverses direction by gradually changing from the concentration during outflow to the prescribed boundary condition during inflow. In the base scenarios, Neumann boundary conditions are imposed on the downstream boundaries and Dirichlet conditions in the upstream boundary. The sediment concentrations imposed on the upper boundaries are based on the van Rijn [2017] measurements (Table 4.4) which are in accordance with approximations of yearly-averaged sediment concentrations on mass balances determined by Amsler et al. [2007]. In the model scenario designed to assess the occurrence of tidal import, homogeneous Dirichlet boundary conditions are imposed on the downstream boundaries with a Thatcher-Harleman return time of one hour.

4.5. Model calibration and validation

Calibration and validation of the model results was done in several phases. Table 4.3 displays the steps, including the calibration parameter, the data used for calibration and the result of the calibration

phase. In the subsequent paragraph, a detailed account of the calibration/validation procedure and the results is given below.

Table 4.3: Model calibration and validation phases (B.C. = Boundary Condition)

	Calibration parameter	Validation data	Result
1a	n (Manning coefficient)	Water level measurement stations	n selection
1b	n	HEC-RAS 1D model results	n validation
1c	n	Discharge measurements [Morale et al., 2018]	n validation
2	Downstream B.C.	March 2022 discharge measurements	B.C. adjustment

1. Calibration of Manning coefficient
Calibration of the Manning coefficient n was primarily done by comparing measured water levels with observed water levels at various stations in the modelled domain. The Manning formulation is a well-known and often used concept in hydrodynamic modelling of environmental flows, and it has been used as well in reference modelling practices by Happee [2019] and Sabarots Gerbec and Pablo E. Garcia [2018]. Two distinct values for the Manning coefficient n were used, one for the main river branches and one for the channel network, as factors such as differences in water depth, bed soil composition and the presence of vegetation can influence hydraulic friction. The spatial variation in roughness coefficient is displayed in Figure 4.5. The calibration period was chosen to be 1 March - 31 August 2019. The following was considered in the selection of the calibration period:

- Hourly water level data was available at Arroyo Carapachay, Canal Seoane and Paraná Mini and daily data at Dique Luján. The hourly data is of importance as the tidal variation is included. The significance of measurements stations Arroyo Carapachay and Canal Seoane is emphasised because theses are located inside the channel network and thus inside the area of interest.
- The calibration period lies only a few years in the past, which could imply at least a significant resemblance in channel bed bathymetry at the time and bed levels measured during the 2021 and 2022 field surveys which were used as topography input.

Note that the calibration period is not the same as either base scenario periods. This is due to the fact that the calibration period was chosen based on the availability and quality of validation data and the scenario periods were based on the quality of boundary condition data.

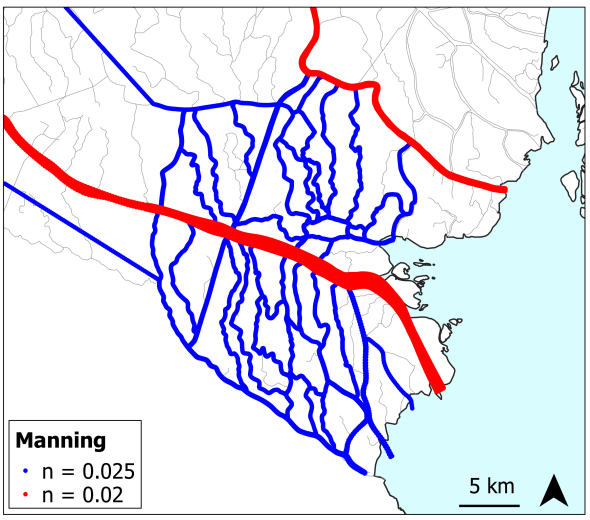

Figure 4.5: Spatial variation Manning coefficient

Discharge time series used to force the model for validation (Paraná de las Palmas, Paraná Mini) are displayed in Figure 4.6. More on the generation of these discharge time series can be found in Appendix F. For the Río Luján and Caraboles Grandes boundaries, constant discharges of 10 and 150

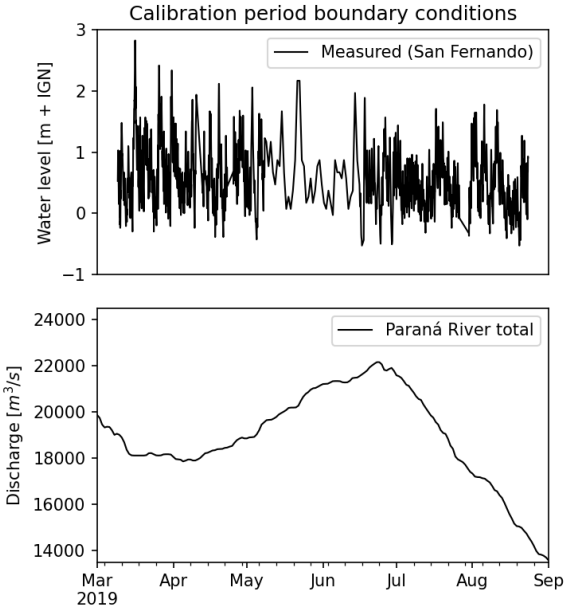

Figure 4.6: Calibration period boundary conditions

m ^{3}/s were assumed, as mentioned in Section 4.4. Downstream boundary conditions are measured hourly water level time series at San Fernando, including the northward water level slope mentioned in Section 4.4 and Table 4.2.

In the first run, a spatially uniform Manning coefficient of 0.02 was applied for both the channels and the river branches. This initial value was based on based on previous modelling practices by Happee [2019] and typical values for muddy beds [van Maren et al., 2015a]. Based on the results, (spatially) varying values were applied in subsequent runs. The complete results of the calibration runs are included in Appendix J. The selected values of the manning coefficient are 0.020 for the main river branches and 0.025 for the channel network. The spatial variation is displayed in Figure 4.6.

After selection of the most appropriate value for the Manning coefficient based on water level comparisons, two additional checks were carried out concerning the validity of the selected values for n:

- Artificial water level data in the Paraná de las Palmas, Río Luján and Paraná Mini was extracted from an existing and validated HEC-RAS model used by INA and compared to the model output. The modelled water level in the Paraná de las Palmas displays a slight underestimation during high discharge (first half of the base scenario A0 run) and a slight underestimation in the Paraná Mini during low discharge (second half of the A0 run).
- ADCP velocitiy measurements from Morale et al. [2018] were compared with modelled flow velocities, and for the selected Manning values found to be in reasonable accordance.

The results of the two additional validation procedures are included in Appendix J.

2. Calibration of downstream boundary condition
An second calibration process was included in order to simulate flow velocities as accurate as possible. First, measured flow velocities and discharges in the northern entrance of Arroyo Carapachay on 25 March 2022 were compared to the output of a model run with March 2022 discharge and water level forcing. This procedure lead to the inclusion of downstream boundary locations G and F (Figure 4.1, resulting in a better than previous similarity of the tidal velocity magnitude in the channel entrance. The results are included in Appendix J.

4.6. Model settings and parameters

4.6.1. Horizontal eddy viscosity and diffusivity

The horizontal eddy viscosity is a parametrization of processes that occur in the sub-grid scale. It is therefore dependent on both the spatial resolution of the grid and the magnitude of the velocities of the domain. In reality, velocities vary in temporal and spatial dimensions, and the grid resolution is not constant over the domain. Therefore a high number of varying values for turbulent viscosity would be most appropriate. As this is not feasible for the numerical experiments within this research, a spatially uniform value for the eddy viscosity was chosen based on the Smagorinsky model [Smagorinsky, 1963] and a sensitivity analysis was carried out in order to address the effect of a varying turbulent viscosity value.

The horizontal eddy viscosity will not have a direct influence on the computations in the channel network, as these are modelled in one dimension only. Therefore the scale analysis of the Smagorinsky model is based on flow characteristics in the Paraná de las Palmas as the main river branch is modelled in 2DH. As flow velocities in the Las Palmas during regular conditions are in the order of 0.5 to 1 m/s, a characteristic value of 0.75 m/s is chosen. Grid sizes are in the order of 40 m. The D3D FM default value for C_s was used. The eddy viscosity is calculated in Equation (4.1).

$$v_t = (C_s \Delta x)^2 \sqrt{\frac{\partial u}{\partial x}} = (0.2 \cdot 40)^2 \sqrt{\frac{0.75}{40}} = 8.8 \frac{m^2}{s} \tag{4.1}$$

The horizontal eddy diffusivity was chosen to be equal the value of the horizontal eddy viscosity.

4.6.2. Sediment parameters

Erosion and deposition of fine, potentially cohesive material is included in D3D-FM by the well-known Partheniades-Krone formulations. The flux of cohesive sediment between the water and the bed are computed per sediment fraction as presented in Equation (4.2).

$$\begin{aligned} E &= M \max\left(0, \frac{\tau_{cw}}{\tau_{cr,e}} - 1\right)^n \\ D &= w_s c_b \Gamma \end{aligned} \tag{4.2}$$

With E and D erosion and deposition fluxes in kg m^{-2} s^{-1}, M the user defined erosion parameter, τ_{cw} the occurring bed shear stress due to currents and waves, $\tau_{cr,e}$ the user-defined critical shear stress for erosion, n the user-defined power for erosion, fall velocity w_s, c_b the sediment concentration, Γ the dimensionless reduction factor for deposition which reduces to zero if the occurring bed shear stress exceeds the user-defined critical stress for deposition $\tau_{cr,d}$ or to a user-defined dimensionless deposition efficiency parameter.

For morphological developments it is relevant to compute both the (time-varying) magnitude of sediment concentrations, as well as the spatial gradients in sediment loads. Data on morphological changes in the research area are insufficient to calibrate these parameters properly. In that case it is common to base sediment parameters on expert judgement and analogy with similar situations and areas. The consequences of uncertainty in specific assumptions are further explored by means of sensitivity analyses (Section 4.7).

The characterization of sediment fractions and concentrations in the Paraná de las Palmas by van Rijn [2017] were used as a starting point. More recently obtained data on suspended sediment concentrations during the field surveys (Appendix B) were not regarded to be representative for the sediment load during regular conditions, as during the time of sampling, the river discharge had been historically low for about two years, therefore sediment supply to the delta was expected to have been limited during this period. The van Rijn measurements however were executed during normal conditions, making it a better option to use for the base scenarios. The data by van Rijn includes one sandy, one silty and one clayey cohesive sediment fraction. Only the suspended sediment present in the top of the water column was included in the model. As only this sediment could enter the channel network, bed load transport was completely disregarded, and the sediment fractions included in the model were based on the van Rijn [2017] characterization of sediment that is present in the top 5 meters in the Paraná

de las Palmas water column. Due to the depth-averaged nature of the model, inclusion of the sandy suspended sediment fraction could lead to unrealistically high amounts of this sediment to enter the channel network. To avoid unwanted erosion in the main river branches caused by the exclusion of coarse fractions, a non-erodible layer was applied in the main river branches, as defined in Figure 4.7. The sediment fractions included in the model are are depicted in Table 4.4.

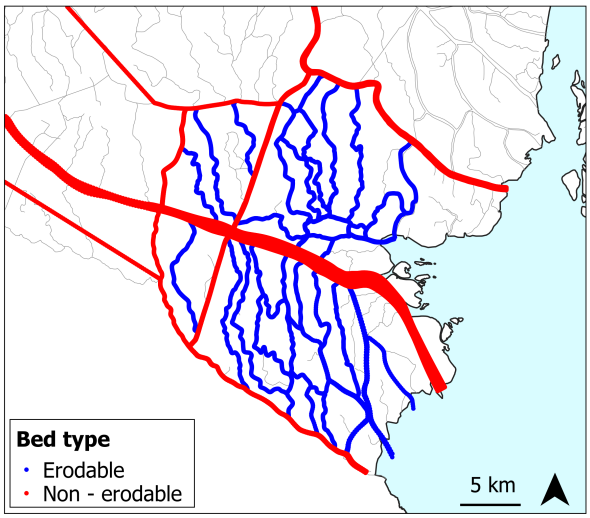

Figure 4.7: Spatial variation erodibility bed

The concentrations presented in Table 4.4 are imposed on all upstream boundaries. The same concentrations are imposed on the entire model domain as initial conditions. In order to prevent non-physically rapid morphological changes right after the stationary initial conditions, morphological updating is activated after 7 days. This way the effect of the stationary initial flow conditions does not effect the computed bed levels.

The selection of the user-defined critical bed shear stress for erosion $\tau_{cr,e}$ and the erosion parameter M is normally based on experimental data or a calibration procedure. The most appropriate values for these parameters are often variable in space and time and can depend on bed characteristics, which may concern electrochemical forcing, organic matter content, pore water characteristics and consolidation state Mengual et al. [2017]. As there is no calibration or experimental data available, the values for these parameters are estimated based on previous modelling practices and literature.

As mentioned in Chapter 2, bed soil samples in the channel network consist of a sand-mud mixture, with silt, clay and sand percentages in the order of 50, 30 and 20 %, respectively. Such a bed composition can be characterised as a light sandy mud bed. The literature on the critical bed shear stresses makes a distinction between pure mud beds and sand-mud mixtures, the latter of which is applicable to this research. Generally, pure mud beds are less resistant to erosion than mud-sand mixtures. High (> 20%) mud percentages can cause increased resistance against erosion due to the cohesive properties, and in addition the presence of sand can improve the drainage, leading to more compaction [van Rijn, 2020].

van Rijn [2020] presents a literature review of experimental data on the critical bed shear stress of mud-sand mixtures. Roughly, critical bed shear stresses for particle and surface erosion of weakly consolidated, light sandy mud beds are in the order of 0.1 to 0.3 Pa. A tentative equation introduced by van Rijn (Equation (4.3)) was used to estimate the the values for $\tau_{cr,e}$ for the silt and clay fractions. By using this equation, slightly higher values for $\tau_{cr,e}$ will be assigned to the fine sediment fractions in the model. This way, the positive effect of sand on $\tau_{cr,e}$ is in some way included, without including the sand fraction in the model itself, for reasons stated before.

Values for $\tau_{cr,0}$ (critical bed shear stress for particle erosion without cohesive effects), were taken from Happee [2019] (0.05 and 0.10 Pa for clay and silt respectively). The fraction of fines p_{fines} is 0.8, and the dry bulk density of the mud $\rho_{dry,fines}$ was assumed to be 300 kg/m^2, indicating a weakly

consolidated bed. Furthermore, $\rho_{dry,sand}$ is 1600 kg/m^2 and the empirical coefficient α equals 2. The outcome of applying the equation to the silt and clay fractions is a value for $\tau_{cr,e}$ of 0.15 and 0.20 Pa for the clay and silt fraction, respectively. These values will be used as the default values for the model runs.

$$\begin{aligned} \tau_{cr,e} &= (1 + p_{fines})^{\beta} \tau_{cr,0} \\ \mathrm{B} &= (1 + \rho_{dry,mixture}/\rho_{dry,max})^{\alpha} \\ \rho_{dry,mixture} &= (1 - p_{fines})\rho_{dry,sand} + p_{fines}\rho_{dry,fines} \end{aligned} \tag{4.3}$$

Typical values of the erosion parameter M in the Partheniades-Krone formulations are generally in the order of 10 e^{-6} to 50 e^{-5} kg m^{-2} s^{-1}. Again, values are dependent on local bed conditions such as consolidation state and the presence of biota [Winterwerp et al., 2012]. Values for M used in the model runes are are 6 e^{-5} and 8 e^{-5} for clay and silt, respectively, which are taken from Happee [2019], who calibrated the parameter for (fine) sediment deposited in Canal Emilio Mitre in the Río de la Plata. These estuarine deposits are not based on identical physical principles as the deposition in the deltaic channel network, but in the absence of field-specific calibration or experimental data, the values determined by Happee can be regarded as a good approximation.

The sediment thickness in the erodable beds is limited to 1 meter. This is done in order to prevent extreme erosion to take place in some of the more energetic channels in the model domain that might in reality be sand-dominated, which could lead to unrealistic results. The initial sediment composition consists of silt, as the sediment characteristics of this fraction are similar to the characteristics of the analysed bed soil samples (see Appendix B).

Table 4.4: Sediment fractions present in the top 5 meter of the water column as determined by van Rijn [2017], and model parameters $\tau_{cr,e}$ and M

	c [mg/l]	w_s [mm/s]	D_{50} [μm]	$\tau_{cr,e}$ [N/mm^2]	M [kg m^{-2} s^{-1}]
Clay	115	0.005	8	0.15	6 e^{-5}
Silt	100	0.7	30	0.20	8 e^{-5}

4.7. Sensitivity Analysis

The uncertainties that come with the use of a morphological model in the absence of a validation procedure for the morphological changes are assessed with a sensitivity analysis. As stated in the previous sections, various model parameters of the base scenarios were selected based on literature and previous modelling practices, the values chosen are referred to as 'selected'. After running Base Scenario A0 with the selected parameters, minimum and maximum values for the parameters were applied to the model, while keeping the rest of the input identical to the default model run. This has lead to 14 different sensitivity model runs. The parameters included in the sensitivity analysis and the selected, maximum and minimum values are given in Table 4.5.

Table 4.5: Sediment parameters used for the base scenario (selected) and the values used for the sensitivity analysis

	Selected	**Min**	**Max**	
$w_{s,silt}$	0.7	0.4	1	mm/s
$w_{s,clay}$	0.005	0.003	0.007	mm/s
M_{silt}	8e^{-5}	5e^{-5}	11e^{-5}	kg m^{-2} s^{-1}
M_{clay}	6e^{-5}	4e^{-5}	8e^{-5}	kg m^{-2} s^{-1}
$\tau_{cr,silt}$	0.20	0.15	0.25	N/m^2
$\tau_{cr,clay}$	0.15	0.10	0.20	N/m^2
v_t and D_t	8.6	5	10	m^2/s

Tuning the sediment parameters for the clayey fraction did not influence the results significantly. As will become clear in the next chapter, the sediment dynamics in the system is dominated by the silty

fraction. The clayey fraction mostly stays in suspension, varying values for M_{clay}, $\tau_{cr,clay}$ and $w_{s,clay}$ generally do not change the total volume of morphological changes by more than 5 percent.

The eddy viscosity parameter does not have a significant influence either. A high value for v_t causes the water level in the Paraná de las Palmas to increase slightly, leading to a small increase in discharge in channels connected to las Palmas, leading to slightly less deposition in these channels.

The magnitude of the silt parameters are highly influential to the modelled morphological changes. The following bullets summarize the influence of each of the Parameters.

- Increasing M_{silt} leads to significant increases in erosion. This effect is mostly concentrated in the channels located near the deltaic front. These channels in general are more energetic than upstream located channels. The more frequent exceedance of the critical bed shear stress leads to a more influential effect of the erosion parameter M_{silt}. Decreasing the parameter value has the opposite effect.
- Increasing and decreasing the settling velocity $w_{s,silt}$ generally leads to net deposition and erosion, respectively. A lower value leads to depositional features in channel entrances to be spread out, and contain less volume in total. The effect again is largest in the downstream located channels.
- The general effect of increasing the critical shear stress $\tau_{cr,silt}$ leads to less erosion in the model domain, with the downstream channels being affected most. In one of the most upstream and northern located channel divisions, increasing $\tau_{cr,silt}$ leads to opposite results than expected. This is because one of the channels becomes more accessible for flow as the other channel is starting to close off due to the increased $\tau_{cr,silt}$. This eventually leads to higher flow velocities in the accessible channel, leading to increased erosion. This demonstrates that sediment parameters do not only have large effect on the deposited and eroded volumes but also on the configuration of the channels.

5

Numerical Experiments - Model Scenarios and Results

The hypotheses listed at the end of Chapter 3 are tested by running a number of model scenarios. The purpose of these simulations is to identify the influence of various physical processes and anthropogenic activities on the morphodynamic behaviour. Table 5.1 lists the model scenarios, the relevant hypothesis per scenario and the alterations made to the base scenarios associated with every scenario run.

Table 5.1: Scenarios overview (Q is discharge, SSC is suspended sediment concentration, B.C. is boundary condition, z_b is bed level)

nr.	Description	Hypothesis	Alteration to base scenario
A0	Base scenario A: regular conditions	-	-
A1	No sediment import from Río de la Plata	1b	Downstream SSC Dirichlet B.C.
A2	No tidal motion	1abc	No tidal motion
A3	Storm surge	2c	Storm surge + lateral discharge
A4	No dredging	5ab	Paraná de las Palmas bed increase
A5	No newly excavated canals	5c	Art. channels z_b = 2 m +IGN
B0	Base scenario B: high discharge	2a	-
B1	Undo past catchment changes I	4a	reduce SSC B.C.
B2	Undo past catchment changes II	4a	” + reduce Q B.C.
B3	Future climate variability I	4bc	increase Q B.C.
B4	Future climate variability II	4bc	increase Q and SSC B.C.

The following must be noted regarding the description of the model results in this chapter:

- Although the model results are quantitative, the assessment of results is mostly qualitative. Absolute modelled quantities of sedimentation/erosion are irrelevant as the sediment parameters were not calibrated against measured bed level changes due to unavailability of validation data.
- The modelled morphodynamic behaviour of the non-base scenarios will be mostly described as relative to the base scenarios. In every model scenario, a figure displaying the relative bed level changes compared to the base scenario is displayed. Appendix K contains more complete, location specific model results.
- The assessment of the model results in this chapter are structured based on the relevant physical processes that are associated with the scenario runs, in stead of discussing every scenario run separately. This is done in order to avoid repetition and to briefly and effectively describe the principal results. In the beginning of each chapter, the relevant hypotheses and model scenarios are repeated and a brief description of the model scenario setup is given. The following structure is used in this chapter:

  - Section 5.2 - Influence of fluvial processes
  - Section 5.3 - Tidal influence
  - Section 5.4 - Influence of varying river discharge
  - Section 5.5 - Influence of varying sediment load
  - Section 5.6 - Influence of topography changes based on dredging/excavation
  - Section 5.7 - Influence of a storm surge event

- In Section 5.1, the hypotheses that are not tested with the numerical model are repeated, and the reasons for disregarding the hypotheses given.

In Appendix K, the spatial characterization of the model result is done by dividing the model domain in sub-domains. For descriptive purposes, these spatial characterizations will not be used in this chapter. In this chapter, simply the terms 'upstream' and 'downstream' will be used to characterize channels by their distance from the deltaic front. In addition, difference between channels 'north' and 'south' of the Paraná de las Palmas are mentioned. This characterization often used in this chapter is depicted in Figure 5.1. Whenever specific channels are mentioned, the locations will be specified in a separate figure.

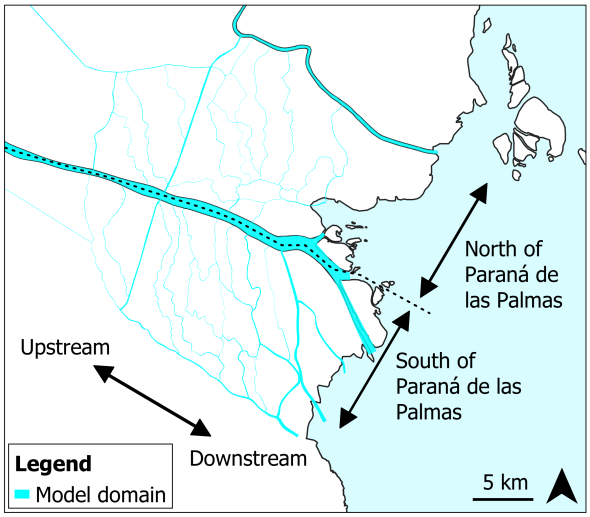

Figure 5.1: Spatial characterization terminology used in Chapter 5

5.1. Disregarded hypotheses

Hypotheses 3 and 5d as defined in Chapter 3 are repeated in the grey frames. These hypotheses are not tested with the model, the reasons for which are given below.

3. **Riparian vegetation** ***Hypothesis***

   The abundance of riparian vegetation in the Lower Delta Channel network facilitates local patterns of sediment deposition

The presence of reed along the Lower Delta channel banks is widespread but also differs highly per channel (section). Assessing the effect of the localized presence of vegetation on the hydraulic conditions requires a close assessment of the exact locations and more detailed information on the vegetation. Such specific data is not available, which makes incorporating the effect of vegetation in a 2DH hydrodynamic model (increased friction) a rather arbitrary practice.

5. **Dredging activities and channel excavation** ***Hypothesis***

   (d) Deposition of dredged material nearby a channel entrance can lead to unwanted sediment supply into the channel network.

Potential transport of disposed dredged material is highly dependent on the local hydrodynamic conditions at the location. The scale of the process is too small to include in the 2DH model, and field-specific data is needed to make an assessment on the occurrence and effects of a dredging plume.

5.2. Influence of fluvial processes

Hypothesis 1a, repeated below, considers the influence of fluvial processes.

1. **Tidal and fluvial processes** ***Hypothesis***

   (a) Channel sedimentation is mainly caused by the supply and deposition of fluvial sediment

   Three fluvial processes are expected to play a significant role in the morphological development of the channel network:

   - Flow of the Paraná de las Palmas decelerates in the downstream end due to the presence of a M1 backwater curve during regular conditions, leading to widespread sedimentation near the deltaic front;
   - Sediment carried by the Paraná River is directly deposited due to decelerations in flow velocity when entering the secondary channel network;
   - Sediment carried towards the deltaic front experiences decelerations due to widening of the channel, leading to the formation of mouth bar deposits in the downstream reaches of (terminal) channels.

The results of model scenarios A0 (base scenario regular conditions) and A2 (no tidal motion) are used in order to analyze and isolate the effect of the fluvial processes listed above. Figure 5.6 displays the downstream boundary conditions of the A0 and A2 model scenario runs. Description of the model results in this section are given in in subsections 5.2.1, 5.2.2 and 5.2.3, following the order of the bullets as given in the hypothesis 1a frame.

5.2.1. M1 backwater curve

The effect of the backwater curve present in the Delta on the channel morphology can not fully be captured with the numerical model. This is due to the large scale nature of the backwater phenomenon, and the dynamics of the channel network are influenced by small scale processes (as will become clear in later sections). However, the presence of a M1 backwater curve is produced in the model; the water level gradient of the Paraná de las Palmas decreases as the river approaches the downstream boundary (see Figure 5.2. This implies that it is at least likely that there is some influence of the backwater curve on the nearshore flow decelerations and the occurrence of sedimentation.

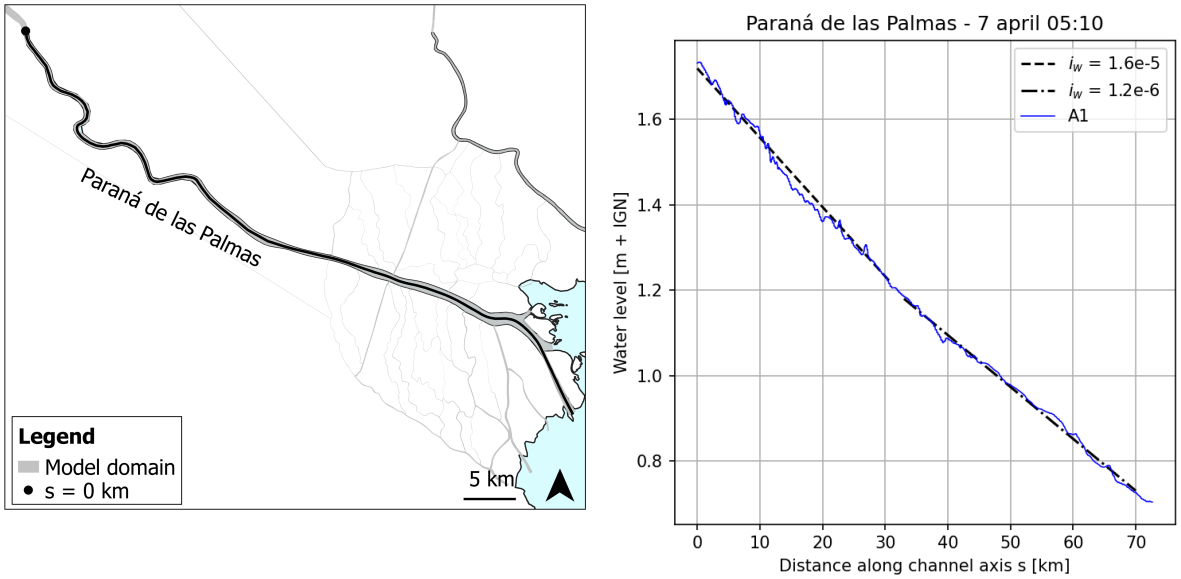

Figure 5.2: Water level in the Paraná de las Palmas, scenario A2 (no tidal motion)

5.2.2. Deceleration in channel entrances

High rates of sedimentation occur in the various inflow locations of the channel network connected to the Paraná de las Palmas. This occurs both in scenario A0 (base scenario) and to a similar extent in A2 (no tidal motion). Due to the high flow velocities in the Las Palmas (0.5 - 1 m/s), the sediment concentrations entering the channel network exceed the equilibrium concentrations in the smaller, low energy channels. A good example of this observation is Arroyo Caraguata (Figure 5.4). This effect of deceleration and subsequent deposition is to a lesser extent present in the northern channel entrances, connected to the Paraná Mini. Flow velocities in the Parana Mini (0.2 - 0.3 m/s) are already in the same order as the velocities in the channel network. This leads to overall higher rates of sedimentation in the channels south of the Las Palmas than the northern channels, which are mostly supplied by the Paraná Mini. Some results of morphological changes in channel entrances are displayed in Figure 5.3.

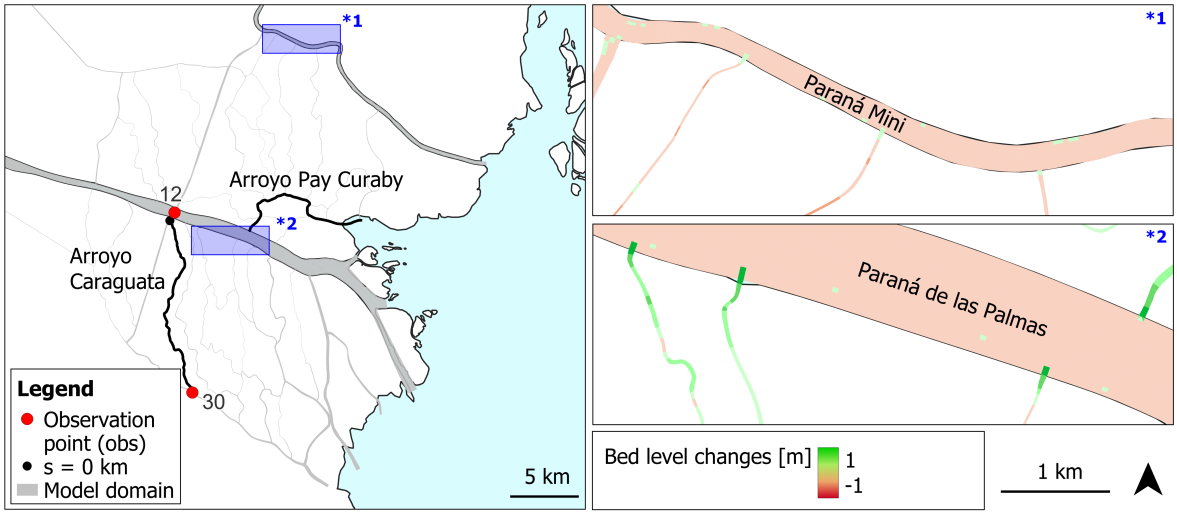

Figure 5.3: Cumulative erosion/sedimentation various channel entrances. The blue frames indicate the location of the close-ups on the right.

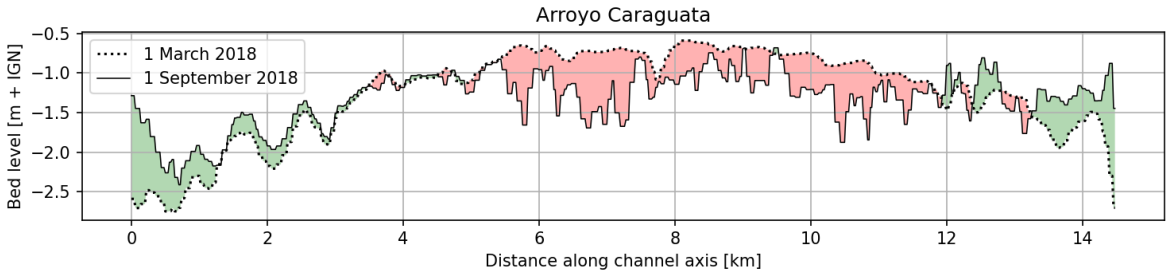

Figure 5.4: Bed level changes in Arroyo Caraguata during scenario A0

5.2.3. Occurrence of mouth bar deposits

Mouth bar deposits can form when the cross sectional area in a river (or channel) rapidly increases, leading to reduced flow velocities and bed shear stresses. The model reproduces similar patterns in some of the terminal channels where the most downstream located reach have a relatively low bottom level. In this region the channel network flows into the subaquatic deltaic front, where accretion leads to the progradation of the coastline. Figure 5.5 displays the modelled bed level changes and initial bed level in the two terminal channels and downstream boundary conditions in the channel network north of the Paraná de las Palmas.

Although the model produces such patterns, two model limitations could have lead to an exaggeration of the deposited volumes in the downstream endings:

- In reality, the region around the terminal channel outflows might be an intertidal area. If during high water these areas inundate, sediment might enter the floodplain and be deposited. After deposition on the intertidal area, sediment poor water flows back towards the estuary. As this process is not included in the model, all the sediment stays inside the channel, possibly leading to an exaggeration of the deposited volumes.
- The water level boundary condition imposed on the terminal channels is the same as the water level at San Fernando. In reality, the funnel shaped bathymetry downstream of the terminal channels displayed in Figure 5.5 could cause an increase in tidal energy, leading to higher tidal velocities in the channel endings which could flush the channel and thus counteract deposition.

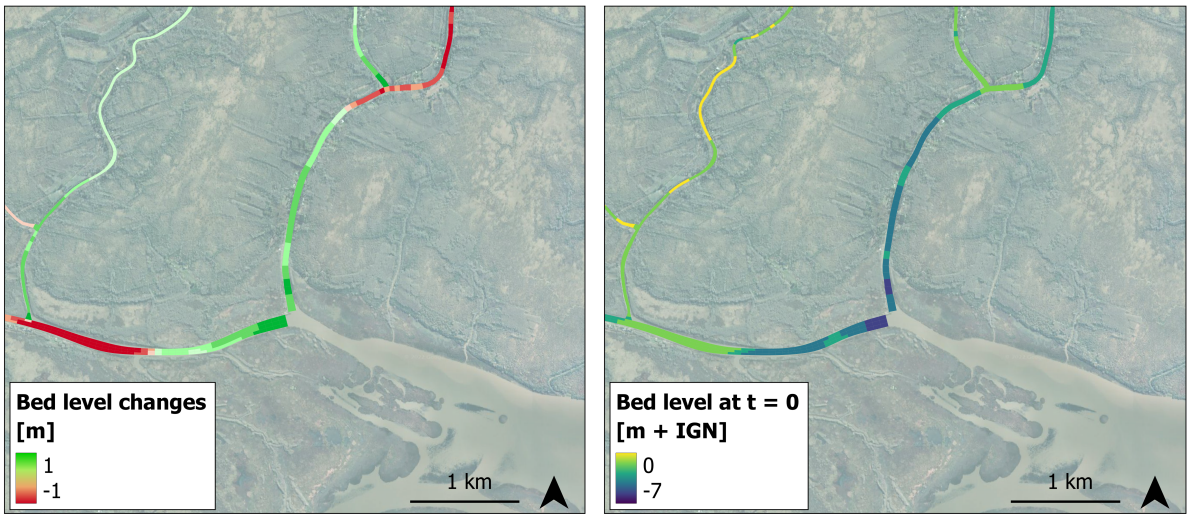

Figure 5.5: Bed level changes (left) and initial bed level in two terminal channels

5.3. Tidal influence

5.3.1. Import of sediment by tidal currents

Hypothesis 1b, repeated below, considers the import of sediment from the estuary due to tidal motion:

> 1. **Tidal and fluvial processes** ***Hypothesis***
>
> (b) Due to the relative magnitude of the tidal velocities and the insignificance in slack water duration asymmetry, import of sediment is not expected to play a significant role in shaping the bathymetry of the Lower Delta channel network

In order to assess the effect of sediment being transported from the downstream boundary into the channel network, the Neumann boundary condition from the base scenario A0 was replaced with a homogeneous Dirichlet boundary condition (scenario A1, see Table 5.2), equating all sediment concentrations on outflow boundaries to zero. This effectively causes sediment poor water to enter the domain during the rising tide if the flow changes direction. A Harleman Thatcher timelag of 60 minutes was applied in order to facilitate a smooth decline of the sediment concentration at the boundary after flow reversal.

Table 5.2: Downstream boundary conditions for sediment concentration (coordinate n perpendicular to the boundary)

A0	Neumann	$\partial c/\partial n$	$= 0$
A1	Dirichlet	c	$= 0$

The changes of scenario A1 relative to A0 are small. Overall differences in deposited/eroded volumes are below 3 percent and manifest mostly in the most downstream located channels. During normal conditions, flow reversal in the downstream boundaries barely occur, and if it occurs, the influence of the sediment-poor water entering the model domain on the overall morphological development of the channel network is small.

5.3.2. Influence of tidal motion

In order to asses the overall effect of tidal motion on the hydro- and morphodynamic patterns in the channel network, the downstream water level boundary conditions were adjusted such that only the subtidal constituent remained. The downstream water level boundary of base scenario A0 and the subtidal time signal of scenario A2 are given in Figure 5.6.

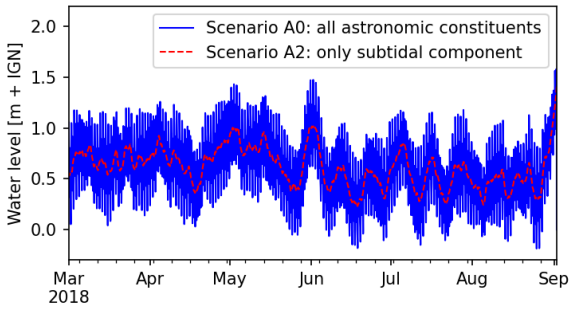

Figure 5.6: Downstream boundary condition scenario A0 and A2

Sedimentation rates are relatively high in scenario A2, indicating that the tide has a stabilizing effect on the overall development of bathymetries and channel configuration in the Lower Delta. The effect is rather spatially uniform, in the majority of the channels the average bed level rise increased. An exception is the entrance of Pay Curaby (Figure 5.3), where the sedimentary deposits in the entrance reduced in volume with approximately 20 cm. Some other exceptions are various channels south of the Las Palmas, close to the deltaic front, with a slight erosive effect i.r.t. scenario A0.

Figure 5.8 displays the comparison between scenarios A0 and A2 in bed level change of various channels. Overall, channels located further away from the deltaic front (Arroyo Caraguata, Arroyo Leber)

are minimally influenced by excluding tidal motion. The effects are mostly limited to a reduction of the sediment deposits in the channel entrances or outflow. In channel Feliciara it can be seen that, without tides, channel sedimentation tends to occur more over the entire length of the channel. This would eventually lead to closing of a channel. Tidal motion counteracts this mechanism, leading to the redistribution of sediment during ebb flow and the export of some of the deposited material.

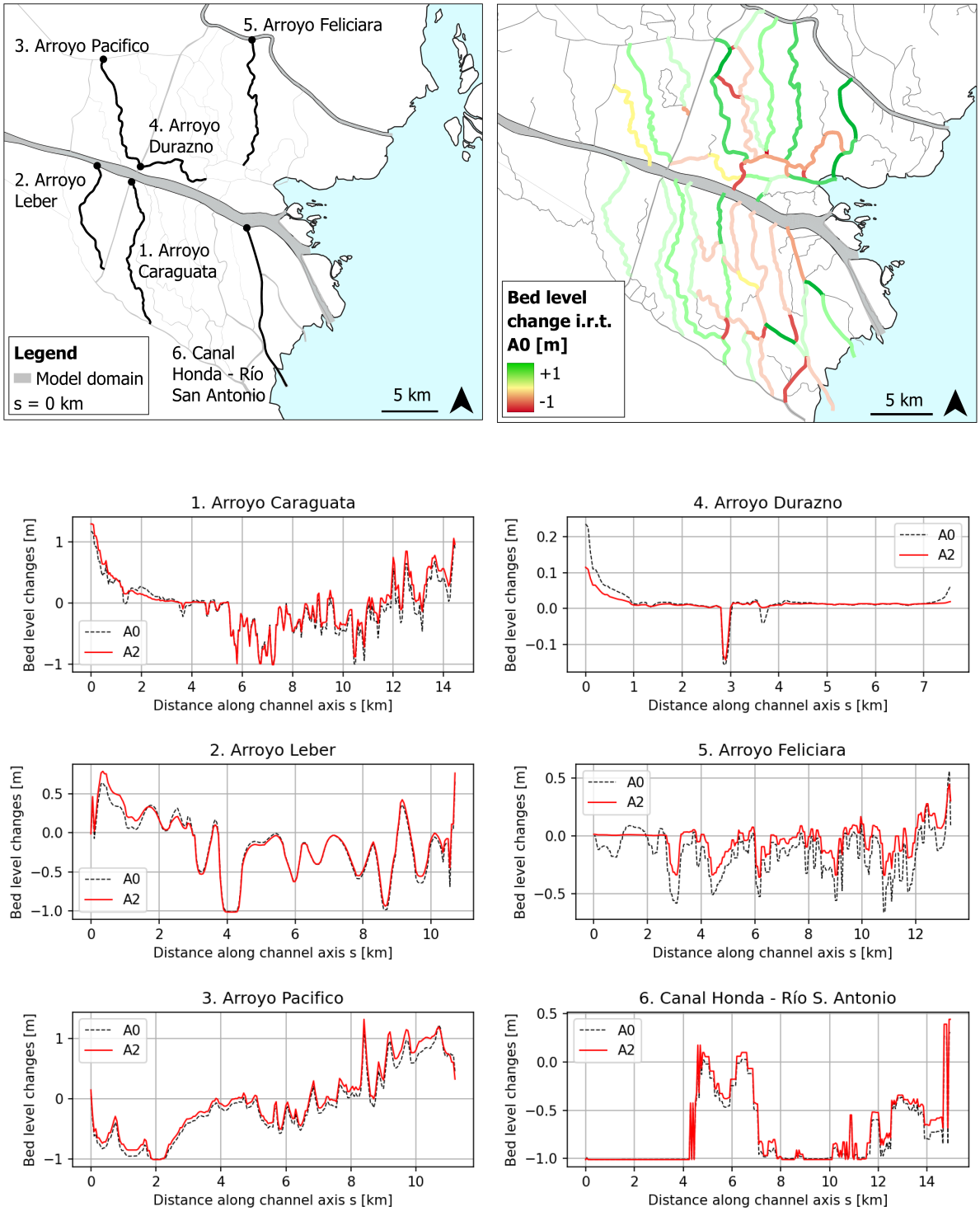

Figure 5.8: Bed level changes various channels scenario A0 and A2

5.3.3. Occurrence of tidal divides

Hypothesis 1c, repeated below, considers the import of sediment from the estuary due to tidal motion.

1. **Tidal and fluvial processes** ***Hypothesis***

   (c) Deposition of sediment occurs at tidal divides inside the channel network

The modelled patterns of sedimentation and erosion in Arroyo Caraguata (Figure 5.4) and various other channels south of the Las Palmas seem to be counteracting the existing, convex-upward bed level profile. This is not in accordance with the expected patterns of sedimentation associated with a tidal divide. To assess the occurrence of a tidal divide in Arroyo Carapachay, the bed shear stresses and water levels over a tidal cycle are plotted and analyzed. In Figure 5.9 it can be seen that the tidal wave enters the northern channel entrance approximately 20 minutes later than the souther entrance. This phase difference is small enough to allow for a tidal divide to occur. Bed shear stresses over the upstream reach (connected to the Paraná de las Palmas) remain low and constant in time compared to the stresses in the downstream reach. This could imply the following:

1. Flow velocities associated with the tidal variation entering the channel from the upstream are lower than in the downstream reach. In Figure 5.9 it can be seen that the tidal range in the northern entrance is lower than in the southern entrance. This is due to the longer distance from the deltaic front and the differential in river flow velocities between the Luján and Palmas rivers, both leading to more damping and lower tidal energy in the channel entrance connected to the Paraná de las Palmas.

2. A part of the tidal prism that enters the channel from the north, leaves the channel from the south. This causes high stresses in the middle and downstream (right side in the Figure 5.9 plots) reach during ebb flow, as this increased tidal prism and the residual river flow have the same direction. This mechanism essentially flushes the middle and downstream part of the channel. In the most downstream part, bed shear stresses are low due to widening of the channel as it approaches Río Luján.

3. The water level gradient during low water is approximately 2e-5, which is low but not negligible. This indicates that river discharge is significant, counteracting the formation of a tidal divide. In addition, the river discharge flows through the shallower middle reach of the channel. This reduction in cross section leads to higher flow velocities and bed shear stresses, leading to (more) erosion in the middle reach.

The influence of the residual (river) discharge through a channel such as Arroyo Caraguata seems to be the main factor counteracting the formation of a tidal divide. To assess the occurrence of tidal divides during lower residual flow conditions (and thus lower river discharge), an addition A0 base simulation was run with 50% of the discharge input of the original A0 run. During these low flow conditions, significantly higher tidal flow velocities are present in the upstream (northern) entrance of Arroyo Caraguata. Longitudinal profiles of the bed shear stress much more resemble the typical stress distribution associated with a tidal divide (see Figure 5.9). This indicates that during normal conditions, the river discharge prevents the occurrence of hydraulic tidal divides in the channel. During low discharge conditions, point 2 is still valid; the majority of the tidal prism leaves the channel through the downstream end, causing high bed shear stresses in the middle and downstream reaches, counteracting deposition that could have occurred in the middle of the channel during the calm conditions around high water slack.

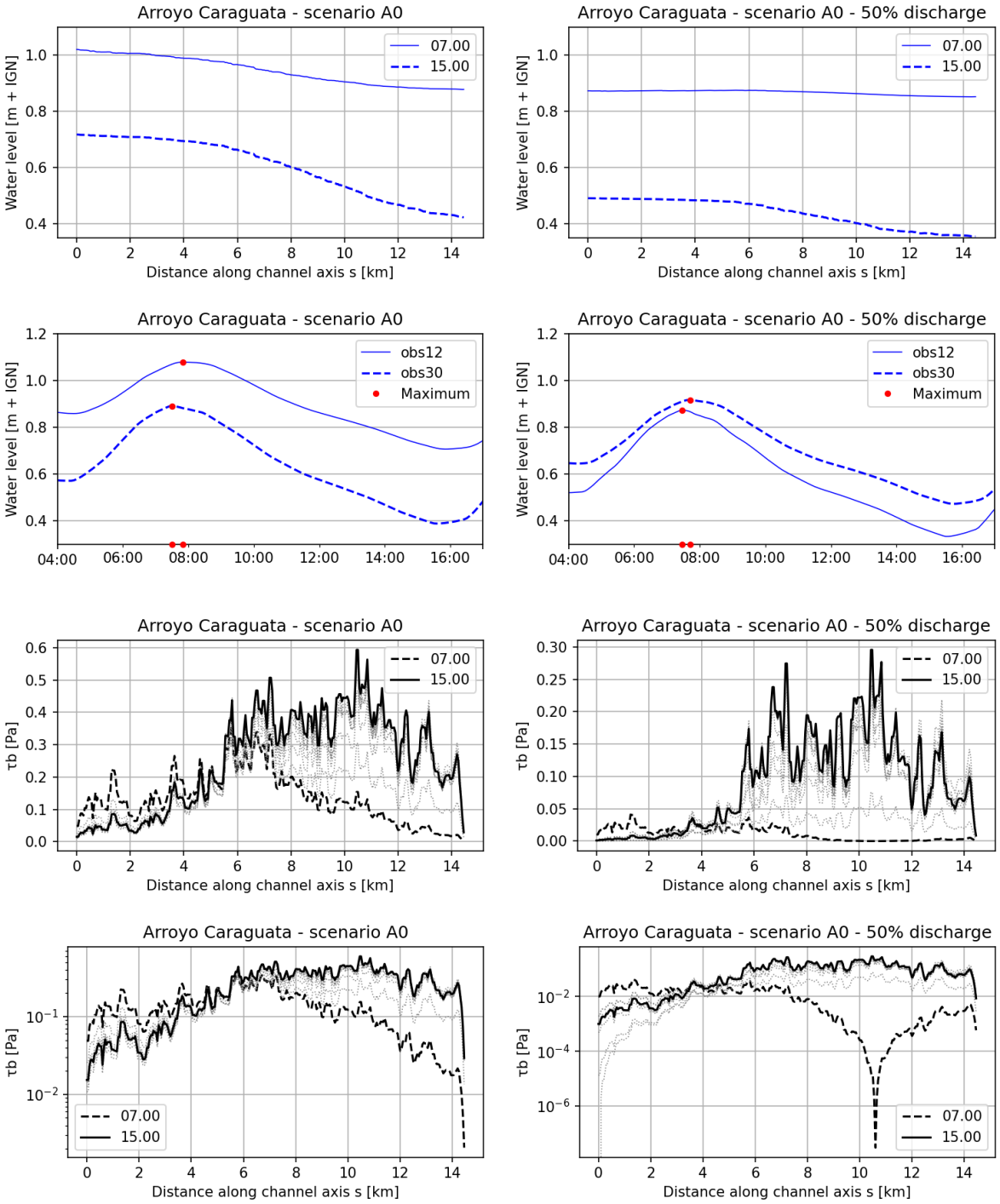

Figure 5.9: Water level and shear stress distribution during a tidal cycle scenario A0 (top) and A0 with a 50% reduction in discharge (middle and bottom), note that the bottom plot is on a logarithmic scale. Locations of observation points 12 and 30 and the s = 0 km point are displayed in Figure 5.3.

5.4. Influence of varying river discharge

As elaborated upon in previous chapters, discharge variability in the Paraná river occurs on seasonal, multi-annual and multi-decadal time scales. By means of various model scenario runs, the influence of variability in river discharge is assessed. Hypotheses 2a, 4a and 4b, repeated below, consider the influence of discharge variability on channel network morphodynamics:

2. **Extreme discharge events and storm surges** ***Hypothesis***

   (a) Extreme river discharges cause erosion or counteract deposition in the Lower Delta channel network compared to regular discharge conditions, due to increased flow velocities and sediment transport capacity.

4. **Historic and future changes in sediment input and river discharge** ***Hypothesis***

   (a) The combination of an overall increased river discharge, manifesting mainly in increased discharge peaks, and increased sediment load from the Bermejo region between 1960 and 2000 caused by increased precipitation patterns and land use change have had a positive effect on the annually averaged sediment concentrations entering the delta, which subsequently lead to increased sedimentation rates in the Lower Delta channel network.

   (b) The projected increase in discharge peaks in the 21st century will counteract depositional patterns in the Lower Delta, essentially 'flushing' the channel system.

The following model scenarios are related to the variability in discharge of the Paraná River. An overview of the B scenarios is given in Table 5.3.

- **Scenario A0** simulates typical regular conditions. The discharge signal of the Paraná River includes a typical seasonal variation between approximately 21,000 and 13,500 m^3/s.
- **Scenario B0** simulates the 2016 high discharge conditions. Such extreme flow conditions are related to the multi-annual variability associated with an El Niño event.
- **Scenario B2** simulates pre 1960 conditions, 'reversing' the land use change and precipitation increases that have caused significant increases in river discharge during the second half of the twentieth century.
- **Scenario B3** simulates a future climate scenario, with a 20% discharge increase related to scenario B0.

Table 5.3: B scenarios, changes relative to scenario B0

	Discharge	Sediment concentration
B1	-0 %	c_{silt} = 74 mg/l, c_{clay} = 85 mg/l (*-26 %*)
B2	-21 %	c_{silt} = 74 mg/l, c_{clay} = 85 mg/l (*-26 %*)
B3	+20 %	c_{silt} = 100 mg/l, c_{clay} = 115 mg/l (*+ 0 %*)
B4	+20 %	c_{silt} = 118 mg/l, c_{clay} = 136 mg/l (*+18 %*)

By analysing the results of above mentioned model scenario runs, the effect of both moderate and extreme discharge variability on the morphological development of the channel network are determined and described in Sections 5.4.1 and 5.4.2.

5.4.1. Moderate seasonal discharge variation

The temporal variation of the magnitude of residual discharges and velocities in the channels follow the trend of the total river discharge input. During relatively high flow conditions (first part of model run A0) the discharge and velocities in most channels was higher than in the low flow half of the model run. This lead to overall higher rates of sedimentation in the second half of the simulation, caused by the reduction in flow velocities.

Total sedimentation/erosion in in March - June 2018 (Scenario A0, low flow) : -4.86e-5 m^3
Total sedimentation/erosion in in June - September 2018 (Scenario A0, low flow) : -2.16e-6 m^3

The volumes mentioned above indicate almost a factor 5 of eroded material between the low and high flow conditions. Although modelled absolute volumes of sediment are not representative of reality, the large difference between modelled morphological development during seasonal high and low flow conditions does show that there is a strong dependence of the magnitude of the river discharge on the channel network development.

5.4.2. Extreme discharge events

The overall effect on the channel network morphological development of extreme discharges is net erosion. Velocities in the channel network increase significantly, leading to more erosion/less deposition.

The erosive effect of the increased Paraná River discharge is mostly present in the channels located south of the Paraná de las Palmas. North of the Paraná de las Palmas, the erosive effect is minimal and for some channels the effect is slightly depositional. The cause of this asymmetry in morphological response is a shift in hydraulic gradient between the Paraná Mini, Paraná de las Palmas and Río Luján. Although the discharge increase of the Paraná Mini and the Paraná de las Palmas are in proportion, the water level in the Paraná de las Palmas increases more than in the Paraná Mini and Río Luján. The increased water level gradient between Paraná Mini and Las Palmas lead to similar or slightly decreased flow velocities and a neutral to slight depositional morphological response. The increased water level gradient between Las Palmas and Río Luján cause increased flow velocities and an erosive response. The principle is schematically depicted in Figure 5.11. In Figure 5.10 the difference in modelled bed level changes between scenarios B0 (current extreme conditions) and B3 (+20% discharge increase) display the asymmetric shift in morphological response.

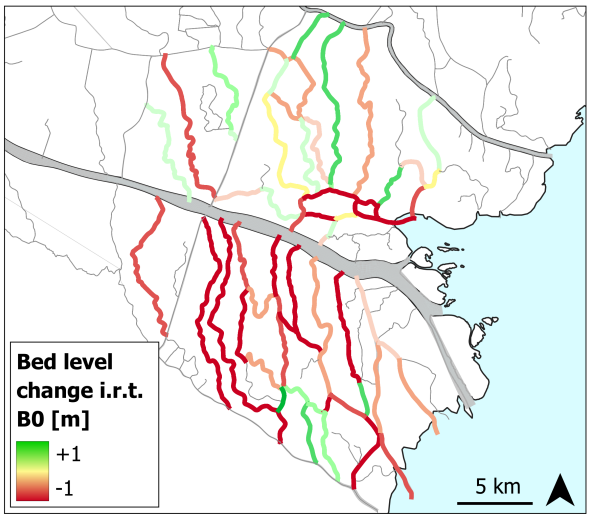

Figure 5.10: Bed level changes scenarios B3 i.r.t. B0

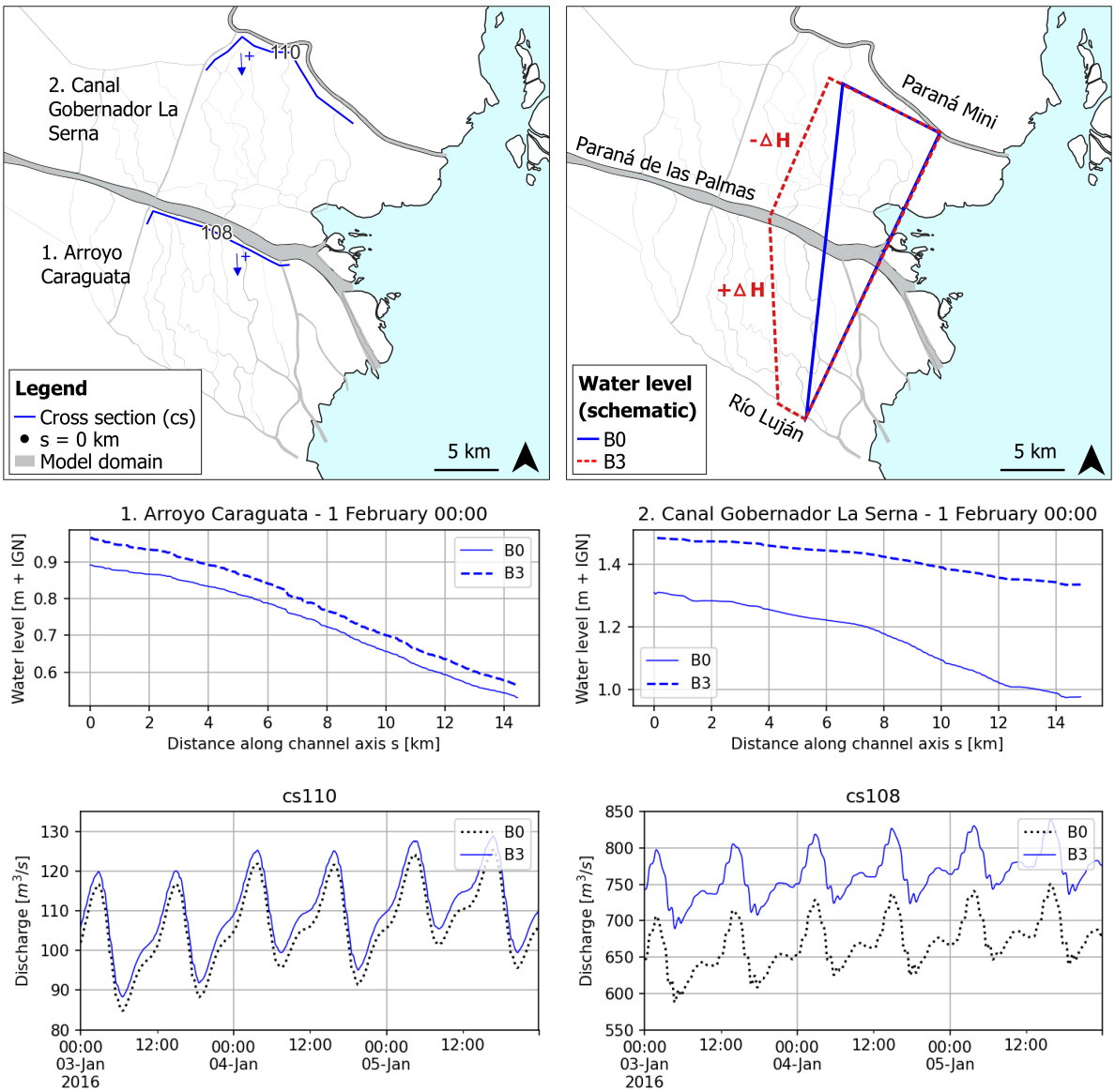

Figure 5.11: Change in discharge and hydraulic gradient scenario B3 i.r.t. B0

5.5. Influence of varying sediment load

By means of two model scenario runs, the influence of variability in sediment load is assessed. Hypotheses 4a and 4c, repeated below, consider the influence of sediment supply variability on channel network morphodynamics.

4. **Historic and future changes in sediment input and river discharge** ***Hypothesis***

   (a) The combination of an overall increased river discharge, manifesting mainly in increased discharge peaks, and increased sediment load from the Bermejo region between 1960 and 2000 caused by increased precipitation patterns and land use change have had a positive effect on the annually averaged sediment concentrations entering the delta, which subsequently lead to increased sedimentation rates in the Lower Delta channel network.

   (b) When considering the possibility of higher sediment loads during a future discharge peak, the overall sediment concentrations in the Lower Delta will increase, leading to an increase of net sedimentation rates in the Lower Delta channel network.

Model scenarios B1 and B4 (see Table 5.3) are related to the variability in sediment load of the Paraná River:

- **Scenario B1** simulates pre 1960 conditions, 'reversing' the land use change and precipitation increases in the Bermejo region that have caused for significant increases in sediment load during the second half of the twentieth century;
- **Scenario B4** simulates a future climate scenario, with a large increase in river discharge and sediment load supplied from the Bermejo Region.

Merely reducing the sediment input without changing the discharge (scenario B1) has an overall erosive effect. The erosive effect is primarily noticeable in channels south of the Las Palmas, and to a lesser extent in channels located close to the deltaic front. The following two points consider this spatial heterogeneity:

- The Paraná Mini supplies sediment to most of the channels north of the Paraná de las Palmas. As the Paraná Mini has a lower transport capacity than the Paraná de las Palmas, the difference in sediment entering these northern channels is less than the southern channels, compared to scenario B0. Therefore the morphological response to decreasing the sediment input is less in the northern channels. Figure 5.12 displays the (change in) sediment input in combined channels connected to the Paraná de las Palmas (cs108) and the Paraná Mini (cs110).
- Downstream located channel bathymetries experience net erosion to a lesser extent. This encapsulates the notion that the morphology of upstream channels are influenced more by the supply of fluvial sediment and the downstream channels are more dependent on marine forcing.

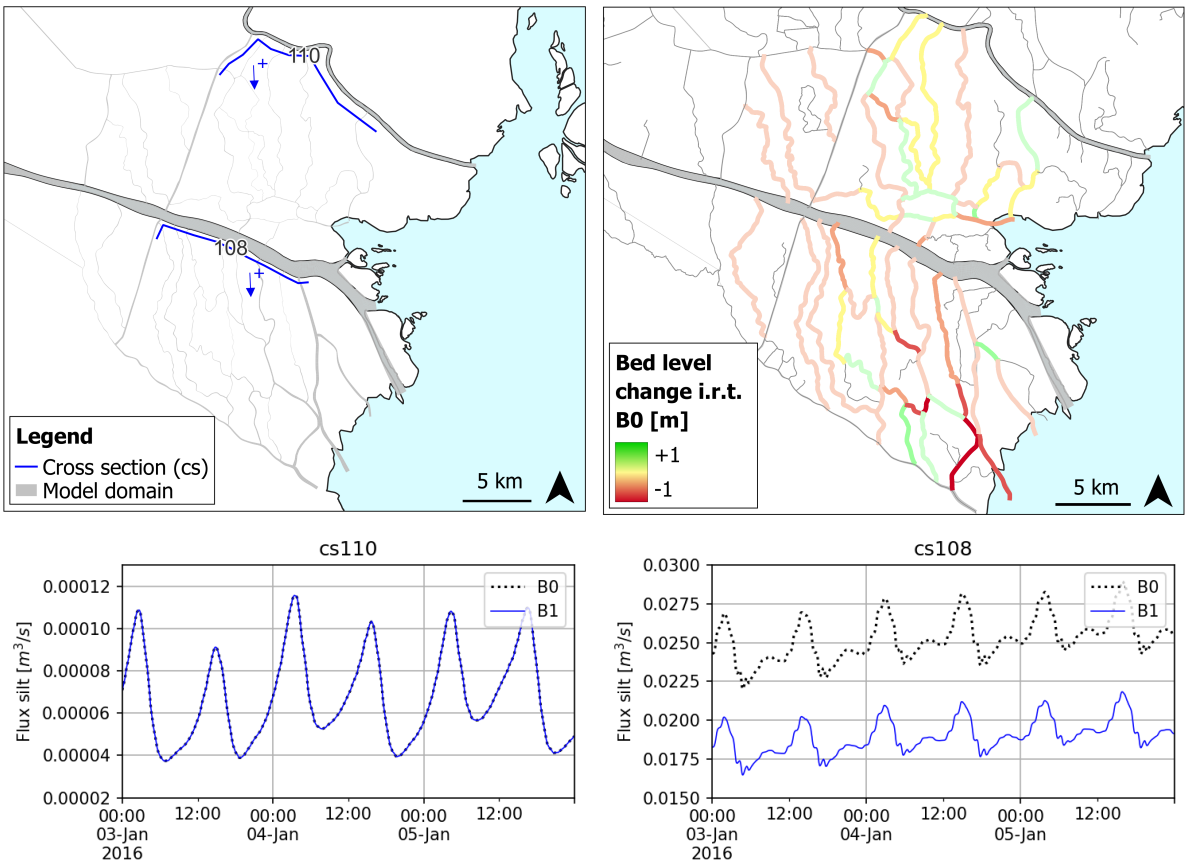

Figure 5.12: Change in sediment flux (silt) scenario B1, south direction is positive

Increasing the sediment supply has a domain-wide effect of slight increased rates of sedimentation. Similarly to scenario B1, changing the sediment supply mostly influences upstream located channels and channels south of the Paraná de las Palmas. Figure 5.13 displays that sediment supply into northern channels are to a lesser extent dependent of upstream sediment boundary conditions as the transport capacity subceeds the concentration imposed.

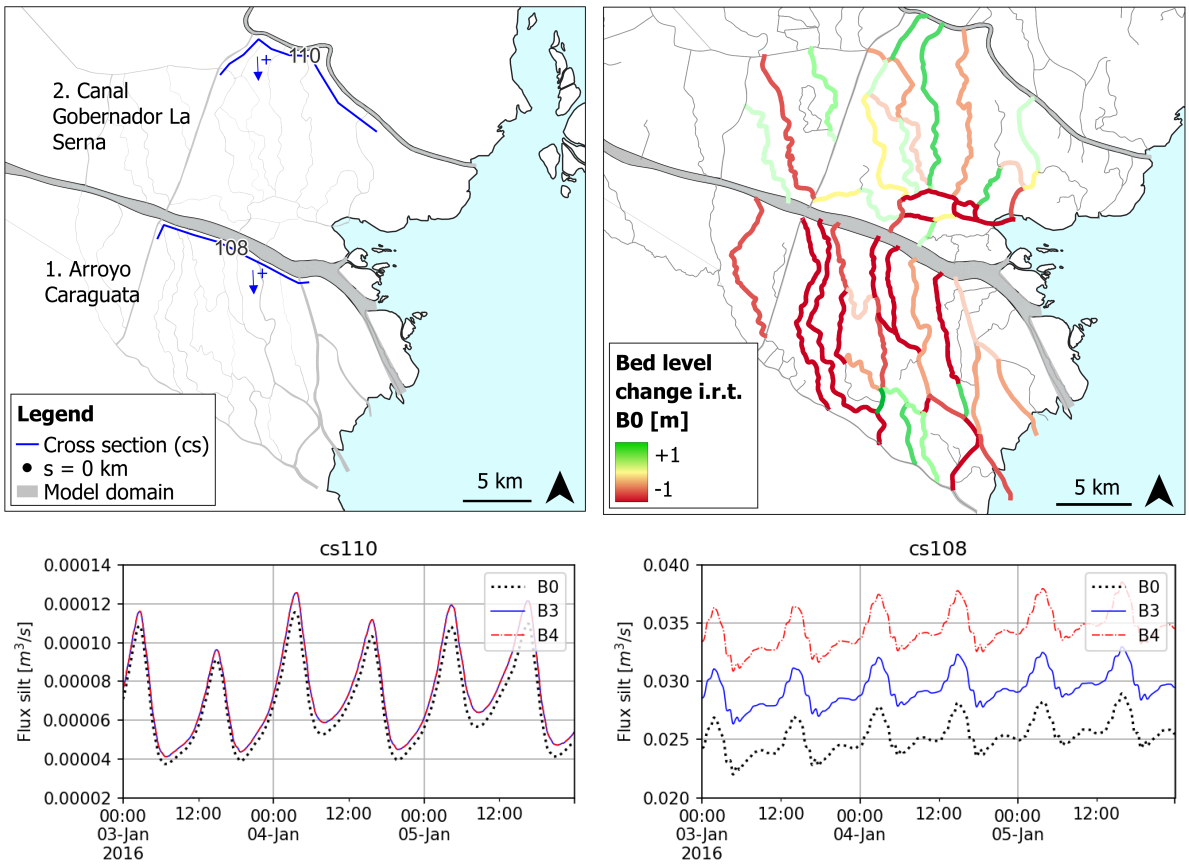

Figure 5.13: Change in discharge and hydraulic gradient scenario B4, south direction is positive

5.6. Influence of topography changes based on dredging / channel excavation

Hypotheses 5a, 5b, 5c and 5d consider the influence of current and historic dredging/excavation activities in the Lower Delta. Hypothesis 5d is not assessed through the numerical model for reasons mentioned in Section 5.1.

5. **Dredging activities and channel excavation** ***Hypothesis***

   (a) Deepening the main channel of a river can enhance tidal amplification or change the celerity of the tidal wave, altering the hydraulic conditions at the boundaries of a channel and changing the location of tidal divides.

   (b) Deepening a river branch will attract flow, leading to a repulsion of flow in nearby channels, lowering the sediment transport capacity in these channels and thus inducing channel accretion.

   (c) The excavation of artificial channels has decreased the river discharge through the existing, natural channels, and the subsequent reduction in sediment transport capacity has had positive effect on deposition in the channel network.

   (d) Deepening a river branch will attract flow, leading to a repulsion of flow in nearby channels, lowering the sediment transport capacity in these channels and thus inducing channel accretion.

5.6.1. Deepening the Paraná de las Palmas

Model scenario A4 is used to asses the effect of artificially keeping the Paraná de las Palmas downstream reach at the depth required for navigation. In scenario A4 the depth of the navigation channel in the downstream reach of the Paraná de las Palmas is decreased in such a way that the river cross sections have a more natural shape. This way, the situation that would occur when dredging efforts have ceased for several years is approximated. Note that the most downstream reach of the river (the most upstream part of Canal Emilio Mitre) is made more shallow, while in the current situation this reach keeps itself at depth. This implies that the Canal Emilio Mitre in the estuary, just downstream of the model domain, has filled up significantly, hindering the flow through the canal, effectively decreasing the flow velocities through the shallow channel. Model run A4 thus not only excludes dredging in the Las Palmas branch, but also dredging in the Emilio Mitre Canal in the Río de la Plata estuary.

Changing the bathymetry input the Paraná de las Palmas results in a difference in total volume between scenario A0 and A4 of roughly $8.35e^6$ m^3 over a distance of 19 km, corresponding to an average decrease in conveyance area of roughly 440 m^2. The current conveyance area of the downstream reach of the Paraná de las Palmas is in the order of 7000 to 9000 m^2 (Appendix D), implying a decrease of roughly 5 to 6 %. A decrease in conveyance area of 440 m^2 over the approximately 150 m wide navigation canal corresponds to a depth decrease of 3 meters. Considering the dredging volumes of the Paraná de las Palmas (Chapter 3), this corresponds to sedimentation of roughly 10 regular, non-ENSO years or 2 to 3 El Niño years with a high sediment supply. The bathymetries associated with scenario A0 and A4 are displayed in Figure 5.14, as well as some cross sections visualizing the decreased channel depth.

The overall effect of scenario A4 compared to A0 is erosive. Increasing the bed level of the Paraná de las Palmas causes an increase in water level, leading to higher discharges into and increased transport capacity in the channels that are supplied directly by the Paraná de las Palmas. These channels include most channels located south of the Paraná de las Palmas and Arroyo Pay Curaby (Figure 5.3). In Figure 5.15 the erosive effect in these channel is displayed.

For various channels connected to the Paraná Mini, the effect is different than stated in the previous paragraph. A decrease in flow velocity induced increased rates of sedimentation compared to base scenario A0. The mechanism behind this spatial asymmetry in morphodynamic response to increasing the bed level of the Las Palmas is that the longshore hydraulic gradient between the Paraná de las Palmas and the Río Luján/Paraná Mini increases/decreases, respectively. The water level increase in the Paraná de las Palmas (10 to 20 cm) is larger than the increase in Río Luján and Paraná Mini (both

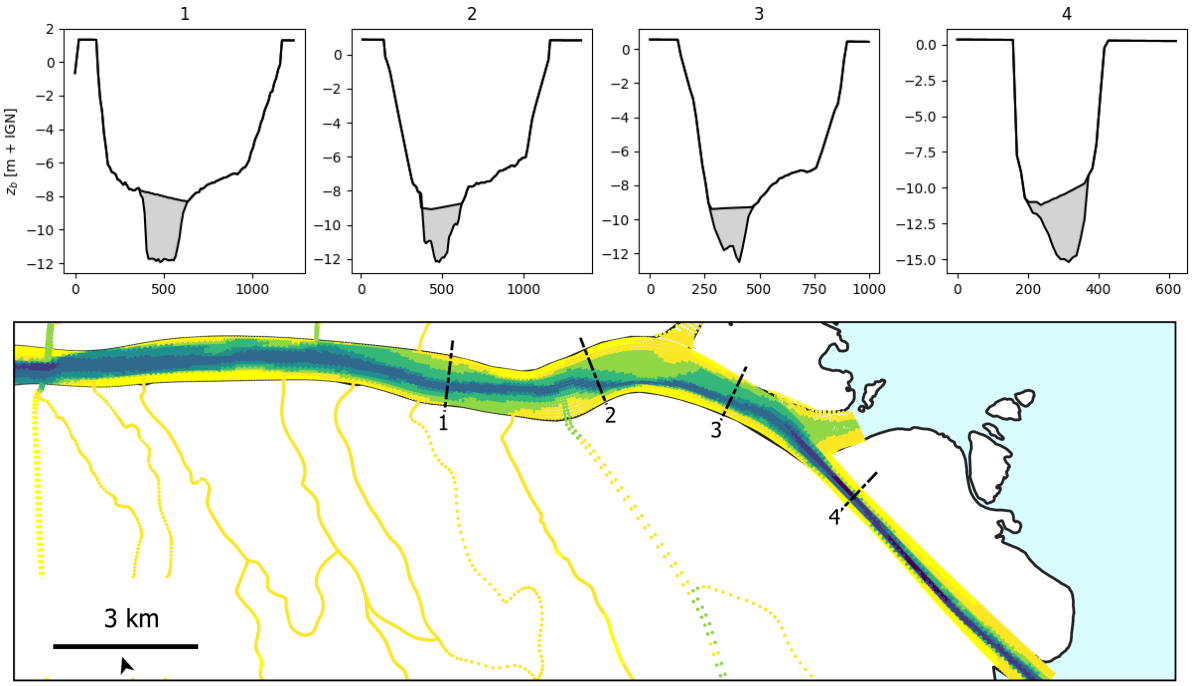

Figure 5.14: Paraná de las Palmas bathymetries of the base scenario (A0) and 'No Dredging' scenario (A4)

approximately 5 cm). Because the main flow directions are south-east directed, the result is an increase in transport capacity in channels south of the Las Palmas and a decrease in channels confluencing with the Pay Curaby channel. The shift in hydraulic gradient (symbol H) is schematically depicted in Figure 5.16.

The characteristics of the tidal wave changed. The tidal amplitude 21 km from the deltaic front decreased with approximately 19-35 % (depending on the magnitude of the discharge), indicating a significant increase in tidal damping. Furthermore, the celerity of the tidal wave decreased from approximately 5.1 to 3.8 m/s leading to a delay of approximately 15 minutes at the location where the Paraná de las Palmas meets Canal Gobernador La Sera (Figure 5.16).

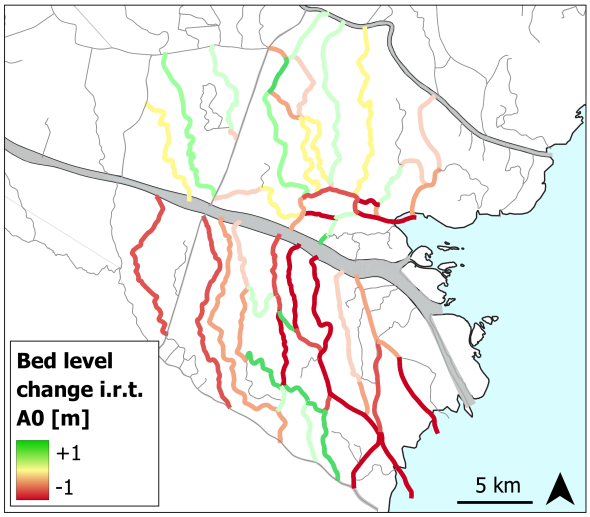

Figure 5.15: Bed level changes scenario A4 i.r.t. A0

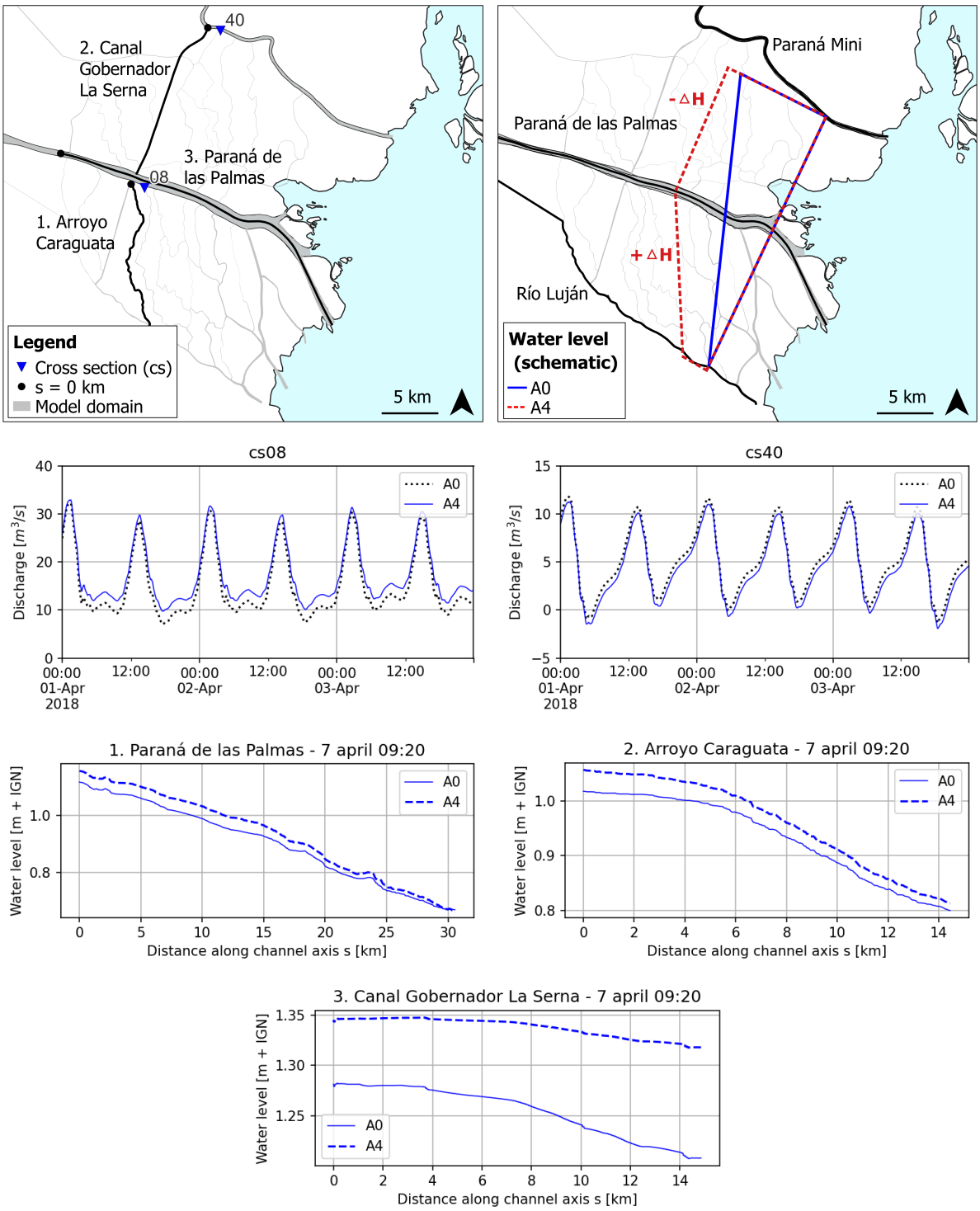

Figure 5.16: Hydraulic gradient and discharge changes scenario A4, bed level changes scenario A4 i.r.t. A0 (right bottom)

5.6.2. Newly excavated channels

In scenario A5 the effect of the excavation of navigation channels in the Lower Delta in the early nineteenth century is assessed. This is done by altering the bathymetry of scenario A0, which is based on the current situation, by filling up some the channels that are know to be man-made. The main artificial canals in the Lower Delta are Canal Gobernador Arias and La Serna, both located at approximately 19 km from the deltaic front with a perpendicular orientation with the Paraná de las Palmas. These two canals, and some smaller canals attached, are excluded in scenario A4. Other artificial canals are not

excluded, such as Canal Honda and Canal Estudiante. These canals are deemed to be too much of a integral part of the channel network to be left out. Figure 5.17 displays the channels that are excluded in the A5 computation, as well as the channel that are man-made in reality.

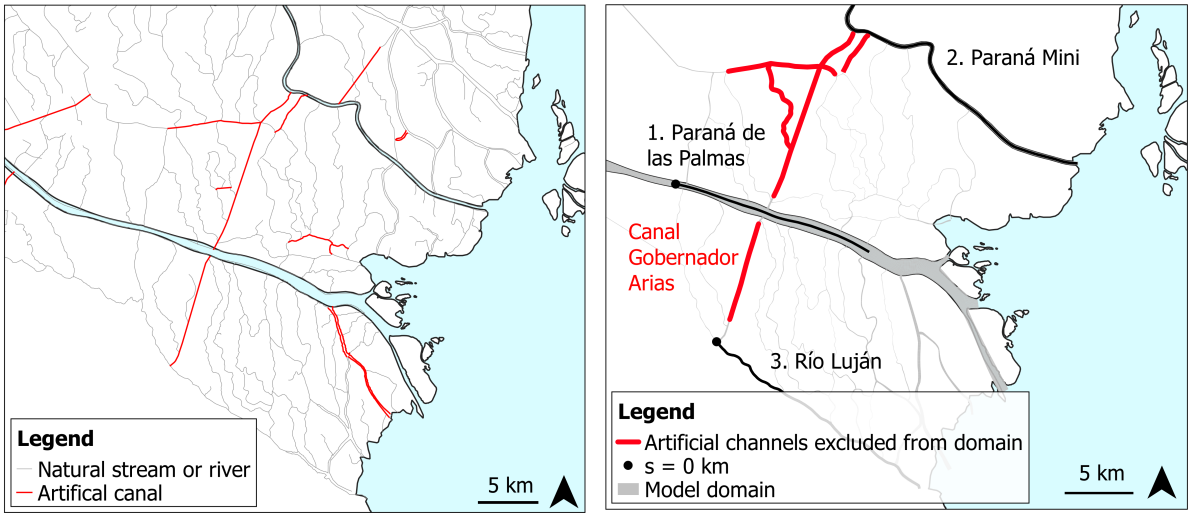

Figure 5.17: Artificial channels, reality (left) and model setup scenario A5

The effects of scenario A5 is overall erosive, and most pronounced in channels located in the direct vicinity of the channel(s) excluded from the domain. A small increase in water level of 1 to 3 cm occurred in the Las Palmas. The water level in Río Luján changed drastically, with a decrease of 30 cm at around 20 km from the deltaic front. The cause is the closing of Canal Gobernador Arias, which in current conditions supplies the majority of the downstream continuation of Río Lujan. The water level in the Paraná Mini increased significantly. The result is an increase in hydraulic gradient between the Paraná Mini, the Paraná de las Palmas and Río Luján, leading to erosion in most of the channels between (see Figures 5.18 and 5.19).

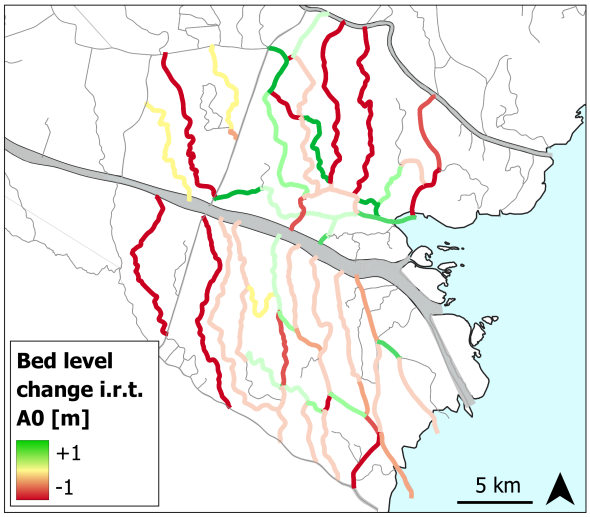

Figure 5.18: Bed level changes scenario A5 i.r.t. scenario A0

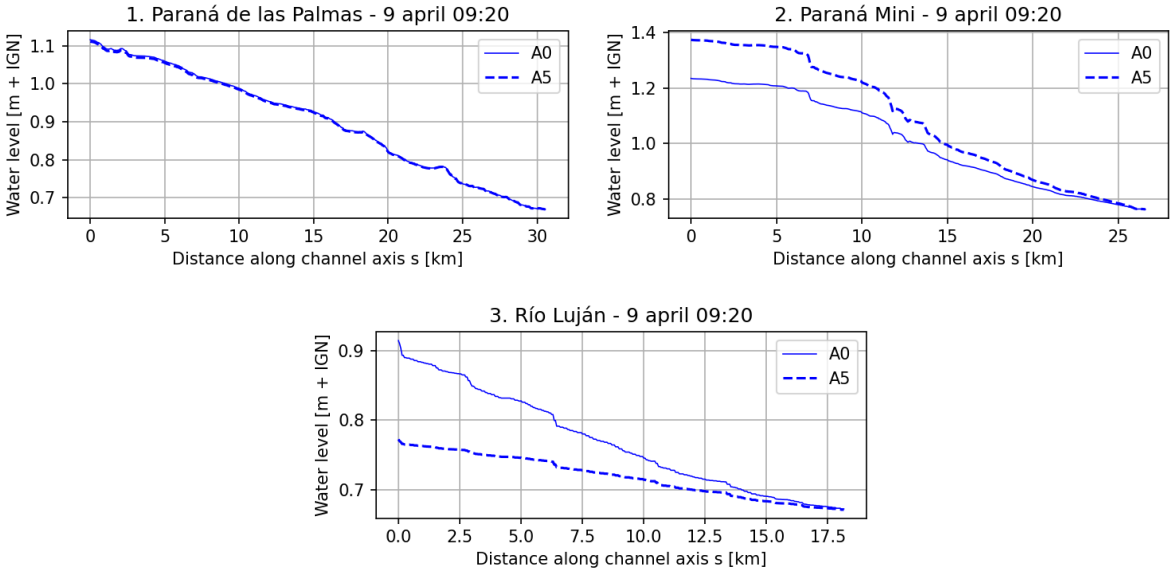

Figure 5.19: Water levels scenario A5 and A0, locations and directions of the longitudinal sections are displayed in Figure 5.16)

5.7. Influence of a storm surge event

Hypothesis 2b, repeated below, considers the influence of a storm surge on the morphological development of the Lower Delta channel network:

> 2. **Extreme discharge events and storm surges** ***Hypothesis***
>
> (b) The sediment-depleted return flow after a flood instigated by a storm surge can pick up sediment from the channel beds, leading to a net erosive effect of the storm surge event and the flood.

In Scenario A3, a storm surge is imposed on the downstream water level boundary of scenario A0. The storm surge spans 2 to 3 days, reaching a water level of 3.0 m + IGN at San Fernando (see Figure 5.20). A storm surge of such duration and water level increase corresponds with events that occur several times per decade. As mentioned in Chapter 2, measured water level timeseries at Arroyo Carapachay show that flooding occurs when water levels exceed 1.7 m + IGN. The effect of flooding of the islands between the channels is included in the model by making use of the lateral discharge functionality in D3D-FM. By specifying discharge timeseries and a sub-selection of the model domain, volume is extracted and inserted into the cells within the subdomain. The functionality weighs the discharge per cell based on the cell area. In the following bullets, the method by which the discharge timeseries was obtained is described below.

- The total volume to be extracted from and later inserted to the model is calculated by multiplying the total area of the floodplains with the difference between the maximum storm surge level and the bankfull level at Arroyo Carapachay:

$$V_{Total} = A_{Floodplains} \cdot (3.0 - 1.7) \tag{5.1}$$

- The volume V_{Total} is extracted during the rising period when the water level exceeds the bankfull level. The lateral discharge is inserted back inserted during the falling period while the water level exceeds the bankfull level.
- The discharge timeseries are assumed to have a Gaussian shape, peaking around the highest values of the temporal water level gradient and changing sign at the flood peak (see Figure 5.20). Integration of the applied discharge timeseries yields the total volume V_{Total}.
- During various test runs, using V_{Total} for the total lateral discharge volume lead to the near-emptying of some cells, leading to non-physically high flow velocities and timesteps approaching zero. To avoid these numerical errors, a reduction factor α was applied to V_{Total}. The maximum value of α was iteratively determined to be 0.175.

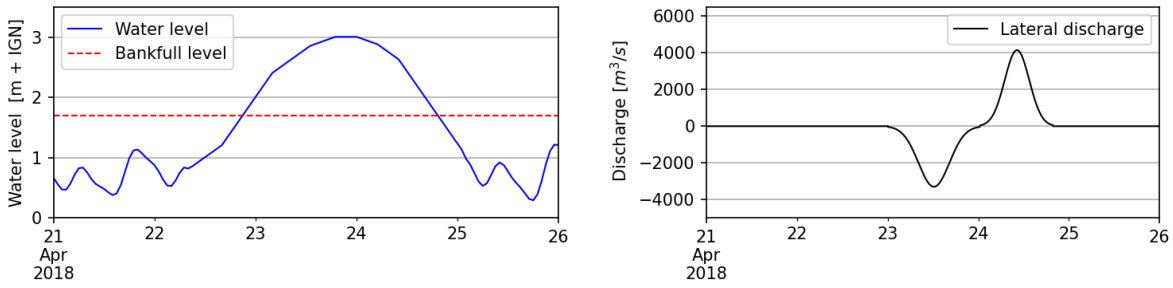

Figure 5.20: Water level boundary condition (San Fernando, left figure) and lateral discharge during the storm surge

Model run A3 with the lateral discharge functionality had a slight depositional effect compared to the base scenario A0, with high spatial variability between the different parts of the domain. Inspection of

the flow patterns inside the channel network during the storm surge showed that the effect of the lateral discharge caused unrealistic results. An A3 model run without the lateral discharge functionality was carried out in order to isolate its effect. The following paragraph describes the discrepancy between realistic and modelled behaviour and the expected reason:

In the model, the water levels in the channels do not communicate with the floodplain but only with the surrounding grid cells. By definition, the lateral discharge functionality extracts/adds a volume from/to every cell weighted by cell area, i.e. the water level difference due to the lateral discharge is equal for every cell. However, the model results show that water level differences due to the lateral discharge are much higher in cells surrounded by few other cells (i.e. in the middle of the channel network) than in the cells surrounded by many cells (i.e. at channel in- and outflow and the river branches). In other words, the water level in the middle of the channel reacts more abrupt to the lateral discharge. An explanation for this phenomena is that the main river branch is much more accessible for a 'restoring' force (i.e. river discharge from upstream or tidal discharge from the downstream boundary). This causes the reaction of the water level in a main river branch to be much more diffuse than in the middle of the channel network. As can be seen in Figure 5.21, this leads to unrealistic high water level differences and extreme flow velocities inside the channel network. The morphological response in the channel newtork is dominated by this artificial phenomena, leading to overall unreliable results.

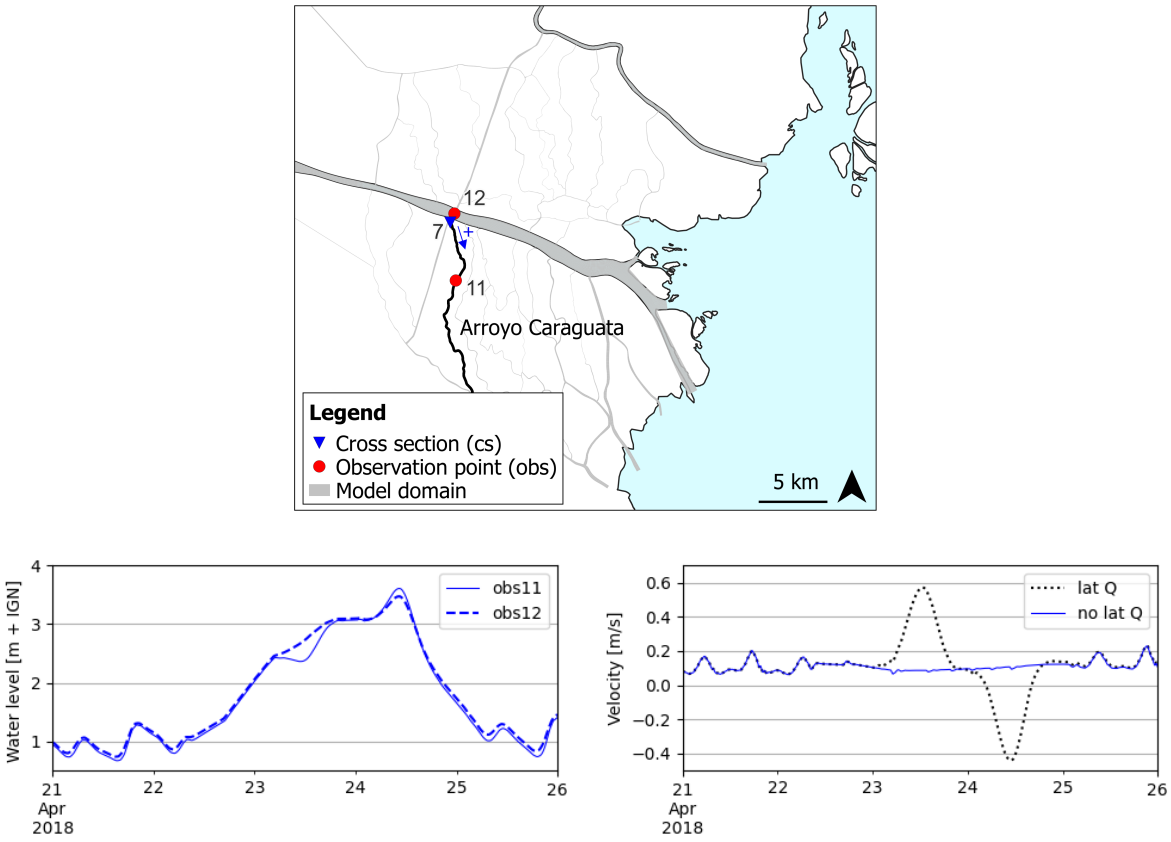

Figure 5.21: Water level in the middle and the side of Arroyo Carapachay (left) and the flow velocity in cross section 07 in Arroyo Carapachay (right) during the storm surge

Figure 5.22 further demonstrates the effect of (not) including the lateral discharge functionality on modelled bed level changes in the channel network. Without including the lateral discharge functionality, the water becomes stagnant during the rising period (23 April 00:00), leading to low shear stresses and sedimentation. During and after the falling stage, the return flow causes higher than normal shear stresses, leading to net erosion after the storm surge. Including the lateral discharge functionality causes an non-physical peak in bed shear stress due to the mechanism described above, during which

much of sediment is put in suspension and transported. At the location depicted (observation point 11) this lead to a large depositional effect.

Overall it can be stated that the model run without the lateral discharge functionality more resembles realistic morphological development, as the return flow causes erosion which leads to the effect of the scenario compared to the base scenario being erosive. One could argue that in reality, the erosive effect would be even larger as the sediment that would be deposited on the flood plain does not leave the model domain. Figure 5.22 displays the net bed level changes of model scenario A3, excluding the lateral discharge functionality, i.r.t. base scenario A0.

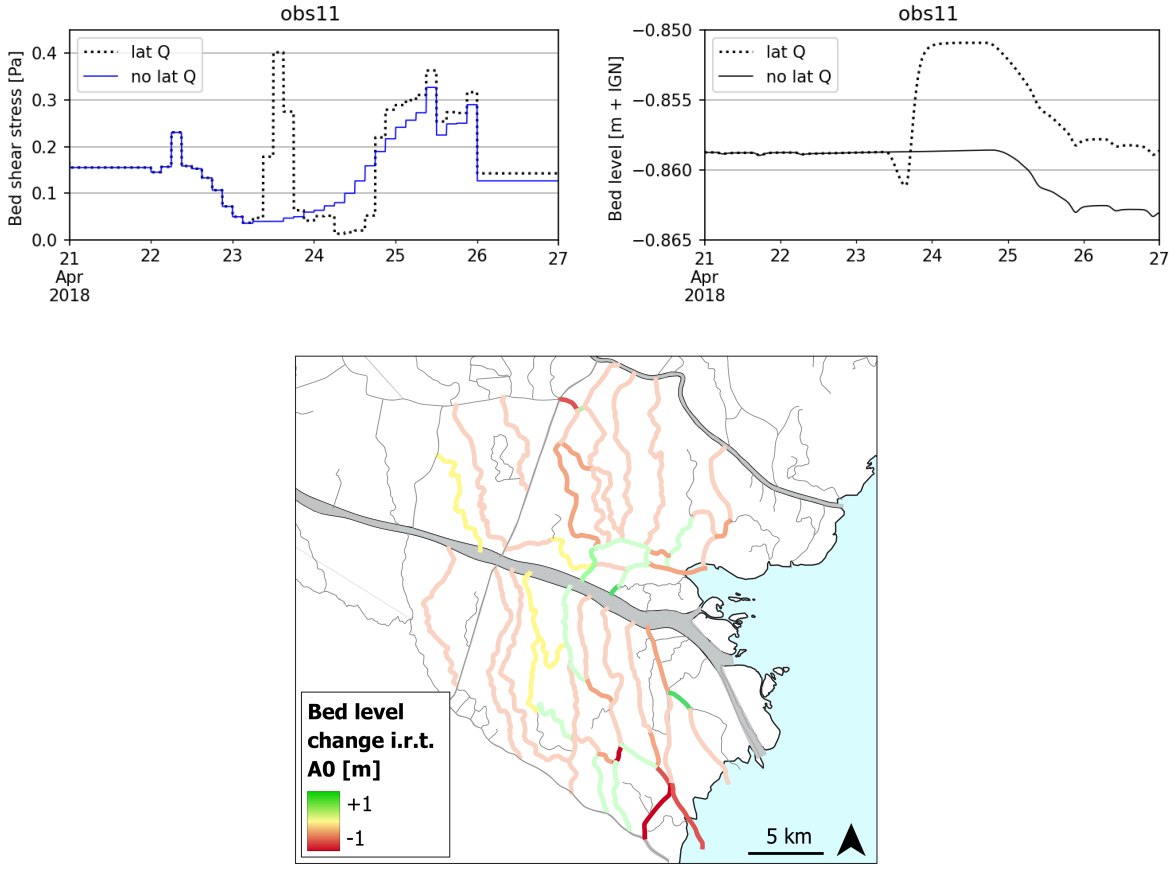

Figure 5.22: Bed shear stress (left) and bed level changes (right) at observation point 11, with and without the lateral discharge functionality. Bottom figure shows the relative bed level changes of the A3 scenario without lateral discharge i.r.t. scenario A0.

6

Discussion of Results

The numerical model has provided several insights on the hydrodynamic and morphodynamic behaviour of the Lower Paraná Delta. In Section 6.1, practical implications of the research results on the current dredging strategy are touched upon. Limitations of the numerical model applied in the context of this research are discussed in Section 6.2. Concrete recommendations on future research on the hydro- and morphodynamic behaviour of (several parts of the) Lower Paraná Delta are also provided in Section 6.2.

6.1. Practical implication: Dredging strategy

Whereas the purpose of this research is primarily to gather knowledge on the (natural) system that is the Lower Paraná Delta, some of the model results have practical implications for (future) dredging activities in the research area. Primarily, it is likely that historic deepening of the downstream reach of the Paraná de las Palmas for navigational purposes has caused deposition in the channels located south of the Paraná de las Palmas and Arroyo Pay Curaby. In contrast, the modelled the effect of deepening the Paraná de las Palmas is erosive for the northern channels, confined by the Paraná Mini and Arroyo Pay Curaby. Whether the effect of dredging activities can be seen as positive or negative with regards to small-scale navigation depends on which region of the channel network is most extensively used for this purpose. Based on incidental presence in the region by the author (during the field surveys, see Appendix I) and conversations with Martín Sabarots Gerbec, the assumption that the channel network located south of the Paraná de las Palmas are more intensively used for navigation than the northern channels is safe to make. Much of the navigation activity is related to tourism and the small scale supply of goods. Most of the accommodations and housing in the Lower Delta are concentrated near the port of El Tigre, therefore navigation is expected to be more frequent in the most south-eastern region of the research area. If this is the case, the effect of deepening the Las Palmas can generally be regarded as negative for navigation in the Lower Delta channel network.

In addition to these potential negative effects of current dredging activities on the navigability of the channel network, the result of keeping the Paraná de las Palmas and Canal Emilio Mitre at depth also includes large financial costs. Personal contact with Pablo Arrecco and as Happee [2019] stated in the discussion chapter of her thesis, an alternative entrance to the Paraná waterways system, using Canal Martin Garcia and the Paraná Guazú tributaries Bravo, Guazu and Talavera (BGT) could hold advantages over the current route (see Figure 6.1). Happee mentioned the following 2 advantages:

- The alternative waterway has a larger natural depth, thus less dredging will be required to maintain the minimum depth for navigation
- The alternative waterway contains larger curvatures than the current route, making it more accessible for larger ships

To these (potential) advantages of the alternative shipping route, the following can be added based on the research presented in this thesis:

- Using the alternative waterway will lead to a reduced need to keep the Paraná de las Palmas at depth. Seizing or reducing these dredging activities will likely lead to less deposition in the channels located south of the Paraná de las Palmas and thus have a positive influence on the navigability of these channels.

Figure 6.1: Alternative entrance to the Paraná waterway: BGT and Canal Martin Garcia (Figure by Happee [2019])

6.2. Model limitations and future research

As mentioned, the modelling strategy chosen is based on gaining system-wide knowledge regarding the various different processes that influence channel morphodynamics in the Lower Delta. This rather broad approach does have the consequence that certain processes or behavioural aspects of the system are not captured. The following numbered list provides a description of the model limitations and specific recommendations concerning future research and modelling practices on the Lower Delta channel network:

1. In order to increase the accuracy with which the numerical model simulates reality, more validation data is needed. In the specific case of the Lower Delta channel network, discharge and/or velocity measurements inside the channels are valuable. Due to unforeseen circumstances, the number of times the author could execute ADCP measurements in the channel network was reduced to one. In order to, for example, measure the occurrence of hydraulic tidal divides, ADCP data covering a significant portion of the tidal cycle at multiple locations along a channel are highly preferred.

2. Several measured channel bed display longitudinal convex-upwards profiles, resembling patterns that imply the presence of a morphological and thus hydraulic tidal divide. Modelled bed level changes do not produce similar patterns, as the influence of fluvial forcing does not allow for semi-permanently calm conditions to exist in channels during regular conditions. Only during low discharge conditions and high water slack, hydraulic tidal divides are modelled. There can be several reasons for this inconsistency between modelled and observed behaviour:

    - The model does not produce tidal discharges inside a channel correctly, see point 1;
    - Natural processes that are not included in the model cause the modelled morphological patterns:
        - The abundance of vegetation in the middle reaches of the channels can significantly increase the hydraulic friction, leading to sediment deposition and a positive feedback mechanism inducing more vegetation growth (as described in Hypothesis 3);
        - Hydraulic friction in reality is depth dependent. In the model, one friction coefficient was selected for the channel network. In reality, the more shallow middle sections of the channels could cause more dissipation of tidal and fluvial energy than modelled, leading to sedimentation in the middle reaches.

3. In order to accurately model volumes and locations of sedimentary deposits, more bathymetrical data is needed taken at different times. This way it can be established where exactly most morphological changes take place.

4. It is probable that in the near-shore channels with relatively high velocities, sandy material is more abundant compared to the majority of the channel network (where the bed soil samples during the field surveys were taken, see Appendix I). In order to model the morphological development in these energetic channels, bed sediment analyses for these channels should be carried out and, depending on the soil characteristics, modelling practices might have to include a coarse, non-cohesive sediment fraction. Such a model is preferred to be three-dimensional, in order to prevent unrealistic amounts of sand that are in reality present in the bottom of the water column to enter the shallow channel network.

5. The limited domain used in the model disregards any 'communication' with excluded channels and river branches. For example, the Paraná Mini has its origin in the Paraná Guazú river branch. Hydraulic gradient changes associated with the deepening of the Paraná de las Palmas and/or high discharges will have an effect on the flow partitioning between the Paraná Guazú and the Paraná mini. In addition, the sediment supplied by the Paraná Mini to the channel network might be underestimated, as the Paraná Guazú can carry higher loads of suspended sediment and the concentration inside the Paraná Mini might not have adjusted to the equilibrium concentration associated with the low flow velocities in the Paraná Mini when the flow enters the channel network. For future modelling, increasing the model domain or using a nested approach could decrease these uncertainties.

6. Accurately modelling the effect of storm surges and the return flow requires including the floodplains in the model. The lateral discharge approach used in model scenario A3 caused non-physical flow to occur inside the channel network, leading to inaccurate model results. The storm surge model run without lateral discharge had a slight erosive effect on the channel network. It can be hypothesised that in reality the erosive effect will be higher, as there is no export of sediment in in the mentioned model run.

7. In order to assess the potential influence of dredging plumes supplying additional sediment to the channel network (hypothesis 5d), high resolution data on the flow conditions during the deposition of material is needed, as well as the exact method and material used during disposal.

8. Any three-dimensional processes, such as entrainment lag or bathymetry effects in the distribution of sediment at bifurcations, are not included in the model. Inclusion of a third dimension in future modelling practices can give insight in the relevance of such processes.

9. The consolidation state of the bed can play a large role in preventing the bed from eroding. Although the bed sediment samples taken during the field surveys were all soft, it is possible that at other locations, (weakly) consolidated clay forms the (under)layer of the bed. Taking more bed sediment samples at different locations and analysing them without de-flocculating the sample beforehand can give insight in the occurrence of consolidated layers in the Lower Delta (channel network).

10. The (small scale) morphological behaviour in the model in general is very dependent on initial conditions and the sediment parameters. Any numerical modelling practice is an approximation of reality. Especially in a dynamic system such as the Lower Paraná Delta, conditions and characteristics change with the variation in forcing. Sediment parameters and quantities are dependent on precipitation in the Bermejo Region, the friction factor can be highly variable in space and time due to bed forms, vegetation or (man-made) obstructions of the flow. In addition, the behaviour of the model at channel bifurcations or confluences is highly dependent on the conditions and chosen parameters. A good example of this is described in the model sensitivity analysis (Chapter 4) where changing the critical bed shear stress led to faster siltation in one channel and increased erosion in the other. In reality, an infinite amount of parameter values and characteristics are present in the a natural system, and the results of a numerical model of a complex system such as the Lower Paraná Delta must be interpreted accordingly.

7

Conclusion

In this chapter, the results of this research is summarized by answering the research questions as defined in Chapter 1, which are presented in bold below.

1. **What are the occurring patterns of sedimentation and erosion in the Lower Delta's secondary channel network?**

   (a) **What are the main sedimentary, morphological and hydraulic characteristics of the Lower Delta and its channel network?**

Hydraulic characteristics
The Lower Paraná Delta is a system both influenced by tidal and fluvial forcing. River discharge supplied by the Paraná river flows through the complex network of mostly natural channels, mostly in south-eastern direction. This leads to that most channels are supplied by a river branch located north of the channel. The micro-tidal, co-oscillating tide approaches the delta from the shallow, funnel-shaped Río de la Plata estuary and penetrates into the river network up to 400 km upstream. Various (terminal) channels located near the deltaic front attract relatively high river and tidal discharge, while more upstream located channels are generally subject to less energetic conditions.

Sedimentary characteristics
High loads of fine sediment, mostly originating from the Bermejo sub catchment in Bolivia, are transported to the Deltaic front, leading to progradation of the deltaic front and sedimentary deposits in the main river branches, the Río de la Plata estuary and the channel network. The muddy beds in the channel network consist of a mixture of silt, clay and fine sand, with silty fractions dominating the distribution of the samples obtained and analysed for this research. Nominal diameters of the muddy channel beds are in the order of 10 to 30 μm, while coarser sediment is present in the beds of the two main river branches, the Paraná Guazú and the Paraná de las Palmas.

Morphological characteristics
The main river branches have mild slopes of around 10e-5 over the length of the delta. The Paraná de las Palmas has an upward slope in the most downstream reach, where it transitions into the shallow Río de la Plata Estuary. Some of the measured bed levels (eg. Arroyo Caraguata, Arroyo Carapachay) in the channel network display convex-up profiles, with typical depths of 2 to 4 meters. Channels located more downstream (eg. Arroyo Pay Curaby, Canal Honda) are often deeper and are presumably kept at depth naturally by the higher fluvial and tidal energy. The islands separated by the channel network that comprise the Lower Delta have slight depressions in the middle and natural embankments near the watercourses. These characteristics are caused by the land-inward fining of sediment deposits during storm surges.

1. (b) **How do local hydrodynamic processes influence the occurring morphodynamic patterns?**

Fluvial processes
From the model results it follows that sedimentation is likely to occur in the channel entrances south of the Paraná de las Palmas, due to the deceleration of the flow that takes place when entering the channel network. Less sedimentation is expected to occur in the channel network north of Arroyo Pay Curaby. In various terminal channels, high sedimentation rates are likely to occur, manifested in mouth bar deposits.

Tidal processes
The numerical model has shown that the tide likely has an overall stabilizing influence on the channel network morphology, as it counteracts deposition in most channels, redistributing sediment over channel beds and exporting some of it into the main river branches and estuary. This effect is most noticeable in channels nearby the deltaic front, as the tidal energy is dampened with increasing distance from the shore. Convex-upward longitudinal bed level profiles in the channel network (subquestion 1a) could be the result of tidal divides occurring inside various channels. However, hydraulic and morphological tidal divides are not produced in the numerical model and hydraulic tidal divides only during low flow conditions, leaving the occurrence and influence of tidal divides an unanswered hypothesis.

Storm surges
During strong south-eastern winds ('Sudestadas'), the water level in the Río de la Plata and the Lower Delta can rise several meters. Every year, few of these storm surge events occur, causing the low lying islands separated by the channels to flood. During high water, some sedimentation in the channels occurs while the floodplains inundate. Sediment is deposited on the floodplains with land inward fining of the deposited fraction, causing the return flow during the falling stage to be sediment-poor and induce erosion in the channels. This second mechanism is expected to be dominant, leading to storm surges having a net erosive effect on the channel beds. A model scenario without a mechanism subtracting and adding flood water to the model resulted in net erosion compared to the base scenario. This implies that in reality, when sediment does leave the channel network, erosive capacities are potentially higher than modelled.

2. **How do climatic and meteorological variability and anthropogenic activities influence the morphodynamic development of the Lower Delta's secondary channel network**

   Subquestions 2a and 2b are answered together as both are related to increases in river discharge and sediment input.

   (a) **What is the influence of the El Niño Southern Oscillation phenomenon on the morphological development?**

   (b) **What is the influence of climate change scenarios on the future morphological development?**

Influence of climatic and ENSO and climate change on the river discharge and sediment supply
Periods of extreme river discharge mostly occur during El Niño years. Dredging reports indicate that during these periods, the input of sediment by the Paraná River into the Delta is significantly higher than during regular, non El Niño periods. IPCC scenarios indicate that the discharge of the Paraná River is likely to increase with 10 to 20 % by the end of the 21st century. These changes are expected to manifest in an intensification of rainfall and subsequent river discharge during El Niño years. There is a large uncertainty on the future sediment load of the Paraná River. Overall precipitation in the Bermejo region is expected to decrease, but the increase in intensity of rainfall events might increase the sediment load from the Bermejo region with up to 40%.

Influence of an increase in fluvial sediment supply on channel development
An increase in sediment load of the Paraná river will have an overall depositional effect. The model showed that a change in the sediment load primarily influences Arroyo Pay Curaby and the channels south of the Paraná de las Palmas as these are supplied by the energetic Paraná de las Palmas. Northern channels are to a lesser extent affected by changes in sediment load of the Paraná River. Figure 7.1 displays the general morphological response of the channel network to an increase in sediment supply.

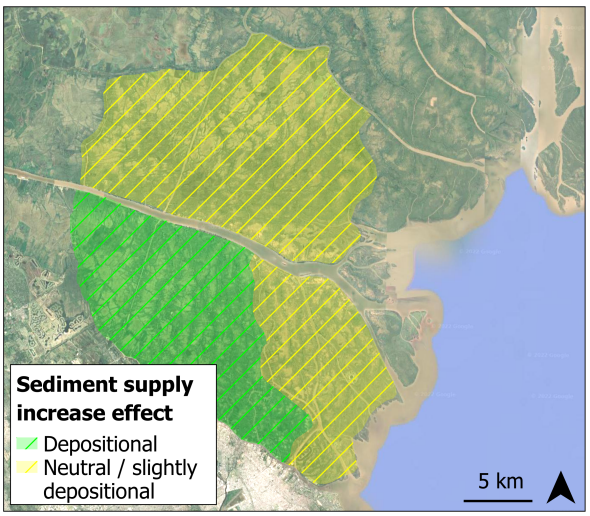

Figure 7.1: General morphological response to a sediment input increase

Modelling the discharge peak in 2016 provided insight in the behaviour of the system under extreme forcing. High discharge lead to a water level increase in the Paraná de las Palmas. The water levels in Río Luján and Paraná Mini do not increase as much, leading to a shift in the longshore hydraulic gradient. This increase in hydraulic gradient between the Paraná de las Palmas and Río Luján causes increased flow velocities and an overall erosive effect in the channel network south of the Las Palmas, as well as in Arroyo Pay Curaby. The channels north of the Paraná de las Palmas generally experience a very small increase or decrease in transport capacity, leading to similar bed level changes as during regular conditions. The spatial variation in the morphological response of varying discharge and sediment supply is displayed in Figure 7.2.

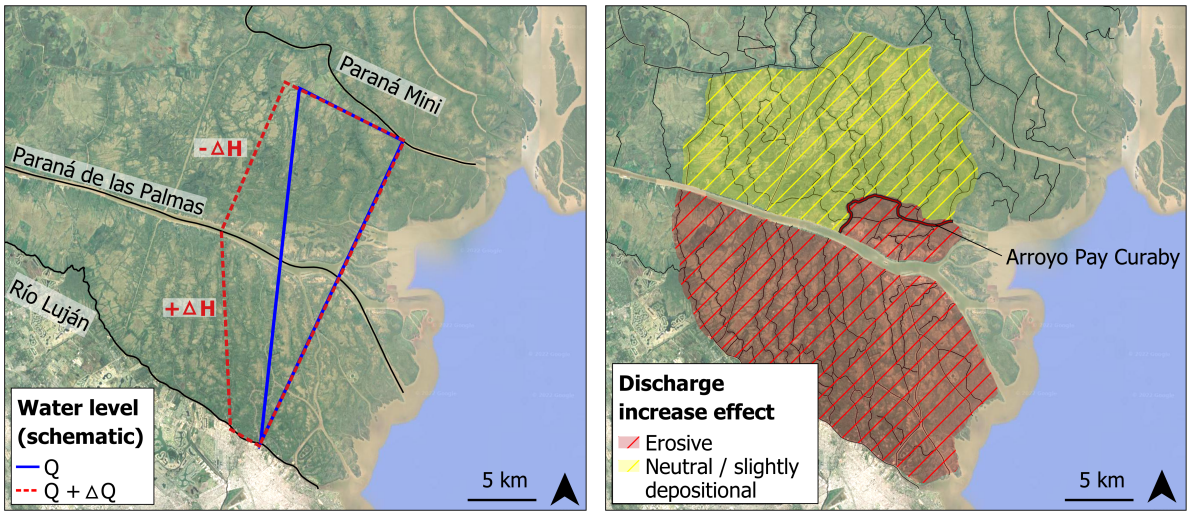

Figure 7.2: Overall hydraulic (left) and morphological (right) response to a discharge increase

2. (c) **What is the influence of anthropogenic activities on the morphological development?**

Land use change in the La Plata basin
Since 1960, extensive deforestation has caused an increase in surface runoff, contributing to the Paraná river discharge increase in the order of 30 to 40 %. In addition, land use change in the Bermejo region has caused the sediment load in the Paraná River to increase with approximately 30% during the same period. The effect of increases in sediment load and discharge were addressed under subquestions 2a and 2b and in Figure 7.1 and 7.2.

Deepening the Paraná de las Palmas
The most downstream located reach of the Paraná de las Palmas is artificially kept at depth in order to facilitate sea-going vessels to navigate upstream. The model results imply that deepening the Paraná de las Palmas has lead to decreased flow in Arroyo Pay Curaby and the channels south of the Paraná de las Palmas, leading to increased rates of sedimentation. Due to the increase in longshore in hydraulic gradient between the Paraná Mini and the Paraná de las Palmas, deepening the Paraná de las Palmas has leads to increased sediment transport capacities in channels between Pay Curaby and The Paraná Mini. The hydraulic and morphological response of dredging the Paraná de las Palmas is schematically depicted in Figure 7.3.

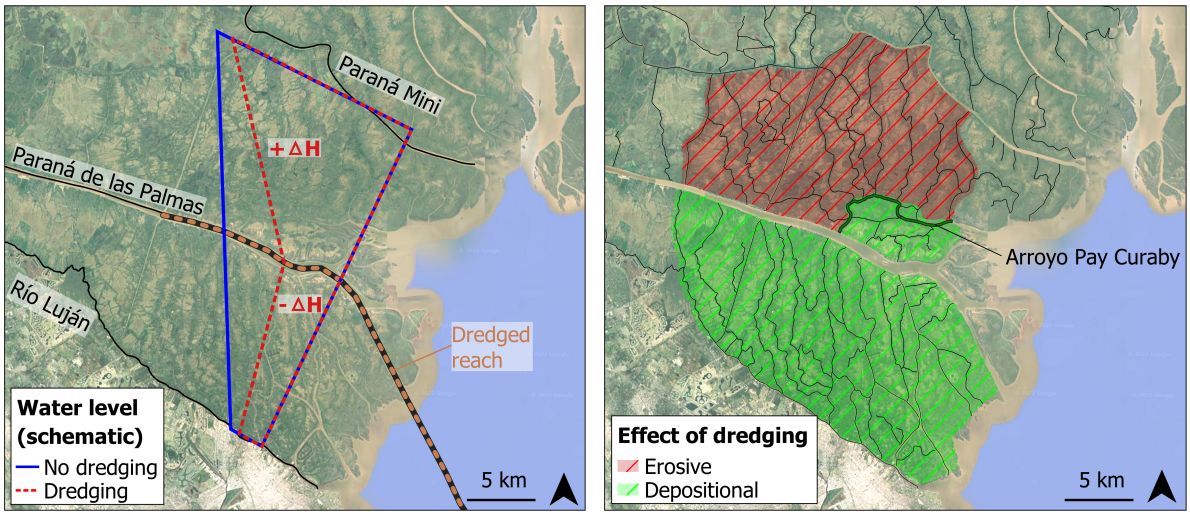

Figure 7.3: Hydraulic (left) and morphological (right) response to deepening the Paraná de las Palmas

Newly excavated channels
The excavation of several artificial channels in the early twentieth century is expected to have had negative influence on the discharge in the surrounding natural channels. The excavated channels attract and redirect flow, mostly connecting the main river branches (Paraná Mini, Paraná de las Palmas, Río Luján). Excluding the artificial channel Gobernador Arias led to a large decrease in discharge and water level in Río Luján, leading to a increase in hydraulic gradient between Paraná de Las Palmas and Luján and to significant erosion in the channel beds.

3. **Which of the morphodynamic patterns are limiting the navigability of the channel network?**

Naturally, depositional patterns are limiting to navigability. From the model base scenario simulating regular conditions, it follows that sedimentation is likely to occur in the channel entrances south of the Paraná de las Palmas, due to the deceleration of the flow that takes place when entering the channel network. Less sedimentation is expected to occur in the channel network north of Arroyo Pay Curaby.

Sedimentation occurring in the mouth of the various terminal channels, either mouth bar deposits or sedimentation over the entire channel width, are disadvantageous for navigability into and from the Río de la Plata estuary.

Deepening of the Paraná de las Palmas since 1990 has caused increased sedimentation in channels supplied by the Paraná de las Palmas, limiting the navigability in these channels. The excavation of new channels in the early 20th century has had a similar effect in channels nearby Canal Gobernador Arias and La Serna. Historic and (projected) future increases in river discharge have an opposite effect, as the shift in hydraulic gradient will likely lead to increased transport capacities in channels supplied by the Paraná de las Palmas.

A

Theoretical framework

A.1. Open Channel Flow

The movement of water is described by the Navier-Stokes (N-S) equations, which are based on mass conservation principles and three-dimensional momentum conservation. In order to mathematically describe water movement over large temporal and spatial scales, the N-S equations are often simplified. Depending on the application, specific terms in the N-S equations are neglected in order to make analysis feasible. A widely used approximation is the Long Wave or Shallow Water (SW) approximation. The SW equations are a set of hyperbolic partial differential equations that describe the movement of the free surface. An important criterion for the application of the SW approximation is that the characteristic horizontal scales (horizontal velocity, wavelength) greatly exceed the vertical scales (vertical velocity, water depth). This validates neglecting vertical acceleration in the equations of motion. In process-based numerical modelling of hydrodynamics, the LW equations are one of the main equations that are approximated. The LW equations are given in Equations (A.1), (A.2) and (A.3). More forcings can be added to the momentum equations such as a barotropic pressure term and coriolis.

The LW or SW approximation is used for many applications in natural, large scale phenomena relating to hydrodynamic flow. Examples of long waves are translatory waves, tsunamis, river flood waves and tidal waves, the latter two of which especially relevant when considering coastal, riverine and estuarine processes.

$$\frac{\partial \eta}{\partial t} + \frac{\partial hU}{\partial x} + \frac{\partial hV}{\partial y} \tag{A.1}$$

$$\frac{Du}{Dt} = \frac{\partial}{\partial x}\left(v_h \frac{\partial u}{\partial x}\right) + \frac{\partial}{\partial y}\left(v_h \frac{\partial u}{\partial y}\right) + \frac{\partial}{\partial z}\left(v_v \frac{\partial u}{\partial z}\right) - g\frac{\partial \eta}{\partial x} - \frac{1}{\rho_0}\frac{\partial p_{atm}}{\partial x} \tag{A.2}$$

$$\frac{Dv}{Dt} = \frac{\partial}{\partial x}\left(v_h \frac{\partial v}{\partial x}\right) + \frac{\partial}{\partial y}\left(v_h \frac{\partial v}{\partial y}\right) + \frac{\partial}{\partial z}\left(v_v \frac{\partial v}{\partial z}\right) - g\frac{\partial \eta}{\partial y} - \frac{1}{\rho_0}\frac{\partial p_{atm}}{\partial y} \tag{A.3}$$

When describing the orientation of water levels, the conventional description as displayed in Figure A.1 is used. Water surface elevation ζ is described in relation to a fixed reference level. Instantaneous water level h is the sum of ζ and the water depth in relation to the reference level.

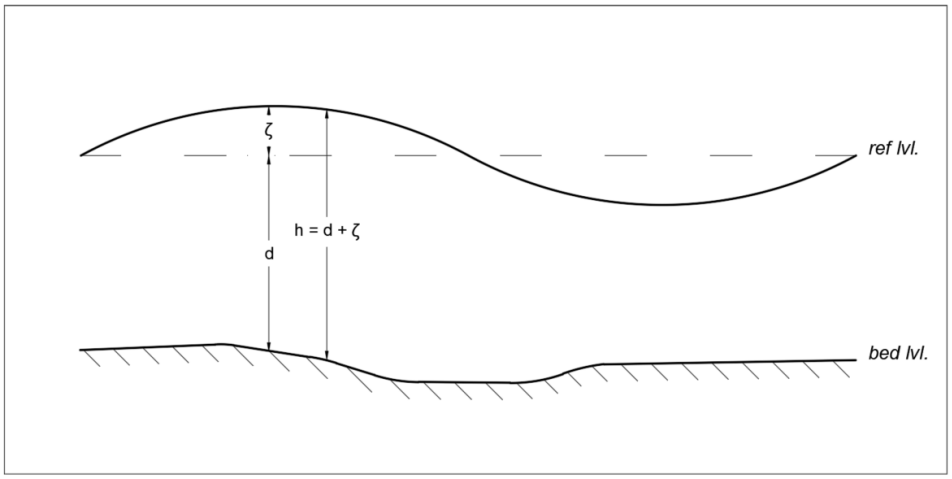

Figure A.1: Reference levels defintions

A.1.1. Long wave propagation

The propagation speed c of a long wave can be derived by differentiating the one dimensional momentum equation with respect to time and the continuity equation with respect to the spatial dimension s, resulting in a secondary partial differential equation (the **elementary wave equation**, Equation (A.4)), describing a perturbation in the water level to propagate with velocity $c_0 = \sqrt{\frac{gA_c}{B}}$, which in the case of a rectangular cross section reduces to $c_0 = \sqrt{gh}$. This relation can be used as a first order approximation of the celerity of a tidal wave. Note that in this approximation, the effect of non-linearities and friction are not incorporated, hence the subscript 0.

$$\frac{\partial^2 2h}{\partial t^2} = c_0^2 \frac{\partial^2 h}{\partial s^2} \tag{A.4}$$

The discharge associated with long wave propagation is equal to $Q = B \cdot c \cdot \zeta$, with ζ the surface elevation anomaly or wave amplitude. Assuming that in a long wave, the flow velocities are evenly distributed over the depth, this leads to a velocity of $U = \frac{Q}{B \cdot h} = \frac{B \cdot c \cdot \zeta}{B \cdot h}$, substituting $c = c_0 = \sqrt{gh}$ gives the formulation of the characteristic magnitude of flow velocity associated with a long (eg. tidal) wave, see Equation A.5.

$$\hat{U} = \hat{\zeta}\sqrt{g/h} \tag{A.5}$$

A.1.2. Tidal propagation through a canal

Formulations of a tidal wave propagating through a canal are presented below. The assumptions valid for this approaches are:

- Linear wave ($\zeta << h$)
- Uni-directional wave, spatial coordinate s
- Sinusoidal wave in the form $\zeta(s,t) = \hat{\zeta}(s)\cos(\omega t - ks + \alpha)$
- Propagation through a infinitely long channel, i.e. no reflection occurs. This assumption is valid in a tidal river.
- Linear friction, proportional to the flow velocity or discharge, the form $\sigma = \frac{8}{3/\pi} c_f \frac{\hat{Q}}{\omega A_c R} = \frac{8}{3/\pi} c_f \frac{\hat{U}}{\omega R} Q)$ and $\delta = \frac{1}{2}\arctan\sigma$

Frictionless harmonic wave

When neglecting friction, the discharge related to a tidal wave is simply $Q = B \cdot c \cdot \zeta$, i.e. the discharge and velocity are in phase with the surface level elevation.

Harmonic wave including friction
When a tidal wave enters shallow waters, the influence of the bottom friction starts to play a significant role in the propagation and the shape of the wave. The influence of friction is demonstrated by considering the analytical formulation of a tidal wave propagating through a canal/river branch. Formulations for wave related surface elevation $\tilde{\zeta}(s,t)$ and discharge $\tilde{Q}(s,t)$ are dependant on time t and location along the channel axis s. Linear friction is assumed, proportional to the flow velocity or discharge, the form $\sigma = \frac{8}{3/\pi} c_f \frac{\hat{Q}}{\omega A_c R} = \frac{8}{3/\pi} c_f \frac{\hat{U}}{\omega R}$) and $\delta = \frac{1}{2} \arctan \sigma$. The full derivation is presented in Battjes and Labeur [2017].

$$\tilde{\zeta}(s,t) = \hat{\zeta}^{+}(s) \cos(\omega t - ks + \alpha) + 0 \tag{A.6}$$

$$\hat{\zeta}^{+}(s) = \hat{\zeta}^{+}(s=0) \exp -\mu s \tag{A.7}$$

The space dependency of the wave amplitude $\hat{\zeta}^{+}(s)$ comes from friction, dampening the wave as it propagates further in the channel. In the case of a spatially uniform cross-section, the damping leads to an exponentially decaying surface elevation $\tilde{\zeta}$ along the channel axis according to Equation (A.7).

$$\tilde{Q}(s,t) = \tilde{Q}^{+} + \tilde{Q}^{-} = Bc\hat{\zeta}^{+}(s) \cdot \cos(\omega t - ks + \alpha + \delta \cos(\delta) + 0 \tag{A.8}$$

Where in the frictionless case the discharge Q was in phase with the surface level elevation, when including the linear friction term the phase of the dischare advances in by an angle δ.
With the initial phase at $s = 0$ equal to α and the damping modulus μ related to the linear friction and proportional to the wave number via $\mu = k \tan \delta$.

When including the linear friction term in the linearized wave equation, the wave celerity under the influence of friction c can be derived, and is displayed in Equation (A.9).

$$c = c_0 \cdot \sqrt{1 - \tan^2(\delta)} \tag{A.9}$$

Tidal amplification
In many alluvial rivers, the result of a exponentially decaying discharge distribution over the river reach is a decrease sediment transport capacity along the river's axis. The long-term morphological response of the estuary is the development of an exponentially decreasing conveyance area, or a typical 'funnel' shaped estuary. Most alluvial tidal rivers are in a such a state of near-equilibrium characterized by a uniform distribution of the maximum tidal current velocities and surface elvation amplitudes along the river. A detailed description of this mechanism is given by Savenije [2005].

A.2. Sediment transport

A.2.1. Sediment and soil classification

Sediments are traditionally classified according to the mass-equivalent (nominal) diameter d_n or median diameter d_{50} of an individual particle. The main types of marine and fluvial environments are sand, silt, and clay. In estuarine environments, organic material can take up significant fractions of the soil. Table A.1 displays the widely used grain size based classification of sediments by the American Geophysical Union.

The silt-sand demarcation separates cohesive from non-cohesive sediments, as silt and clay particles can display tendencies to assemble into flocs, settling more rapidly than the individual particles. The physical principle behind cohesiveness is the limited relative magnitude of the gravitational force on a small particle versus the electromagnetic Van der Waals forces, which is unidirectional and can lead in attraction between particles. The 'flaky' or 'pallete' - like shape of individual clay particles make for additional cohesiveness, as surface forces dominate gravitational forces.

Table A.1: Grain size classification by American Geophysical Union

	d_n [mm]	Cohesiveness
Coarse sand	0.5 - 2	Non-cohesive
Fine sand	0.063 - 0.5	Non-cohesive
Coarse silt	0.032-0.063	Sometimes cohesive
Fine silt	0.008-0.033	Weakly cohesive
Clay + very fine silt	< 0.008	Cohesive

In estuarine environments, cohesive sediments will always play some role in the shaping of the system. The composition of soil mixtures can vary spatially and temporarily due to varying conditions. A soil mixture classificaiton based on composition percantages of different grain types was taken from van Rijn [2020] and repeated in Table A.2. Generally, sand-mud mixtures start to behave cohesively at clay contents higher than 5 to 10%. More on the implications of cohesive sediment dynamics is given in Section A.2.5.

Table A.2: Mud-sand classification by van Rijn [2020]

	Cohesiveness [mm]	% Organic material	Clay + Fine silt	Silt	Sand
Sand	Non-cohesive	0 %	0 %	0 %	100 %
Muddy sand	Weakly cohesive	0 - 10 %	0 - 5 %	20 - 40 %	60 - 80 %
Sandy Mud	Cohesive	0 - 10 %	5 - 10 %	30 - 60 %	60 - 30 %
Mud	Cohesive	0 - 20 %	10 - 20 %	50 - 70 %	0 - 10 %
Silty mud	Cohesive	0 - 20 %	10 - 40 %	60 - 80 %	0 %
Clayey Mud	Cohesive	0 - 20 %	40 - 60 %	40 - 60 %	0 %

A.2.2. Initiation of motion

Sediment particles will start moving when the bed shear stress τ_b on a grain of sediment exceeds a certain treshold value. For non-cohesive sediments, the only force counteracting the movement due to waves or currents is gravity. The bed shear stress is intrinsically related to the flow velocity u and the density of water ρ via a non-dimensional friction factor c_f, see Equation (A.10). As the bed shear stress τ_b is proportional to the square of the flow velocity, there exists a critical flow velocity u_{cr} for which a particle starts to move.

$$\tau_b = c_f \rho u^2 \tag{A.10}$$

Shields (source) introduced a parameter θ_{cr} that relates the critical shear stress to the soil characteristics. He found that typical values of the critical shields factor lie between 0.03 and 0.06. The validity of this empirical constant ceases to be valid in the case of laminar flow, bed ripples, non-uniform flow, poorly sorted sediment and cohesive sediment, however it still provides aid in estimating the critical velocities of granulate sediments in environmental open channel flow.

$$\theta_{cr} = \frac{\tau_{b,cr}}{(\rho_s - \rho) g D} = C \tag{A.11}$$

The friction factor c_f introduced in the previous section, is an non-dimensional coefficient relating bed stress to the flow conditions. In many formulations describing hydrodynamics, the shear velocity u_* is used. This non-physical parameter has the unit of velocity (m/s) but it represents the shear stress. The shear velocity is related to the velocity and bed shear stress via Equation (A.12).

$$\begin{aligned} u_* &= \frac{\sqrt{\tau_b}}{\rho} \rightarrow \tau_b = \rho u_*^2 \\ u_* &= u\sqrt{c_f} \end{aligned} \tag{A.12}$$

In traditional hydraulics, empirical relations are used to quantify this proportionality, the most famous and widely used examples being Chezy (Equation (A.13)) and Manning (Equation (A.14)). *p. 25 bed bank shore protection.* These formulations are widely used in hydrodynamic theory and modelling practices. Typical values of the manning and Chezy coefficients for low-lying, natural rivers and streams

are in the order of 35 - 70 $m^{1/2}/s$ (C, Chezy) and 0.015 - 0.02 $s/m^{1/3}$ (n, Manning) [Shaw, 1999]. For muddy, hydraulically smooth beds, typical values of n are in the order of 0.01 [van Maren et al., 2015b]. Equivalent dimensionless friction coefficients c_f are in the range of 0.005 - 0.04 and around 0.002 for smooth muddy beds.

$$\overline{u} = C\sqrt{Ri_w}$$
$$C = \sqrt{\frac{g}{c_f}} \tag{A.13}$$

$$\overline{u} = \frac{1/n}{R}^{2/3}\sqrt{i_w}$$
$$n = R^{1/6}\sqrt{\frac{c_f}{g}} \tag{A.14}$$

A.2.3. Transport modes

Sediment transport mode classification can be done by considering the transport mechanism or the origin of the material (Figure A.2). Bed material load are particles that are the same size and type of the material that composes the bed. Bed material load can be transported as bed load, rolling and sliding over the bed, or in suspension. Wash load is very fine material (fine silt and clay) that only settles during very low or non existent flow.

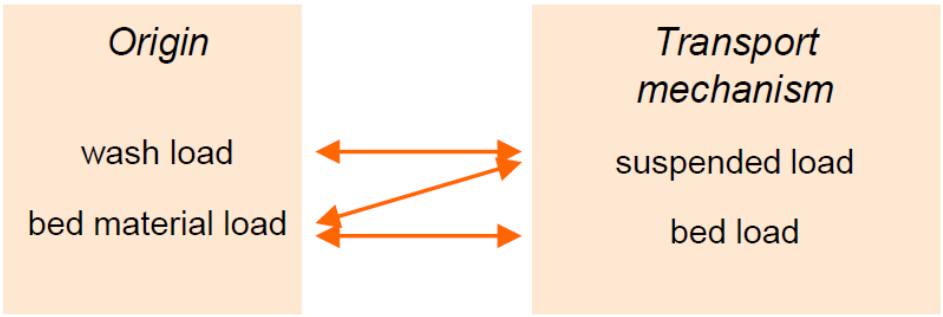

Figure A.2: Transport modes [Blom, 2019]

A.2.4. Suspended sediment transport

Silt, clay and finer sand fractions are often transported in suspension. The sediment is put and kept in suspension by turbulent motions induced by lateral flow velocity gradients. The net vertical transport due to these turbulent fluctuations is balanced by the settling of particles due to gravity. The Rouse number Rou is a dimensionless number used to approximate this concentration profile of the sediment concentration in a water column. $Rou = \frac{\sigma_T w_s}{\kappa u_*}$ is the ratio between the sediment fall velocity and the upwards turbulent fluctuations, represented by the von Karman Coefficient κ and shear velocity u_*. The Rouse number represents determines the equilibrium concentration profile c_e. This is demonstrated in Equation (A.15) and typical Rouse profiles are displayed in Figure A.3.

$$c = c_e = c_a\left(\frac{a}{h-a}\frac{h-z}{z}\right)^{\frac{\sigma_T w_s}{\kappa u_*}} \tag{A.15}$$

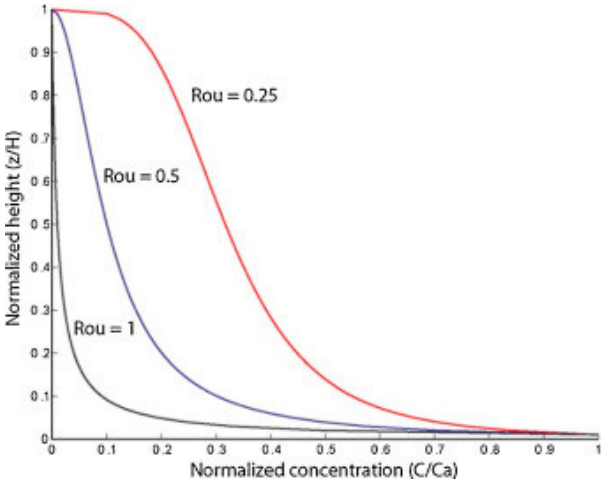

Figure A.3: Typical Rouse profiles Teles et al. [2016]

When describing the gradients in suspended sediment transport, distinction must be made between (quasi) equilibrium transport and non-equilibrium transport. **Equilibrium transport** refers to a situation where there are no spatial gradients in sediment transport quantities, i.e. net sedimentation and erosion are zero. Equilibrium transport is a concept that does not occur in large, natural systems due to the presence of spatial and temporal gradients in forcings and conditions. **Quasi equilibrium transport** refers to the type of transport that is solely determined by local flow conditions, i.e. the rate of sediment transport at a certain location directly responds to the sediment transport capacity of the current. This type of transport is based on the notion that the fall velocity of a particle w_s is large enough to greatly exceed the timescale of change in forcing. This implies that quasi equilibrium transport is applicable to sediment with large settling velocity, i.e. coarse fractions. Generally, suspended load of bed material can be considered quasi-equilibrium transport. In quasi equilibrium transport, erosion and/or sedimentation do occur, and is only determined by local hydrodynamic conditions. Resulting from this notion is the assumption that the sediment flux can be approximated by equating the sediment concentration c to the equilibrium concentration c_e. Changes in morphology could thus be approximated/modelled by only considering the spatial gradient in hydrodynamic forcing, see Equation (A.16).

$$\frac{\partial s}{\partial x} = \frac{\partial ucd}{\partial x} \approx \frac{\partial uc_e d}{\partial x} \tag{A.16}$$

Non-equilibrium transport refers to the situation where the fall velocity of the sediment is sufficiently small to cause a significant time lag in the change of hydrodynamic conditions and bed level and thus in erosion or deposition rates. These conditions make the assumptions underlying the equilibrium (Rouse) concentration profile invalid. The fine clay and silt particles are transported as wash load, and are generally uniformly distributed over the water column. Due to the time dependency of the settling process, a transport equation of the form advection-diffusion equation must be solved in order to approximate/model gradients in sediment transport and subsequent changes in bathymetry. Equation (A.17) represents a generic 2 dimensional transport equation.

$$\frac{\partial c}{\partial t} + \frac{\partial uc}{\partial x} + \frac{\partial vc}{\partial y} + \frac{\partial}{\partial x}\left(\epsilon_x \frac{\partial c}{\partial x}\right) - \frac{\partial}{\partial y}\left(\epsilon_y \frac{\partial c}{\partial y}\right) = S \tag{A.17}$$

A.2.5. Muddy beds

Flocculation

Cohesive particles can display tendencies to assemble into flocs, settling more rapidly than the individual particles. This flocculation process can be initiated and amplified by high suspended sediment concentrations and the presence of a chemical coagulant (salt in estuarine environments)

Consolidation

Consolidation is a basic occuring processing in low-energy environments with muddy (mixture of clay, silt and sand) soil. Fundamentally, consolidation is the downward movement of soil particles and the

upward movement of pore water, resulting in a strengthened bond between the particles and a (much) higher critical shear stress needed to erode. The consolidation process can be divided into various distinct phases [Rijn and Barth, 2018]:

- Hindered settling; particles and flocs move downward in the water column, hindered by upward moving displaced water. Density is approximately 10 to 150 kg/m^{3}m, timescale is hours
- Transitional phase during which the particles form a slurry, the settling velocity decreases. Density is approximately 150 kg/m^3, timescale is days
- Weakly consolidated: Primary consolidation phase, pore water starts flowing out, a 'buttery type' matrix is formed. Density is approximately 600 kg/m^3, timescale is weeks to months.
- Firmly consolidated: Secondary consolidation phase, the soil network further strengthens to firm soil. Density is approximately 1100 kg/m^3, timescale is months to years.

Erosion
For muddy beds, three main types of erosion can be distinguished [van Rijn, 2020] [Winterwerp et al., 2012]:

- **Floc erosion** is the pick up of individual particles and flocs from the fluffy toplayer. Turbulent fluctuations are the main instigators of this erosion type. Floc erosion could be seen as an equivalent of the pick up of individual, non-cohesive sediment particles, however depending on the relative intensity of the turbulent fluctuations, floc erosion may already occur when $\tau b < \tau cr$. Typical values for τb lie around 0.10 to 0.15 N/m^2.
- **Surface erosion** occurs after the structural failure of a network of particles and/or flocs, leading to the movement of one or more layers of soil. Surface erosion is said to occur at higher values of bed shear stress ($\tau_b = 1.5$ to $3\tau cr$). Surface erosion is a drained process.
- **Mass erosion** is the undrained process occurring when the fluid stresses in the soil exceed the undrained soil strenghts, large lumps of bed material start moving, exposing deeper soil layers. Mass erosion can start occurring at $\tau_b > 3\tau cr$

Critical bed shear stresses for weakly consolidated mud for surface erosion and mass erosion are in the order of 0.35 and 0.9 N/m^2, respectively. Firmly consolidated mud has a critical bed shear stress of around 1 to 1.5 N/m^2 [van Rijn, 2020].

A.3. Riverine processes

A.3.1. Dynamic equilibrium

The equilibrium state of a river or river reach is defined as the state that the river flow, sediment supply and bed level approach during constant values of upstream river discharge and downstream water level. In equilibrium flow, the bed slope is equal to the hydraulic slope, implying a constant sediment composition and morphology. This theoretical principle helps in understanding the one dimensional, large scale behaviour of a river reach and the fluvial sediment it carries. Equilibrium flow parameters are derived by balancing the stream-wise component of gravitational force on the water column with the friction induced by the flow over the bed. The result of this derivation leads to an expression of the equilibrium, or 'normal' flow depth d_e, whch is given in Equation (A.18).

$$d_e = \left(\frac{q^2}{g} \frac{c_f}{i_b} \right)^{1/3} \tag{A.18}$$

In a real, physical rivers system, equilibrium flow is never truly reached as conditions are never constant in time. Variation in precipitation and catchment characteristics impose non-steady discharge forcing on a river system, tidal fluctuations and offshore meteorological events cause downstream located variations in time. By taking into account the temporal variations in a natural river, Van Bendegom and De Vries supplemented the equilibrium theory. The concept is based on the notion that the timescale of morphological changes greatly exceeds discharge variability. Therefore in a dynamic equilibrium,

several discharge regimes can lead to a stable morphological state where all sediment supplied from upstream can be transported.

Deviations from a (dynamic) equilibrium state will induce morphological changes that make the river approach its equilibrium state. Long-term morphological changes can have various causes, all of which fundamentally change a parameter of the equilibrium state (Equation (A.18)). Without (yet) considering the different causes of long-term change in the Paraná Delta, a morphodynamic pattern seemingly applicable to the Paraná Delta is presented in Figure A.4. It displays two backwater curves, one of which can occur in subcritical flow. the M1 backwater curve (blue) is present when the downstream boundary exceeds the equilibrium flow depth. The water depth increases downstream, implying downstream a downstream reduction in flow velocity and transport capacity, leading to sedimentation. The M2 backwater curve (red) induces accelerating flow and can thus induce erosive patterns at the downstream end.

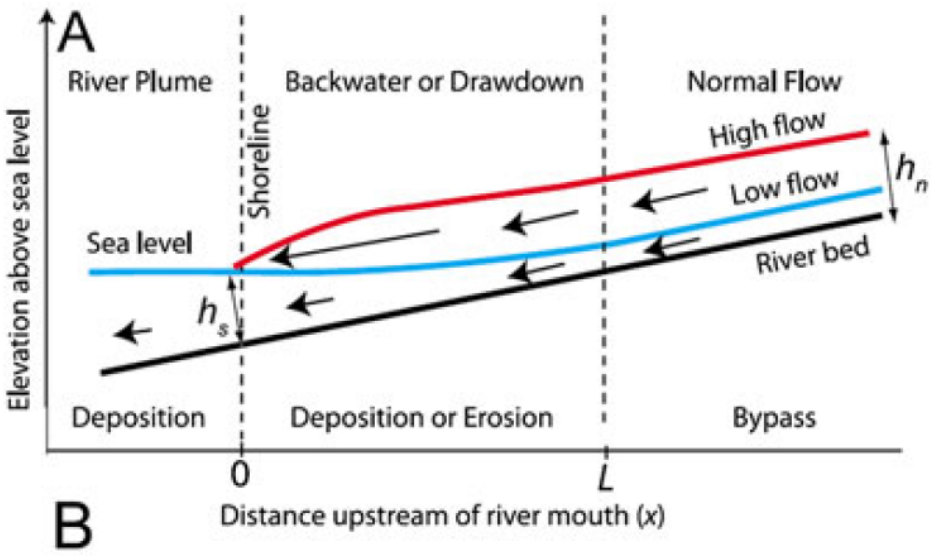

Figure A.4: Backwater curves for varying river discharges [Hoitink and Jay, 2016]

A.3.2. Confluences and bifurcations

Confluences and bifurcations are typical features of river systems, both are schematically depicted in Figure A.5.

At confluences, the difference between the regimes Q_3' and Q_2' is a dominating factor. For $Q_1' > Q_2'$ strong backwater effects can be found in river 2'. Hence the supply of sediment from river 2' to the main river 0' can be irregular. Therefore in river 2' there is direct link between Q_2 and S_2' near the confluence Jansen [1979].

The discharge distribution at a bifurcation is such that the water levels at the bifurcation match. Therefore downstream characteristics and boundary conditions are a determining factor, especially in short channels where backwater effects can be noticeable. The local characteristics upstream at at the bifurcation can play a large role in the distribution of sediment between the two arms. Four typical mechanisms influencing the sediment distribution are described below Mosselman [2020].

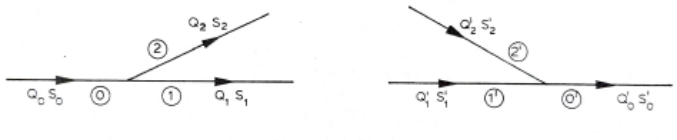

Figure A.5: Schematic depiction of a bifurcation (left) and confluence Jansen [1979]

1. **Bulle effect**

In 1962, Bulle found that a disproportionate amount of bedload entered a lateral irrigation channel, while the main channel continued its course. This can be explained by the occurrence of helical flow due to curved streamlines. This helical flow copmrises of an outward surface flow and an inward bottom flow. As more sediment is present at the lower part of the water column and on the bed, more sediment is transported into the side channel Mosselman [2020]. The main control of the Bulle effect is the angle between the main channel and the bifurcations.

2. **Gravity pull along bed slopes** When the slope of the bed is higher towards a river branch, gravity will cause a larger amount of bed load to enter this branch.

3. **Asymmetrical approach conditions**

   If the bathymetric or the granulometric characteristics vary over the width of the river approaching a bifurcation, this will influence the distribution of sediment over the downstream branches. Course sediment is less likely to be picked up, therefore if coarse material is predominantly located at one side of the approach channel, the downstream reach at this side will retrieve less sediment. The same is true for varying depths over the width of the approach channel, as flow velocities and thus sediment transport rates are larger in deeper water. These are dominant mechanism at the Pannerdensche Kop in the Dutch Rhine.

4. **Flow separation**

   Bifurcation channels with sharp angles in relation to the main channel can cause flow separation and eddy formation. The eddy will attract sediment, resulting in sedimentation at the location of the eddy. This sedimentation can 'squeeze' the entrance of the bifurcation, resulting in a more narrow bifurcation entrance and thus negatively influencing the conveyance capacity of the bifurcation.

In a one-dimensional analysis of a river reach, these effects on the sediment distribution can be imposed via a nodal point relation (Equation **x)**, describing the disproportionality of the sediment and discharge distribution via an exponent p.

$$\frac{Q_{s1}}{Q_{s2}} = \left(\frac{Q_1}{Q_2}\right) \tag{A.19}$$

A.4. Tidal processes

A.4.1. Tidal asymmetry

As a tidal wave approaches more shallow waters, the amplitude to depth ratio becomes larger, reducing the applicability of the linear wave assumption. As the shallow water wave length equals $c = \sqrt{g(h+\eta)}$, the relative effect of η increases, the crest of the wave will propagate with a higher velocity resulting in an asymmetrical tidal signal. The peak of the wave will heighten and the crest of the wave will flatten. The duration of the flood phase will decrease, while the duration of the ebb phase increases. This principle will cause increased flow velocities during the flood phase, and as as sediment transport generally obeys a power law, net transport of fines into the direction of the tidal flood wave will occur. This phenomenon is called **flood dominance**. In a case where intertidal storage areas are present, the friction caused by these shallow areas may decrease flood tide velocities significantly, to the case where they are exceeded by ebb velocities. Net transport of sediment will be in the direction of the ebb flow, hence it is called **ebb dominance**. As the concept of sediment transport being only dependant on the local flow conditions imply quasi equilibrium flow conditions, flood and ebb dominance have a predominant effect on medium to coarse sediments.

Another type of asymmetry considers the difference in high and low slack water periods. This type of saw tooth-asymmetry around the horizontal originates from the dependency of the temporal gradient in velocity $\frac{\partial u}{\partial t}$ on the landward basin area and conveying cross section. In the case of little intertidal storage and shallow channels, high water slack duration is longer than low water slack. The inverse is true at a basin where vast storage-offering tidal flats and deep channels are present. Due to the time dependency of fine sediment dynamics, this type of asymmetry is dominant in influencing net tidal im- or export of fine, suspended matter.

A.5. Estuarine aspects

There are various definitions for the term 'estuary', all of which exhibit small differences in the defining characteristics. Some state that estuarine waters must per definition be significantly influenced by the salinity of the oceanic waters [Wolanski, 2007]. However, due to the size of the Río de la Plata, salinity intrusion is negligible near the deltaic region. For the sake of clarity, the submerged Río de la Plata will be called an 'estuary' throughout this research, and the areas of land around the river channels conveying water and sediment into the estuary will be called the 'delta'.

One way to distinguish between estuarine features at a large scale is by considering the magnitude of the influence different physical processes have in the formation and behaviour of the system. This process-based classification of estuaries considers the fluvial, wave and tidal influences on the coastal region and establishes typical geometrical, sedimentary and morphological characteristics. A first distinction is made between shoreline progression or transgression. Transgression is shoreline retreat due to a rise in sea level and/or insufficient sediment supply. A progradating coast is characterized by a falling sea level and/or abundant sediment supply. In the prograding case, alluvial sediment deposits at the river mouth due to decreased flow velocities. With low tidal and wave energy, the sediment forms elongated banks next to its main course. at high river discharges, the bank will overflow and new channels can be formed, resulting in a bird foot type of coastal shape. In the presence of predominantly tidal or wave energy, respectively tidal flats or elongated features caused by longshore currents can be observed. In the transgressive case, the coast will more probably have a typical estuarine, funnel-shaped geometry. The sediment at the deltaic front does not have to be predominantly fluvial, as flood tides and/or waves can bring in sediment from the sea. Typical coastal features in wave dominated regime sandy barriers redistributing fluvial sediment along the coast, possibly resulting in low-energy lagoons. Tide dominated transgressive coasts will have pronounced tidal channels and bars, formed by the strong tidal currents directed perpendicular to the coast [Bosboom and Stive, 2015]. Figure A.6 displays typical features based on estuarine classification based on forcing.

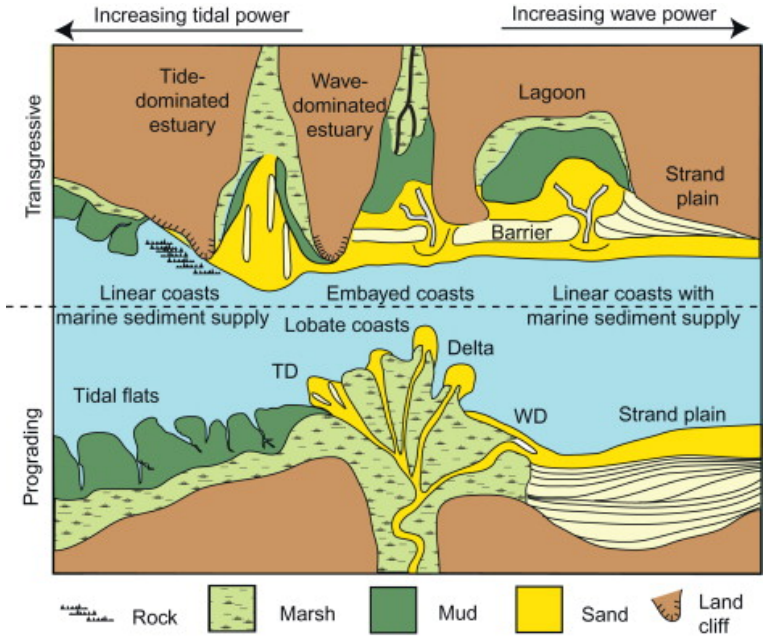

Figure A.6: Coastal shapes for different process-based classifications Harris et al. [2012]

A.5.1. River or tidal dominated channels

In a natural estuarine system, connected channels are in constant competition with neighbouring channels, attracting flow and sediment carried by the flow. This competition indicates that the (morpho)dynamics of a single channel can not not considered independently from neighbouring channels [Cathcart, 2019]. From an energetic point of view, one could state that there is only a certain amount of potential hydrodynamic energy available to transport the sediment supplied from upstream through the channel. Channel abandonment is a naturally occurring phenomena of which irreversible accreting patterns lay

at the basis. Deeper channels will attract more flow, causing more shallow channels to fill up and eventually close off. The abandonment of channels can be initiated by the alteration of main flow directions (avulsion) or historic changes in sediment supply [Gugliotta et al., 2021]. The timescales at which channel (networks) respond to changes in water and/or sediment supply vary from decades to millennia [Cathcart, 2019].

Across a delta plain, multiple relative magnitudes of forcings (river, tide or wave) can vary, locally effecting morphologies of individual channels. In a channel where river discharge dominates the flow regime, morphological patterns related to the equilibrium theory could be observed, such as the natural tendency to form a uniform bed slope, with morphological changes often starting downstream and propagating upstream. Another typical characteristic is the downstream fining of sediment, caused by the general deceleration of flow in the downstream direction.

When considering only riverine equilibrium theory, it can be understood that river-dominated deltas stimulate the continuation or growth of main river branches at the cost of small distributaries. The equilibrium flow velocity u_e is proportional to $\sqrt{d_e}$, eg. an increase in depth due to erosion of a factor 1.1 leads to an increase in discharge and flow velocity of $\sqrt{1.1}$ and erosive capacity (bed shear stress) of 1.1. This can lead to more erosion and thus more flow being attracted to the channel in question. In practice, this leads to river-dominated deltas to contain relatively few distributary channels. However, two mechanisms in fluvial dominated areas can be responsible for the formation of distributary channels. Mouth bar formation occurs when sediment carried by the river is directly deposited at the river mouth, causing a local obstruction of the flow and forcing the river to bifurcate [Mikhailov, 1966]. The second mechanism is avulsion, which occurs during high discharge events. When a river is flooded, a part of the flow changes direction due to a slope advantage, causing the river to bifurcate, and possibly abandoning its original channel [Stouthamer et al., 2011].

The influence of the tide on the morphology of channels is less well-understood compared to fluvial dominated channels. Tidal motion through distributary channels can have a net deposotional effect if there is an abundant supply of sediment in the nearshore region. If this is not the case, tidal motion can have a modulating effect on the channel morphology, counteracting fluvial deposition. When tidal amplitudes reduce in the upstream direction, this potential modulating effect increases in the downstream direction, often causing upstream channels to silt up more than more nearshore located channels. Tidal divides can play a role in defining locations of high depositional volumes, in turn influencing water and sediment flow patterns into other channels in the delta.

The following list is a summary of typical characteristics of distributary channels formed by fluvial (channel bar, avulsion) and tidal processes. It is based on a description by Kästner et al. [2017], who more thoroughly assesses these characteristics, as well as the relevant historic literature. Figure A.7 displays three examples of the channel types, all from the Paraná Delta.

1. Mouth bar channels (fluvial)
    - Fractal appearance
    - Wide and shallow
    - Width and depth decrease in downstream direction due to decreasing discharge with bifurcation order
    - Requires sufficient fluvial sediment input
2. Avulsion (fluvial)
    - Anabranching pattern if frequency of avulsion is higher than channel abandonment
    - Width to depth ratio similar to single thread rivers
3. Tidal creek
    - Channels branch off in perpendicular directions
    - Channels interconnect to form islands
    - Channel inlet size related to tidal prism, therefore depth reducing in upstream direction

- Strongly meandering, reducing in downstream direction
- Very low width to depth ratio
- Possible downstream coarsening of bed sediment

Figure A.7: Mouth bar channels at the Paraná de las Palmas mouth (a), indications of avulsions in the Middle Paraná Delta (b), tidal creek at the deltaic front (c)

B

Sedimentological and geomorphical analysis

This analysis on the sedimentological characteristics and geomorphology of the Paraná River and its delta contains the outcome of multiple sources and the data analysis. This chapter and its most important points is summarized in Chapter 2.

B.1. Geomorphology of the Parana Delta

The geomorphological evolution of the Paraná delta occurred during the Holocene, and it comprises of four main phases. Its current phase can be described as *a fluvial period with channel deposits and deltaic deposits advancing into the Río de la Plata*. The subaerial delta has a gentle slope 10^{-5} in the upstream direction.

The Lower Delta, indicated with 'delta' in Figure B.1, consists of islands separated by wide channels with naturally developed levees. The islands and levees consist of fine sands or silt, with the finer sediments located in the island centres. The substratum contains of fine sand, carried as bed load by the Paraná River. This fine sand and silty material form a more or less continues body of soil to a depth of 5 m. The areas around the main river branches (indicated with 'Bar-and-meander belts in Figure B.1) have less homogeneous stratigraphic characteristics due to the more energetic fluvial conditions. Typical stratigraphic profiles are given in Figure B.1 [Iriondo, 2004].

As will become clear in Section 2.3, the Paraná Guazú bed material is relatively coarse compared to that of the Paraná de las Palmas, and the concentration of fines is higher in the Las Palmas branch. Drago and Amsler [1998] presented a theory on the cause of this asymmetry in sedimentological characteristics between the Guazú and Las Palmas river branches. They proposed quaternary epeirogenic movements to have induced deviations from a solely south-western river thalweg resulting into north-west directed secondary channels and the diversion of the main channel into the Guazú and Las Palmas branches. This induced a larger hydraulic gradient in the Guazú channel and a subsequential increased amount of river discharge and (mostly sandy) sediment load to be diverted to the Paraná Guazú. It currently captures the majority of the water and solid discharge of the Paraná River, characterizing the Guazú branch as a true continuation of the alluvial stream that is the Paraná River, with a predominantly sandy bed up to the Río de la Plata estuary. The Paraná de las Palmes has morphologically evolved differently, incising its channel in plastic clay and Pleistocene silts (visible on Figure B.1). This is reflected in the composition of the Palmas bed sediment with higher clay and silt percentages in almost its entire length.

In an unpublished research by Dr. Ricardo Nicolás Szupiany, he showed that at the entrance of the Delta, the river had not yet mixed horizontally completely after confluencing with the Paraguay river approximately 600 km upstream, causing a non-uniform lateral distribution of sediment concentrations. This finding on the river's mixing length could be a driving forcer of the asymmetry in suspended sediment concentrations between the las Palmas and Guazú branches, implying that the sediment-rich

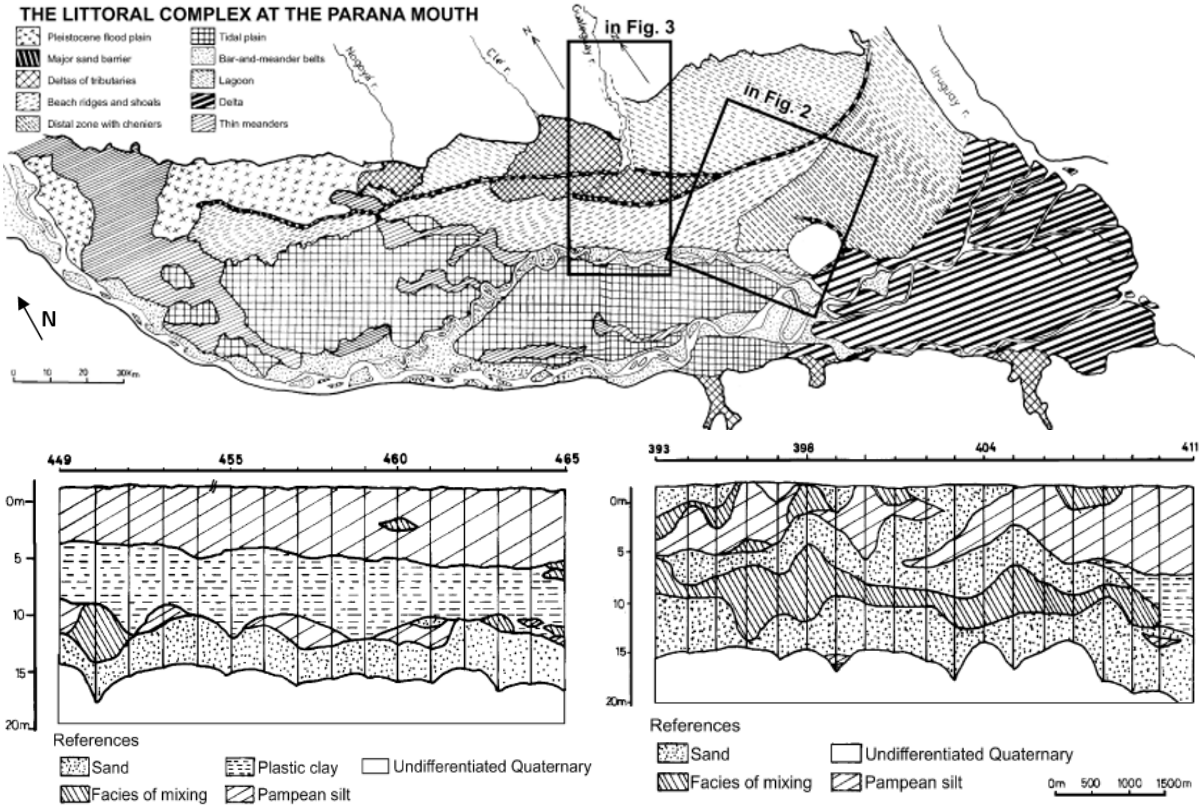

Figure B.1: Map of the littoral complex of the Paraná Delta (top) and typical stratigraphic profiles of the Lower Delta (left) and the bar-and-meander belts (right) [Iriondo, 2004]

water originating from the Paraguay river enters the las Palmas branch, and the sediment-poor water from the Upper Paraná mostly reaches the Paraná Guazú.

B.2. Sedimentary analysis

The majority of the (fine) sediment entering the Paraná Delta originates from the sub-basin of the Bermejo River. Sediment concentrations measured in El Colorado, Bermejo indicate mean annual sediment loads of approximately 6500 g/m^3 [Amsler and Drago, 2009], with extreme flows during which concentrations can exceed 100 kg/m^3 [Amsler et al., 2007]. Figure B.2 also shows that maximum concentrations and very fine sediment proportions were observed in April.

Table 5.3 Maximum and minimum percentages of wash load and clay fraction with the corresponding mean diameters and standard deviations (averages at the sampling vertical in the mid channel) (from: Drago and Amsler 1988)

	Wash load parameters			
Date	d_g [a] (μm)	σ_g [b]	Wash load (%)	Clay fraction (%)
28/10/76	16	3.07	66	22
27/01/77	12	3.25	73	36
01/03/77	14	3.34	66	31
28/03/77	6	2.08	97	55
13/04/77	7	2.39	93	51
25/04/77	7	2.46	92	51
09/05/77	7	2.51	92	49
23/05/77	7	2.41	94	47
06/06/77	7	2.48	92	47
25/07/77	12	2.87	77	31
08/08/77	14	2.87	73	23
31/10/77	15	2.99	67	22
14/11/77	11	2.77	81	26

[a]Mean diameter
[b]Geometric standard deviation of the size distribution

Figure B.2: Maximum and Minimum percentages of wash load and clay fraction with the corresponding mean diameters and standard deviations Amsler et al. [2007]

Drago and Amsler [1988] determined the separation between bed material and wash load specifically for the Paraná River. Based on bed sediment samples, they concluded that 31.2 μm is the limit between wash load and the suspended coarser fractions. Lelievre and Navntoft [1980] estimated this threshold to be around 37 μm. Drago and Amsler also showed that 60.8% of the suspended sediment falls within the fine silt range (8-16 μm).

B.2.1. Sediment fluxes

There is not much consistent and quantitative data available of sediment fluxes in different parts along the Paraná river reaches. Spatial and temporal variations of physical mechanisms related to sediment transport complicate the definition of a uniform description of sediment (transport) characteristics, therefore data found in literature can vary widely. The following values should thus be interpreted with care.

- Isupova and Mikhailov [2018] analyzed multiple data sources and summarized typical long-term suspended sediment yields in the Paraná River system. At Corrientes (just downstream of the confluence with the Paraguay river), data on the Paraná River's yield varies from 80 to 120 Mt/year.
- Isupova and Mikhailov reported that the suspended sediment yields of the Paraná river and Uruguay river into the estuary are estimated at 80-90 Mt/year and 10-11 Mt/year, respectively
- [Amsler et al., 2007] reported total sediment transport averages of 133 Mt/year at Paraná City, just upstream of the delta's entrance. Approximately 5 to 10% is bed material load (sand fractions) of which 91% is transported in suspension.

B.2.2. Sediment in the Río de la Plata

The fine sediments carried by the Paraná River are discharged into the Río de la Plata estuary. Fine, suspended sand and coarse silt fractions [Menéndez et al., 2009] are deposited near the river discharge zones, resulting in a significantly progradating shoreline (25 m/year at Guazú, up to 75 m/year at Palmas, see Figure 2.9) and the growth of the Oyarvide and Martín García islands, located just offshore the Paraná Guazú mouth. Finer fluvial sediment settles as it enters the estuary, resulting in decreasing concentrations along the estuary axis. The Paraná Guazú, de las Palmas and Uruguay river all have

distinct corridors of flow through the Río de la Plata with little mixing between them [Piedra-Cueva and Fossati, 2007]. This causes suspended sediment concentrations near the Argentian coast to be significantly higher than near the Uruguayan shore. Concentrations of suspended sediment in the Río de la Plata estuary are highly variable in space and time. Fossati et al. [2014] researched the sediment dynamics in the estuary. Her modelling efforts indicate that during regular weather conditions, sediment concentrations in the middle of the water column are in the order 30 mg/l. During stormy weather, values lie around 150 mg/l. Re-suspension of sediment by wave action plays an important role in the shallow estuary [Fossati et al., 2014]. Simionato et al. [2013] collected turbidity profiles and compared them to MODIS satellite observations calibrated with an algorithm that estimates the sediment concentration by means of a spectral analysis of the reflectance bands. Simionato et al. computed multi-annual seasonal averages of the suspended matter concentrations, reporting minima (20-30 mg/l) and maxima (60-80 mg/l) in the austral summer and winter, respectively.

B.2.3. Paraná de las Palmas: 2017 van Rijn measurements

van Rijn [2017] performed an analysis on bed and suspended sediment characteristics as part of a study with the purpose of estimating siltation quantities in a newly constructed harbour basin in the Paraná de las Palmas near Campana. The following points describe some relevant sedimentological and morphological aspects of his study and its findings:

- van Rijn measured bed forms (mega-ripples) of approximately 20 to 60 m in length and 0.3 to 1 m in height. The propagation speed was around 0.5 to 1 m/day.
- van Rijn took soil samples and analyzed the particle size distribution based on a laser-diffraction instrument. He found that all bed samples in depths larger than 16 m are sandy with d_{50} values of 300 to 400 μm. Sediment found in depths smaller than 13 meter are silty-muddy with d_{50} of 20 to 50 μm.
- A bulk sample of various suspended sediment samples indicated the presence of a clay fraction (<8μm) of 35%, a silt fraction (between 8 and 63 μm) of 50% and a fine sand fraction (between 63 and 250 μm) of 15 %.
- Based on the observed propagation of bed forms and verification by the Van Rijn Transport formula, bed load at the project location is approximately 0.01 to 0.02 kg/m/s for the mentioned d_{50} values of 300 to 400 μm.
- Based on sediment balance and discharge distributions, van Rijn estimated the annual-average wash load to be 300 mg/l. In-situ measurements indicated depth-averaged sediment concentrations of 250 to 330 mg/l.

  van Rijn [2017] measured sediment concentrations at multiple depths near the city of Campana. Measurements were taken on 2 May 207 at 0.2, 0.5, 1, 2, 4 and 8 meter above the bed.

Height above bed (m)	Flow velocity (m/s) and sediment concentration (mg/l)							
	8.45 hrs	9.45 hrs	10.45 hrs	11.45 hrs	12.45 hrs	13.45 hrs	14.45 hrs	15.45 hrs
0.2	0.38; 980	0.35; 912	0.34; 896	0.26; 780	0.28; 715	0.33; 735	0.35; 806	0.36
0.5	0.47; 836	0.43; 750	0.41; 774	0.36; 675	0.35; 630	0.43; 613	0.45; 693	0.44
1	0.53; 592	0.49; 687	0.52; 687	0.44; 593	0.43; 513	0.49; 523	0.54; 615	0.49
2	0.67; 561	0.60; 565	0.58; 563	0.47; 518	0.52; 442	0.56; 442	0.61; 505	0.54
4	0.69; 381	0.67; 379	0.65; 450	0.54; 379	0.60; 311	0.63; 297	0.73; 347	0.68
8	0.76; 296	0.72; 296	0.65; 304	0.55; 293	0.53; 236	0.58; 233	0.67; 262	0.73
Water depth (m)	13.5	13.5	13.5	13.5	13.5	13.5	13.5	13.5
Depth-mean velocity (m/s)	0.7	0.7	0.65	0.55	0.6	0.6	0.75	0.7
Depth-integrated suspended transport (kg/m/s)	3.1	3.1	3.0	2.4	2.0	2.1	2.8	
Depth-mean concentration (mg/l) $c_{mean}=10^3 q_s/q$ $q=u_{mean}h$	330	330	340	320	250	260	280	

Figure B.3: Suspended sediment measurement results in the Paraná de las Palmas, Campana [van Rijn, 2017]

van Rijn [2017] conceptualized the suspended sediment transport by identifying three distinguished sediment types, based on the survey of 2 May 2017 during a velocity of 0.6 - 0.8 m/s. Results are depicted in Figure B.4. If these measurements were to be assumed as representative for the Paraná de las Palmas, the following could be said about the sediment entering the secondary channel network:

- 115 mg/l of clay is present in the top few meters of the water column and can therefore enter the channel network
- An average of 100 mg/l of silt is present in the top few meters of the water column. This could enter a channel with a depth close to this 5 meters, shallower channels could receive slightly less silt as silt concentrations are not uniform over the depth.
- Although concentrations in the Paraná River are highly dependant on supply from the Bermejo Region, the proposed values approximately reflect average conditions, as the mean total suspended sediment concentrations in Figure B.4 (330 mg/l) are similar to yearly-averaged values determined by Amsler et al. [2007] (250-300 mg/l).

Type of sediment	Depth-mean Sediment concentration (mg/l)	Fraction percentage of suspended sediment	Particle size range (μm)	Mean size (μm)	Settling velocity at temperature of 15° C (mm/s)
Clay	115 (uniform over depth)	35%	< 8 μm	8 μm	0.005 mm/s
Silt	165 (100 mg/l in upper 5 m of the depth)	50%	8-63 μm	30 μm	0.72 mm/s
Fine sand	50 (0 mg/l in upper 5 m of depth)	15%	63-250 μm	100 μm	7 mm/s
Total	330 mg/l (215 mg/l in upper 5 m of the depth)	100%			

Figure B.4: Identified fractions of suspended sediment, Campana, 2 May 2017 [van Rijn, 2017]

B.2.4. Paraná River system: 1998 soil samples

Drago and Amsler [1998] executed an extensive research project on the granulometric characterization of bed sediments in the Paraná and Paraguay River system. He found that the majority of the bed sediments in the systems consists of medium to fine well-sorted sands. Some sample locations and results of soil sample analyses from the River's thalweg in the Lower Delta are presented in Figure B.5 and Table B.1.

Table B.1: Soil sample characteristics, with mean particle diameter (Dg) and percentages coarse (S.C), medium (S.M), fine (S.F) and very fine (S.VF) sand and silt (s) and clay (c) fractions, and hydraulic characteristics at the sample site with depth-averaged velocity u_m and hydraulic radius h [Drago and Amsler, 1998]

	Dg	S.C	S.M	S.F	S.VF	s	c	u_m	h
	[mm]	*[%]*	*[%]*	*[%]*	*[%]*	*[%]*	*[%]*	*[m/s]*	*[m]*
45	0.140	0.4	2.4	62	33	1	4	1.20	22.6
46	-	-	-	-	-	23	75	0.92	19.3
47	-	-	-	-	-	2	97	1.21	18.0
48	0.340	14.5	51	33	0.7	-	-	0.94	11.5
49	0.290	6.6	64	27	0.6	1	2	-	32
50	0.168	0.2	2.3	88	7.7	1	1	0.99	12.0
51	0.235	0.1	56	44	0.5	0	1	0.84	5
52	0.106	0.03	0.2	24	50	12	12	0.19	1.8

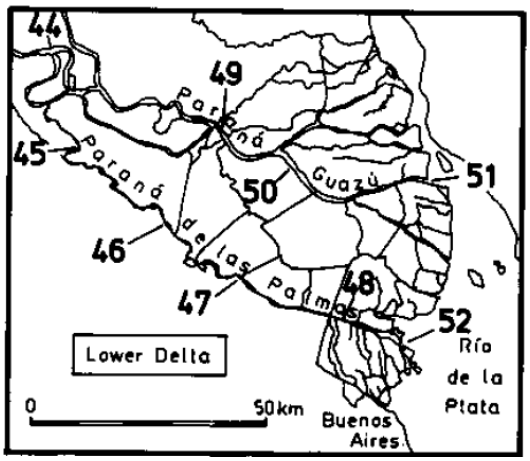

Figure B.5: Locations of the soil samples [Drago and Amsler, 1998]

B.2.5. Granulometric analysis deltaic front

Marcomini et al. [2018] executed a granulometric analysis on various morphological units in the deltaic front near San Fernando, near the mouth of the Paraná de las Palmas. Marcomini found that the soil composure is silt dominated with significant fractions of cohesive material. The locations of the soil samples are displayed on Figure B.6 and the results on Table B.2.

Table B.2: Sand, silt and clay fractions of the soil samples by Marcomini et al. [2018]

	Location description	Sand *[%]*	Silt *[%]*	Clay *[%]*
D01	Distribution channel (Luján river)	4.8	79.8	15.4
D02	Distribution channel (Luján river)	0.6	86.2	13.2
D03	Distribution channel	0.3	85.1	14.6
D10	Distribution channel (La Paloma)	2.1	82.2	15.7
D11	Distribution channel (San Antonio)	3.1	79.9	17.0
D15	Distribution channel (San Antonio)	7.5	80.0	12.5
D09	Island	0	70.4	29.6
C24	Island	0.2	65.4	34.4
C35	Island	0.2	67.0	32.8
C42	Island	1.8	70.4	27.8
D13	Tidal flat on bar	22.3	68.7	9.1
D12	Bar	92.4	5.8	1.8
D14	Channel between bars	8.1	79.2	12.7

Figure B.6: Locations of soil samples [Marcomini et al., 2018]

Sanci and Panarello [2018] analysed soil samples on an island of the Lower Delta, between the Arroyón and Sáalos streams. She took soil samples at 3 locations (on a levee, in the middle of the island and in between) at 6 depths (20 to 120 cm). She found high silt percentages in the middle of the island, with decreasing clay percentages varying from 15 to 5 %. At the levee the clay percentage was as high as 17.5% near the surface, with lower values between 5 and 10% around a meter deep.

B.2.6. Q-S curve Zarate and Brazo Largo

A curve relating the river discharge in the Bermejo river and the transport of fine sediment in the Paraná de las Palmas branch (located at Zarate) and the Paraná Guazú (Brazo Largo) was computed by Re et al. [2009]. The following notions on the generation of this relation are stated:

- A Q-S curve at El Colorado (city at the Bermejo river) was constructed based on data between 1993 to 2008
- It is assumed that the sediment discharge from the Bermejo river is representative for sediment discharge at the city of Paraná (Tunel Subfluvial)

- A 'base concentration' was incorporated in the formulation to correct for measured sediment concentrations during times of low discharge from the Bermejo Region
- A correction was made to account for the travelling time of sediment from the Bermejo river to the Delta, resulting in a delay of roughly 9 days.
- An additional correction was made to account for the deposition of sediment between the Bermejo region and the delta, resulting in a reduction in solid flow of 10 million t/y, which is defined to only occur during times with sediment concentrations exceeding 600 mg/l
- The obtained sediment discharge at Tunel Subfluvial is assumed to be evenly distributed between the Palmas and Guazú branches, i.e. the sediment concentrations for both branches are the same.
- Furthermore, it is assumed that the transport of sandy bed material is fully realized by the Paraná Guazú. The Engelund-Hansen transport formulation was used, verified and found to produce reasonable predictions for bed transport in the Guazú branch.

Figure B.7 displays 2-monthly sediment transport data at Zarate (Paraná de las Palmas) based on the Q-S curve. ADCP discharge measurements were used to approximate the concentrations. During the 2016 ENSO event, Sediment concentrations were similar to those computed during non-ENSO periods. Absolute values of transported fines were slightly higher during the 2016 ENSO event. As can be seen in Table B.3, the anomaly is rather small. This is not in accordance with the extremely high volumes of sediment deposited and dredged during the 2016 ENSO period. As deposited volumes are a robust indicator of sediment transport and deposition, the validity of the QS curve must be interpreted with great care. Another indicator for the limited validity of the QS curve is that average concentrations (order 60 mg/l) seem to greatly subceed the concentrations mentioned in various other literature (order 300 mg/l), as described in the sections above. Note that the extremely high value of over 7000 kg/s in transport and 1800 mg/l was assumed to be a measurement error, as the date in question (April 2014) was not preceded by significantly high discharges or sediment supply.

Table B.3: Average fine sediment transport computed with the Q-S curve at Zarate during the 2014-2016 ENSO event and in the periods before and after

	Sediment concentration *[mg/l]*	Total load of fines *[kg/s]*
2010 - May 2014	68.2	345.0
May 2014 - June 2016 (ENSO)	73.8	366.8
June 2016 - Jan 2021	73.5	342.1

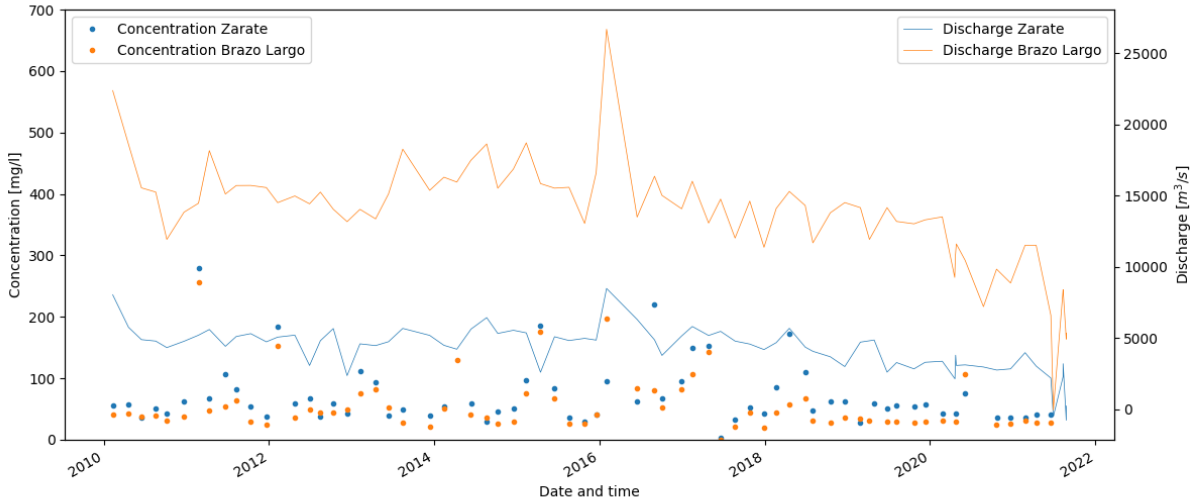

Figure B.7: Concentrations of fines computed with the Q-S curve and discharges measured by ADCP

B.2.7. Suspended sediment measurements

Sabarots Gerbec et al. [2017a] describe the execution and results of suspended sediment concentration measurements in the Paraná Guazú and las Palmas branches. Measurements were taken only at 1 meter below the water surface due to limitations of the measuring device. The measuring locations are depicted in Figure B.8 and the results in Table B.4.

Table B.4: Suspended sediment measurement details [Sabarots Gerbec et al., 2017a].

#	Location	Date	Concentration [mg/l]
1	Paraná Guazú upstream Barca Grande	24/05/2017	53
2	Paraná Guazú downstream Barca Grande	24/05/2017	45
3	Paraná de las Palmas	03/07/2017	66
4	Paraná Guazú	03/07/2017	47
5	Talavera	03/07/2017	33

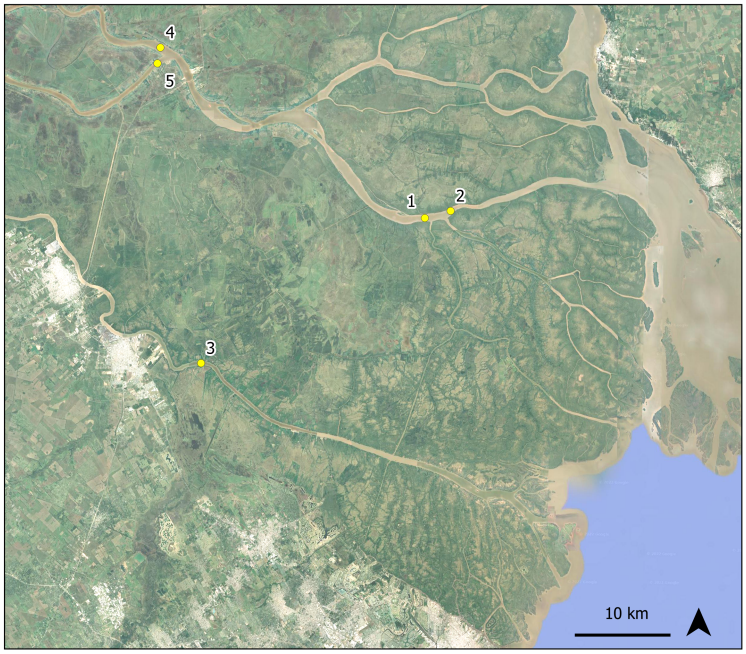

Figure B.8: Locations of suspended sediment measurements, numbers according to B.4 [Marcomini et al., 2018]

B.2.8. December 2021 Soil samples

Bed soil and suspended sediment samples were carried out in December 2021 and March 2022. Appendix I describes the methodology of the sampling. Figure B.9 displays the median diameter D_{50} of the bed sediment. The table on the next page gives the statistical characteristics and the percentages silt, sand clay in each of the samples. Samples in the table indicated with *1 are not taken inside the channel network and *2 is deemed to be not representative for typical channel characteristics. Note that not all samples specified in the table are displayed in Figure B.9. The following remarks are made regarding the bed sediment:

- Sediment in the Paraná de las Palmas thalweg is predominantly sand
- Typical values of D_{50} are in the order of 10 - 30 μm in the channel network.
- One sample in the channel network (”Arroyo Espera”) with a D_{50} of 76.6 μm is expected to be either a measurement error or a sample not representative for the characteristic sediment type. Due to the strong bimodal character of the distribution (see Figure B.10, it is likely that some very coarse sediment from an artificial source was included in the analysis. It is unlikely that large amounts of sandy material is naturally transported to the specified location, as the distance to the deltaic front and the Palmas river branch is large.
- Typical percentages of clay, silt and sand in the channel network bed are roughly 30, 50 and 20 % respectively
- No spatially uniform patterns concerning bed sediment size variation (eg. downstream coarsening or fining) are observed.

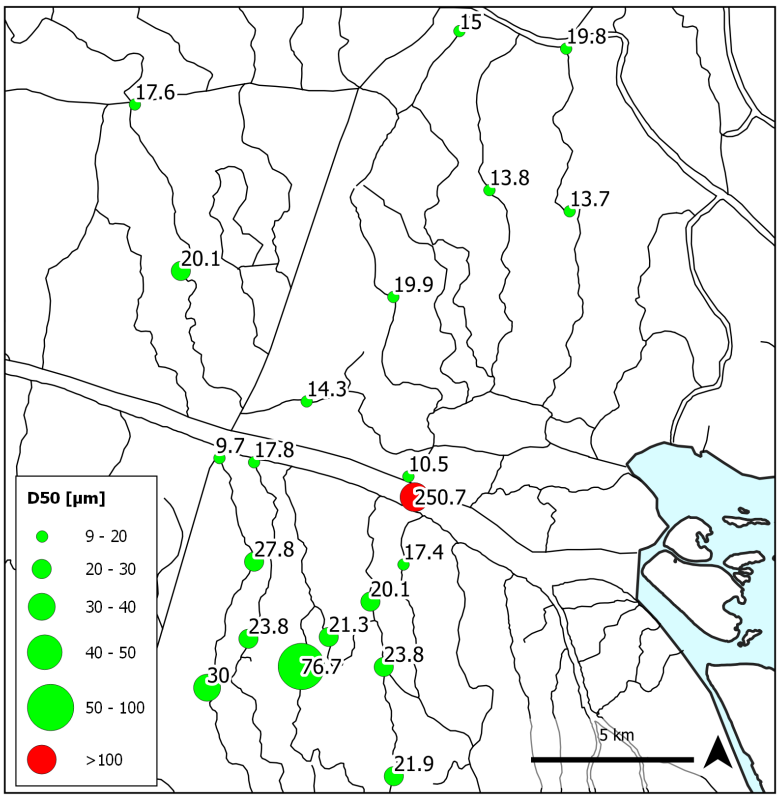

Figure B.9: Median diameter analyzed bed samles

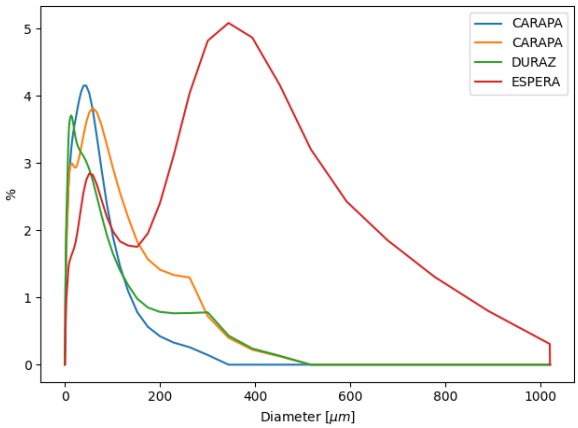

Figure B.10: Particle size distibutions of the faulty measurement (Espera) and nearby samples

Name	Median [µm]	Mean [µm]	Variance [µm^2]	SD [µm]	Mode [µm]	Sand (> 63 µm) %	Silt %	Clay (< 8 µm) %
18338_PENTAMAR	17.63	51.7	7309	85.5	16.24	21	50	29
*1 18818_PTE_AVE	203.91	216.2	22507	150	245.3	83	12	5
*1 18878_M1	49.74	65.29	4379	66.17	94.85	45	31	24
18879_M2	12.44	37.44	3656	60.46	9.43	18	44	38
ANTEQ_1	17.44	42.15	3562	59.68	14.17	22	48	29
BANCO_1	20.05	47.43	4642	68.13	14.18	25	48	27
CARAG_1	30	42.34	2115	45.99	48.13	25	53	23
CARAG_2	27.83	46.18	2867	53.54	63.05	29	45	26
CARAG_3	9.72	16.45	607	24.64	12.38	4	54	42
CARAPA_1	17.84	30.84	1379	37.13	41.91	16	54	31
CARAPA_2	23.84	47.88	3783	61.51	55.08	27	47	26
DURAZ_1	14.33	35.3	3118	55.84	12.38	17	50	33
*2 ESPERA_1	76.73	172.4	37860	194.6	321.8	55	31	14
FELIC_1	19.78	38.22	2426	49.25	48.15	21	48	30
FELIC_2	13.73	55.84	13446	116	10.81	19	47	34
FREDES_1	13.81	34.99	3300	57.44	12.38	16	51	33
GELVEZ_1	21.88	53.6	8009	89.49	24.4	22	55	23
*1 M1_PARANA_MINI_v2	17.52	36.28	2187	46.76	55.01	21	49	31
*1 M2_PARANA_MINI_v2	25.83	45	2925	54.09	55.15	27	48	25
*1 M3_PARANA_MINI	9.69	24.2	1030	32.1	8.24	14	43	43
*1 M4_PARANA_MINI	13.38	33.68	3171	56.31	12.39	15	52	34
*1 M5_PARANA_MINI	33.9	45.09	2038	45.14	55.16	29	52	20
PACIF_1	20.11	34.83	2076	45.57	36.72	16	57	27
PACIF_2	17.62	46.38	5198	72.1	14.17	21	49	29
*1 PALMAS_1	250.71	266.6	16679	129.2	246.6	95	3	2
PAYCA_1	10.45	30.32	4285	65.46	12.36	10	50	40
PAYCA_2	19.94	37.12	2313	48.09	47.97	19	53	28
PAYTO_1	14.97	36.61	4125	64.23	16.24	15	52	33
TORO_1	21.29	35.56	1728	41.57	48.13	20	52	28
TORO_2	23.77	39.11	2353	48.5	42.05	20	54	25

B.2.9. March 2022 suspended sediment samples

During the March 2022 field surveys, suspended sediment samples were taken at various locations in the Lower Delta. The results of the samples indicated below are the samples taken with the DH-45 sampler at 1 meter depth only. At the time of writing, samples taken at multiple depths taken with the peristaltic pump are not yet analyzed. Although the samples are taken at only one depth, the results still present characteristic values of sediment concentrations, mostly of fine material, present in the

Lower Paraná Delta river and channel network during regular (17 March) and storm surge (18 March) conditions. Analysis was done by filtering, drying and weighing the samples.
The locations and results of the analysis are presented below. The following remarks are made concerning the results of the sampling and analysis:

- Sediment concentrations in the top of the water column are generally in the order of 100 to 300 mg/l. This is in reasonable accordance with concentrations measured by Van Rijn and concentrations calculated with annual sediment transport quantities in the Paraná River.
- There is no significant observed difference between sediment concentrations during regular conditions (17 March) and during the storm surge on 18 March.

Day	Time	#	Volume [ml]	MPS [mg/l]	Average [mg/l]
17-03-22	09:28:00	1	200	137	
17-03-22	10:00:00	2	200	278	
17-03-22	10:29:00	3	200	263	
17-03-22	11:19:00	4	100	243	
17-03-22	11:33:00	5	100	254	214
17-03-22	12:05:00	6	100	211	
17-03-22	13:23:00	7	200	33	
17-03-22	15:18:00	8	100	300	
17-03-22	16:31:00	9	100	205	
18-03-22		10	100	145	
18-03-22		11	100	273	
18-03-22		12	100	137	222
18-03-22		13	100	201	
18-03-22		14	100	310	
18-03-22		15	100	267	

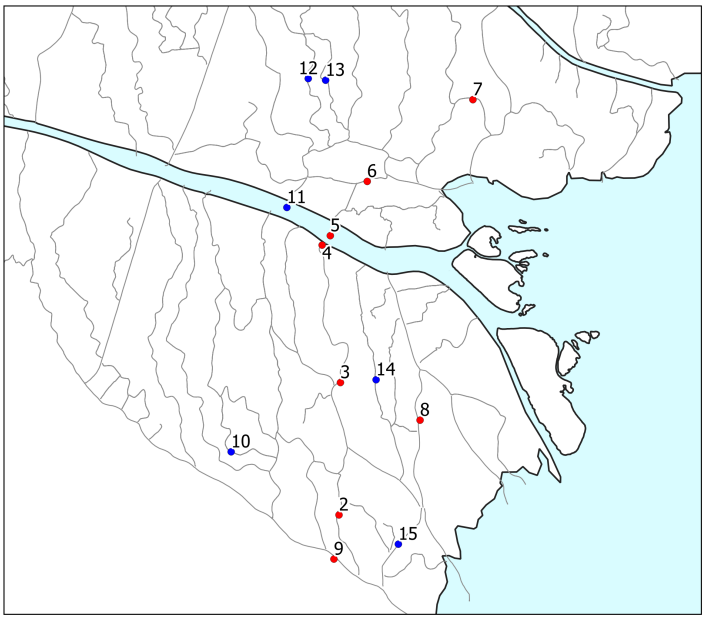

Figure B.11: Results suspended sediment samples

C

Spatial analysis

C.1. Spatial analysis: Procedure

To establish a better understanding on the spatial characteristics of the channel network and to generate attribute files for the numerical model (Chapter 4), satellite imagery was used to create a more detailed picture of the Lower Delta channel network. Various methods on automated water detection algorithms were considered or tested [Cordeiro, 2020, Google, 2021], but the small channel widths and the widespread presence of vegetation next to the channels made a manual analysis of the satellite imagery most suitable. The following steps were carried out using QGIS3, freely available remote sensing imagery from Google Earth and post processing algorithms in Python 3:

1. Manual drawing of polygons around the water bodies in the secondary channel network.

   - Distinction was made between channels that are (nearly) permanently inundated and channels that appear dry on the satellite imagery.
   - Distinction was made between channels that are a continuous link in the network and channels that seem to only exist as a 'dead end.

   Use the algorithm ID *native:jointattributesbylocation* to assign region numbers to the individual channel features. Use the Sort and Number plugin to assign unique channel ID values to the individual channel features, sorted by region and type (regular, dry, dead end).

2. Generate channel centerlines with the GRASS voronoi skeleton algorithm (ID: *grass:v.voronoi.skeleton*) with a low smoothness factor without inducing numerical instability (eg. 0.05).

3. Generate points along the centerlines at a fixed distance ds (ID: *native:pointsalonglines*). Use *native:dissolve* to merge multiple centerlines belonging to one channel ID.

4. Generate transect lines on the points, perpendicular to the centerlines (ID: *native:geometrybyexpression*). Expression:

   extend(
   make_ line(
   $geometry,project (
   $geometry,50, radians ("angle"-90))
   ),50,0)

5. Clip the transects with the channel polygons as mask layer (ID: *native:geometrybyexpression*). Using the following expression in stead of *native:clip* will clip the transects only to the associated channel polygon:

   intersection(
   & geometry, geometry(

get_ feature
('Channel transects layer name','channel ID','channel ID'
))

The procedure 1 to 5 is depicted in Figure C.1. The complete results of the analysis are provided under Section C.2 The following spatial and geometrical characteristics of individual channels and the network were obtained:

- Channel length;
- Water surface area;
- Channel width per transect and averaged per channel.

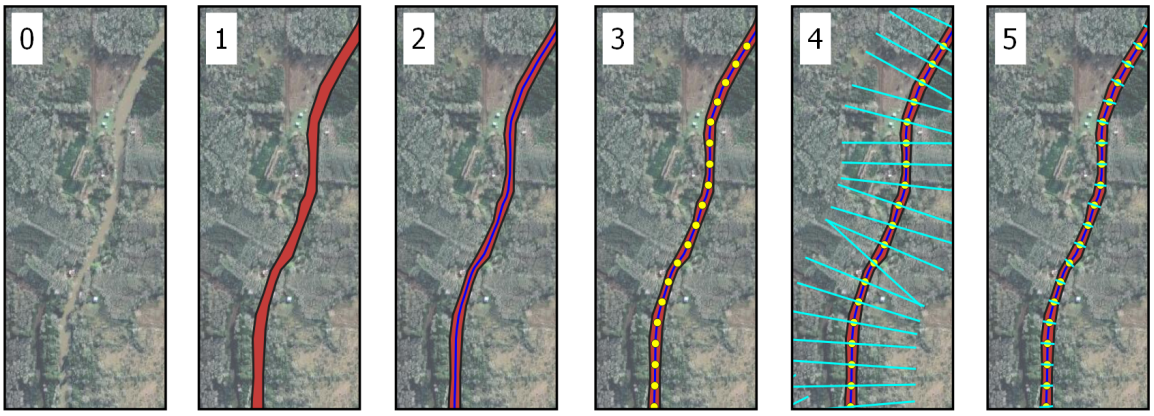

Figure C.1: Procedure spatial analysis

Table C.1: Spatial characteristics of the Lower Delta channel network

	Region				
	I	II	III	IV	V
Area [km^2]					
Total	15.99	5.64	4.63	3.61	10.62
Regular	15.61	5.01	3.42	2.40	8.84
Dry	0.04	0.32	0.90	0.77	0.68
Dead end	0.34	0.31	0.32	0.55	1.11
Length [km]					
Total	305	213	187	141	266
Regular	288	174	119	78	158
Dry	3	19	49	40	46
Dead end	14	20	19	23	62

C.2. Spatial analysis: Results

For descriptive purposes, the Lower Delta and its channel network is divided into five regions (see Figure C.2), confined by the Luján river in the south, the Paraná Guazu (tributary Paraná Bravo / Río Gutierrez) in the north, the Río de la Plata estuary and the Canal 'Coronel Martín Irigoyen' as the upstream limit.

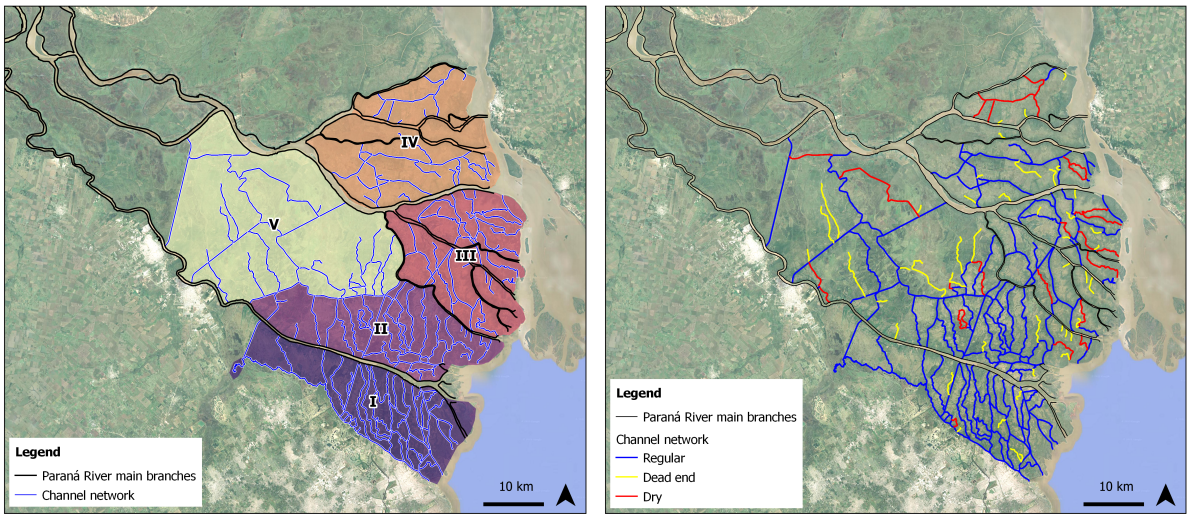

Figure C.2: Lower Paraná Delta regions (left) and channel network classification

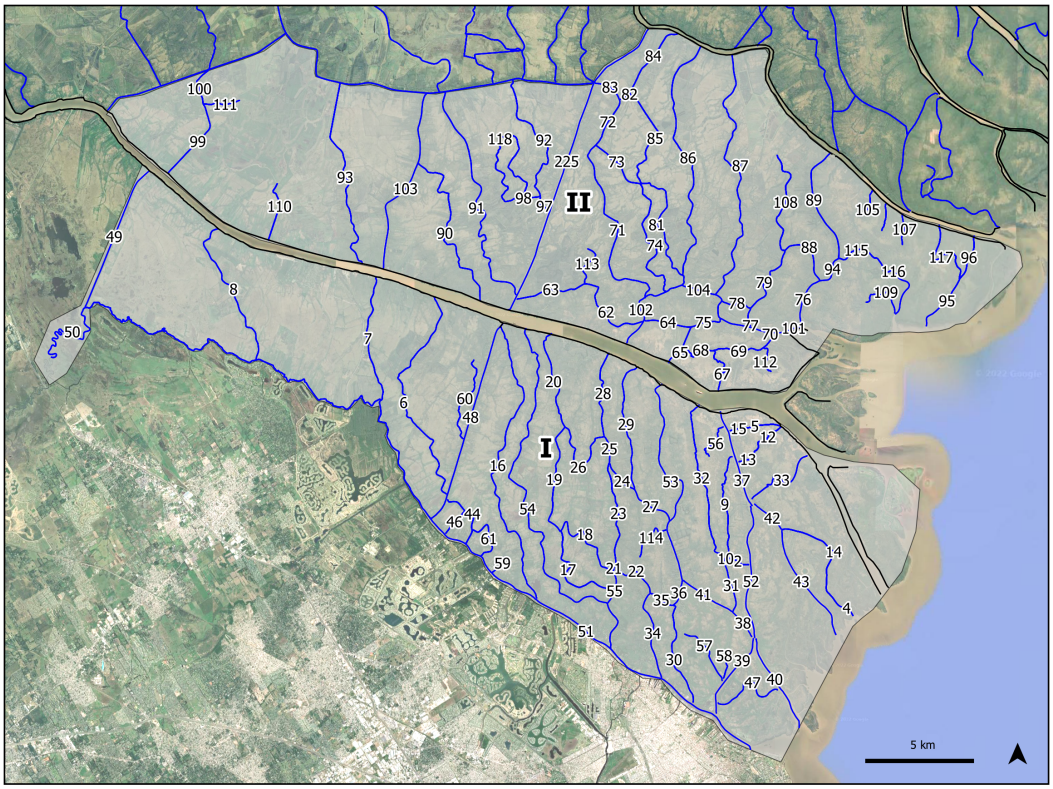
I
II
5 km

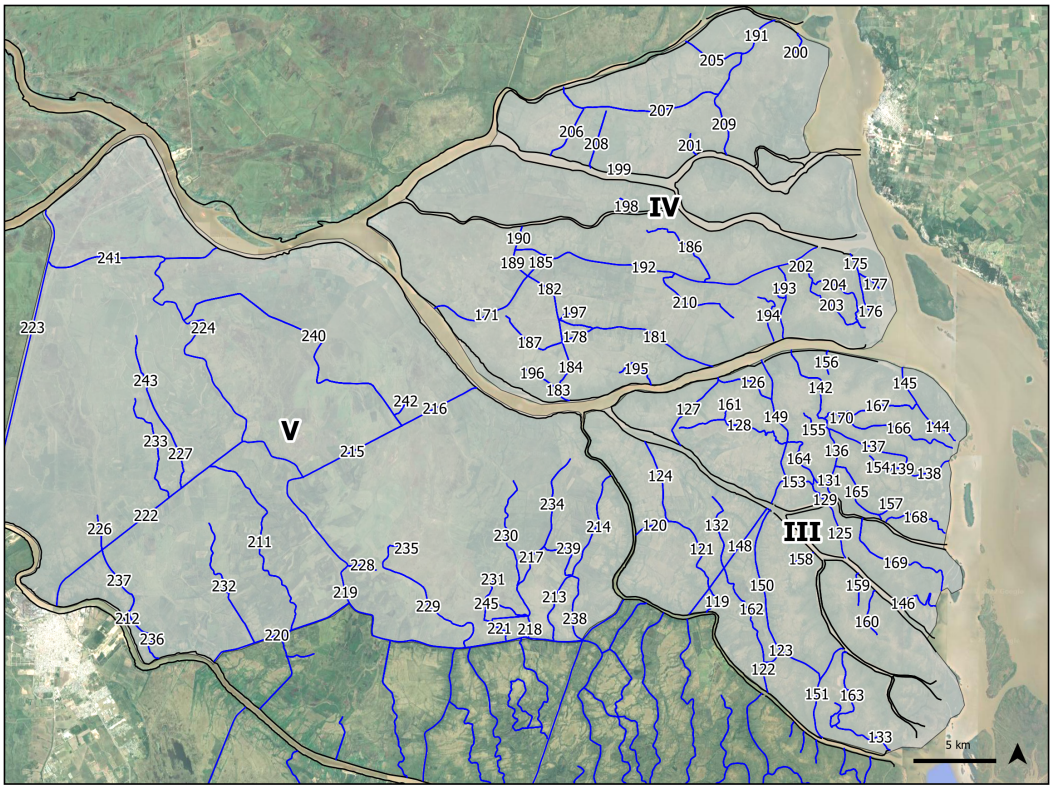
III
IV
V
5 km

channel_ID	Type	Region	Length [m]	Area [m2]	Width [m]	channel_ID	Type	Region	Length [m]	Area [m2]	Width [m]
1	Regular	I	175	3940	22.5	67	Regular	II	2417	36768	15.2
2	Regular	I	1111	16547	14.9	68	Regular	II	2124	19987	9.4
3	Regular	I	2961	46104	15.6	69	Regular	II	2460	31551	12.8
4	Regular	I	6352	169804	26.7	70	Regular	II	1066	25607	24.0
5	Regular	I	2355	22840	9.7	71	Regular	II	9323	276987	29.7
6	Regular	I	11499	299831	26.1	72	Regular	II	2442	54934	22.5
7	Regular	I	6114	156700	25.6	73	Regular	II	2972	57349	19.3
8	Regular	I	7472	190511	25.5	74	Regular	II	6569	88558	13.5
9	Regular	I	5058	101386	20.0	75	Regular	II	1525	35079	23.0
10	Regular	I	180	3948	21.9	76	Regular	II	2459	136627	55.6
11	Regular	I	2967	46112	15.5	77	Regular	II	868	26316	30.3
12	Regular	I	2967	46112	15.5	78	Regular	II	1481	40903	27.6
13	Regular	I	2967	46112	15.5	79	Regular	II	3505	86796	24.8
14	Regular	I	6352	169804	26.7	80	Regular	II	485	14460	29.8
15	Regular	I	2355	22844	9.7	81	Regular	II	6085	160787	26.4
16	Regular	I	14423	478802	33.2	82	Regular	II	513	10873	21.2
17	Regular	I	5206	77618	14.9	83	Regular	II	1445	47788	33.1
18	Regular	I	4534	137331	30.3	84	Regular	II	3811	75811	19.9
19	Regular	I	5462	144712	26.5	85	Regular	II	5189	80995	15.6
20	Regular	I	5039	154167	30.6	86	Regular	II	12099	312130	25.8
21	Regular	I	303	11371	37.5	87	Regular	II	13421	401193	29.9
22	Regular	I	2439	121806	49.9	88	Regular	II	2888	93045	32.2
23	Regular	I	5035	77832	15.5	89	Regular	II	5664	209210	36.9
24	Regular	I	1691	55949	33.1	90	Regular	II	8870	209028	23.6
25	Regular	I	1291	39559	30.6	91	Regular	II	12107	371777	30.7
26	Regular	I	4336	112441	25.9	92	Regular	II	6733	115548	17.2
27	Regular	I	2331	114685	49.2	93	Regular	II	9435	194909	20.7
28	Regular	I	4224	99148	23.5	94	Regular	II	1558	66064	42.4
29	Regular	I	6142	198856	32.4	95	Regular	II	2830	78428	27.7
30	Regular	I	4980	155551	31.2	96	Regular	II	2178	26116	12.0
31	Regular	I	2488	119497	48.0	97	Regular	II	987	24391	24.7
32	Regular	I	7969	167060	21.0	98	Regular	II	783	10782	13.8
33	Regular	I	4120	124797	30.3	99	Regular	II	4052	109087	26.9
34	Regular	I	4279	286576	67.0	100	Regular	II	1828	41307	22.6
35	Regular	I	1280	68560	53.6	101	Regular	II	3961	267561	67.5
36	Regular	I	1247	69366	55.6	102	Regular	II	2671	156040	58.4
37	Regular	I	4639	885916	191.0	103	Regular	II	8819	568405	64.5
38	Regular	I	1481	192185	129.8	104	Regular	II	4862	170620	35.1
39	Regular	I	4099	649649	158.5	105	DeadEnd	II	951	13893	14.6
40	Regular	I	4695	965084	205.6	106	DeadEnd	II	1321	16129	12.2
41	Regular	I	2651	325307	122.7	107	DeadEnd	II	1469	24101	16.4
42	Regular	I	1755	188623	107.5	108	DeadEnd	II	5275	59969	11.4
43	Regular	I	5631	657442	116.8	109	DeadEnd	II	2441	60899	24.9
44	Regular	I	2215	34335	15.5	110	DeadEnd	II	2915	37342	12.8
45	Regular	I	702	10702	15.2	111	DeadEnd	II	1742	35125	20.2
46	Regular	I	1363	16406	12.0	112	DeadEnd	II	1505	20243	13.5
47	Regular	I	3911	154317	39.5	113	DeadEnd	II	2126	45769	21.5
48	Regular	I	9817	808218	82.3	114	DeadEnd	I	2327	66484	28.6
49	Regular	I	7033	731490	104.0	115	Dry	II	2012	32205	16.0
50	Regular	I	31933	767338	24.0	116	Dry	II	3838	148544	38.7
51	Regular	I	18955	2281047	120.3	117	Dry	II	4058	47145	11.6
52	Regular	I	6324	1087020	171.9	118	Dry	II	9162	88537	9.7
53	Regular	I	10536	861057	81.7	119	Regular	III	1925	24207	12.6
54	Regular	I	19495	787459	40.4	120	Regular	III	2224	36075	16.2
55	Regular	I	1560	46450	29.8	121	Regular	III	5717	115568	20.2
56	DeadEnd	I	2031	36327	17.9	122	Regular	III	1913	62409	32.6
57	DeadEnd	I	3028	106291	35.1	123	Regular	III	1377	32363	23.5
58	DeadEnd	I	1486	33847	22.8	124	Regular	III	5219	93631	17.9
59	DeadEnd	I	926	32175	34.7	125	Regular	III	3638	246668	67.8
60	DeadEnd	I	4360	61529	14.1	126	Regular	III	3891	63600	16.3
61	Dry	I	2643	44839	17.0	127	Regular	III	5493	151912	27.7
62	Regular	II	4308	105800	24.6	128	Regular	III	8039	120589	15.0
63	Regular	II	3301	70518	21.4	129	Regular	III	1286	35745	27.8
64	Regular	II	2210	46501	21.0	130	Regular	III	383	8466	22.1
65	Regular	II	768	21596	28.1	131	Regular	III	1323	24125	18.2
66	Regular	II	1258	33962	27.0	132	Regular	III	4959	62706	12.6

channel_ID	Type	Region	Length [m]	Area [m2]	Width [m]
133	Regular	III	4123	104706	25.4
134	Regular	III	1124	41653	37.1
135	Regular	III	944	36110	38.3
136	Regular	III	2394	77513	32.4
137	Regular	III	5865	233154	39.8
138	Regular	III	3254	175448	53.9
139	Regular	III	524	7383	14.1
140	Regular	III	229	6897	30.1
141	Regular	III	526	9196	17.5
142	Regular	III	5812	83409	14.4
143	Regular	III	284	10620	37.4
144	Regular	III	3315	217973	65.8
145	Regular	III	2476	134669	54.4
146	Regular	III	1556	16190	10.4
147	Regular	III	2801	41993	15.0
148	Regular	III	8124	251800	31.0
149	Regular	III	9858	385747	39.1
150	Regular	III	12317	325066	26.4
151	Regular	III	6252	182602	29.2
152	DeadEnd	III	2384	34040	14.3
153	DeadEnd	III	1291	13114	10.2
154	DeadEnd	III	2169	70721	32.6
155	DeadEnd	III	2224	42710	19.2
156	DeadEnd	III	1522	18732	12.3
157	DeadEnd	III	1093	20936	19.2
158	DeadEnd	III	1307	18989	14.5
159	DeadEnd	III	2075	32039	15.4
160	DeadEnd	III	3112	56094	18.0
161	DeadEnd	III	1368	10141	7.4
162	Dry	III	6972	146440	21.0
163	Dry	III	5942	82537	13.9
164	Dry	III	3740	49563	13.3
165	Dry	III	4607	79940	17.4
166	Dry	III	7294	165358	22.7
167	Dry	III	5361	81922	15.3
168	Dry	III	4655	79281	17.0
169	Dry	III	8803	177573	20.2
170	Dry	III	1891	33893	17.9
171	Regular	IV	7227	172001	23.8
172	Regular	IV	2050	42381	20.7
173	Regular	IV	2528	110085	43.5
174	Regular	IV	678	10695	15.8
175	Regular	IV	1364	37957	27.8
176	Regular	IV	2436	90409	37.1
177	Regular	IV	1594	20474	12.8
178	Regular	IV	2046	29533	14.4
179	Regular	IV	1359	25232	18.6
180	Regular	IV	2199	18996	8.6
181	Regular	IV	8081	292553	36.2
182	Regular	IV	3610	58131	16.1
183	Regular	IV	1030	27980	27.2
184	Regular	IV	3252	67352	20.7
185	Regular	IV	1537	34100	22.2
186	Regular	IV	6103	148944	24.4
187	Regular	IV	4513	50597	11.2
188	Regular	IV	2245	28456	12.7
189	Regular	IV	2061	33686	16.3
190	Regular	IV	1490	16317	11.0
191	Regular	IV	3089	88109	28.5
192	Regular	IV	17622	997507	56.6
193	DeadEnd	IV	1411	21227	15.0
194	DeadEnd	IV	3808	113843	29.9
195	DeadEnd	IV	3004	48611	16.2
196	DeadEnd	IV	2412	25137	10.4
197	DeadEnd	IV	1089	14477	13.3
198	DeadEnd	IV	1645	27491	16.7
199	DeadEnd	IV	948	13833	14.6
200	DeadEnd	IV	1389	25610	18.4
201	DeadEnd	IV	1436	35222	24.5
202	Dry	IV	1755	36545	20.8
203	Dry	IV	4469	108168	24.2
204	Dry	IV	5078	110971	21.9
205	Dry	IV	3996	82274	20.6
206	Dry	IV	3652	44441	12.2
207	Dry	IV	13704	275086	20.1
208	Dry	IV	3731	36638	9.8
209	Dry	IV	4082	75001	18.4
210	DeadEnd	IV	6295	118818	18.9
211	Regular	V	13676	349096	25.5
212	Regular	V	405	6861	16.9
213	Regular	V	4618	108514	23.5
214	Regular	V	7088	170108	24.0
215	Regular	V	6856	271871	39.7
216	Regular	V	5184	159125	30.7
217	Regular	V	3109	69945	22.5
218	Regular	V	3416	77988	22.8
219	Regular	V	30843	1476881	47.9
220	Regular	V	9170	334914	36.5
221	Regular	V	3992	69207	17.3
222	Regular	V	15561	658100	42.3
223	Regular	V	18928	2254810	119.1
224	Regular	V	20589	894810	43.5
225	Regular	V	15002	1933915	128.9
226	DeadEnd	V	2218	10972	4.9
227	DeadEnd	V	4363	76710	17.6
228	DeadEnd	V	1835	14112	7.7
229	DeadEnd	V	10467	275485	26.3
230	DeadEnd	V	7309	179054	24.5
231	DeadEnd	V	4628	50481	10.9
232	DeadEnd	V	8798	132210	15.0
233	DeadEnd	V	7313	126092	17.2
234	DeadEnd	V	5971	90564	15.2
235	DeadEnd	V	1484	21672	14.6
236	Dry	V	3642	62415	17.1
237	Dry	V	4933	65787	13.3
238	Dry	V	4765	98049	20.6
239	Dry	V	3906	58912	15.1
240	Dry	V	19445	233892	12.0
241	Dry	V	7434	149942	20.2
242	DeadEnd	V	1518	17950	11.8
243	DeadEnd	V	5883	114663	19.5
244	Dry	V	518	2185	4.2
245	Dry	V	1105	4299	3.9

C.3. Historic planform changes

For one of the wider channels in the Lower Delta, it was possible to use historic satellite imagery to detect changes in channel width. The vegetation line has retreated over the last decades at several locations along the channel banks. The channel in question is the Río Union, and it is one of the most nearshore located distributary channels of the Paraná de las Palmas. In 45 years, its increase in width is approximately 40 meters at some locations. The evolution is displayed in Figure C.3.

No other significant changes in planform or river/channel width were detected using satellite imagery.

Figure C.3: Evolution of the Río Union [Imagery by Google Earth]

D

Analysis bathymetrical data

D.1. Main river branches

A Digital Elevation model (DEM) of the delta, including the main river branches, some major artificial and natural channels and a part of the Río de la Plata, was constructed by combining and manipulating data from various sources [Sabarots Gerbec et al., 2017b]. Figure D.1 presents the DEM in the Lower Delta. The bathymetries of the main Paraná river branches are analysed and described in the following sections.

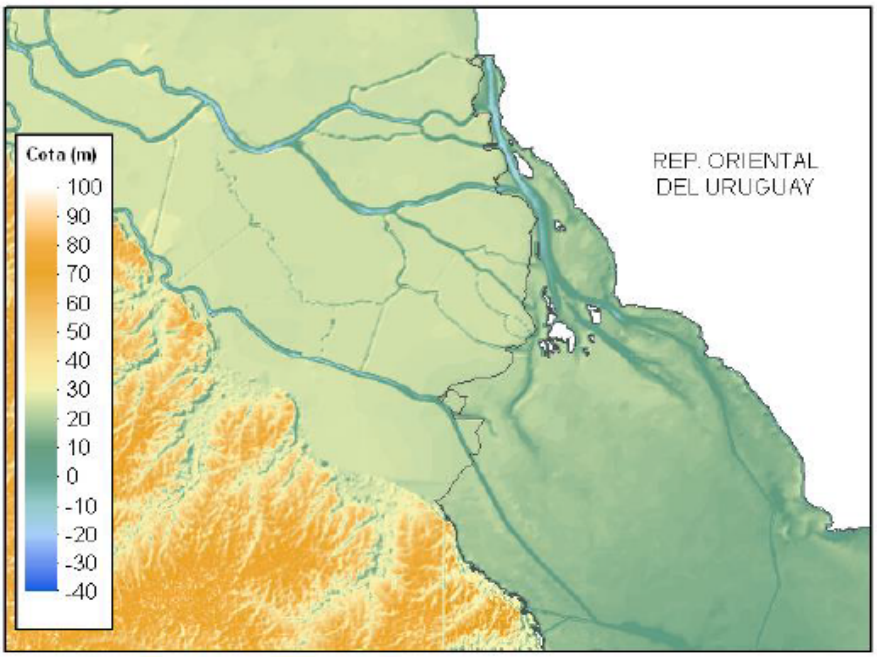

Figure D.1: Digital Elevation Model Lower Paraná Delta [Sabarots Gerbec et al., 2017b]

D.1.1. Longitudinal sections

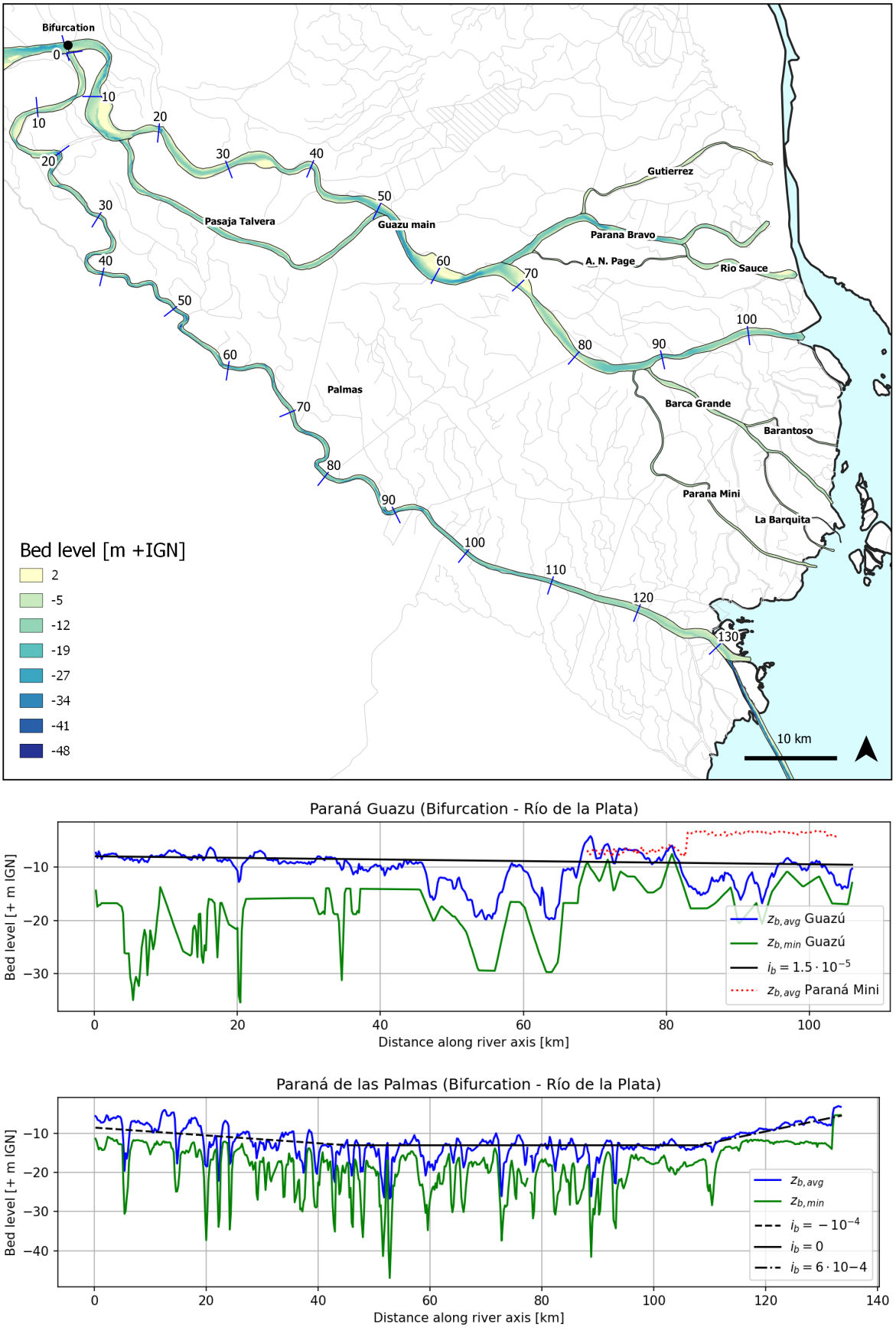

Figure D.2: Paraná Guazú and Las Palmas average (z_{avg}) and thalweg bed level (z_{avg}) in the Lower Delta

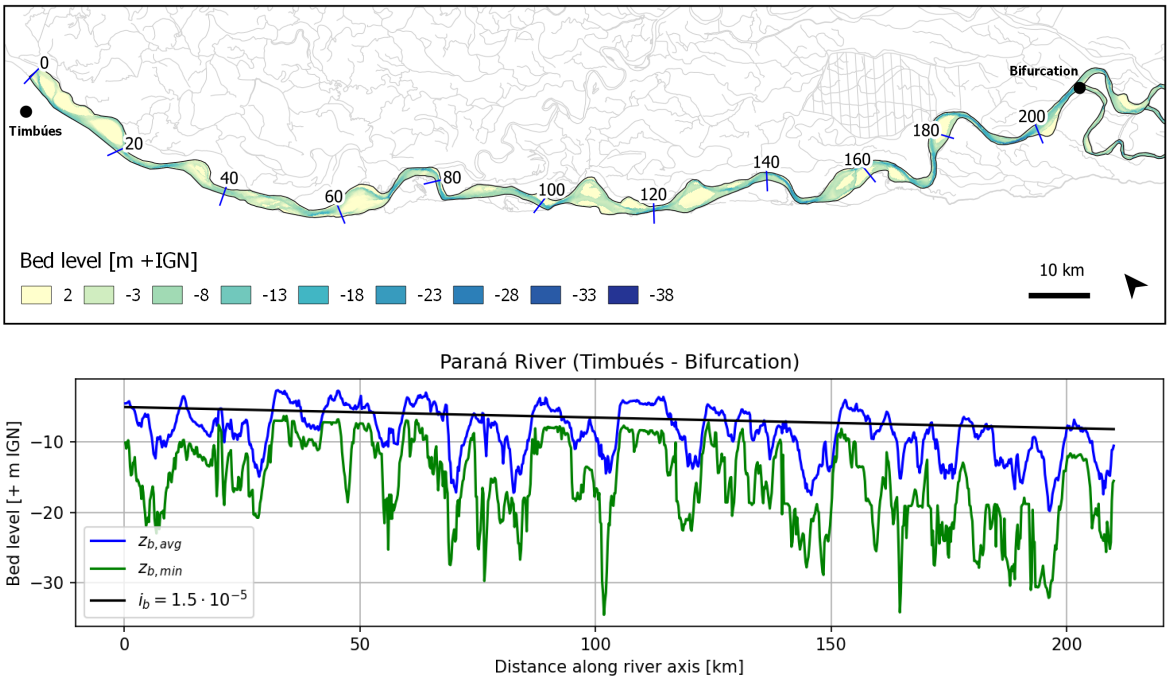

Figure D.3: Paraná River average (z_{avg}) and thalweg bed level (z_{avg}) from Timbues to the Palmas-Guazú bifurcation

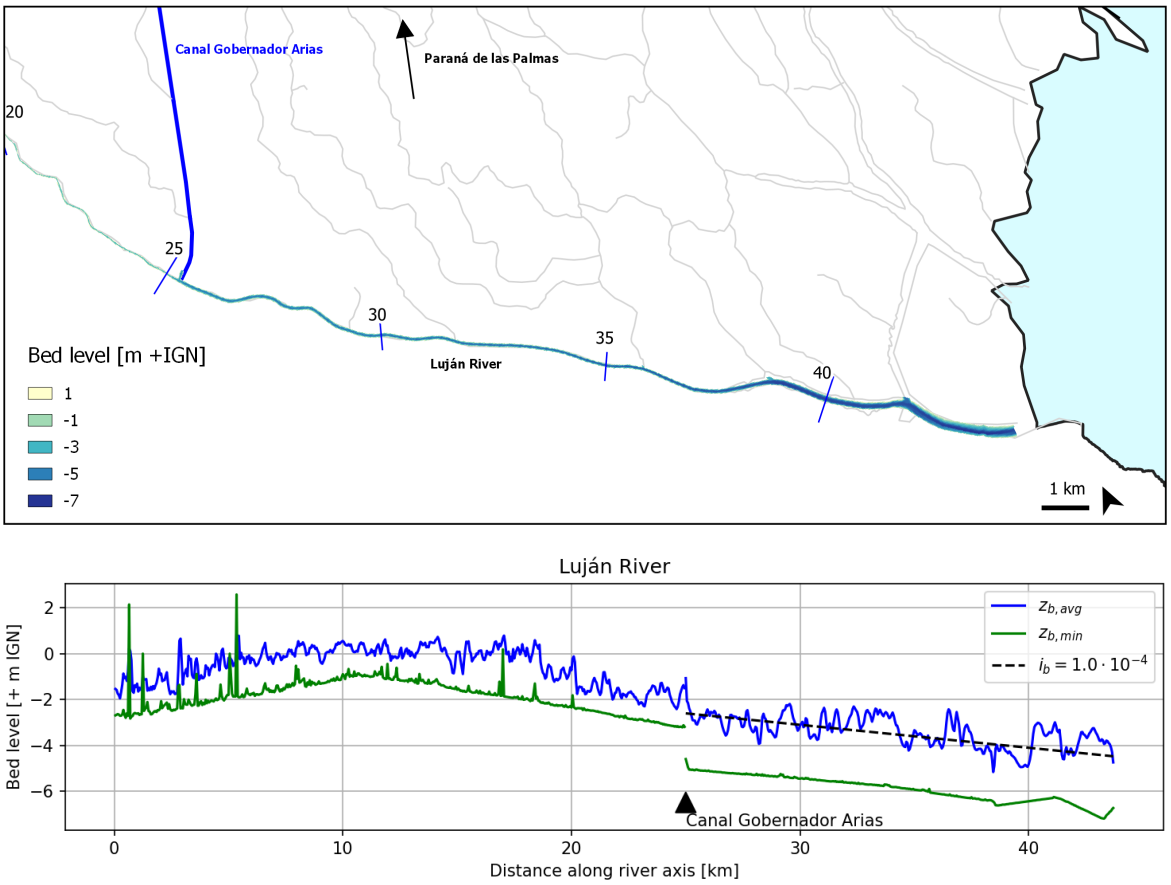

Figure D.4: Luján River average (z_{avg}) and thalweg bed level (z_{avg}), only downstream section displayed on map

D.1.2. Cross sections Paraná de las Palmas

Figure D.5 displays various cross sections of the Paraná de las Palmas. The distance labels are in accordance with those presented in Figure D.2. Multiple cross sections are shown in the most downstream, heavily dredged reach (120-130 km). An indication of the conveyance area A_c is given for a water level at 0.5 m + IGN.

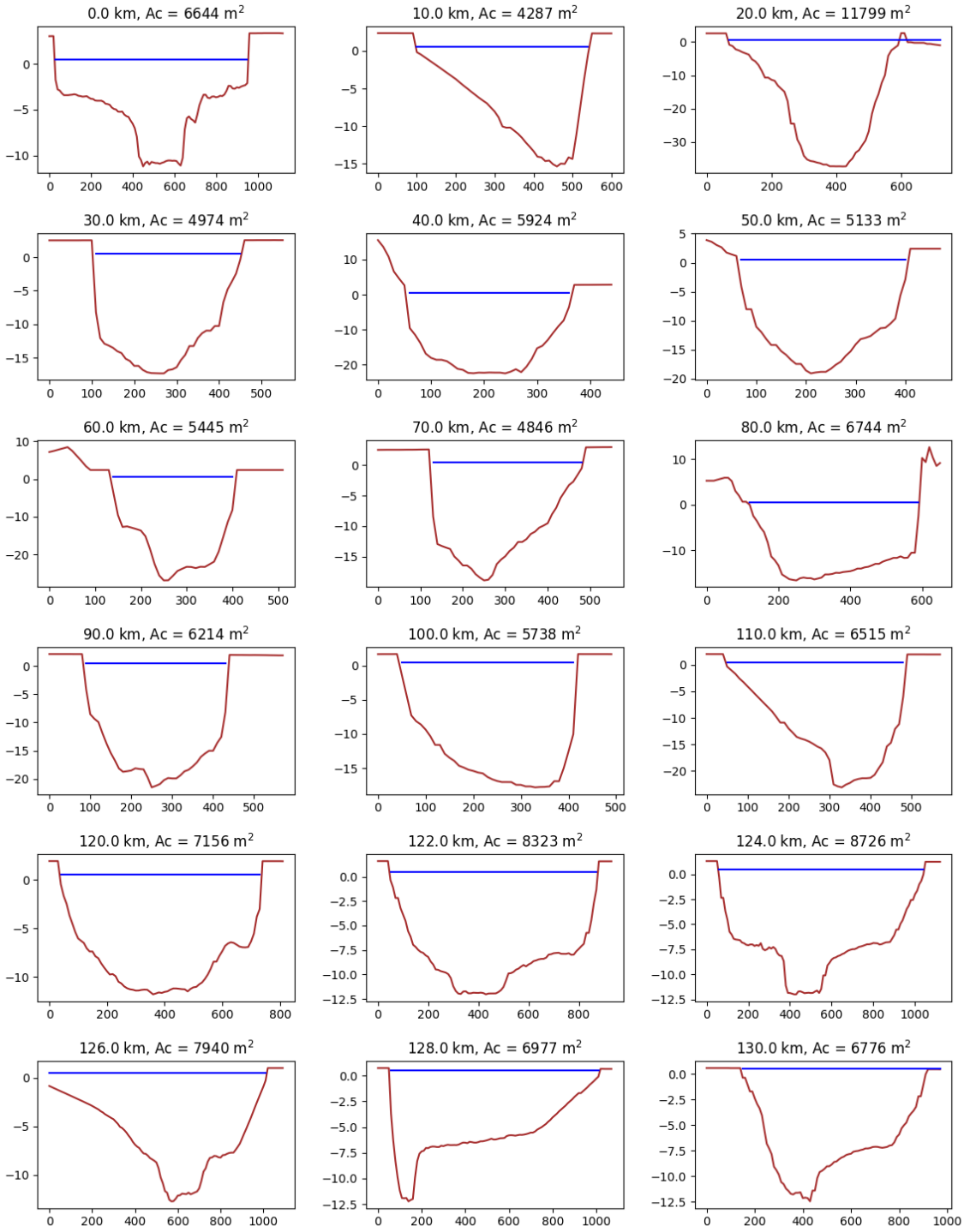

Figure D.5: Paraná de las Palmas cross sections

D.2. Channel network

D.2.1. Individual channels - depth measurements 2021 - 2022

Field surveys were carried out in December 2021 and March 2022 (see Appendix I for the survey report). These surveys included taking depth measurements by Echo Sounder in various channels in the Lower Delta channel network near the deltaic front. The measured bed levels of the channel centrelines are displayed in Figure D.6. It can be observed that i) more inland located channels are

generally shallower than channels located nearshore and ii) various channels display reducing depths as the distance from a main river branch increases.

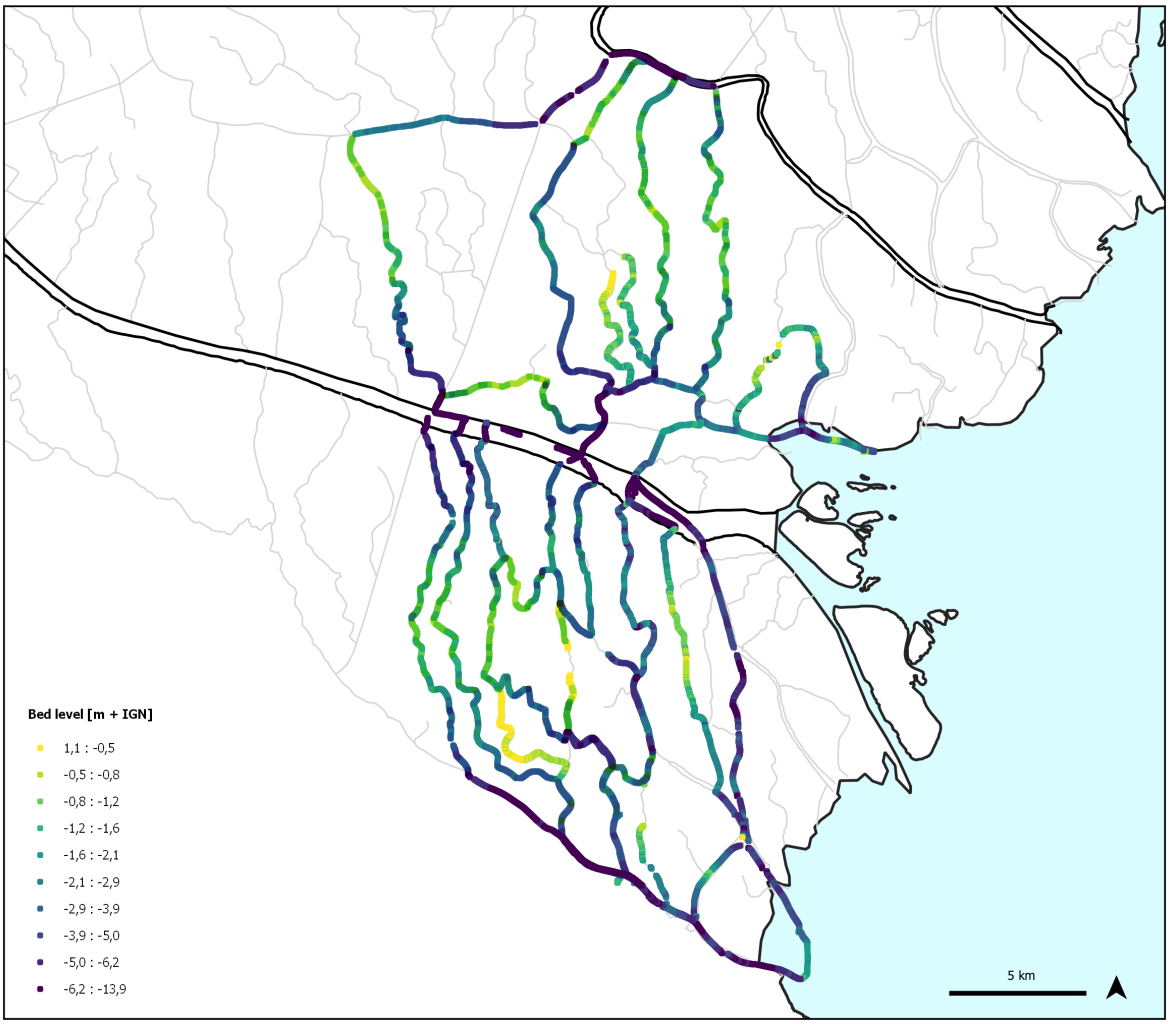

Figure D.6: Echo sounder centerline depth measurements, field surveys December 2021 and March 2022

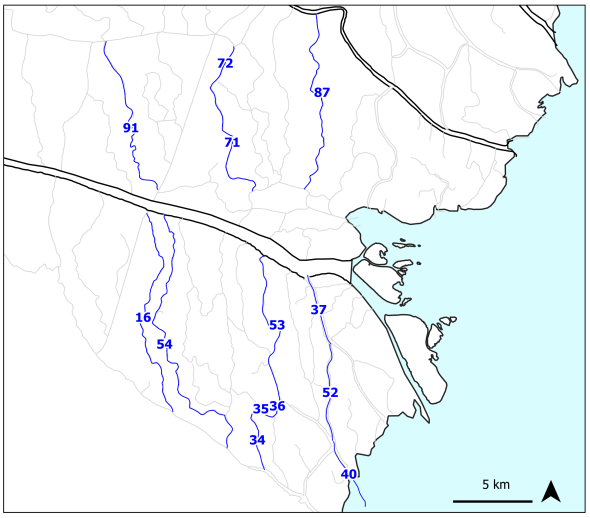
72
87
91
71
16
54
53
37
52
35
36
34
40
5 km

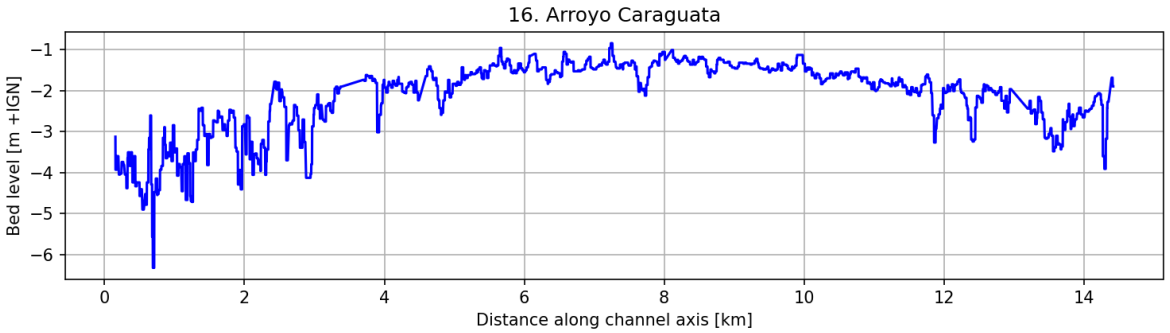
16. Arroyo Caraguata
Bed level [m +IGN]
Distance along channel axis [km]

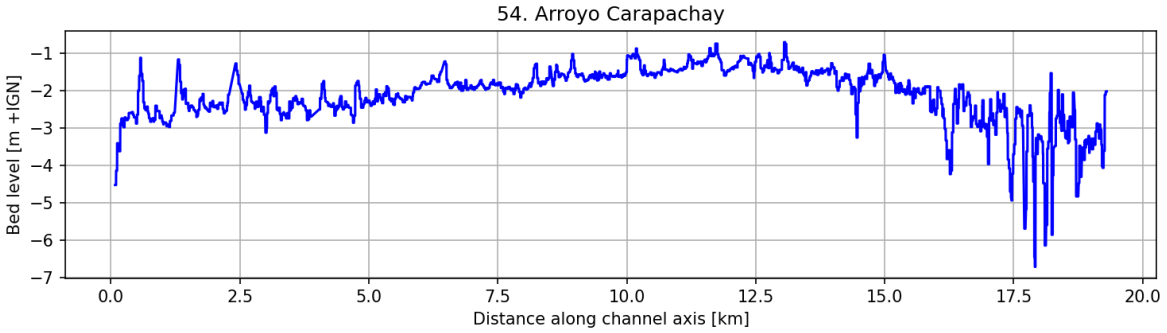
54. Arroyo Carapachay
Bed level [m +IGN]
Distance along channel axis [km]

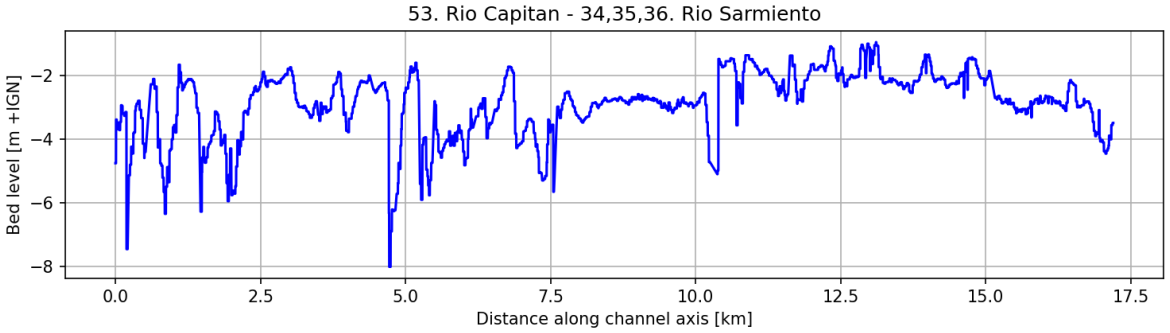
53. Rio Capitan - 34,35,36. Rio Sarmiento
Bed level [m +IGN]
Distance along channel axis [km]

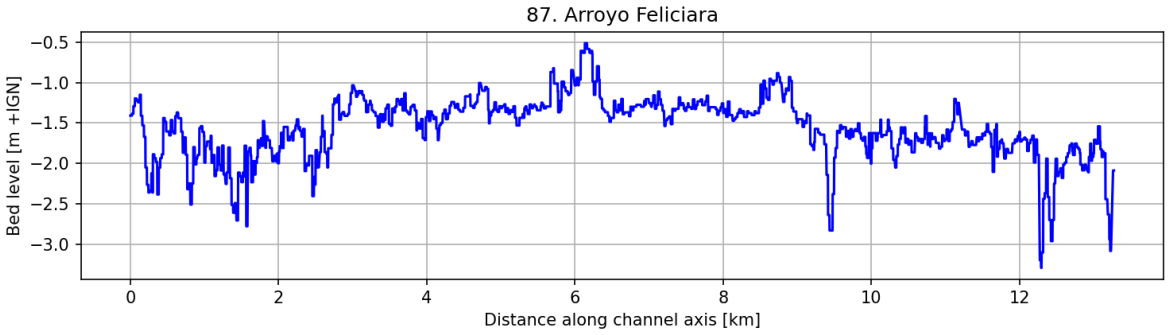
87. Arroyo Feliciara
Bed level [m +IGN]
Distance along channel axis [km]

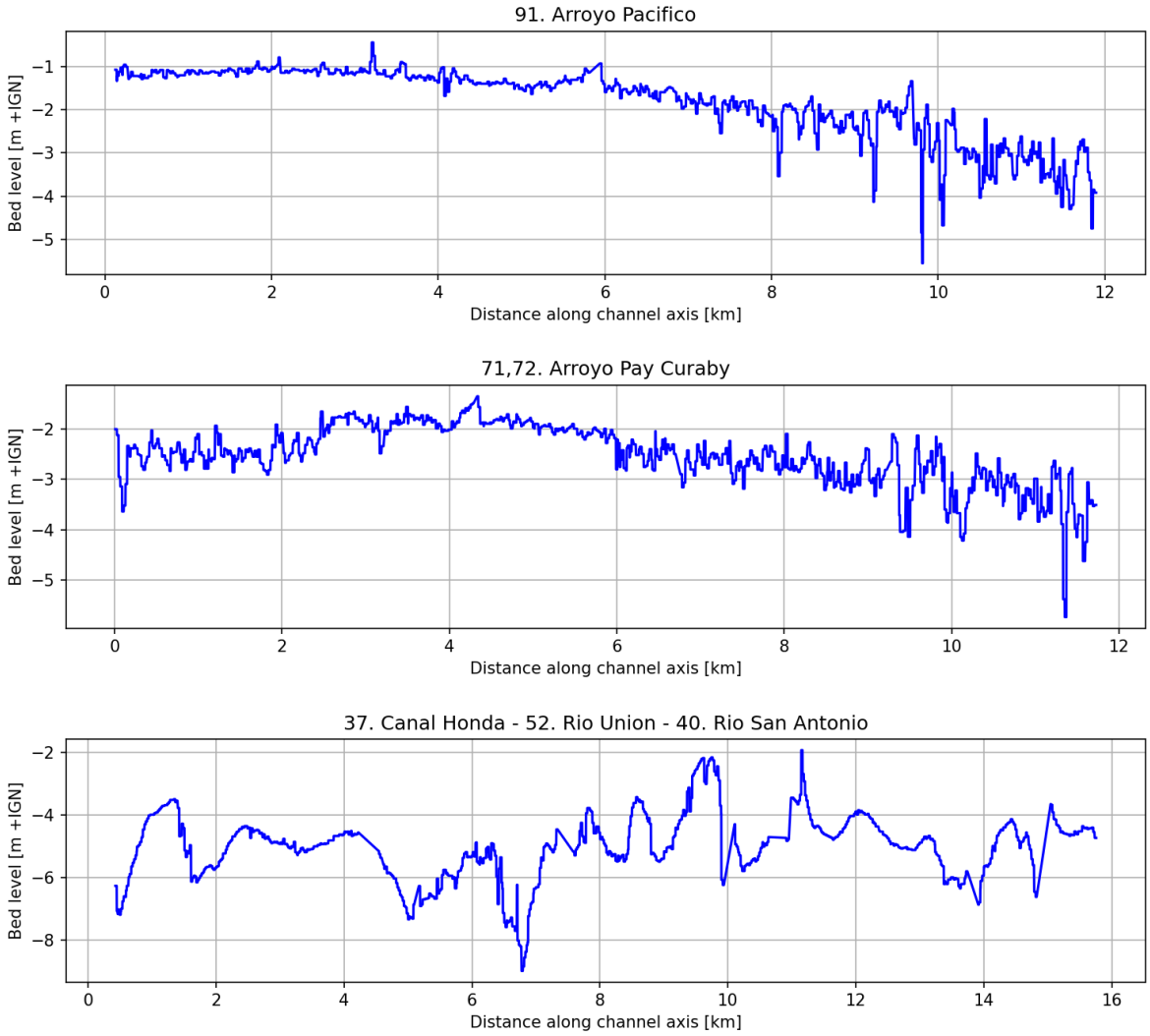

D.3. Procedure - bathymetrical data preparation numerical experiments

As described in Chapter 2, bathymetrical data on the main river branches was used as input for the numerical model. In order to obtain usable bathymetry input data for the 1D channel network in Delft3D FM, a data manipulation procedure using QGIS 3 was applied to the point data obtained during the field surveys in December 2021 and March 2022. The following section describes the procedure and argues the assumptions made.

Measurement data obtained with the Echo Sounder (field report; see section X) exists of point measurements along the channel axis and cross sections at approximately every 1 to 3 km, with the bed level referenced from IGN and spatial coordinates. The cross sections can be used to generate an hydrologically accurate DEM by interpolating along the channel centreline. This is however not applicable to the 1D cell network as i) input for the 1D cell network must consist out of *single depth values per cell* and ii) various parts of the 1D cell network are simplified, resulting in a difference between the location of the cell and the coordinates of the point measurements. Steps 1 to 12 describe the steps taken in order to generate a bathymetry that can be used as modelling input for the 1D cell network in Delft3D FM.

1. Manually extract the point measurements in the cross sections, resulting in a layer with only the channel axis measurements.
2. The resulting values for the bed levels should not directly be used in the numerical model, as

the measurements represent the bed levels in the channel axis and the values in the model should represent the *bed level based on the average depth* as this term is present in the one-dimensional balance equations. In order to obtain the ratio between the minimum bed level h_{min} and $h_{avg} = A_c/B$, approximately 30 cross sections were extracted from the DEM based on field surveys in 2017 and 2018 The shape of the channels is assumed to be accurately represented in this DEM. The ratio h_{avg}/h_{min} was generated by executing the steps 3 to 10.

3. Using the Points along geometry algorithm (ID: *native:pointsalonglines*), generate points on the selected cross sections from step 2.
4. Use the Sample raster values algorithm (ID: *native:rastersampling*) to assign bed level values from the DEM to the points layer.
5. Manually extract all points with bed level values exceeding z = +0.5 m IGN (based on the average water level at San Fernando).
6. Compute the water depths by adding 0.5 to the point values ($-z_b$).
7. Use the algorithm Join attributes by nearest (*ID: native:joinbynearest*) to assign unique cross section ID's to the point layer from step 6.
8. Use the algorithm Statistics by categories (ID: *qgis:statisticsbycategories*) to extract a non-geometrical layer with statistical parameters on the depth attribute, categorized by the unique cross section ID.
9. Use the Field calculator to generate a new attribute *ratio* = *mean/min*.
10. Use the Basic statistics for fields algorithm (ID: *native:basicstatisticstofields*) to obtain the average value of the *ratio* attribute generated in step 8.

The ratio between h_{avg}/h_{min} results from step 9, and was approximately 0.635. This is approximately in accordance with the ratio between the minimum and mean depth for a perfect parabolic cross section (see Figure D.7). Multiplying this value with the measured depth would imply that the points measurements were the deepest points in the cross sections. Although the measurements in the channel centerline can be considered located in the deepest regions of the channel, assigning the absolute maximum depth to this measurements would be an unrealistic assumption. Therefore, a ratio h_{avg}/h_{min} of 0.7 is assumed to be more realistic. The water depth point measurements will thus be multiplied with 0.7 before translating to bed levels and executing steps 10 to 12.

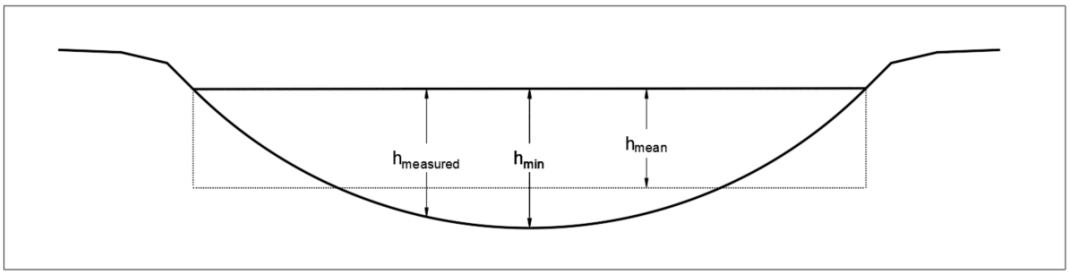

Figure D.7: Depth ratios

11. Use the rasterize: vector to raster (ID: *gdal:rasterize*) algorithm to convert the point measurements with the corrected bed level elevations to raster pixels.
12. convert the raster pixels to Delft3D FM compatible .xyz files with the algorithm r.out.xyz (ID: *grass7:r.out.xyz*.)
13. Using triangular interpolation in the Delft3D FM suite to interpolate the xyz samples to the grid points results in an accurate representation of the depths in the grid cells. This is only the case if the grid and the samples are located sufficiently close to each other, as visualized in Figure D.8.

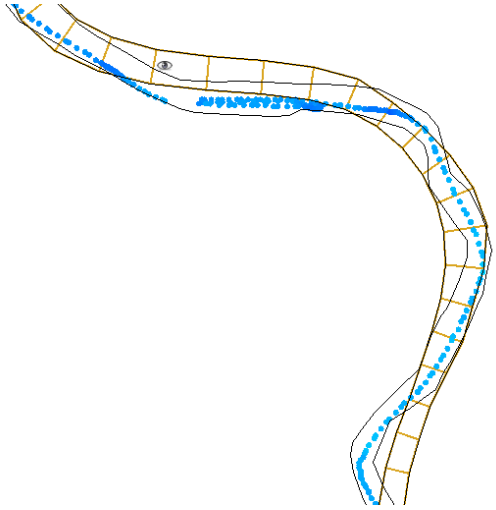

Figure D.8: Point samples (blue) slightly offset from the grid cells (orange)

14. At some locations, there is a discrepancy between the generated grid from the DEM of the main branches and the channel network, resulting in some of the channels to be closed off. The bathymetries at these locations are smoothed out manually by using the Overwrite value operation in the Delft3D FM Spatial Operations tab (Figure D.9).

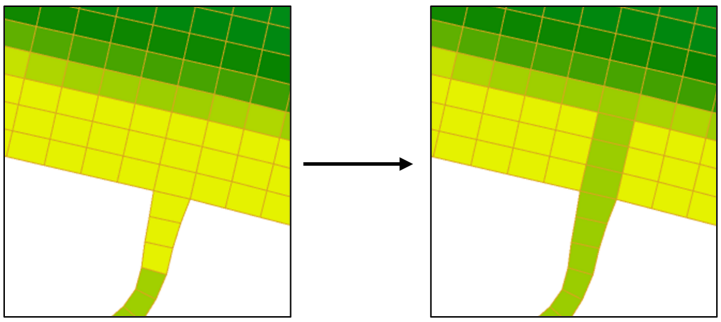

Figure D.9

E

Water level data analysis

The various water level measurement stations that are present in the Paraná Delta are displayed in Figures E.1 and E.2.

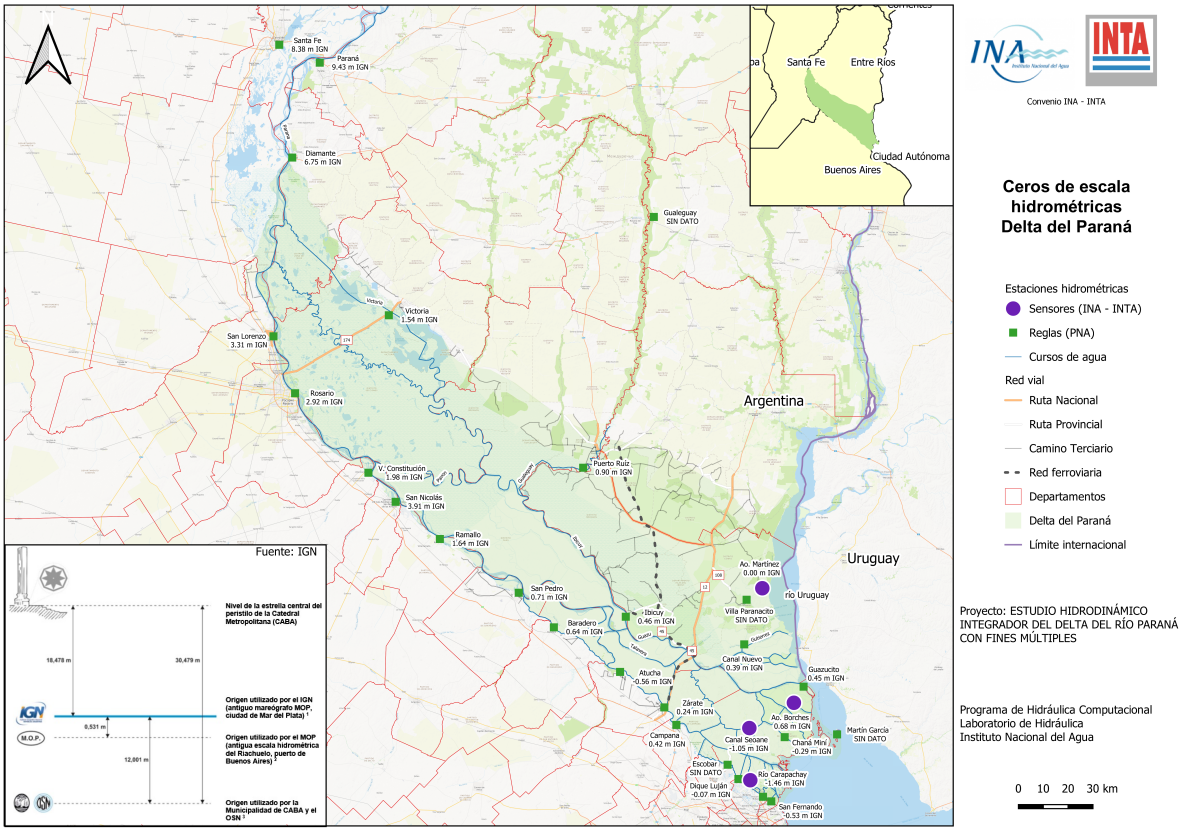

Figure E.1: Measurement stations in the Paraná Delta. Source: Website INA (https://www.argentina.gob.ar/ina)

The majority of the measurement stations are owned by the the *Prefectura Naval Argentina* (PNA) or the *Subsecretaría de Puertos y Vías Navagables* (SSPyVN). Distinction is made between measurement stations by the PNA where daily or sub-daily water level data are retrieved , and stations governed by the SSPyVN where water level data is retrieved (sub-)hourly [Sabarots Gerbec et al., 2017a]. The latter type is particularly suitable for analysing the tidal propagation in the delta, as the period between measurements significantly subceeds the tidal period. Some of the water level measurement stations require manual reading of a scale, some are equipped with a FdX water level measurement device that uploads the data with by mobile phone network [Morale et al., 2018].

E.1. Average water level San Fernando

As input for the downstream boundary condition in the numerical experiments (Chapter 4), the average water level at San Fernando was determined. For the base scenario including yearly-averaged, regular conditions, the average water level in the non-ENSO periods in 2010-2020 were determined. For the water level during a high discharge event, the average water level between January and May in 2016 was considered. The results are displayed in Table E.1.

Table E.1: Average water level at San Fernando during different conditions (2010 - 2020)

	Period	Water level [m + IGN]
Regular conditions	2010 - January 2016	0.51
	May 2016 - 2020	0.61
High discharge	January - May 2016	0.81

E.2. Tidal propagation

The tidal signal of the high-frequency measurement stations in the Lower Delta were analyzed. In Figure E.2 the damping coefficient α (as defined in Equation (E.1) of the tidal wave in relation to the wave height in San Fernando (SF) is presented. It must be noted that the analysis was carried out manually over several tidal cycles during regular conditions. These are approximate average values, during high water levels, the influence of friction decreases while during low water levels the influence of friction increases. The yellow arrow indicates the maximum influence of the tidal wave during regular conditions, located near Villa Constitución.

$$H_{Location} = \alpha \cdot H_{SanFernando} \tag{E.1}$$

In the right figure of Figure E.2, the delay in the tidal signal compared to the San Fernando signal is displayed. The tidal delay in Canal Seoane (CS) and Arroyo Carapachay (AC) obtained from the timeseries can be used to verify the behaviour of the tidal wave in the numerical model.

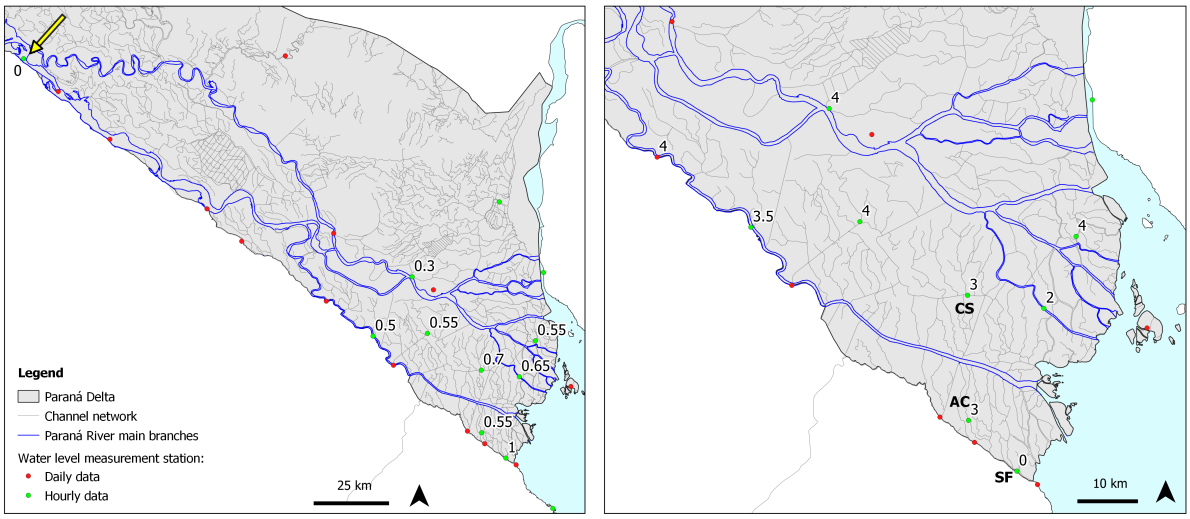

Figure E.2: Damping of the tidal wave in relation to the amplitude in San Fernando (yellow arrow indicates the upstream limit of the tidal influence during regular conditions) and the delay of the tidal wave [hrs] in the Lower Delta (right figure)

E.3. Bankfull water level

A storm surge event occurred at the end of January 2021. From comparing the water level records at in the estuary (station Buenos Aires) and Arroyo Carapachay, the bankfull water level can be estimated. In Figure E.3 it can be seen that the rate of water level increase at Arroyo Carapachay significantly decreases around 1.7 m+ IGN. At Zarate, the bankfull level lies around 2 m+ IGN.

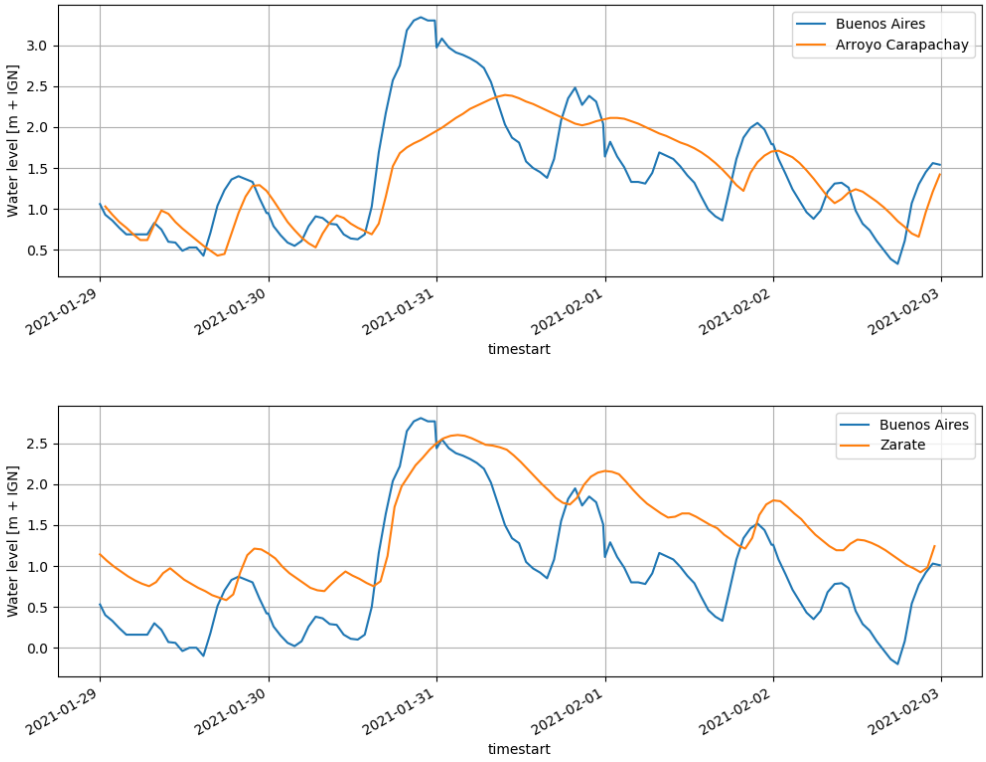

Figure E.3: Water level records around the January-February storm surge in 2021

F

Discharge data analysis

F.1. Direct discharge measurements and Q-H curve

Q-H curves relating measured water level data points to a fitted curve of discharge is available in Rosario, Timbues and Santa Fé. The discharge curves in Timbues and Santa Fé are updated every 2 months by means of new ADCP discharge measurements. Another QH curve is available in Corrientes, upstream of the Paraná Delta, just downstream of the confluence with the Paraguay River. All data is freely available at [https://snih.hidricosargentina.gob.ar/]. At Zarate (Paraná de las Palmas) and Brazo Largo (Paraná Guazú), 2-monthly ADCP discharge measurements are available.

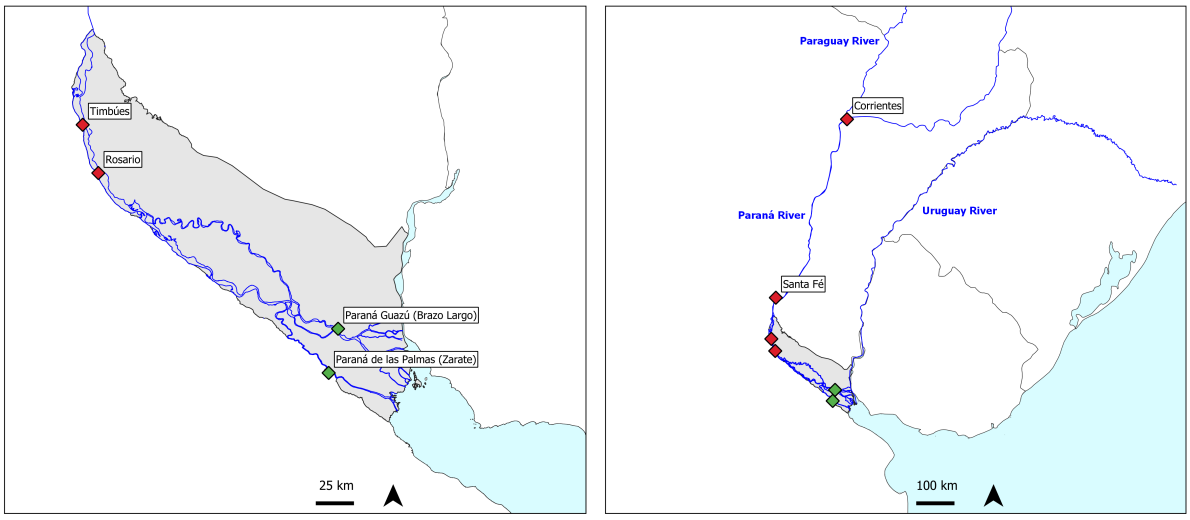

Figure F.1: Discharge data locations in the Paraná Delta (left) and the Middle Paraná River

Figure F.2 compares the computed QH curve in Timbués with the 2-monthly point measurements in Zarate and Brazo Largo. It can be seen that during irregularly high or low flows, the Q-H curve does not give accurate results, as the discharge in Zarate and Brazo Largo combined should add up to the discharge in Timbués. When the discharge in Timbues exceeds roughly 25,000 m^3/s, flood plains start to inundate, and this effect is not taken into account in the QH curve. When considering high discharges, the Timbués discharge can be represented by multiplying the Santa Fé discharge with 1.19, as Happee [2019] suggested. The multiplication factor is based on the average ratio between Santa Fe and Timbués discharges, which exists due to the Colastine and Coronda tributaries not being included in the Santá Fe measurements. To obtain continues time series for the Palmas and Guazú branches, the linear relation from Re et al. [2009] (see Chapter 2 of the main report) was used to approximate the ratio of the Guazú discharge with the total discharge (here: the corrected discharge in Timbues). It can be seen that the computed values of the Guazú and Palmas discharges are in

reasonable accordance with the 2-monthly measured values. These computed values of the separate branches can be used for numerical modelling of individual river branches.

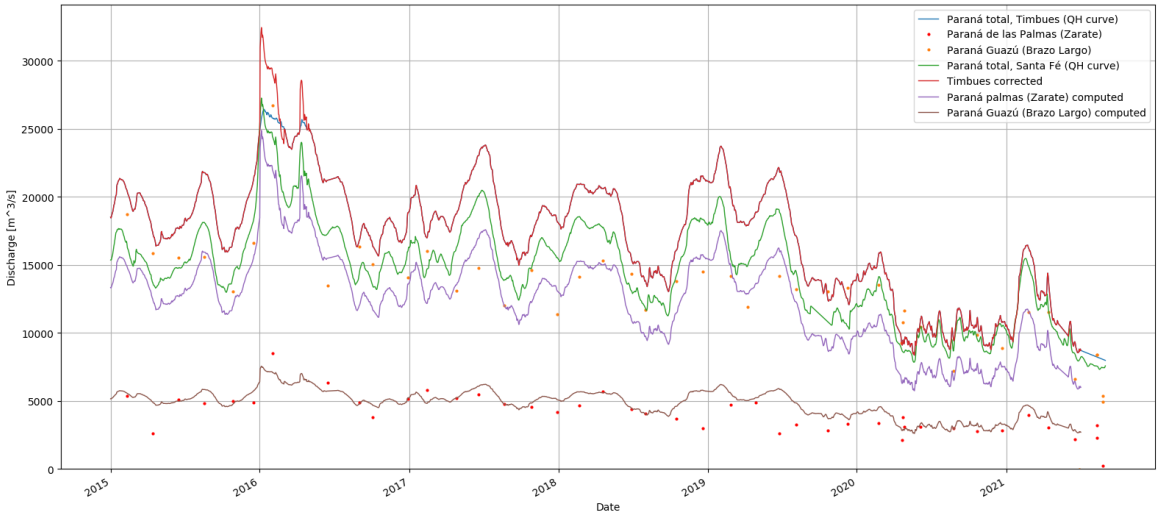

Figure F.2: Comparison of the QH curve in Timbues, computed discharges in Timbues, Zarate and Brazo largo and measured discharges in the Guazú and Las Palmas branches

F.2. Short-term analysis (2010-2020)

As can be seen in Figure F.2, rather high discharges were experienced in during the first half of the El Niño year 2016, and low discharges in 2020, which have persisted to at least 2022. The average discharge at Timbués (representative for the total discharge in the Lower Delta) during the El Niño event of 2014-2016 and 2020 were compared to the periods before and after and displayed in Table F.1, as well as the pre-, and post- average discharges and the discharge during the period of historically low water, persistint untill the moment of writing. As can be seen in Figure F.2, the extreme discharges in 2016 exceeded 30,000 m^3/s.

Table F.1: Average discharge [m^3/s] at Timbués (corrected) during the periods pre-, during and post the 2016 ENSO event

		Discharge
pre-ENSO	2010 - 2016	18331
ENSO	Jan - May 2016	24278
post-ENSO	May 2016 - 2020	18561
Dry period	2020 - 2022	11532

F.3. Long-term analysis (1904-2020)

In order to establish a better understanding on the long-term discharge variability of the Paraná River and the potential influence of land use change during the 1960's and 1970's, discharge (Q-H curve) records were analysed to detect trends in monthly and yearly averaged flows. The occurrence of discharge maxima is not considered, as the QH is considered not to represent peak flows well due to the effect of flood plains on the water level during extreme discharge events. The severity of this effect differs per location, as in Timbúes this effect is more pronounced than in Santa Fé [Happee, 2019]. The results as presented in Table F.2 should be interpreted with the uncertainties associated with Q-H curves in hindsight. These uncertainties are addressed explicitly in Chapter 7.

Table F.2: Montlhy averaged discharges [m^3/s] during the periods pre- and post extensive land use change in the La Plata Basin

	[1904-1960]	[1990-2020]	Absolute change	Relative change
Corrientes	16227	18780	+2553	+16%
Tunél Subfluvial	13222	15418	+2196	+17%
Timbúes (corrected)	14260	17956	+3566	+26%

F.4. ADCP measurements 25 March 2022

As part of the series field surveys executed in 2021 and 2022 (See Appendix I), stationary ADCP measurements were executed on 25 March 2022. The goal of the stationary measurements was to capture the tidal dynamics in the entrance of a channel. Figure F.3 displays the discharge and the main velocity. Water level series at the Arroyo Carapachay measurement station display that when the measurements started around 12:00, the water level was approximately at its highest point. Therefore the maximum tidal velocities would have occurred several hours earlier. This implies that flood velocities could be around twice as high as ebb velocities.

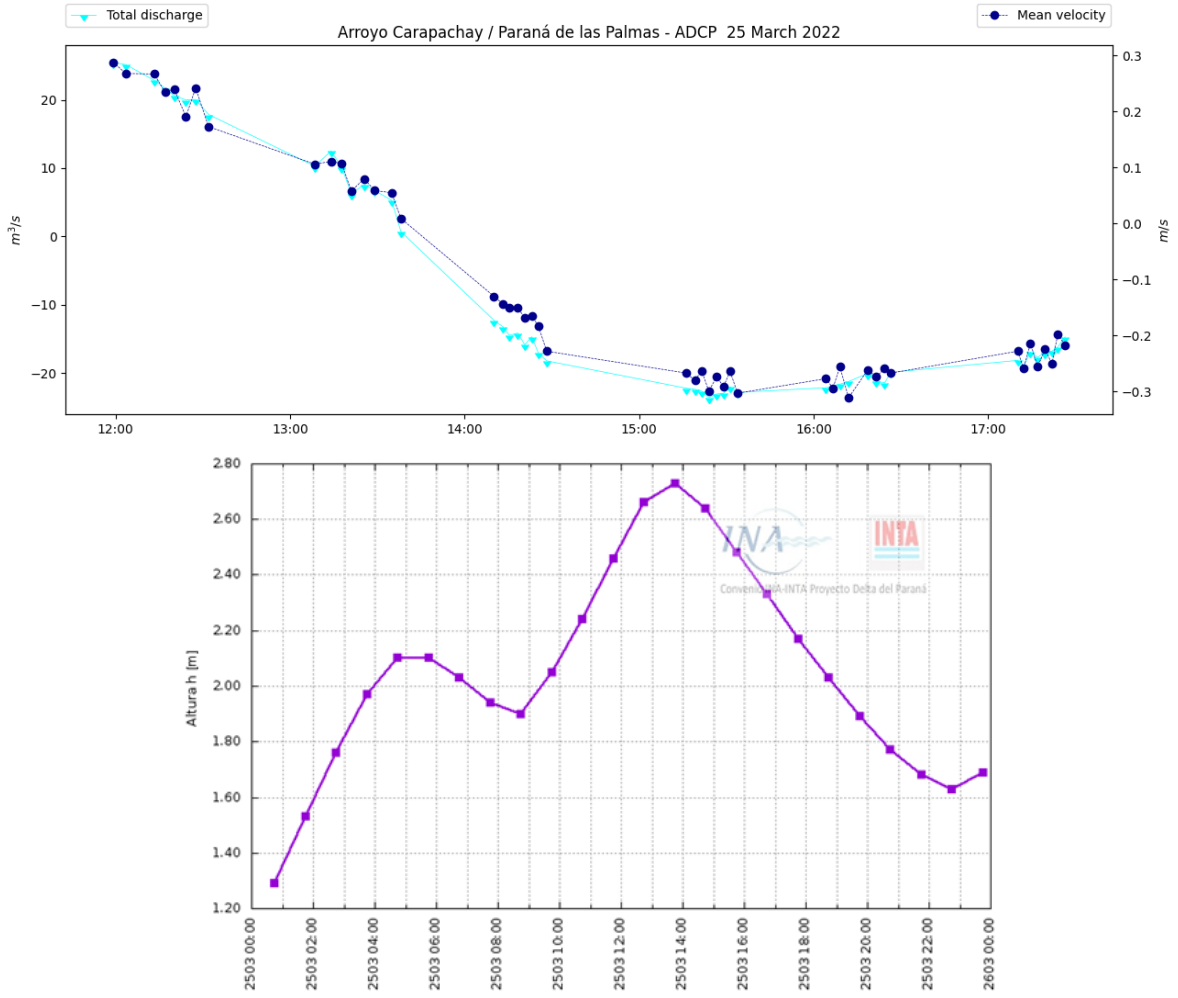

Figure F.3: ADCP results and water level data on 25 March

G

Dredging data

G.1. Reach definition Paraná de las Palmas

PARANA DE LAS PALMAS

Paso	Progresiva	Este	Norte	Curva	Radio	Ancho de Solera	Veril Verde	Veril Rojo
ILU19-02-10	49.800	5637347.923	6203212.649			140.0	1/4	1/4
ILU19-02-10	49.991	5637200.171	6203334.186	SI	2709.560	140.0	1/4	1/4
ILU19-02-10	51.402	5635931.673	6203913.067			140.0	1/4	1/4
ILU19-02-10	53.011	5634344.961	6204182.002	SI	4309.133	140.0	1/4	1/4
ILU19-02-10	54.571	5632886.890	6204712.447			140.0	1/4	1/4
ILU19-02-10	56.997	5630793.378	6205938.884	SI	6014.295	140.0	1/4	1/4
ILU19-02-10	57.927	5629958.514	6206344.928			140.0	1/4	1/4
ILU19-02-10	58.400	5629518.031	6206518.527			140.0	1/4	1/4
ILU-TOR19-02-10	58.400	5629518.031	6206518.527			140.0	1/4	1/4
ILU-TOR19-02-10	59.151	5628819.196	6206793.946	SI	6116.353	135.7	1/4	1/4
ILU-TOR19-02-10	59.797	5628206.665	6206998.699			132.0	1/4	1/4
ILU-TOR19-02-10	61.202	5626852.996	6207373.010			124.1	1/4	1/4
ILU-TOR19-02-10	61.562	5626506.079	6207468.939			122.0	1/4	1/4
ILU-TOR19-02-10	62.215	5625876.383	6207643.061	SI	19163.940	122.0	1/4	1/4
ILU-TOR19-02-10	63.285	5624854.002	6207956.725			122.0	1/4	1/4
ILU-TOR19-02-10	69.347	5619110.228	6209895.830	SI	3920.757	122.0	1/4	1/4
ILU-TOR19-02-10	69.733	5618738.530	6210001.225			122.0	1/4	1/4
ILU-TOR19-02-10	75.167	5613444.724	6211224.030	SI	6749.132	122.0	1/4	1/4
ILU-TOR19-02-10	78.441	5610553.565	6212691.045			122.0	1/4	1/4
ILU-TOR19-02-10	83.096	5607029.676	6215732.915	SI	4603.095	122.0	1/4	1/4
ILU-TOR19-02-10	83.919	5606457.819	6216323.530			122.0	1/4	1/4
ILU-TOR19-02-10	84.088	5606353.871	6216457.062			130.5	1/4	1/4
ILU-TOR19-02-10	84.779	5605939.615	6217009.887			165.0	1/4	1/4
TOR19-02-10	84.8	5605939.615	6217009.887			165.0	1/4	1/4
TOR19-02-10	85.245	5605673.845	6217366.456	SI	1500.012	165.0	1/4	1/4
TOR19-02-10	86.717	5604394.738	6217968.094			165.0	1/4	1/4
TOR19-02-10	87.015	5604096.618	6217952.884			165.0	1/4	1/4
TOR-HNJ19-02-10	87.015	5604096.618	6217952.884			165.0	1/4	1/4
TOR-HNJ19-02-10	87.080	5604031.379	6217949.556	SI	4565.736	165.0	1/4	1/4
TOR-HNJ19-02-10	88.608	5602547.437	6217620.518			165.0	1/4	1/4
TOR-HNJ19-02-10	88.610	5602544.901	6217619.489			165.0	1/4	1/4
TOR-HNJ19-02-10	87.015	5604096.618	6217952.884			165.0	1/4	1/4
TOR-HNJ19-02-10	87.080	5604031.379	6217949.556	SI	4565.736	167.3	1/4	1/4
TOR-HNJ19-02-10	88.608	5602547.437	6217620.518			222.0	1/4	1/4
TOR-HNJ19-02-10	88.610	5602544.901	6217619.489			222.0	1/4	1/4
HNJ19-02-10	88.600	5602544.901	6217619.489			222.0	1/4	1/4
HNJ19-02-10	89.252	5601941.223	6217372.053	SI	673.618	222.0	1/4	1/4
HNJ19-02-10	90.306	5601064.297	6217735.423			222.0	1/4	1/4
HNJ19-02-10	90.406	5601025.625	6217827.884			222.0	1/4	1/4
HNJ-CAP19-02-10	90.406	5601025.625	6217827.884			222.0	1/4	1/4
HNJ-CAP19-02-10	92.156	5600384.496	6219456.251			165.0	1/4	1/4
CAP19-02-10	92.200	5600384.496	6219456.251			165.0	1/4	1/4
CAP19-02-10	92.349	5600330.622	6219594.854	SI	3271.704	165.0	1/4	1/4
CAP19-02-10	93.351	5599831.449	6220458.985			165.0	1/4	1/4
CAP19-02-10	93.651	5599643.323	6220693.085	SI	1304.456	165.0	1/4	1/4
CAP19-02-10	94.378	5599057.097	6221107.301			165.0	1/4	1/4
CAP19-02-10	94.432	5599006.434	6221125.017	SI	2091.005	165.0	1/4	1/4
CAP19-02-10	95.956	5597516.731	6221083.336			165.0	1/4	1/4
CAP19-02-10	96.011	5597465.711	6221062.224	SI	3381.862	165.0	1/4	1/4
CAP19-02-10	96.762	5596745.551	6220854.135			165.0	1/4	1/4
CAP19-02-10	96.805	5596702.809	6220846.788	SI	1650.656	165.0	1/4	1/4
CAP19-02-10	97.378	5596133.007	6220848.633			165.0	1/4	1/4
CAP19-02-10	97.545	5595968.575	6220877.996	SI	2270.657	165.0	1/4	1/4
CAP19-02-10	98.693	5594936.191	6221350.748			165.0	1/4	1/4
CAP19-02-10	98.997	5594699.637	6221542.876			165.0	1/4	1/4

CAP-EST19-02-10	98.987	5594699.637	6221542.876			165.0	1/4	1/4
CAP-EST19-02-10	99.683	5594174.420	6221999.003			248.0	1/4	1/4
EST19-02-10	99.700	5594174.420	6221999.003			248.0	1/4	1/4
EST19-02-10	100.122	5593866.555	6222287.626			258.6	1/4	1/4
EST19-02-10	100.134	5593858.160	6222295.496	SI	444.427	258.6	1/4	1/4
EST19-02-10	101.088	5594056.156	6223051.332			258.6	1/4	1/4
EST19-02-10	101.097	5594065.233	6223053.460			257.0	1/4	1/4
EST19-02-10	101.300	5594262.641	6223097.557	SI	806.405	221.6	1/4	1/4
EST19-02-10	101.400	5594359.016	6223125.481			204.0	1/4	1/4
EST19-02-10	102.433	5594892.025	6223928.874			204.0	1/4	1/4
EST19-02-10	102.791	5594872.386	6224285.758	SI	1151.246	204.0	1/4	1/4
EST19-02-10	103.568	5594580.520	6224990.499			204.0	1/4	1/4
EST19-02-10	103.598	5594560.511	6225012.844			204.0	1/4	1/4
EST-BAR19-06-10	103.598	5594560.511	6225012.844			204.0	1/4	1/4
EST-BAR19-06-10	103.985	5594302.037	6225301.490	SI	1745.149	164.9	1/4	1/4
EST-BAR19-06-10	104.870	5593573.000	6225786.379			122.0	1/4	1/4
EST-BAR19-06-10	105.787	5592707.292	6226086.159			122.0	1/4	1/4
EST-BAR19-06-10	106.979	5591691.993	6226694.295			122.0	1/4	1/4
EST-BAR19-06-10	107.037	5591649.048	6226733.981	SI	2888.768	122.0	1/4	1/4
EST-BAR19-06-10	107.482	5591420.969	6227109.484			122.0	1/4	1/4
EST-BAR19-06-10	108.533	5591143.844	6228123.209	SI	797.695	122.0	1/4	1/4
EST-BAR19-06-10	108.987	5590941.310	6228526.019			122.0	1/4	1/4
EST-BAR19-06-10	111.238	5589552.275	6230297.689	SI	1140.125	122.0	1/4	1/4
EST-BAR19-06-10	111.625	5589337.497	6230619.165			122.0	1/4	1/4
EST-BAR19-06-10	112.128	5589090.852	6231056.956	SI	2548.309	122.0	1/4	1/4
EST-BAR19-06-10	112.429	5589005.932	6231343.812			122.0	1/4	1/4
EST-BAR19-06-10	112.564	5588997.529	6231477.920	SI	669.737	122.0	1/4	1/4
BAR19-06-10	112.600	5588997.529	6231477.920				1/4	1/4
BAR19-06-10	112.867	5588977.403	6231744.421	SI	4055.963	122	1/4	1/4
BAR19-06-10	113.424	5588897.565	6232294.975				1/4	1/4
BAR19-06-10	113.487	5588884.233	6232356.724	SI	1346.227	166	1/4	1/4
BAR19-06-10	114.240	5588532.824	6233011.799				1/4	1/4
BAR19-06-10	114.345	5588460.023	6233086.562	SI	1393.088	166	1/4	1/4
BAR19-06-10	115.817	5587106.255	6233461.594				1/4	1/4
BAR19-06-10	116.851	5586106.624	6233197.607	SI	2246.352	122	1/4	1/4
BAR19-06-10	117.210	5585753.876	6233134.028				1/4	1/4
BAR19-06-10	117.494	5585471.323	6233106.118	SI	2596.650	122	1/4	1/4
BAR19-06-10	118.343	5584627.340	6233161.164				1/4	1/4
BAR19-06-10	119.315	5583680.918	6233381.480	SI	769.001	205	1/4	1/4
BAR19-06-10	120.142	5583113.489	6233927.669				1/4	1/4
BAR19-06-10	120.256	5583083.459	6234037.539	SI	905.730	199	1/4	1/4
BAR19-06-10	120.599	5582932.940	6234344.068				1/4	1/4
BAR19-06-10	121.033	5582671.652	6234690.601	SI	1018.400	186	1/4	1/4
BAR19-06-10	121.313	5582474.910	6234888.143				1/4	1/4
BAR19-06-10	121.320	5582468.961	6234892.667				1/4	1/4
BAR-ANT19-02-10	121.300	5582468.961	6234892.667			186.0	1/4	1/4
BAR-ANT19-02-10	122.580	5581421.329	6235628.104			122.0	1/4	1/4
BAR-ANT19-02-10	123.148	5580956.443	6235954.455			122.0	1/4	1/4
BAR-ANT19-02-10	125.068	5579384.667	6237057.842			198.4	1/4	1/4
ANT19-02-10	125.000	5579384.667	6237057.842			218.0	1/4	1/4
ANT19-02-10	125.396	5579063.107	6237289.202	SI	545.004	238.0	1/4	1/4
ANT19-02-10	126.440	5579072.657	6238180.710			238.0	1/4	1/4
ANT19-02-10	126.541	5579156.149	6238238.098	SI	514.974	245.0	1/4	1/4
ANT19-02-10	127.556	5579142.071	6239096.219			245.0	1/4	1/4
ANT19-02-10	127.575	5579125.901	6239106.154			243.1	1/4	1/4
ANT19-02-10	127.979	5578778.178	6239311.068			202.4	1/4	1/4
ANT-ALM19-02-10	127.979	5578778.178	6239311.068			202.4	1/4	1/4
ANT-ALM19-02-10	128.363	5578448.376	6239509.516	SI	1272.664	183.4	1/4	1/4

ANT-ALM19-02-10	128.716	5578175.129	6239730.575			166.0	1/4	1/4
ANT-ALM19-02-10	128.776	5578135.102	6239775.443			166.0	1/4	1/4
ANT-ALM19-02-10	128.818	5578108.261	6239807.001			166.0	1/4	1/4
ALM19-02-10	129.100	5578108.261	6239807.001			166.0	1/4	1/4
ALM19-02-10	129.464	5577880.246	6240091.015	SI	1500.003	166.0	1/4	1/4
ALM19-02-10	130.346	5577163.111	6240582.057			166.0	1/4	1/4
ALM19-02-10	130.510	5577004.764	6240622.819			182.4	1/4	1/4
ALM19-02-10	130.566	5576949.450	6240633.882			188.0	1/4	1/4
ALM19-02-10	130.603	5576912.741	6240641.225	SI	985.031	188.0	1/4	1/4
ALM19-02-10	131.676	5576160.508	6241330.627			188.0	1/4	1/4
ALM19-02-10	131.714	5576150.563	6241367.233			189.3	1/4	1/4
ALM19-02-10	132.038	5576071.637	6241681.603			200.0	1/4	1/4
LIM19-02-10	132.038	5576071.637	6241681.603			200.0	1/4	1/4
LIM19-02-10	132.390	5575985.923	6242023.008			214.0	1/4	1/4
LIM19-02-10	132.425	5575977.294	6242057.378	SI	699.992	214.0	1/4	1/4
LIM19-02-10	133.544	5575109.540	6242560.968			214.0	1/4	1/4
LIM19-02-10	133.589	5575066.397	6242547.363			209.7	1/4	1/4
LIM19-02-10	133.699	5574962.508	6242510.872			200.0	1/4	1/4
LIM-PEL19-02-10	133.699	5574962.508	6242510.872			200.0	1/4	1/4
LIM-PEL19-02-10	133.700	5574961.904	6242510.660	SI	6208.536	200.0	1/4	1/4
LIM-PEL19-02-10	134.246	5574439.086	6242352.616			200.0	1/4	1/4
LIM-PEL19-02-10	134.399	5574290.730	6242316.741			206.3	1/4	1/4
LIM-PEL19-02-10	134.400	5574289.755	6242316.518			206.3	1/4	1/4
PEL19-02-10	134.400	5574289.755	6242316.518			208.0	1/4	1/4
PEL19-02-10	134.405	5574284.880	6242315.406	SI	6110.338	208.0	1/4	1/4
PEL19-02-10	134.748	5573948.430	6242248.537			208.0	1/4	1/4
PEL19-02-10	134.751	5573945.528	6242248.043	SI	828.303	208.0	1/4	1/4
PEL19-02-10	134.801	5573896.033	6242241.147			208.0	1/4	1/4
PEL19-02-10	135.801	5573068.707	6242688.159			208.0	1/4	1/4
PEL19-02-10	135.882	5573035.496	6242761.951			214.2	1/4	1/4
PEL19-02-10	136.064	5572968.961	6242931.403			228.0	1/4	1/4
PEL19-02-10	136.097	5572957.048	6242961.742	SI	599.968	228.0	1/4	1/4
PEL19-02-10	136.727	5572485.819	6243336.056			228.0	1/4	1/4
PEL19-02-10	136.790	5572423.122	6243341.930			228.0	1/4	1/4
PEL19-02-10	136.811	5572401.910	6243342.422			226.9	1/4	1/4
PEL19-02-10	137.232	5571981.475	6243344.752			206.8	1/4	1/4
PEL-LPT19-02-10	137.214	5571981.475	6243344.752			206.8	1/4	1/4
PEL-LPT19-02-10	137.400	5571795.727	6243345.682	SI	1429.045	197.5	1/4	1/4
PEL-LPT19-02-10	137.705	5571493.187	6243379.625			182.3	1/4	1/4
PEL-LPT19-02-10	137.911	5571292.378	6243424.201	SI	24897.470	172.0	1/4	1/4
PEL-LPT19-02-10	138.910	5570312.509	6243621.163			122.0	1/4	1/4
PEL-LPT19-02-10	139.106	5570119.799	6243655.110			122.0	1/4	1/4
PEL-LPT19-02-10	139.299	5569929.686	6243687.828			122.0	1/4	1/4
LPT19-02-10	139.300	5569929.686	6243687.828			122.0	1/4	1/4
LPT19-02-10	139.900	5569338.670	6243791.268			186.0	1/4	1/4
LPT19-02-10	139.939	5569299.767	6243798.077	SI	1012.001	186.0	1/4	1/4
LPT19-02-10	141.600	5568492.038	6245038.709			186.0	1/4	1/4
LPT19-02-10	142.858	5569388.896	6245803.322			186.0	1/4	1/4
LPT19-02-10	142.898	5569428.736	6245805.903			182.1	1/4	1/4
LPT19-02-10	143.338	5569868.365	6245825.692			139.0	1/4	1/4
LPT19-02-10	143.768	5570297.930	6245845.028			182.0	1/4	1/4
LPT19-02-10	143.808	5570338.035	6245846.833	SI	1099.997	182.0	1/4	1/4
LPT19-02-10	146.042	5571251.276	6247477.874			182.0	1/4	1/4
LPT19-02-10	146.082	5571231.283	6247512.540			178.2	1/4	1/4
LPT19-02-10	146.220	5571160.182	6247630.790			165.0	1/4	1/4
LPT19-02-10	146.479	5571026.683	6247852.819			165.0	1/4	1/4
LAR19-02-10	146.400	5571026.683	6247852.819			165.0	1/4	1/4

LAR19-02-10	146.919	5570756.193	6248295.738	SI	1499.996	165.0	1/4	1/4
LAR19-02-10	147.349	5570587.354	6248689.707			165.0	1/4	1/4
LAR19-02-10	147.772	5570477.944	6249098.506	SI	1199.967	176.0	1/4	1/4
LAR19-02-10	149.088	5569571.856	6249961.244			176.0	1/4	1/4
LAR19-02-10	149.187	5569475.867	6249981.959	SI	1500.045	166.1	1/4	1/4
LAR19-02-10	149.198	5569464.703	6249984.413			165.0	1/4	1/4
LAR19-02-10	150.550	5568441.148	6250796.695			165.0	1/4	1/4
LAR19-02-10	150.572	5568431.880	6250816.275			163.3	1/4	1/4
LAR19-02-10	150.730	5568365.173	6250959.874			151.0	1/4	1/4
LAR19-02-10	151.271	5568137.375	6251450.250	SI	2294.666	151.0	1/4	1/4
LAR19-02-10	152.776	5567115.594	6252519.037			151.0	1/4	1/4
LAR19-02-10	153.557	5566423.326	6252879.297	SI	2362.897	151.0	1/4	1/4
LAR19-02-10	153.922	5566087.881	6253022.155			151.0	1/4	1/4
LAR19-02-10	154.507	5565533.148	6253209.307			151.0	1/4	1/4
LAR19-02-10	154.687	5565362.563	6253266.858	SI	999.868	174.0	1/4	1/4
LAR19-02-10	155.485	5564780.787	6253781.590			174.0	1/4	1/4
LAR19-02-10	155.776	5564654.632	6254044.416	SI	1015.058	174.0	1/4	1/4
LAR19-02-10	156.942	5564793.780	6255138.064			174.0	1/4	1/4
LAR19-02-10	157.114	5564904.875	6255269.793			174.0	1/4	1/4
MCD19-02-10	157.200	5564904.875	6255269.793			174.0	1/4	1/4
MCD19-02-10	157.402	5565035.816	6255423.606			174.0	1/4	1/4
MCD19-02-10	158.011	5565430.864	6255887.662	SI	560.004	234.9	1/4	1/4
MCD19-02-10	158.032	5565443.904	6255903.562			237.0	1/4	1/4
MCD19-02-10	159.389	5564902.155	6256801.250			237.0	1/4	1/4
MCD19-02-10	159.409	5564882.391	6256797.576			237.0	1/4	1/4
MCD19-02-10	159.435	5564856.695	6256792.800			237.0	1/4	1/4
ALI27-02-15	159.400	5564856.695	6256792.800			237.0	1/4	1/4
ALI27-02-15	160.550	5563726.068	6256582.603			122.0	1/4	1/4
ALI27-02-15	160.797	5563483.484	6256537.504	SI	1358.782	122.0	1/4	1/4
ALI27-02-15	161.177	5563104.829	6256520.876			122.0	1/4	1/4
ALI27-02-15	161.270	5563012.306	6256533.008			134.0	1/4	1/4
ALI27-02-15	161.388	5562896.500	6256552.260	SI	3199.960	149.0	1/4	1/4
ALI27-02-15	163.132	5561335.780	6257281.866			149.0	1/4	1/4
ALI27-02-15	163.273	5561228.902	6257373.705			149.0	1/4	1/4
ALI27-02-15	163.332	5561184.359	6257411.980	SI	2499.449	151.9	1/4	1/4
ALI27-02-15	163.746	5560893.915	6257706.713			152.0	1/4	1/4
ALI27-02-15	163.809	5560853.756	6257754.859	SI	1275.225	152.0	1/4	1/4
ALI27-02-15	164.110	5560689.895	6258006.510			152.0	1/4	1/4
ALI27-02-15	164.210	5560645.438	6258096.432			152.0	1/4	1/4
ALI27-02-15	164.313	5560599.805	6258188.731	SI	3000.341	160.2	1/4	1/4
ALI27-02-15	164.681	5560457.204	6258528.116			160.4	1/4	1/4
ALI27-02-15	164.727	5560441.965	6258571.695	SI	1383.093	165.0	1/4	1/4
ALI27-02-15	165.804	5560497.281	6259619.669			165.0	1/4	1/4
ALI27-02-15	165.855	5560519.141	6259665.879			165.0	1/4	1/4
ALI27-02-15	166.034	5560595.829	6259827.991	SI	2597.981	146.7	1/4	1/4
ALI27-02-15	166.276	5560709.174	6260041.327			122.0	1/4	1/4
ALI27-02-15	166.566	5560870.601	6260282.063			152.0	1/4	1/4
ALI27-02-15	168.617	5562595.064	6261291.439			152.0	1/4	1/4
ALI27-02-15	168.745	5562722.103	6261305.500			137.4	1/4	1/4
ALI27-02-15	168.880	5562856.780	6261317.061			122.0	1/4	1/4
ALI27-02-15	170.080	5564052.383	6261419.690			122.0	1/4	1/4
ALI27-02-15	170.260	5564231.724	6261435.084			140.0	1/4	1/4
ALI27-02-15	170.283	5564254.997	6261437.082	SI	3602.163	140.0	1/4	1/4
ALI27-02-15	172.143	5565986.317	6262056.796			140.0	1/4	1/4
ALI27-02-15	173.740	5567302.589	6262960.861			140.0	1/4	1/4
ALB12-01-15	173.600	5567302.589	6262960.861			140.0	1/4	1/4
ALB12-01-15	173.926	5567570.287	6263146.827	SI	1281.096	168.8	1/4	1/4
ALB12-01-15	173.962	5567599.599	6263167.806			172.0	1/4	1/4
ALB12-01-15	174.838	5568080.033	6263879.590			172.0	1/4	1/4
ALB12-01-15	174.869	5568087.728	6263909.482	SI	1355.715	172.0	1/4	1/4
ALB12-01-15	175.221	5568130.490	6264258.116			172.0	1/4	1/4

ALB12-01-15	175.242	5568130.323	6264279.312			172.0	1/4	1/4
ALB12-01-15	175.320	5568129.709	6264357.427			170.2	1/4	1/4
BIF12-01-15	175.300	5568129.709	6264357.427			170.2	1/4	1/4
BIF12-01-15	175.542	5568127.475	6264599.471	SI	2416.919	162.6	1/4	1/4
BIF12-01-15	175.787	5568112.817	6264843.873			155.0	1/4	1/4
BIF12-01-15	176.754	5567819.220	6265758.467			155.0	1/4	1/4
BIF12-01-15	176.763	5567814.821	6265766.285			154.1	1/4	1/4
BIF12-01-15	177.084	5567656.876	6266045.772			122.0	1/4	1/4
BIF12-01-15	177.352	5567524.940	6266279.235	SI	15785.960	122.0	1/4	1/4
BIF12-01-15	177.600	5567401.316	6266494.034			122.0	1/4	1/4
BIF12-01-15	178.492	5566928.820	6267250.473			122.0	1/4	1/4
BIF12-01-15	178.644	5566843.893	6267376.929			137.2	1/4	1/4
BIF12-01-15	178.822	5566744.124	6267523.944			155.0	1/4	1/4
BIF12-01-15	178.958	5566667.561	6267636.764	SI	1980.440	155.0	1/4	1/4
BIF12-01-15	180.412	5565500.231	6268448.202			155.0	1/4	1/4
BIF12-01-15	180.423	5565489.781	6268450.763			155.0	1/4	1/4

G.2. Reach definition Río de la Plata

RIO DE LA PLATA

Paso	Progresiva	Este	Norte	Curva	Radio	Ancho de Solera	Veril Verde	Veril Rojo
EMI(01-05-12)	0.000	6386645.671	6169667.663			212.5	1/8	1/8
EMI(01-05-12)	0.300	6386443.898	6169889.671			100	1/8	1/8
EMI(01-05-12)	4.972	6383301.463	6173347.250	SI	2321.845	100	1/8	1/8
EMI(01-05-12)	5.161	6383168.709	6173481.873			100	1/8	1/8
EMI(01-05-12)	14.064	6376664.836	6179561.065	SI	2193.209	100	1/8	1/8
EMI(01-05-12)	14.253	6376532.239	6179696.188			100	1/8	1/8
EMI(01-05-12)	18.963	6373381.865	6183196.786	SI	6907.926	100	1/8	1/8
EMI(01-05-12)	19.150	6373258.542	6183337.610			100	1/8	1/8
EMI(01-05-12)	20.773	6372205.945	6184572.963			100	1/8	1/8
EMI(01-05-12)	20.893	6372128.150	6184664.265	SI	3460.412	106	1/8	1/8
EMI(01-05-12)	21.526	6371764.061	6185180.467			106	1/8	1/8
EMI(01-05-12)	21.646	6371703.893	6185284.852			100	1/8	1/8
EMI(01-05-12)	27.921	6368570.289	6190721.346	SI	23190.340	100	1/8	1/8
EMI(01-05-12)	28.033	6368514.745	6190818.248			100	1/8	1/8
EMI(01-05-12)	30.774	6367157.228	6193199.890			100	1/8	1/8
EMI(01-05-12)	30.800	6367144.353	6193222.478			100	1/8	1/4
EMI(01-05-12)	36.443	6364349.704	6198125.439	SI	1693.258	100	1/8	1/4
EMI(01-05-12)	36.661	6364254.326	6198321.001			100	1/8	1/4
EMI(01-05-12)	38.147	6363690.097	6199695.650	SI	1623.926	100	1/8	1/4
EMI(01-05-12)	38.349	6363602.082	6199877.103			100	1/8	1/4
EMI(01-05-12)	39.298	6363135.680	6200703.618	SI	1993.419	100	1/8	1/4
EMI(01-05-12)	39.439	6363070.602	6200829.147			100	1/8	1/4
EMI(01-05-12)	40.154	6362764.503	6201474.618			100	1/8	1/4
EMI(01-05-12)	40.274	6362713.075	6201583.064	SI	2002.803	106	1/8	1/4
EMI(01-05-12)	40.944	6362331.024	6202129.611			106	1/8	1/4
EMI(01-05-12)	41.064	6362246.839	6202215.165			100	1/8	1/4
EMI(01-05-12)	41.577	6361886.945	6202580.914	SI	5119.127	100	1/8	1/4
EMI(01-05-12)	42.167	6361449.822	6202976.722			100	1/8	1/4
EMI(01-05-12)	42.508	6361183.878	6203190.992			100	1/8	1/4
ACE(01-05-12)	12.000	6386645.671	6169667.663			210	1/6	1/6
ACE(01-05-12)	12.330	6386970.641	6169610.265			100	1/6	1/6
ACE(01-05-12)	12.400	6387039.574	6169598.090			100	1/9	1/9
ACE(01-05-12)	14.200	6388812.138	6169285.012			100	1/9	1/9
ACE(01-05-12)	14.600	6389206.041	6169215.439			100	1/10	1/10
ACE(01-05-12)	21.800	6396296.296	6167963.125			100	1/10	1/10
ACE(01-05-12)	21.921	6396415.195	6167942.124	SI	2235.226	106	1/10	1/10
ACE(01-05-12)	22.517	6396981.994	6167761.639			106	1/10	1/10
ACE(01-05-12)	22.637	6397090.158	6167710.487			100	1/10	1/10
ACE(01-05-12)	22.800	6397237.512	6167640.803			100	1/14	1/14
ACE(01-05-12)	26.804	6400856.761	6165929.247	SI	7169.567	100	1/14	1/14
ACE(01-05-12)	27.203	6401222.330	6165768.667			100	1/14	1/14
ACE(01-05-12)	28.505	6402428.461	6165278.455	SI	3758.962	100	1/14	1/14
ACE(01-05-12)	28.781	6402687.629	6165184.044			100	1/14	1/14
ACE(01-05-12)	37.000	6410508.252	6162656.071			100	1/14	1/14
RAD(01-05-12)	37.000	6410508.252	6162656.071			100	1/20	1/20
RAD(01-05-12)	38.000	6411459.959	6162348.438			100	1/20	1/20
RAD(01-05-12)	48.544	6421497.474	6159119.933	SI	48281.340	100	1/20	1/20
RAD(01-05-12)	50.416	6423290.474	6158581.354			100	1/20	1/20
RAD(01-05-12)	55.808	6428483.291	6157130.688	SI	3810.476	100	1/20	1/20
RAD(01-05-12)	56.402	6429065.319	6157016.037			100	1/20	1/20
RAD(01-05-12)	56.998	6429657.736	6156946.659			100	1/20	1/20
BCH 20-03-17	57.000	6429657.736	6156946.659			100	1/20	1/20
BCH 20-03-17	61.824	6434448.326	6156379.502	SI	15643.540	100	1/20	1/20
BCH 20-03-17	62.189	6434810.847	6156340.861			100	1/20	1/20
BCH 20-03-17	64.216	6436828.865	6156149.627	SI	4248.013	100	1/20	1/20
BCH 20-03-17	64.782	6437387.740	6156058.762			100	1/20	1/20
BCH 20-03-17	73.313	6445698.007	6154131.632	SI	18938.730	100	1/20	1/20
BCH 20-03-17	74.033	6446396.418	6153955.614			100	1/20	1/20
BCH 20-03-17	77.592	6449829.937	6153020.488	SI	1498.370	100	1/20	1/20
BCH 20-03-17	77.793	6450019.694	6152954.865			100	1/20	1/20

BCH 20-03-17	81.009	6452982.334	6151702.265			100	1/20	1/20
CIM(01-05-12)	81.000	6452982.334	6151702.265			100	1/20	1/20
CIM(01-05-12)	81.403	6453353.083	6151545.450	SI	2461.862	100	1/20	1/20
CIM(01-05-12)	81.807	6453711.218	6151357.932			100	1/20	1/20
CIM(01-05-12)	98.590	6467889.855	6142378.703			100	1/20	1/20
CIM(01-05-12)	98.710	6467991.163	6142314.545	SI	3222.438	106	1/20	1/20
CIM(01-05-12)	99.633	6468690.170	6141716.428			106	1/20	1/20
CIM(01-05-12)	99.753	6468769.248	6141626.227			100	1/20	1/20
CIM(01-05-12)	120.993	6482770.946	6125655.145			100	1/20	1/20
PIN(01-05-12)	121.000	6482770.946	6125655.145			100	1/20	1/20
PIN(01-05-12)	129.484	6488282.145	6119205.259	SI	5810.591	100	1/20	1/20
PIN(01-05-12)	130.252	6488818.472	6118655.692			100	1/20	1/20
PIN(01-05-12)	136.742	6493648.077	6114320.839	SI	32166.150	100	1/20	1/20
PIN(01-05-12)	137.521	6494233.823	6113807.763			100	1/20	1/20
PIN(01-05-12)	142.954	6498363.768	6110277.615			100	1/20	1/20
PIN(01-05-12)	143.074	6498454.971	6110199.657	SI	3372.587	106	1/20	1/20
PIN(01-05-12)	144.994	6500182.914	6109422.721			106	1/20	1/20
PIN(01-05-12)	145.114	6500301.780	6109406.232			100	1/20	1/20
PIN(01-05-12)	146.492	6501666.536	6109216.917	SI	5333.233	100	1/20	1/20
PIN(01-05-12)	147.062	6502234.793	6109168.872			100	1/20	1/20
PIN(01-05-12)	151.939	6507109.208	6109018.431	SI	15513.620	100	1/20	1/20
PIN(01-05-12)	152.295	6507465.309	6109011.531			100	1/20	1/20
PIN(01-05-12)	160.489	6515658.720	6108946.871	SI	7518.048	100	1/20	1/20
PIN(01-05-12)	160.739	6515908.374	6108940.753			100	1/20	1/20
PIN(01-05-12)	169.532	6524694.179	6108579.173	SI	4421.050	100	1/20	1/20
PIN(01-05-12)	169.733	6524894.850	6108575.474			100	1/20	1/20
PIN(01-05-12)	181.460	6536621.980	6108625.276			100	1/20	1/20
PIN(01-05-12)	181.700	6536861.978	6108626.295			160	1/20	1/20
PIN(01-05-12)	183.009	6538171.386	6108631.856	SI	18592.670	160	1/20	1/20
PIN(01-05-12)	183.183	6538344.549	6108631.785			160	1/20	1/20
PIN(01-05-12)	190.076	6545237.454	6108596.684	SI	3639.366	160	1/20	1/20
PIN(01-05-12)	190.170	6545332.152	6108597.434			160	1/20	1/20
PIN(01-05-12)	194.400	6549560.944	6108685.949			160	1/20	1/20
PIN(01-05-12)	194.640	6549800.892	6108690.972			100	1/20	1/20
PIN(01-05-12)	196.020	6551180.445	6108719.848			100	1/20	1/20
PIN(01-05-12)	197.887	6553046.891	6108779.257	SI	8906.749	100	1/20	1/20
PIN(01-05-12)	198.275	6553434.105	6108783.160			100	1/20	1/20
PIN(01-05-12)	202.180	6557339.359	6108737.603	SI	2754.317	100	1/20	1/20
PIN(01-05-12)	202.494	6557652.538	6108716.059			100	1/20	1/20
PIN(01-05-12)	205.293	6560429.787	6108365.114			100	1/20	1/20
PUN(01-05-12)	205.300	6560429.787	6108365.114			100	1/20	1/20
PUN(01-05-12)	206.922	6562039.574	6108165.206	SI	3212.376	100	1/20	1/20
PUN(01-05-12)	207.396	6562512.739	6108141.649			100	1/20	1/20
PUN(01-05-12)	211.911	6567025.899	6108250.251			100	1/20	1/20
PUN(01-05-12)	212.031	6567145.844	6108253.138	SI	5313.756	106	1/20	1/20
PUN(01-05-12)	213.980	6569042.277	6108652.275			106	1/20	1/20
PUN(01-05-12)	214.100	6569153.261	6108698.002			100	1/20	1/20
PUN(01-05-12)	239.075	6592245.247	6118212.232	SI	3519.282	100	1/20	1/20
PUN(01-05-12)	240.360	6593495.671	6118476.440			100	1/20	1/20
PUN(01-05-12)	246.814	6599949.794	6118476.440			100	1/20	1/20

G.3. Dredged volumes per reach

Names of the reaches (”Canal/Paso”) are associated with the three or six digit codes in the reach definitions (previous Sections G.1 and G.2).

Dirección Nacional de Vías Navegables
Departamento Control de Vías Navegables

Al: 13 de mayo de 2019

Suma de VOLUMEN		Años y meses 2018 DRAGA																			
		1995	1996	1997	1998	1999	2000	2001	2002	2003	2004	2005	2006	2007	2008	2009	2010	2011	2012	2013	2014
TRAMO	CANAL / PASO																				
Río de la Plata	Extensión C. Punta Indio			3,003,000	565,000							211,000									
	C. Punta Indio	476,800	9,455,300	5,714,000	4,774,067	8,419,700	6,663,000	6,266,000	7,114,000	5,871,538	8,075,960	7,377,200	7,173,000	4,872,000	7,367,000	9,721,000	5,415,000	6,020,000	4,754,000	5,402,000	3,292,000
	C. Intermedio											392,000	171,000	10,000	22,000	26,000					11,000
	C. Intermedio - Zona de Espera											2,644,000	986,000		20,000	257,000	81,000				
	Zona de Practicaje															37,000					
	Paso Banco Chico		946,859				40,000					119,000	56,000			20,000	16,000	23,000			71,000
	Rada Exterior						7,000	260,000				257,100	240,000			42,000					
	C. Acceso Pto. Buenos Aires	1,659,200	1,534,900	1,173,000	770,000	1,024,100	1,177,000	705,000	414,000	265,295	492,000	960,000	509,000	592,000	631,000	810,000	369,000	473,435	201,000	468,000	270,000
	C. Ing. Emilio Mitre	16,290,360	8,988,500	13,166,168	5,907,520	7,243,450	1,654,000	4,417,000	1,191,000	3,985,000	1,353,000	2,225,000	4,177,000	4,894,000	4,703,000	4,586,000	13,365,500	4,511,000	3,389,000	4,497,500	10,631,300
Río de la Plata Total		18,426,360	20,925,559	23,056,168	12,016,587	16,687,250	9,541,000	11,648,000	8,719,000	10,121,833	9,920,960	14,185,300	13,312,000	10,368,000	12,743,000	15,499,000	19,246,500	11,027,435	8,344,000	10,367,500	14,275,300
Río Paraná de las Palmas	Arriba Obligado																				
	Isla Lucha	464,500	469,000	372,541	827,100	202,000	35,000	181,000	83,000	169,000	28,000	709,000	278,000	407,000	102,000	310,000	1,307,000	513,000	183,000	303,000	449,000
	EV. Isla Lucha/Tordillo												6,000								
	Vuelta del Tordillo														17,000	7,000	21,000		12,000	13,000	18,000
	Vuelta Campana															31,000	10,000		4,000		
	Vuelta del Este	997,314	109,000	277,514	318,000	131,000	152,000	302,000	184,000	103,000	135,800	234,000	361,600	394,000	433,500	616,000	565,000	429,000	450,000	613,000	664,000
	EV. Del Este/de los Barbones													1,000							
	Vuelta de los Barbones		660,100	4,500	13,000				39,000	14,000	23,000	26,000	60,000	127,000	52,000	114,000	163,000	70,000	63,000	84,000	89,000
	Vuelta de San Antonio	972,218	49,000	56,000	180,000	14,000		34,000	29,000	50,000	33,500	68,000	128,000	98,000	95,000	100,000	153,000	82,000	110,000	107,000	118,000
	Vuelta Abajo Las Limas		581,500	1,000	4,000	12,000			4,000							11,000					
	Vuelta Las Limas									8,000	6,000	6,000	8,000	7,000	9,000	25,000	4,000	10,000	67,000	13,000	18,000
	Vuelta del Pelado	104,179	38,000	71,500	30,000	53,000	67,000	116,000	44,000	41,000	70,000	115,000	77,000	135,800	83,000	151,000	207,000	132,000	195,000	215,000	285,000
	EV. Del Pelado/Los Patos												9,000								
	Vuelta Los Patos	32,000	142,000	139,500	143,000	26,000	39,000	183,000	145,000	88,200	145,000	324,000	390,000	557,000	418,000	510,000	459,000	358,000	461,000	530,000	373,000
	Cancha Larga	34,000	155,000	9,000	63,000	9,000	12,000	43,000	21,000	55,000	46,000	100,500	183,000	253,000	192,000	231,000	349,000	254,000	409,000	327,000	285,000
	Zanja Mercadal		1,069,000	94,000	73,000	30,000	45,000	31,000	73,000	51,000	70,000	163,000	165,000	172,000	145,000	164,000	146,000	184,000	211,000	308,000	220,000
	Angostura de la Isleta	459,000	470,000	617,000	517,000	394,000	217,000	353,000	327,000	521,000	408,000	651,000	1,159,000	890,000	625,000	972,000	1,375,000	918,000	925,000	1,097,000	1,108,000
	Angostura de la Base		431,000	27,000	85,000	87,000	31,000	45,000	95,000	74,000	143,000	206,000	113,000	250,000	145,000	394,000	626,000	419,000	461,000	509,000	498,000
	Bifurcación	344,000	436,000	227,000	374,000	239,000	66,000	197,000	206,000	338,000	456,000	961,000	772,000	1,743,000	1,076,000	1,567,000	2,769,000	1,730,000	1,963,000	1,740,000	2,167,000
Río Paraná de las Palmas Total		3,407,211	4,609,600	1,896,555	2,627,100	1,197,000	664,000	1,485,000	1,250,000	1,512,200	1,564,300	3,563,500	3,709,600	5,034,800	3,392,500	5,203,000	8,154,000	5,099,000	5,514,000	5,859,000	6,292,000
Río Paraná Inferior	Abajo Los Ratones				85,000	116,000	124,000	246,000	264,000	320,000	239,000	346,000	359,500	636,000	537,000	446,000	1,231,000	861,000	365,000	508,000	796,000
	Los Ratones	231,000	143,000	59,500	132,500	183,000	96,000	135,000	135,000	112,000	116,000	111,000	298,000	132,000	224,000	241,000	172,000	238,300	114,000	240,000	102,000
	Arriba Obligado																			94,000	602,000
	EP. L Ratones/Abajo I. Herman									14,000			19,000	27,000	6,000	13,000					
	Abajo Las Hermanas	58,500					26,000	68,000	50,000	43,000	44,000	92,000	135,000	140,000	272,000	514,000	925,000	578,300	747,000	645,000	457,000
	Las Hermanas	973,051	1,313,000	1,045,849	1,813,600	968,200	445,500	699,000	716,000	1,106,000	670,000	842,000	1,525,000	1,636,000	1,154,000	1,034,200	2,986,000	1,973,700	1,512,000	1,830,000	2,074,000
	Tonelero - Isla Nueva			68,000	119,400	279,600	296,100	404,000	673,000	602,000	753,000	1,402,000	1,267,000	1,061,000	1,391,000	1,273,000	1,729,000	2,638,000	1,138,000	1,432,000	1,479,000
	Cortada Isla Nueva																				
	Abajo San Nicolás	324,000	341,000	422,000	415,000	468,000	150,000	364,000	360,000	586,000	442,000	630,000	584,000	1,584,000	713,000	769,000	1,811,000	1,334,000	1,388,000	1,495,000	1,839,000
	Yaguarón		101,000	41,000	104,000	63,000	93,000	135,000	96,000	75,000	124,000	455,000	218,000	179,000	350,000	348,000	266,000	157,000	597,000	254,000	149,000
	EP.Yaguarón/Paraguayo															200					
	Paraguayo	207,654	188,000	682,000	606,386	397,100	227,200	591,000	350,000	425,000	248,000	388,000	290,000	269,000	270,000	243,000	958,000	756,000	780,000	955,000	1,131,000
	EP. Paraguayo/Abajo Alvear																				
	Abajo Alvear									224,000	161,000	110,000	318,000	235,000	339,000	292,000	233,000	230,000	426,000	483,000	432,000
	EP. Abajo Alvear/Alvear														22,000						
	Alvear	552,096	748,000	1,287,743	1,328,228	908,200	371,390	549,000	640,000	894,000	438,000	562,000	1,316,000	1,387,000	1,186,000	769,000	1,827,000	1,502,000	1,805,000	1,724,000	2,306,000
	C. Muelles Pto. Rosario	1,614,000	1,600,000	454,815	684,855	909,000	481,000	701,000	260,000	485,000	233,000	193,000	953,000	345,000	481,000	344,000	246,000	377,600	649,000	320,000	310,000
	Borghi	1,158,659	1,197,000	822,000	526,258	761,700	357,000	566,000	221,000	385,000	217,000	267,000	454,200	332,000	439,000	259,000	200,000	267,000	278,000	185,000	164,000
	Bella Vista	104,000	59,000	5,000	507,867	79,000	24,000	119,000	30,000	144,000	85,000	156,000	112,000	469,000	578,000	437,000	1,550,000	1,085,000	873,000	858,000	1,366,000
Río Paraná Inferior Total		5,222,960	5,690,000	4,887,907	6,323,094	5,132,800	2,691,190	4,577,000	3,795,000	5,415,000	3,770,000	5,554,000	7,848,700	8,432,000	7,962,000	6,982,400	14,134,000	11,997,900	10,672,000	11,023,000	13,207,000
Río Paraná Medio	Abajo Correntoso	283,000	90,000	131,000	244,000	166,000	25,000	68,000	33,000	88,000	34,000	195,000	308,000	702,000	335,000	160,000	985,000	841,000	267,000	384,000	570,000
	Paranacito	158,000	90,000	19,000	55,000	77,000	40,000			4,000	28,000	45,000		13,000	80,000	9,000	8,000	36,000	125,000	98,000	46,000
	EP. Paranacito/Tacuaní														3,000						
	Tacuaní	529,000	374,000	299,000	1,485,712	940,200	894,000	1,356,000	882,386	1,323,000	601,000	1,046,000	1,131,000	989,000	834,000	721,000	802,000	731,000	730,000	873,364	701,000
	Abajo Diamante	469,000	457,258	686,000	1,304,395	617,000	646,000	825,000	605,724	179,000	118,000	277,000	289,000	90,000	65,000	38,000		31,000	42,000		
	Los Chivos											48,000	103,000	107,000	114,000	155,000	104,000	9,000			
	Raigones		24,000		8,000	107,000	216,000	31,000	68,323	101,000	183,500	517,000	541,000	621,000	488,000	455,000	394,000	509,000	350,000	259,000	177,000
	EP. Raigones/Paracao													2,000							
	Paracao				22,000	28,000	69,000	222,000	210,811	154,000	5,000		1,000			107,000			9,000		
	Ánimas	141,000	28,000		41,000	315,000	120,000	201,000	2,000	6,000	13,000	139,000	277,000	112,000	228,000	181,000	214,000	196,000	295,000	209,000	99,000
	Tragadero	336,000	277,000	290,800	1,367,600	254,000	183,000	321,000	477,402	713,000	735,000	1,043,000	1,093,000	931,000	898,000	483,000	1,001,000	1,366,400	772,000	1,144,667	691,000
	Colastiné													314,000	578,000	451,000	470,000	518,000	568,000	421,000	385,000
Río Paraná Medio Total		1,916,000	1,340,258	1,425,800	4,527,707	2,504,200	2,193,000	3,024,000	2,279,646	2,568,000	1,717,500	3,310,000	3,743,000	3,881,000	3,623,000	2,760,000	3,978,000	4,237,400	3,158,000	3,389,030	2,669,000
PARO	(blank)																				
PARO Total																					
Grand Total		28,972,531	32,565,417	31,266,430	25,494,488	25,521,250	15,089,190	20,734,000	16,043,646	19,617,033	16,972,760	26,612,800	28,613,300	27,715,800	27,720,500	30,444,400	45,512,500	32,361,735	27,688,000	30,638,530	36,443,300

Dirección Nacional de Vías Navegables
Departamento Control de Vías Navegables

Al: 13 de mayo de 2019

Suma de VOLUMEN		2015	2016	2017	2018	2019	Grand Total
TRAMO	CANAL / PASO						
Río de la Plata	Extensión C. Punta Indio						3,779,000
	C. Punta Indio	2,573,000	3,995,000	4,002,000	4,589,000	3,169,000	142,551,565
	C. Intermedio	36,000					668,000
	C. Intermedio - Zona de Espera						3,988,000
	Zona de Practicaje						37,000
	Paso Banco Chico		25,000	151,000			1,467,859
	Rada Exterior						806,100
	C. Acceso Pto. Buenos Aires	309,000	170,000	757,000	476,000	149,000	16,358,930
	C. Ing. Emilio Mitre	4,233,000	21,384,000	2,238,000	2,280,000	1,499,000	152,809,298
Río de la Plata Total		7,151,000	25,574,000	7,148,000	7,345,000	4,817,000	**322,465,752**
Río Paraná de las Palmas	Arriba Obligado					21,000	21,000
	Isla Lucha	417,000	1,414,000	448,000	424,000	223,000	10,318,141
	EV. Isla Lucha/Tordillo						6,000
	Vuelta del Tordillo	8,000	18,000			5,000	119,000
	Vuelta Campana	11,000	5,000			14,000	75,000
	Vuelta del Este	586,000	553,000	467,000	598,000	157,000	9,830,728
	EV. Del Este/de los Barbones						1,000
	Vuelta de los Barbones	111,000	116,000	49,000	102,000	27,000	2,006,600
	Vuelta de San Antonio	161,000	178,000	139,000	162,000	39,000	3,155,718
	Vuelta Abajo Las Limas	15,000					628,500
	Vuelta Las Limas	38,000	21,000	35,000	109,000	17,000	401,000
	Vuelta del Pelado	218,000	332,000	186,000	300,000	110,000	3,376,479
	EV. Del Pelado/Los Patos						9,000
	Vuelta Los Patos	471,000	299,000	202,000	497,000	223,000	7,154,700
	Cancha Larga	207,000	265,000	214,000	348,000	266,000	4,330,500
	Zanja Mercadal	255,000	132,000	156,000	203,000	188,000	4,348,000
	Angostura de la Isleta	741,000	634,000	881,000	970,000	568,600	17,797,600
	Angostura de la Base	527,000	428,000	373,000	329,000	306,000	6,602,000
	Bifurcación	1,604,000	2,132,000	470,000	414,000	528,000	24,519,000
Río Paraná de las Palmas Total		5,370,000	6,527,000	3,620,000	4,456,000	2,692,600	**94,699,966**
Río Paraná Inferior	Abajo Los Ratones	831,000	915,000	1,026,000	982,000	647,000	11,880,500
	Los Ratones	186,000	267,000	298,000	121,000	47,000	4,134,300
	Arriba Obligado	509,000	708,000	675,000	681,000	284,000	3,553,000
	EP. L Ratones/Abajo I. Herman						79,000
	Abajo Las Hermanas	476,000	537,000	619,000	490,000	135,000	7,051,800
	Las Hermanas	2,459,000	1,884,000	2,212,000	1,945,000	1,051,000	35,868,100
	Tonelero - Isla Nueva	1,888,000	1,415,000	271,000			21,579,100
	Cortada Isla Nueva			3,356,000	1,239,000	604,000	5,199,000
	Abajo San Nicolás	1,810,000	1,644,000	376,000			19,849,000
	Yaguarón	204,000	259,000	238,000	198,000	66,000	4,770,000
	EP.Yaguarón/Paraguayo						200
	Paraguayo	755,000	2,705,000	2,151,000	1,514,000	719,000	17,806,340
	EP. Paraguayo/Abajo Alvear		27,000				27,000
	Abajo Alvear	623,000	474,000	617,000	321,000	114,000	5,632,000
	EP. Abajo Alvear/Alvear						22,000
	Alvear	2,014,000	2,878,000	1,915,000	1,703,000	436,000	31,046,657
	C. Muelles Pto. Rosario	553,000	809,000	850,000	536,000	110,000	14,499,270
	Borghi	159,000	106,000	116,000	221,000	15,000	9,673,817
	Bella Vista	922,000	1,717,000	965,000	907,000	350,000	13,501,867
Río Paraná Inferior Total		13,389,000	16,345,000	15,685,000	10,858,000	4,578,000	**206,172,951**
Río Paraná Medio	Abajo Correntoso	511,000	886,000	422,000	562,000	517,000	8,807,000
	Paranacito	72,000	42,000	130,000	74,000	15,000	1,264,000
	EP. Paranacito/Tacuaní						3,000
	Tacuaní	1,139,000	1,444,000	1,253,000	1,299,000	405,000	22,782,662
	Abajo Diamante						6,739,377
	Los Chivos						640,000
	Raigones	244,000	454,000	305,000	188,000	80,000	6,320,823
	EP. Raigones/Paracao						2,000
	Paracao						827,811
	Ánimas	79,000	2,000	90,000	68,000	27,000	3,083,000
	Tragadero	848,000	1,590,000	1,398,000	1,108,000	735,000	20,056,869
	Colastiné	534,000	258,000	411,000	319,000	55,000	5,282,000
Río Paraná Medio Total		3,427,000	4,676,000	4,009,000	3,618,000	1,834,000	**75,808,541**
PARO	(blank)						
PARO Total							
Grand Total		29,337,000	53,122,000	30,462,000	26,277,000	13,921,600	**699,147,210**

H

Analytical considerations

This appendix contains various simple analytical models and the application of theoretical principles that serve as (additional) substantiation for the hypotheses described in Chapters 2 and 3. Section H.1 describes the conditions and parameters used for the calculations. Subsequent sections cover the hypotheses related to fluvial deposition due to flow acceleration, tidal import, tidal divides, and variation in tidal and fluvial dynamics caused by deepening the Paraná de las Palmas.

H.1. Analytical model - parameters

The analytical models introduced in this appendix include the Paraná de las Palmas and/or Río Luján as main river branches and one or two channels, based on Arroyo Caraguata and Canal Honda/Río Union/Río San Antonio (See Figure H.1). To avoid repetition, the parameters used in these calculations are only stated in Table H.1. The values are roughly based on the analyses of bathymetrical, discharge and water level data (Appendices D, E and F). The very mild or non-existent bed slopes of Arroyo Caraguata and Río Capitan are approximated with $0.33 \cdot 10^{-5}$. A higher friction factor for the channels was assumed due to the high sinuosity and the presence of vegetation compared to the main river branches. Figure H.1 displays the channels, and clarifies the definition of parameter s. If (channel bed) sediment parameters are used in the analytical models, the silty and clayey fractions identified by van Rijn [2017] are used (Table H.2). The sand fraction is disregarded as it is not expected to be present in the upper part of the water column, and will thus not enter the channel network.

Table H.1: Typical river and channel characteristics used in the analytical models

		1 Palmas	2 Luján	3 Caraguata	4 Honda - S. Antonio	
Channel length	L	39	15	14	16	km
Channel width	B	400	50	50	130	m
Water depth	h	12	5	4	5	m
Upstream bed level	z_b	-11	-4	-3	-4.5	m + IGN
Distance inlet - coast	s	-	-	23	8	km
Bed slope	i_b	10^{-5}	10^{-4}	$0.33 \cdot 10^{-5}$	$0.33 \cdot 10^{-5}$	[-]
Friction factor	c_f	0.0015	0.0015	0.0020	0.0020	[-]
Flow velocity	U	0.75		x	x	m/s

Table H.2: Sediment fractions as determined by van Rijn [2017], used in the analytical models. Concentrations are presented as depth averaged values (c_m) and values in the upper 5 m of the water column.

	c_m [mg/l]	c (h ∈ [-5,0 m]) [mg/l]	w_s [mm/s]	D_{50} [μm]
Clay	115	115	0.005	8
Silt	165	100	0.7	30

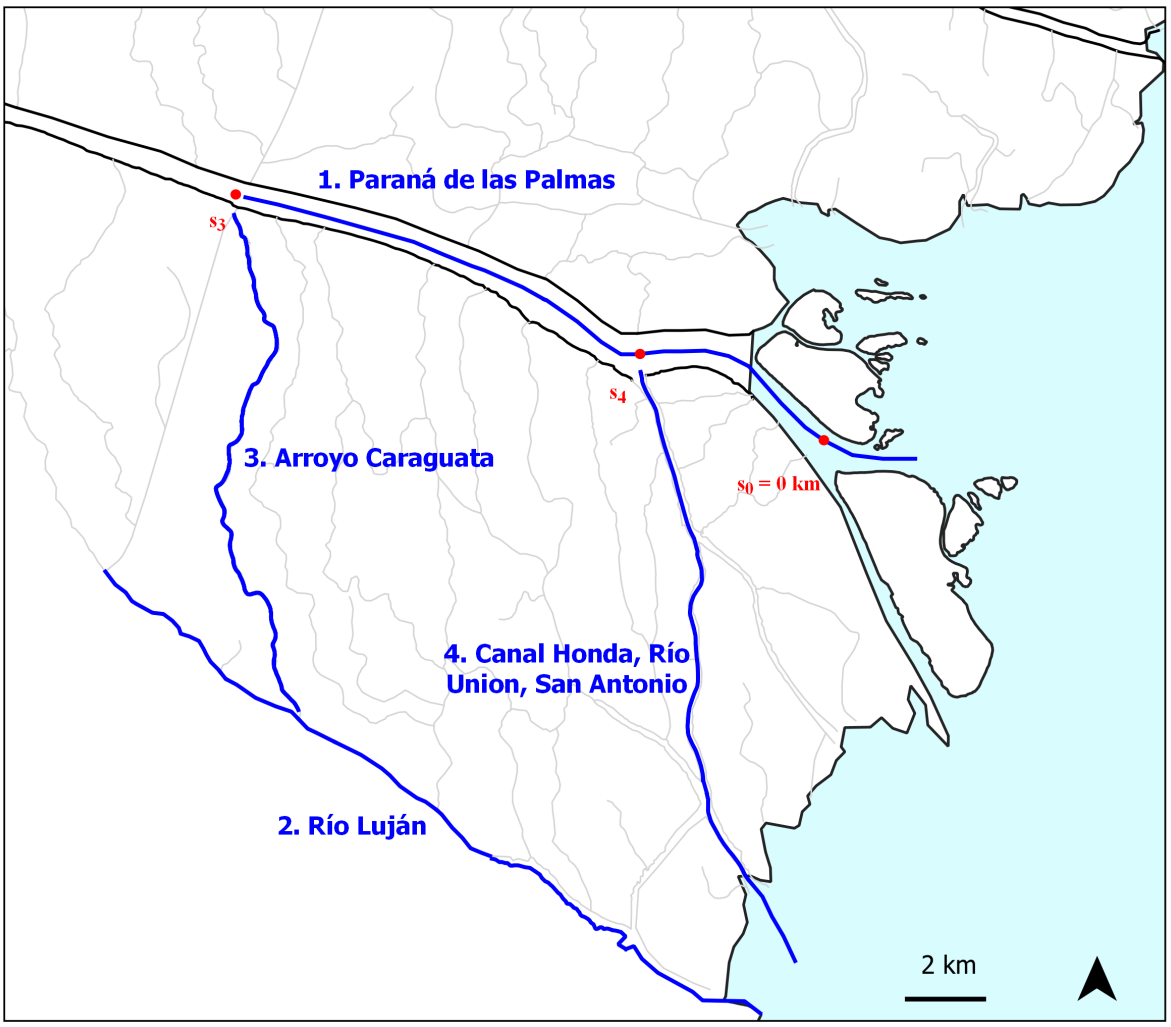

Figure H.1: Channels used in the analytical models

H.2. Flow decelerations in a channel

As river discharge enters the channel network, flow velocities are likely to decrease with a reduction in sediment transport capacity as a result. As elaborated upon in Appendix A, the rate of deposition or erosion for suspended sediments depends on the difference between the equilibrium suspended sediment concentration c_e, which is approximately proportional to the bed shear stress $\tau_b \propto u^2$, the actual sediment concentration c and the relaxation time T. For non-equilibrium transport, the relaxation time T is non-negligible.

$$\begin{aligned} \frac{\partial cd}{\partial t} &= E - D = m(\tau - \tau_c) - \frac{w_s c}{d} \\ \frac{\partial c}{\partial t} &= \frac{1}{d}\frac{m(\tau - \tau_c) - w_s c}{d} = \frac{c_e - c}{T} \\ T &= \frac{d}{w_s}, c_e = \frac{m(\tau - \tau_c)}{w_s} \end{aligned} \tag{H.1}$$

A simplified case of a channel connected to a main river branch is considered. Only sediment in suspension is considered. Deposition occurrence in the side channel is dependant on the following two criteria:

1. A reduction in flow velocity from main channel to side channel must occur

2. The time it takes for water and suspended sediment to travel through the channel t must be at least the same order of magnitude as the relaxation time T

A calculation on the transport capacity of river flow in a channel is given. Typical values of channel characteristics based on 'Arroyo Caraguata' are given in Table H.1. The magnitude of the fluvial flow velocity is approximated by assuming equilibrium flow for the given water depth. For an equilibrium depth of d_e = 4 m, the associated flow velocity in the channel becomes 0.25 m/s. This is in accordance with the flow velocities in channels that are calculated with the numerical model (Chapter 5).

$$u_e = \sqrt{d_e g \frac{i_b}{c_f}}$$
$$u_e = 0.25\ m/s \tag{H.2}$$

ADCP measurements carried out by INA (Figure H.2) and reports by van Rijn [2017] and Drago and Amsler [1998] show that during regular conditions, flow velocities in the Paraná de las Palmas are in the order of 0.5 to 1 m/s. A reduction in velocity from 1 to 0.25 m/s, or roughly a factor 3 to 4 reduction, implies a decrease in bed shear stress by a factor 9 to 16, as $\tau = u^2$. This highly simplified case demonstrates that the transport capacity in a (shallow) channel decreases significantly and thus criterium 1 is likely to be fulfilled when river discharge enters the Lower Delta channel network.

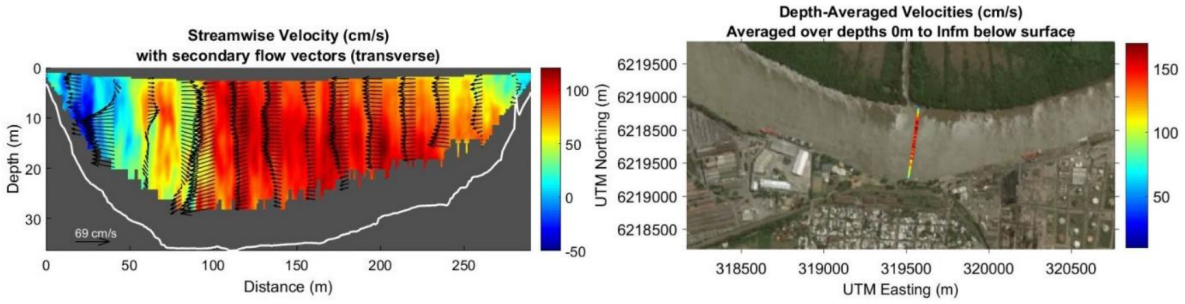

Figure H.2: ADCP flow measurements in the Paraná de Las Palmas near Campana (measurements by INA, Morale et al. [2018])

A silt or clay particle will take characteristic time scale T to fall through the water column. T is calculated via Equation (H.3). Using the approximate dimensions of 'Arroyo Caraguata', T yields approximately 1.5 hours for the silt particle and 220 hours for the clay particle.

$$T = \frac{h}{w_s} \tag{H.3}$$

The time for a particle to flow through the channel is calculated in Equation (H.4), and for a flow velocity of 0.25 m/s is approximately 16 hours.

$$t = \frac{L}{u} = \frac{14000}{0.25} \approx 16\ h \tag{H.4}$$

Which indicates that there is enough time for a silt particle to settle while flowing through the channel. The characteristic settling time scale of a clay particle exceeds t by an order of magnitude, therefore criterion 2 is fulfilled for the silt fraction only. In general, clay fractions are not likely to settle at all during conditions that are somewhat energetic. It is thus likely that mostly silt particles are deposited due to the deceleration of river flow, and as the are more likely to be kept in suspension and carried out of the channel network, into the Río de la Plata. The analasis of bed sediment samples (Appendix B) confirms that the channel beds consist predominantly of silt.

The abundance of suspended sediment in the Río de la Plata, the progradating coastline and the depositional patterns in the Paraná River are all evidence of a heavily sediment laden estuarine system. It is likely that sediment carried by the Paraná River is directly deposited due to decelerations in flow velocity when entering the secondary channel network. It is likely that predominantly silt fractions settle

due to the reduction in river flow inside the channel network, and that clay fractions are more likely to be carried into the Río de la Plata.

H.3. Influence of the tide

H.3.1. Tidal import

Figure H.3 presents the tidal signal at San Fernando, in June 2018, representing typical regular conditions. The rising stage of the tide takes approximately 4 to 5 hours, the falling stage 8. By looking at the tidal signal, it is evident that the signal is flood-dominant, resulting in significantly higher flood velocities. For a friction dominated flow, there is a proportionality between the velocity and the temporal derivative of the water level, see). In a short basin, this proportionality is absolute ($u = \frac{\partial h}{\partial t}\frac{A_b}{A_s}$). Although the assumption of a short basin is not completely valid for a channel in the network, the quantity $\frac{\partial h}{\partial t}$ can be assumed to be somehow representative for the flow velocity in a cross section. The quantity $\frac{\partial h}{\partial t}$ was approximated by means of a first order central difference scheme (Equation (H.3.1)) and displayed in Figure H.3. In Figure H.3 it can be seen that flood velocities would be around twice as high as ebb velocities, therefore criterion 2 would be fulfilled.

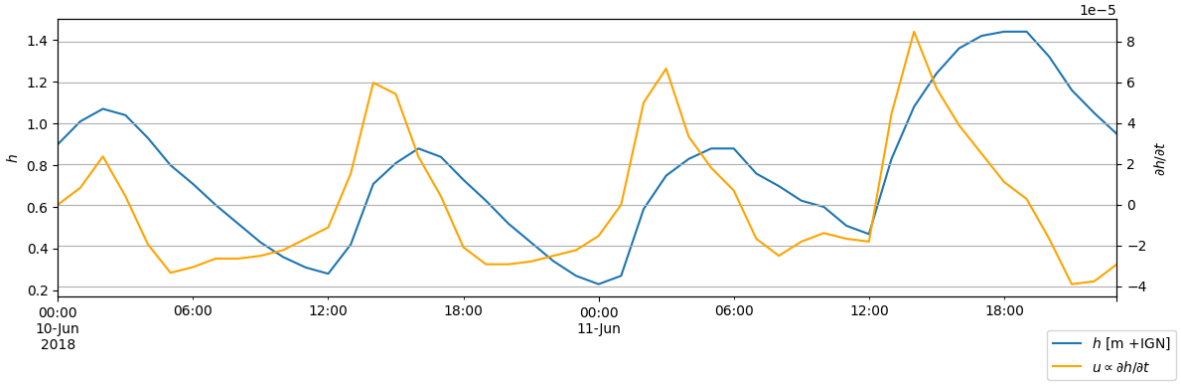

Figure H.3: Tidal signal at San Fernando in June 2018

$$\frac{\partial h}{\partial t}_t \approx \frac{h_{t+\Delta t} - h_{t-\Delta t}}{2\Delta t}$$
$$\frac{\partial^2 h}{\partial t^2} \approx \frac{h_{t+\Delta t} - 2h_t + h_{t-\Delta t}}{\Delta t^2} \quad \text{(H.5)}$$

Slack water duration can be assessed by considering the temporal derivative of the tidal velocity around flow reverse (i.e. when u and thus $\frac{\partial h}{\partial t}$ changes sign). By visual expectation of Figure H.3 a difference in slack water duration is not evident. The second temporal derivative of a longer period of water level time series was approximated by a second order central differences scheme (Equation (H.3.1)) to consider the duration of high water slack (positive values for $\frac{\partial^2 h}{\partial t^2}$) and low later slack (negative values). The average of the absolute values of the maxima and minima were compared, and it was found that the maxima were only slightly larger, the difference seems to be insignificant of magnitude. The results are depicted in Table H.3.

Table H.3: Approximated maxima-minima values of the slack time duration parameter $\frac{\partial^2 h}{\partial t^2}$, August - March 2018

	Maxima	Minima
Number of extreme values	1412	1408
Mean value [m/h^2]	0.110	-0.107

Characteristic settling times for a shallow channel were calculated in Section H.2, and yield approximately 1 hour for silt and 126 hours for clay. It is evident that the settling time for clay particles greatly

exceeds time scales related to a tidal cycle. The settling time for a silt particle is however in the same order as a fraction of the tidal cycle, i.e. it is plausible that the high water slack facilitates enough time for a silt particle to settle.

Import of sediment can go through two 'paths': Direct import from the estuary into a channel and import trough a main river branch with subsequent transport into the channel network. Characteristic magnitudes of tidal flow velocities U_{tide} are determined with formula (H.6) (characteristic flow velocity magnitude of the elementary wave equation, see Appendix A). An analysis of the water level data shows that at the Arroyo Carapachay water level station, the height of the tidal wave has reduced by approximately 50% compared to the deltaic front. Therefore, 50% of the characteristic spring tide wave amplitude of 0.55 m was used for the tidal velocity in the channel network, while it is assumed that 100% of the tidal energy is present in the Río Luján and Paraná de las Palmas.

$$\hat{U}_{tide} = \sqrt{\frac{g}{h}} \cdot \hat{\zeta} \tag{H.6}$$

Direct import from the estuary into the channel network via Canal Honda - Río San Antonio was considered, approximating U_{river} by assuming equilibrium flow. Import via Río Lujan or the Paraná de las Palmas was also considered. Table H.4 shows that it is likely that in the channel network, tidal currents dominate the overall flow. In the main river reaches, characteristic tidal velocities are at most in the same order of river flow velocities. This rises the expectation that significant import of sediment from the Río de la Plata could occur only via the channels that are directly connected to the estuary.

Table H.4: Characteristic river flow and tidal velocities

	U_{tide}	$U_{e,river}$	$\frac{U_{tide}}{U_{river}}$
Paraná de las Palmas	0.50	0.89	0.56
Río Luján	0.77	1.81	0.42
Canal Honda, Río Union, San Antonio	0.77	0.28	2.75
Arroyo Caraguata	0.43	0.25	1.72

The high relative magnitude of tidal currents in the channels, as presented in H.4 could imply that the tidal forcing is dominant over fluvial forcings in shaping the bathymetry of certain channels in the network. A significant difference in slack water duration is not evident, the import of sediment from the estuary into the channel network is therefore expected to be limited. It must be emphasized that the highly simplified given in the previous section do not give any conclusive or exclusive evidence.

H.3.2. Influence of deepening on tidal celerity

Keeping the Paraná de las Palmas at depth could significantly influence the celerity of the tidal wave, changing the temporal character of the water level at the boundary of a channel connected to the river branch. A consequence could be that the location of a tidal divide (see Section 2.5.2) can change after the deepening. The simplified case of the Arroyo Caraguata and the location of the tidal divide was repeated, but with a 0.5 m increase in bed level over the 8.6 km most downstream located reach (ILU) of the Paraná de las Palmas, as this is the most heavily dredged reach in the Paraná de las Palmas. The resulting tidal delay between the entrances of the arroyo Caraguata increased with approximately one minute. This did not change the approximate location of the tidal divide significantly. It is therefore not expected that dredging activities in the Paraná de las Palmas and the Río de la Plata have a significant effect on the timing of the tidal wave in the channel network.

H.3.3. Influence of deepening on tidal damping

As stated in the Theoretical Framework (Appendix **A**), tidal energy is damped due to friction when propagating through a channel. When the conveying cross section of the river does not decrease significantly upstream, the result is a reduction in tidal wave height and the eventual complete dissipation of tidal energy. In the analysis of geometrical data of the Paraná River (Appendix D), it can be seen that in the most downstream located reach, the conveyance area of the Palmas branch is approximately 8,000 m^2. Using the analytical formulation of the surface level elevation as introduced in Appendix A, the influence of changing the depth of a river branch on the dissipation of tidal energy is assessed by

comparing the theoretical damping of the tidal wave with the reduced conveyance area. Equations (H.7) repeat the relevant equations for determining the wave amplitude $\hat{\zeta}$ along the anti-streamwise spatial coordinate s.

$$\begin{aligned} \hat{\zeta}^{+}(s) &= \hat{\zeta}^{+}(s=0)\exp -\mu s \\ \mu &= ktan(\delta) \\ \delta &= \frac{1}{2}arctan(\sigma) \\ \sigma &= \frac{8}{3/\pi}c_f\frac{\hat{Q}}{\omega A_c R} \end{aligned} \tag{H.7}$$

Table H.1 displays the input paramaters of the analytical formulation, based on typical characteristics of the downstream located reach of the Paraná de las Palmas. Figure H.4 displays the wave amplitude reduction factor $\exp -\mu s$ for spatial coordinates $s \in [0, 20]$ km, i.e. the most downstream located reach of the Las Palmas where dredging activities take place. When using a constant friction factor c_f of 0.0015, the damping factor $\exp -\mu s$ reduces from 0.88 to 0.87 when no dredging takes place. This implies an increase in tidal amplitude of roughly 1% or less than 1 cm. This increase greatly subceeds the order of magnitude of the (meteorological) tide and the water level elevation related to the river discharge. When using a higher friction factor for the non-deepened case, the difference in the damping factor becomes significant (0.88 versus 0.84). Depending on the change in bed roughness, depth and overall change in hydraulic friction after deepening, this second case could be more applicable than the case with constant friction factor. The results are displayed in Figure H.4.

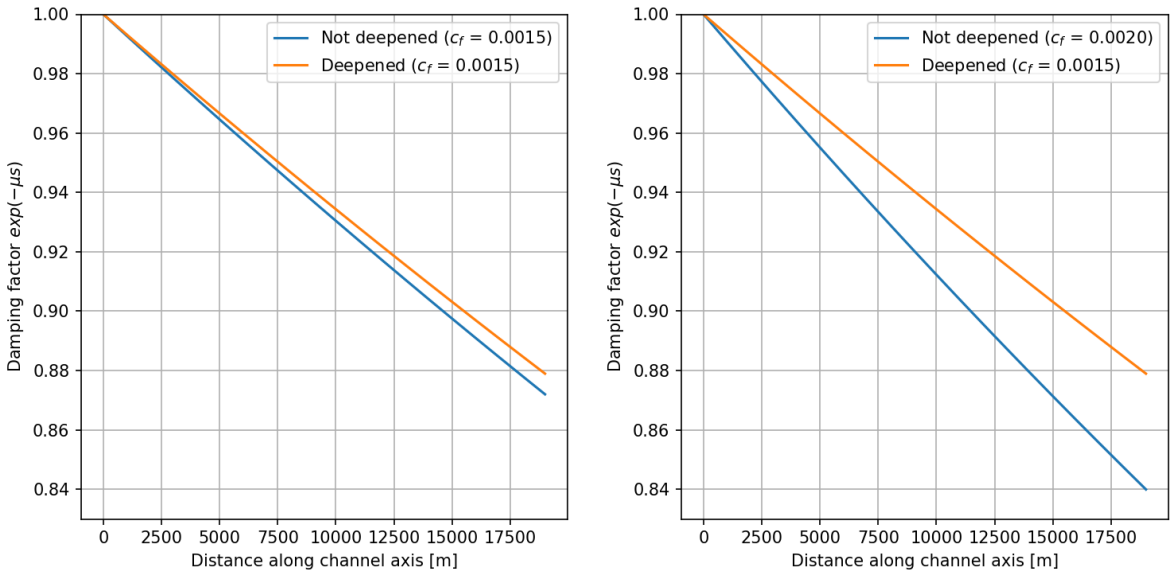

Figure H.4: Damping coefficient with and without deepening of the Paraná de las Palmas

H.3.4. Influence of deepening on channel flow repulsion

Deepening a river branch can alter the water levels at upstream channel bifurcations and can lead to reduced flow velocities in the side channels. A highly schematized case of the Paraná de las Palmas and a side channel is presented, demonstrating the effect that artificially deepening a main channel has on the discharge distribution, and associated changes of sediment transport capacity between the channels. The discharge distribution between main channel 1 and side channel 2 is governed by the downstream boundary conditions, and the conditions at the bifurcation (water level h, discharge Q) described in Equation (H.8).

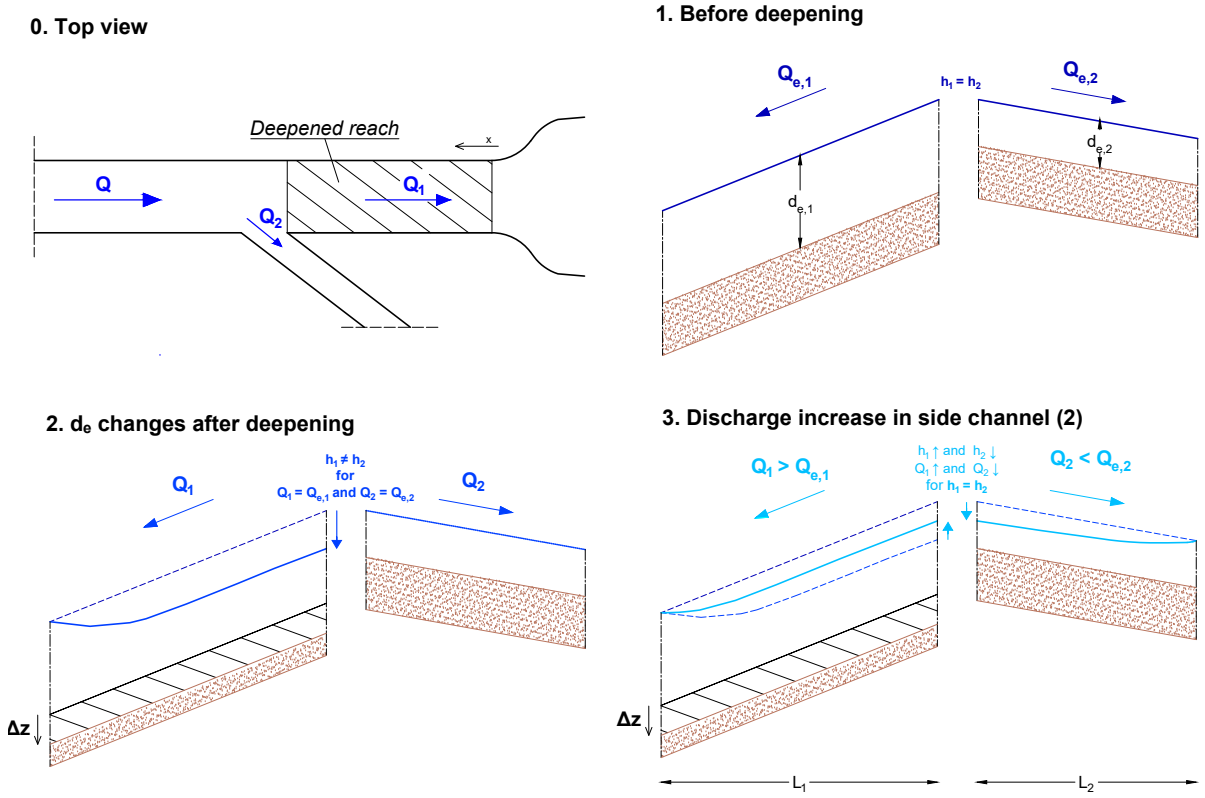

Figure H.5: Top view and theoretical behaviour before and after deepening

$$h = h_1 = h_2$$
$$Q_{total} = Q_1 + Q_2 \tag{H.8}$$

In the schematized model, the following must be noted:

- The channel dimensions and distances are roughly based on the Paraná de las Palmas (Channel 1), Arroyo Carapachay (Channel 2) and Canal Honda - San Antonio (Canal 2, second computation). Typical characteristics of the channels are presented in Table H.1.
- It is assumed that before deepening Channel 1, both rivers are in equilibrium state.
- The main channel is deepened by Δz = 0.5 m
- Deepening of Channel 1 happens instantaneously

The characteristic values in Table H.1 are associated with equilibrium discharges Q_e and mean flow velocities u_e. Based on the current knowledge on the Las Palmas branch and the secondary channels, these values are at least in the right order of magnitude.
$Q_{1,e,Palmas}$ = 4252 m^3/s
$u_{1,e,Palmas}$ = 0.89 m/s

$Q_{2,e,Caraguata}$ = 51 m^3/s
$u_{2,e,Caraguata}$ = 0.25 m/s
$Q_{2,e,Honda - S. Antonio}$ = 485 m^3/s
$u_{2,e,Honda - S. Antonio}$ = 0.28 m/s

After deepening the main channel, a M2 backwater curve is formed in the main channel, lowering the equilibrium water depth and the water level along the reach. The water depth at the bifurcation (location $x = L_1$) can now be approximated with the Empirical Fit to Bresse, which was introduced Appendix A and repeated in Equations (H.9)

$$L_{(1/2)} = 0.24\frac{d_e}{i_b}\left(\frac{d_0}{d_e}\right)^{4/3}$$
$$d(x) = d_e + (d_0 - d_e)2^{\left(\frac{-x}{L_{(1/2)}}\right)} \quad \text{(H.9)}$$

The water level associated with the water depth $d(x = L_1)$ does not match the initial water level at the bifurcation in channel 2. In order for the system to comply with the condition $h_1 = h_2$, the discharges Q_1 and Q_2 will increase and decrease, respectively. The theoretical behaviour of the system is schematically depicted in Figure H.5.

The computation to find the discharge distribution matching the upstream water levels was carried out iteratively for the assumptions presented above. The computation was carried out for both Arroyo Caraguata and Río Union, this way the difference between a more upstream (Caraguata) and downstream located channel can be assessed. The before and after deepening discharges, flow velocities and bed shear stresses were computed. The results are displayed in Table H.5.

Table H.5: Discharge Q [m^3/s, velocity u [m/s] and bed shear stress [N/m^2] before and after deepening the main channel

Channel 2 =		Q_1	Q_2	u_1	u_2	$\tau_{b,1}$	$\tau_{b,2}$
Caraguata	Before deepening	4252	51	0.89	0.25	1.2	0.13
	After deepening	4261	42	0.85	0.21	1.08	0.09
	Difference (%)	+0.2%	-17.6%	-4.5%	-16%	-10.0%	-30.0 %
Honda - S. Antonio	Before deepening	4252	185	0.89	0.28	1.2	0.16
	After deepening	4272	165	0.85	0.25	1.08	0.13
	Difference (%)	+0.5%	-10.8%	-4.5%	-10.7%	-10.0%	-21.9 %

In Table H.5 it can be seen that the transport capacity in Channel 2 is impacted significantly (decrease of 30.0 and 21.9 %), while the effect in the main channel is limited. This highly schematized example displays that the sediment transport capacity in a small side channel can be significantly decreased by deepening of the larger channel. The large difference in channel dimensions and discharges makes for the influence to be mostly one-sided; changes in the main channel can have large influence on the small channel, not vice versa. The effect of reduction in side channel sediment transport capacity decreases as the distance from the river mouth decreases. This could explain the observation of more shallow and permanently dry channels being located more upstream in the Lower Delta, and deeper, more permanently conveying channels near the deltaic front. Due to the backwater effect not influencing the most downstream channels as much, these channels attract more water, which in one observed case (Río Union) can have the widening of the channel as an effect.

H.3.5. Channel feeding by deposition sites

By means of a highly simplified case, the possibility of dredged material being transported into a side channel is considered. The situation at Arroyo Pay Curaby is used as a reference case.

It is assumed that the dredged material originates from nearby, i.e. from the river mouth. Typical soil characteristics at the Paraná de las Palmas mouth were sampled and characterized by Drago and Amsler [1998], described in Chapter 2 and repeated in Table H.6.

Table H.6: Bed sediment at the Paraná de las Palmas [Drago and Amsler, 1998]

	D_n [mm]	Fraction in bed
Fine sand	0.125 - 0.250	24 %
Very fine sand	0.062 - 0.125	50 %
Silt	0.002 - 0.062	12 %
Clay	0.002	12 %

Typical flow conditions during regular conditions are assumed to be similar to those measured by by INA (Morale et al. [2018], see Figure H.2). The flow velocity, near the shore, around the location of deposition is approximately 0.5 m/s. For such conditions, the maximum particle diameter that can be transported is approximated by using the concept of the critical shields factor (see Appendix A). For a critical shields factor θ_{cr} of 0.04, a friction factor c_f of 0.0015 and a dry density of 2650 kg/m^3, the threshold sediment diameter D_{cr} becomes 0.57 mm, implying that the finer sand, silt and clay particles might be transported by the current. Flow decelerations in the channel network could cause the transported material to settle, however the extent of this process is highly dependant on local conditions.

$$\begin{aligned} \theta_{cr} &= \frac{\tau_{b,cr}}{(\rho_s - \rho)gD} \\ 0.04 &= \frac{0.0015 \cdot 0.5^2}{(1650 \cdot 9.81 \cdot D_{cr}} \\ D_{cr} &= 0.57mm \end{aligned} \tag{H.10}$$

Field surveys report

On 5 days in December 2021 and March/April 2022, field surveys were carried out in order to collect hydrometric and sedimentological data. This data mainly served as input and validation data for the numerical modelling practices associated with this research. This appendix describes the activities that were carried out. Table I.1 gives the dates and summarizes the activities carried out. More detailed information on the methodology is iven in the subsequent sections.

Table I.1: Summary field surveys

Date	Activities
6 Dec 2021	depth measurements - bed soil sampling
7 Dec 2021	depth measurements - bed soil sampling
18 March 2022	depth measurements - bed soil sampling - suspended sediment sampling
19 March 2022	depth measurements - bed soil sampling - suspended sediment sampling
25 March 2022	stationary discharge measurements - suspended sediment sampling

All surveys started and ended at the port of El Tigre, where associates of INTA (*Instituto Nacional de Tecnología Agropecuaria*) picked the up participants of the surveys in the morning and dropped them off in the late afternoon. INTA is a governmental institution assigned with executing research and practical activities related to benefiting agricultural activities in Argentina, and that in reality is involved in many other technical and societal issues related to a wide range of subjects [personal contact with M. Sabarots Gerbec].

I.1. Echo Sounder depth measurements

During 4 of the 5 surveys, an Echo Sounder device was used to capture the instantaneous water depth while sailing the routes as displayed in Figure I.1. At various locations, cross sections were measured which can be used to interpolate between in order to create a Digital Elevation Model of the channels. An Echo Sounder uses acoustic waves to determine the distance between the measuring device and the water bottom. It uses the time interval between outgoing and reflected signals with the celerity of sound waves in water to compute the water depth, along with the spatial coordinates (long/lat) and time, and saves this data on a MicroSD card. The principles of Echo Sounder measurements are schematically depicted in Figure I.2.

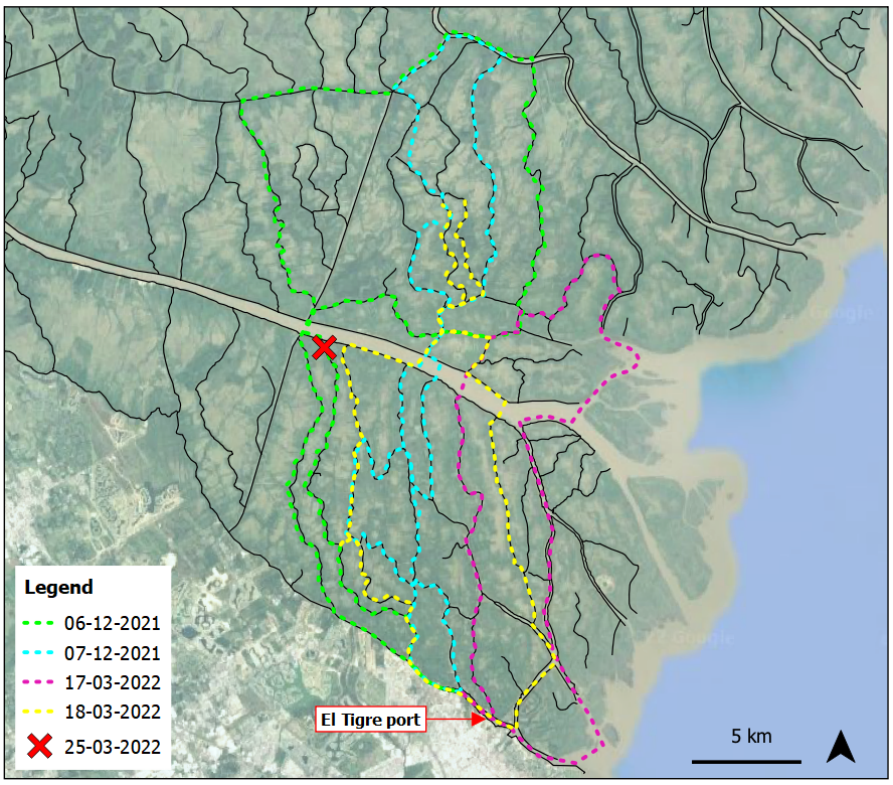

Figure I.1: Sailing routes and location

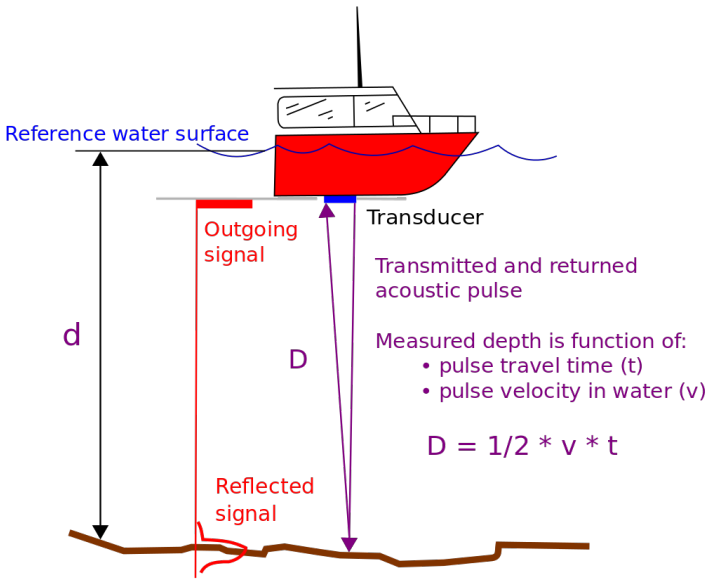

Figure I.2: Principles of Echo sounder measurements (adjusted by Brandon T. Fields, based on [USA, 2013])

The device used was the ***Garmin echoMap™ CHIRP 42cv***. It exists of a controller and a transducer (see Figure I.3). The transducer was placed in a bottom compartment of the boat in a small layer of water, allowing its signals to penetrate the bottom of the boat. The controller was kept in a briefcase with the necessary power supply, as well as a mobile phone saving temporal and GPS coordinates to serve as a backup in case the Echo sounder failed to measure or save either of those data types.

Figure I.3: Echo sounder used during the field surveys

The following must be noted concerning the accuracy of the measurements:

- The error margin of an Echo Sounder is proportional to the water depth, as the transducer is placed manually and will in reality always be placed in a slight inclination to the downward direction. The ship's bobbing motion will also cause slight measurement errors. This makes an echo sounder more suitable for measuring small water depths, as is the case in the Lower Delta channel network.
- The measured data is a function of the celerity of sound waves in water, which is approximately 1500 m/s. The celerity decreases with increasing fluid density, therefore factors such as salinity, sediment concentration and temperature all influence the data output. However, in the conditions present in the Paraná Delta, these factors can be assumed to be of minimal importance.

The accuracy of the measurements are thus highly dependant on the perpendicularity of the transducer to the water level, which is a function of the transducer placement and the boat movement, and the accuracy of the celerity of sound used to calculate the depth. Earlier measurements by INA have implied that measured errors can be in the order of 10 - 20 cm [Personal contact with M. Sabarots Gerbec].
[Garmin, 2016]

I.2. Discharge measurements

On 25 March, hourly discharge measurements were executed with an Acoustic Doppler Current Profiler. An ADCP transmits sound waves which reflect of particles carried by the water current and using the principle of the Doppler effect, the reflected signal can be converted to a relative velocity of the particles.

For large portion of the afternoon, a SonTek M9 ADCP device was used to measure several cross sections at one location in order to capture the variability of the discharge during a part of the tidal cycle. The device was attached to a SonTek foamboard and attached with a string of 5 - 10 meters to the boat, after which several cross sections were measured. For every measurement at a certain time, approximately 8 cross sections were taken and averaged over to generate the final discharge and (mean) velocity signal. The results are displayed in Appendix F. Figure I.4 display some impressions of the survey.

Figure I.4: ADCP device during the 25 March field survey

I.3. Suspended sediment measurements

During the non-stationary surveys, suspended sediment samples were taken at a water depth of 1 m, using a DH-48 sediment sampler (see Figure I.5). The sampler consists of a glass bottle with a nozzle, which is attached to a rod of 1.5 m long. When held under water, the water and sediment enters the bottle via the nozzle.

It is important that the samples should not be kept under water for too long, as the measurements are no longer representative when the container fills up completely. The time the bottle should be kept under water is a function of the ambient flow velocity. Limits in ambient velocity are approximately 0.3 to 3 m/s, associated limits in the filling times are 41 to 4 seconds, respectively [US-FISP, 1999].

At every location a sample was taken. These samples only give information on superficial concentrations, however due to the high percentage of fines these measurements are indicative for concentrations over the water column. Results (Appendix B) are in the order of 150 to 300 mg/l, similar to yearly-averaged concentrations.

On 25 March, stationary suspended sediment samples were taken measurements were taken after every discharge measurement. These samples were taken using a peristaltic pup of the brand Apema (Figure I.5) and a thin glass tube, which allowed for sampling at multiple depths. Samples were taken at 20, 50, 100, 200 centimetres above the bed and 1 meter below the surface.

Figure I.5: DH-48 (left) sampler and the peristaltic pump

I.4. Bed sediment sampling

At the same locations as the suspended sediment samples, bed sediment samples were taken. The heavy, metal sampler (Figure I.5) was attached to a rope and dragged over the channel bed in order for it to capture a sample. Samples were analyzed with a Laser Scattering Particle Size Distribution Analyzer (Horiba LA-910) at the Litoral University of Santa Fe. Results of the analysis are included in Appendix B.

Figure I.6: Bed sediment sampler

J

Calibration results

This appendix describes the calibration procedure and results, as introduced in Chapter 4. Section J.1 describes the main calibration procedure, making use of measured water levels in the lower delta. Section J.4 describes the results of the discharge and velocity measurements on 25 March 2022. Section J.2 gives the additional validation procedure of the selected Manning coefficient based on water level data extracted from an existing and calibration HEC-RAS model.

J.1. Water level measurement stations

The following figures display the results of the calibration of the Manning Coefficient, as described in Chapter 4. The different values for the Manning coefficient for the calibration runs are displayed in Table J.1. Selection of the best combination of friction parameter values was primarily based on water levels of the Arroyo Carapachay and Canal Seoane water level measurement stations (Figure J.1). The Paraná Mini station is located close to the deltaic front, and the model results are thus mostly determined by the downstream boundary condition; no significant differences were detected between the calibration runs. The measured time series of the Dique Luján have a lower frequency and are obtained by manual reading of a water level scale. The accuracy of this data is thus limited, and must be interpreted accordingly.

Table J.1 presents the Manning values applied in the calibration runs. The model run that has the best resemblance with the measured time series is variable over time. During low water levels, lower Manning values seem to be well suitable. Especially in the shallow channel network, the tides induce a large temporal variation in water depth and thus experienced friction. During various periods, run 1, 3 and 4 seem to give a similar quality of results, depending on the instantaneous water level. In the end, run 4 seems to best resemble the measured time series, and was thus chosen to be applied to all model scenario runs and the sensitivity analysis runs. On the subsequent pages, the results of the calibration runs are depicted, both during the entire computational period and during a smaller period, in which the water levels are better identifiable.

Table J.1: Manning coefficients in the calibration model runs

	n_{rivers}	n_{channels}
1	0.020	0.020
2	0.015	0.020
3	0.015	0.025
4	**0.020**	**0.025**
5	0.025	0.025
6	0.025	0.030
7	0.030	0.030
8	0.030	0.035

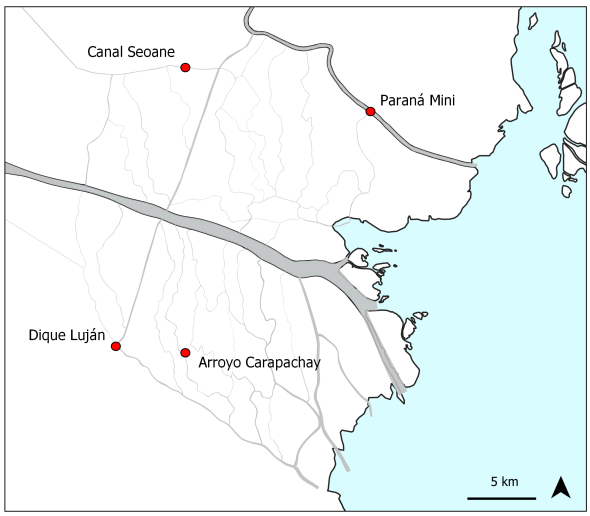

Figure J.1: Locations water level measurement stations

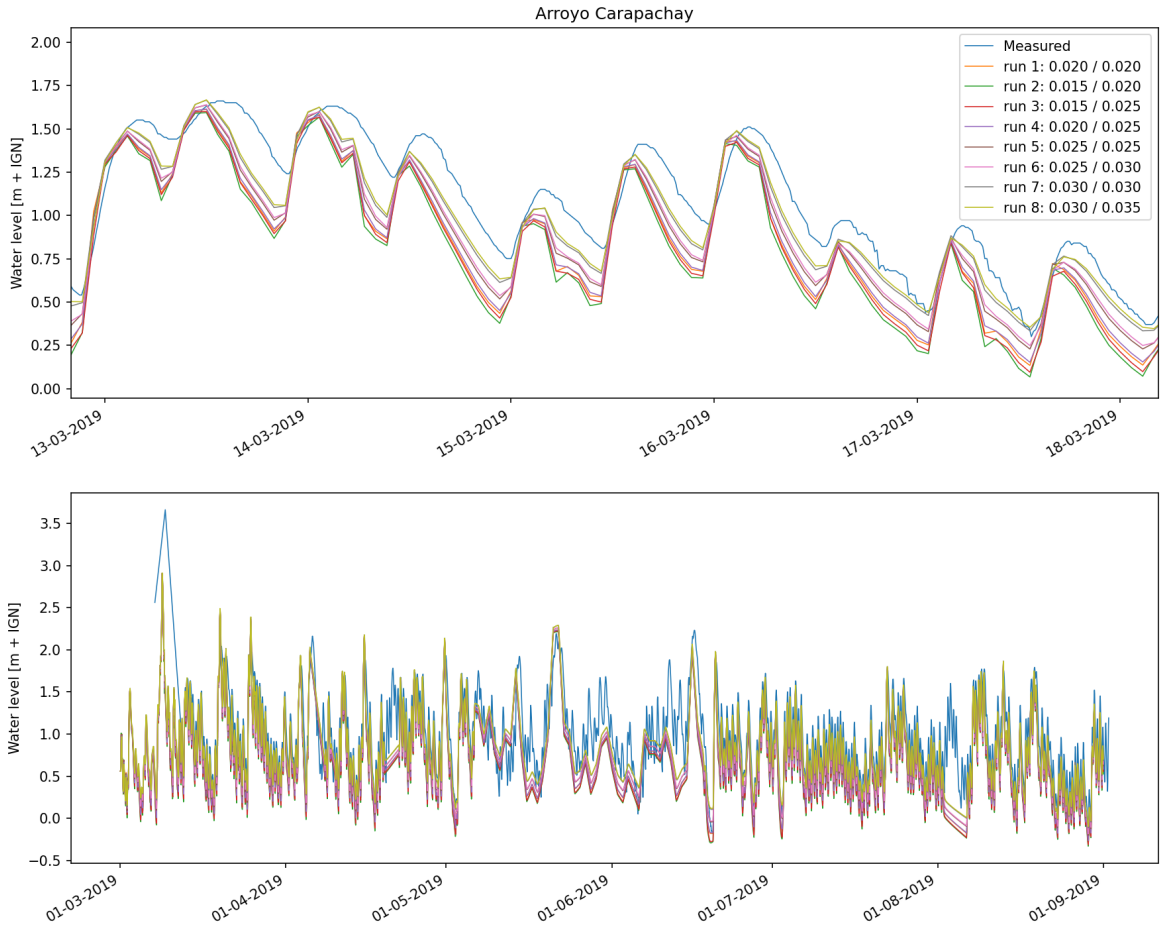

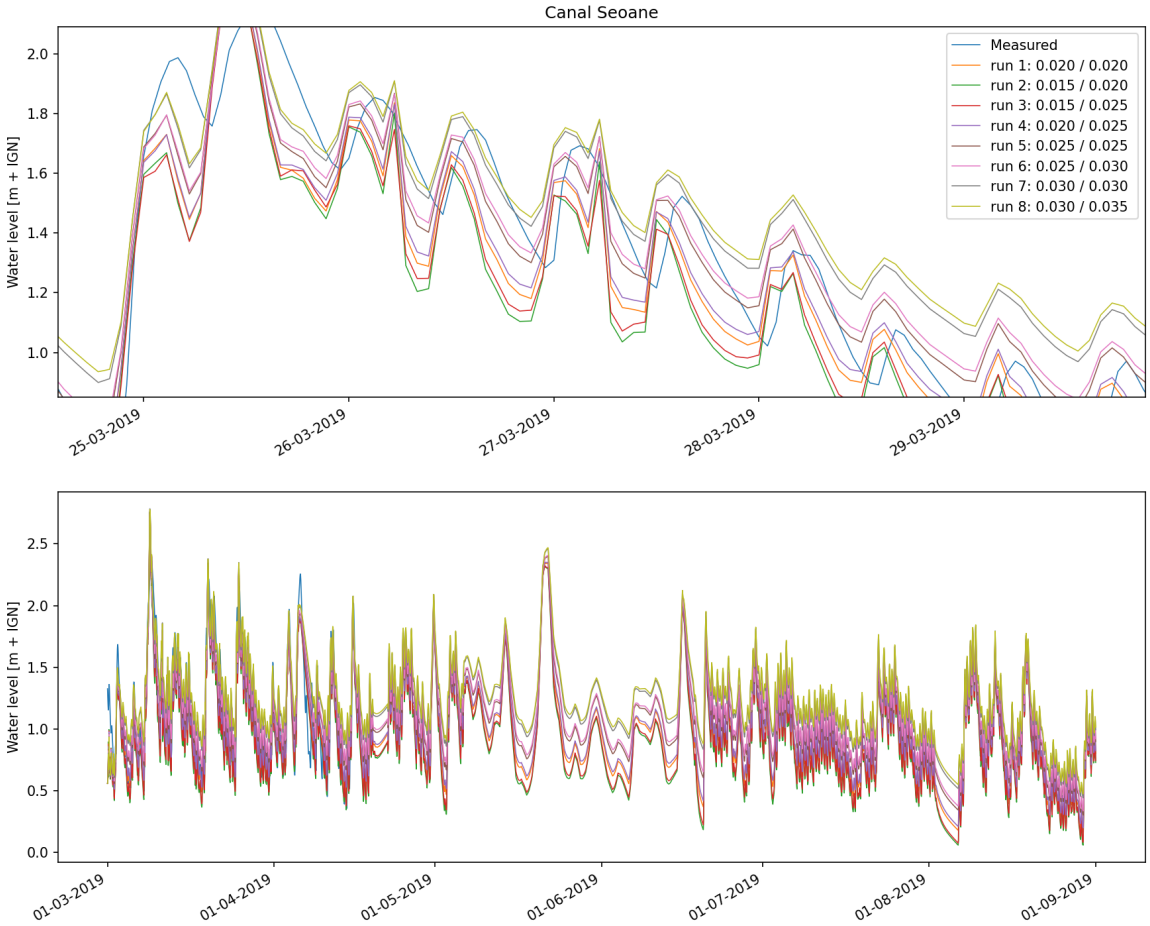
Canal Seoane
Water level [m + IGN]
Measured
run 1: 0.020 / 0.020
run 2: 0.015 / 0.020
run 3: 0.015 / 0.025
run 4: 0.020 / 0.025
run 5: 0.025 / 0.025
run 6: 0.025 / 0.030
run 7: 0.030 / 0.030
run 8: 0.030 / 0.035
25-03-2019
26-03-2019
27-03-2019
28-03-2019
29-03-2019
Water level [m + IGN]
01-03-2019
01-04-2019
01-05-2019
01-06-2019
01-07-2019
01-08-2019
01-09-2019

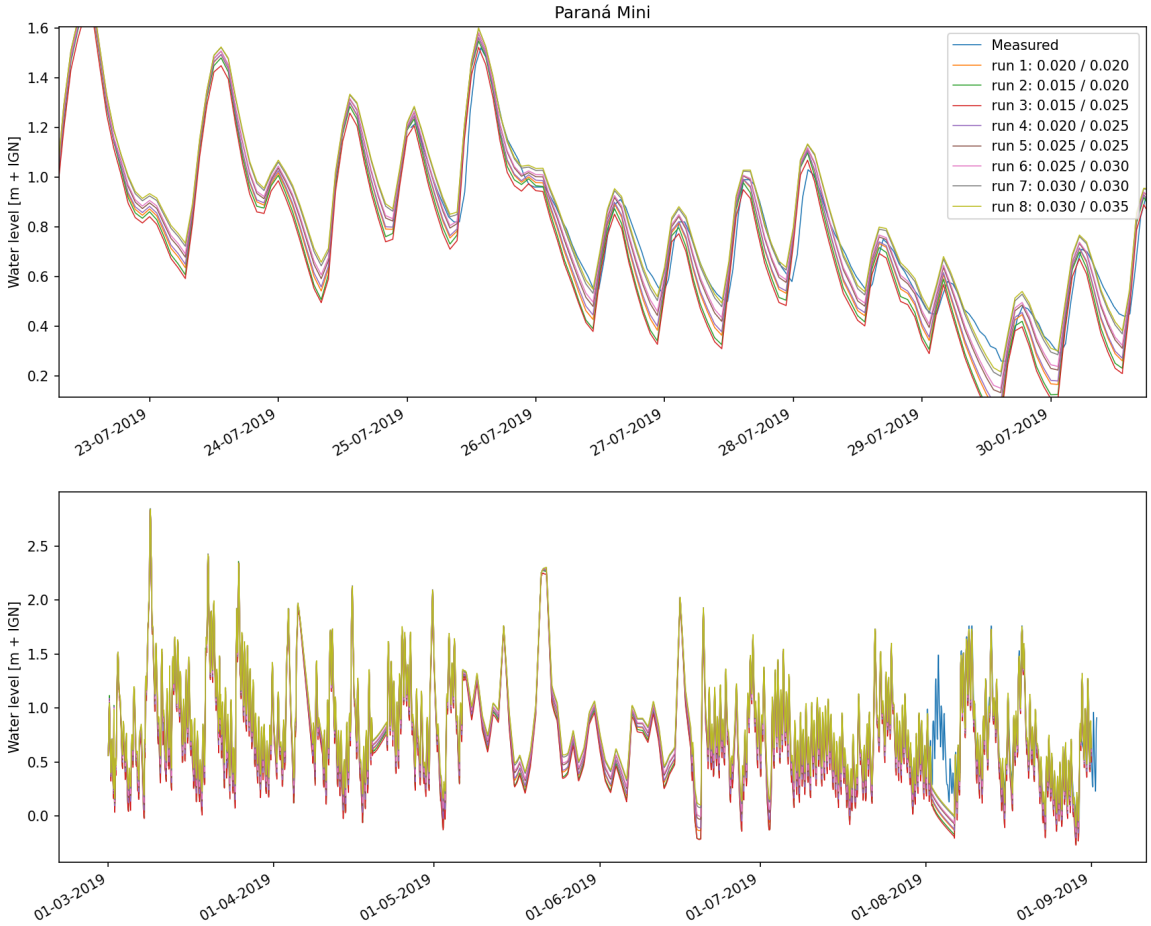
Paraná Mini
Water level [m + IGN]
Measured
run 1: 0.020 / 0.020
run 2: 0.015 / 0.020
run 3: 0.015 / 0.025
run 4: 0.020 / 0.025
run 5: 0.025 / 0.025
run 6: 0.025 / 0.030
run 7: 0.030 / 0.030
run 8: 0.030 / 0.035
23-07-2019
24-07-2019
25-07-2019
26-07-2019
27-07-2019
28-07-2019
29-07-2019
30-07-2019
Water level [m + IGN]
01-03-2019
01-04-2019
01-05-2019
01-06-2019
01-07-2019
01-08-2019
01-09-2019

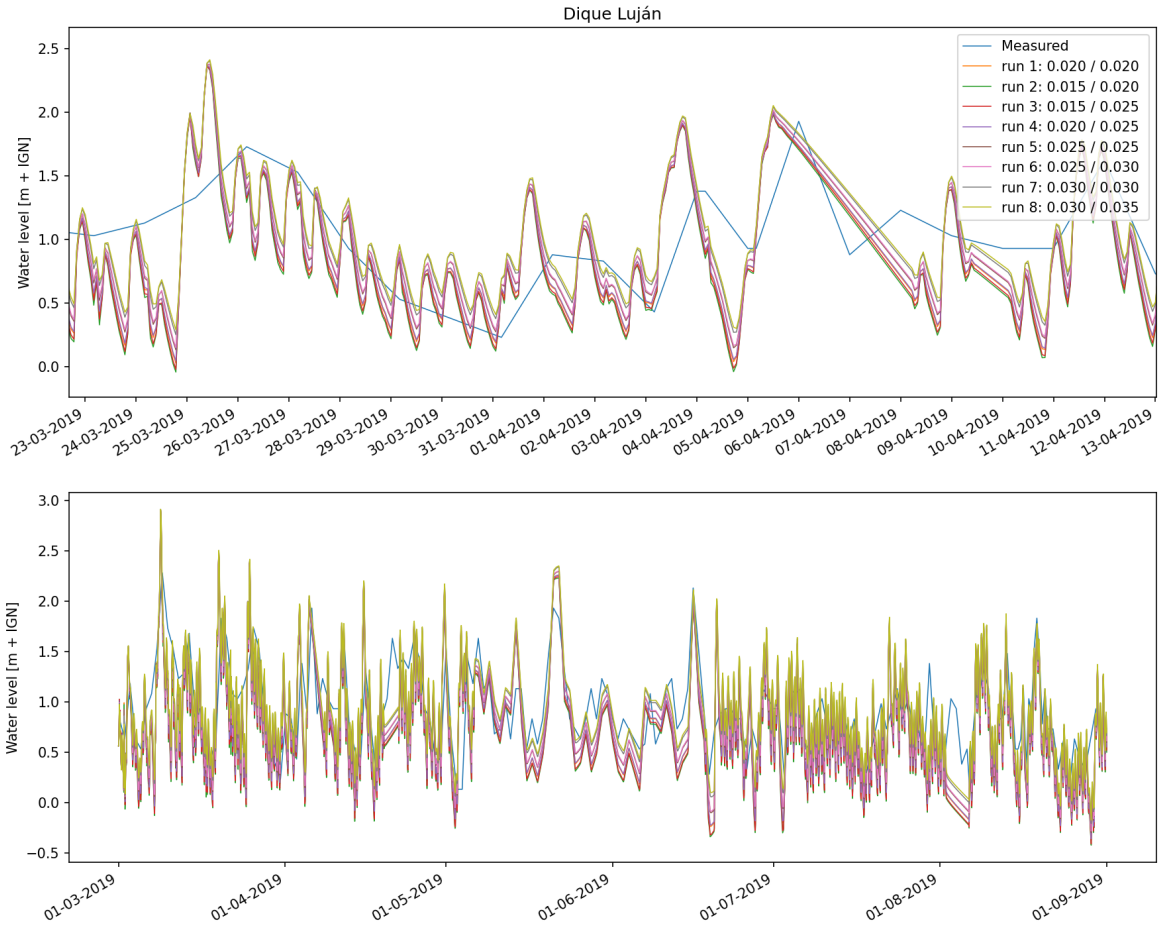

J.2. HEC-RAS water levels

Average water levels in the Paraná de las Palmas, Río Luján and the Paraná Mini extracted from an existing HEC-RAS model were compared with the model output. The modelled water level in the Paraná de las Palmas display a slight underestimation during high discharge (first half of the A0 run) and a slight underestimation in the Paraná Mini during low discharge (second half of the A0 run). Figures J.2 display the locations and results.

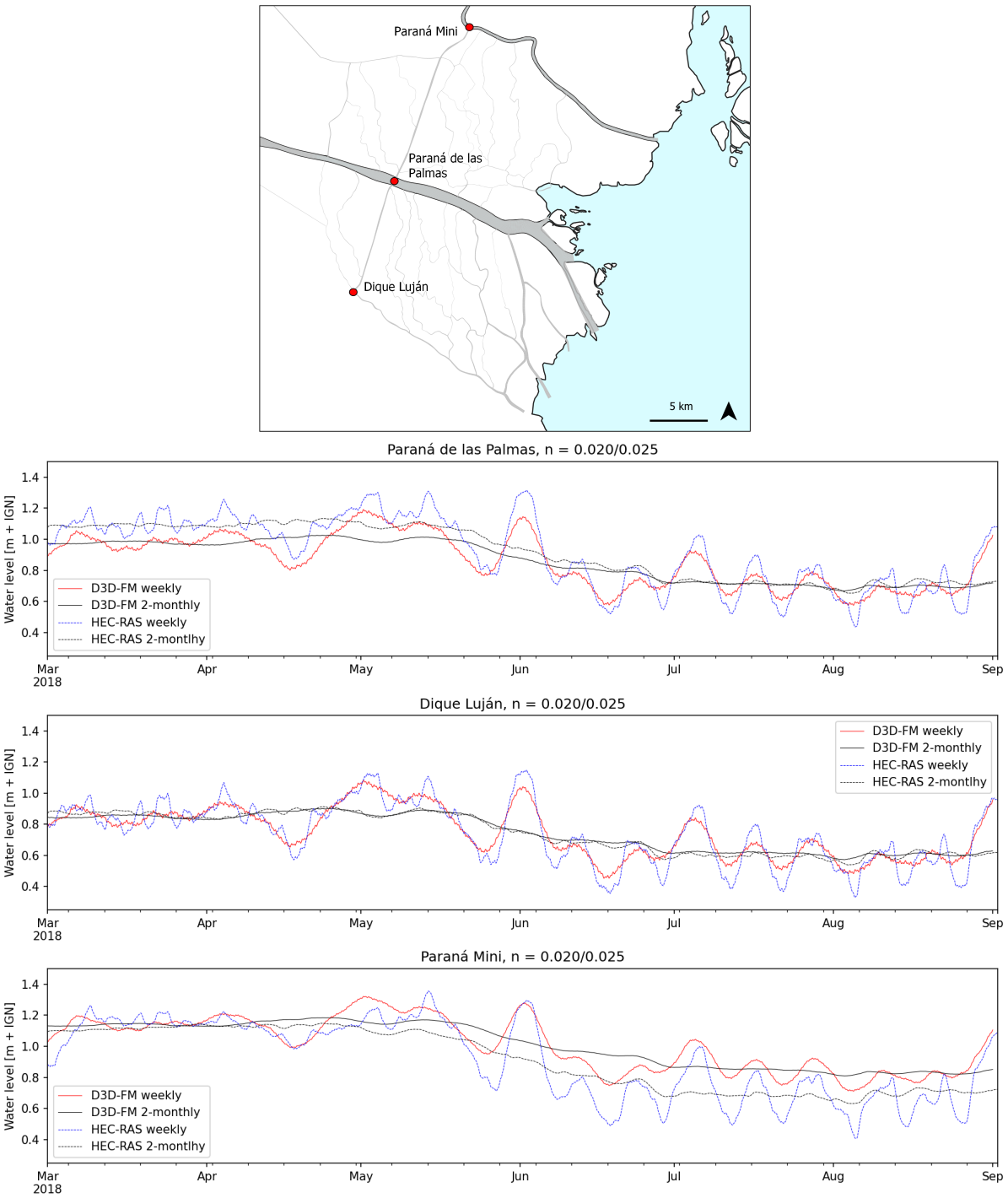

Figure J.2: Locations and results of additional HEC-RAS validation procedure

J.3. Discharge measurements 2018

Morale et al. [2018] executed ADCP discharge measurements in the Paraná de las Palmas. Morale et al. showed that depth averaged flow velocities of the Paraná de las Palmas are in the order of 1 to 1.5 m/s (see Figure J.3). Exact flow conditions during the time of measuring are unknown. In general, 2018 was a year with moderate discharge variation (see the selection of base scenario A0, Chapter 5) therefore the results of these measurements can be assumed to be representative for regular flow conditions.

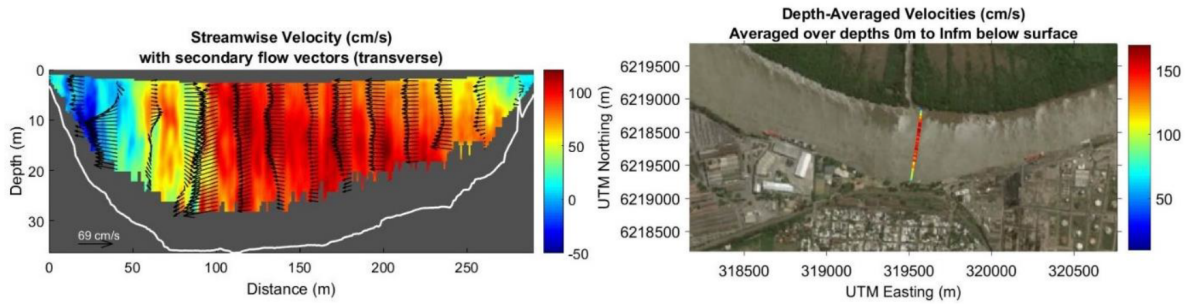

Figure J.3: ADCP measurements, Paraná de las Palmas [Morale et al., 2018]

Modelled flow velocities in the same location as the Morale et al. measurements were compared to the measurements, and found to be of a similar magnitude. As can be seen in Figure J.4., the modelled flow velocities fluctuate between 0.6 and 1.1 m/s , implying a reasonable similarity between modelled and observed flow conditions in the Paraná de las Palmas.

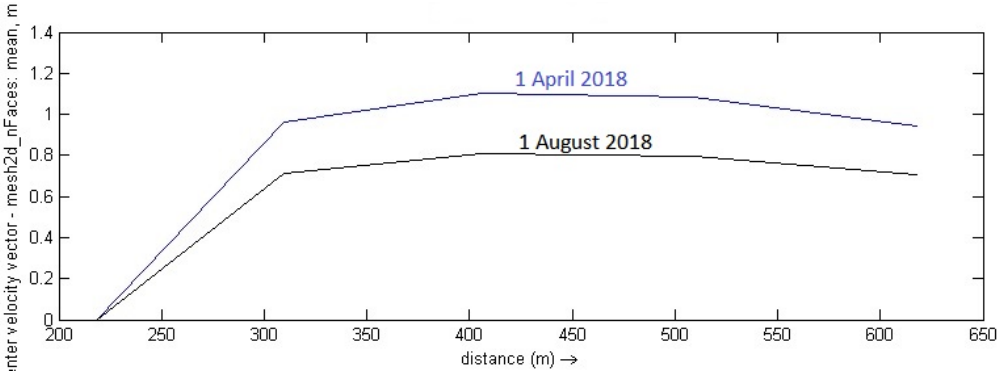

Figure J.4: Modelled flow velocities in the cross section displayed in Figure J.3

J.4. Discharge measurements Arroyo Carapachay 25 March 2022

In addition to the water levels, ADCP discharge and velocity data obtained on 25 march 2022 (see field survey report) were used to verify the flow in the model. In previous model runs (excluding downstream boundary points E and F, see Chapter 4), the model reproduced unrealistically low tidal velocity and discharge values. After including boundary points E and F, slightly more tidal energy entered the Paraná de las Palmas, resulting in a modelled velocity and discharge more closely resembling the measured values. Measured and modelled discharge and velocity data is presented below.

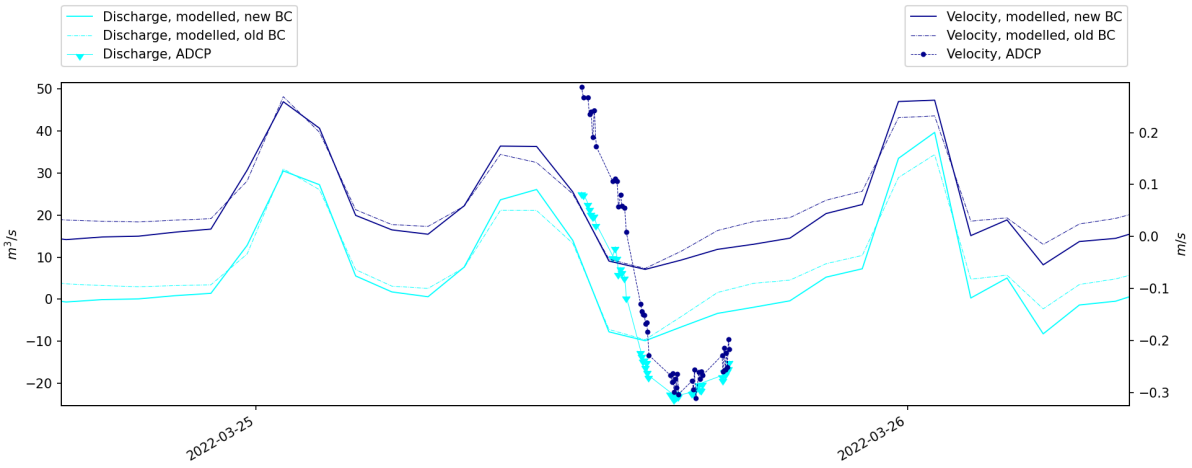

K

Model results

K.1. Bed level changes per region

This section gives the bed level changes categorized per region as displayed in Figure K.1. The 'upstream/downstream' terminology used in Chapter 5 is largely based on these results. Note that for scenario A3 in the table, the scenario run without the lateral discharge functionality is used.

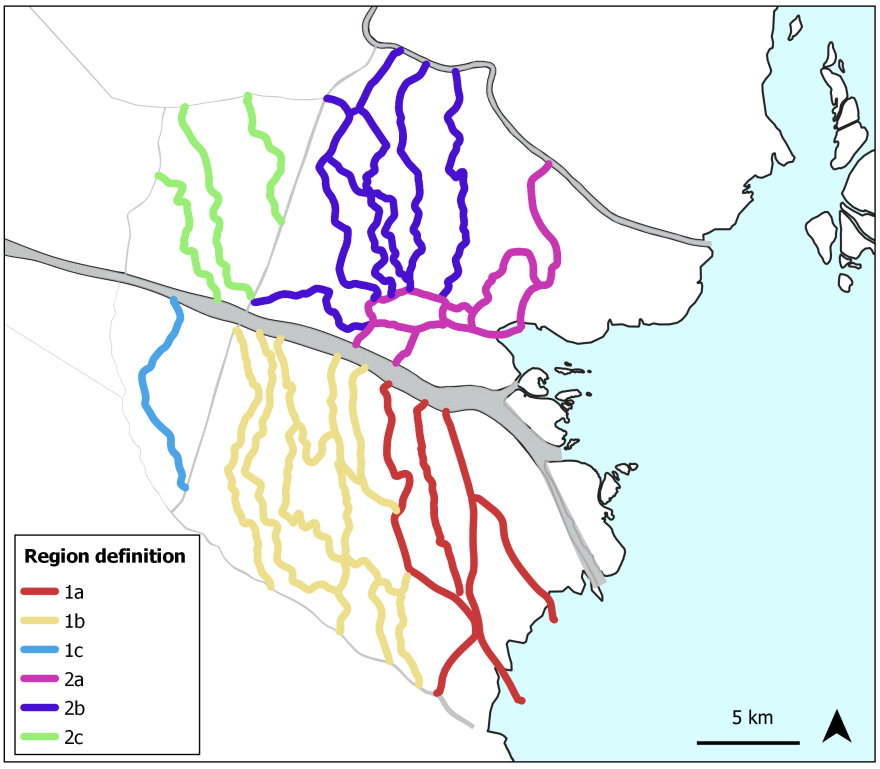

Figure K.1: Model output region definition

K.2. Bed level changes per scenario

The following sections give the cumulative erosion per scenario and the difference with the base scenarios, categorized per channel reach as defined in the Spatial Analysis (Appendix C).

K.2.1. A0

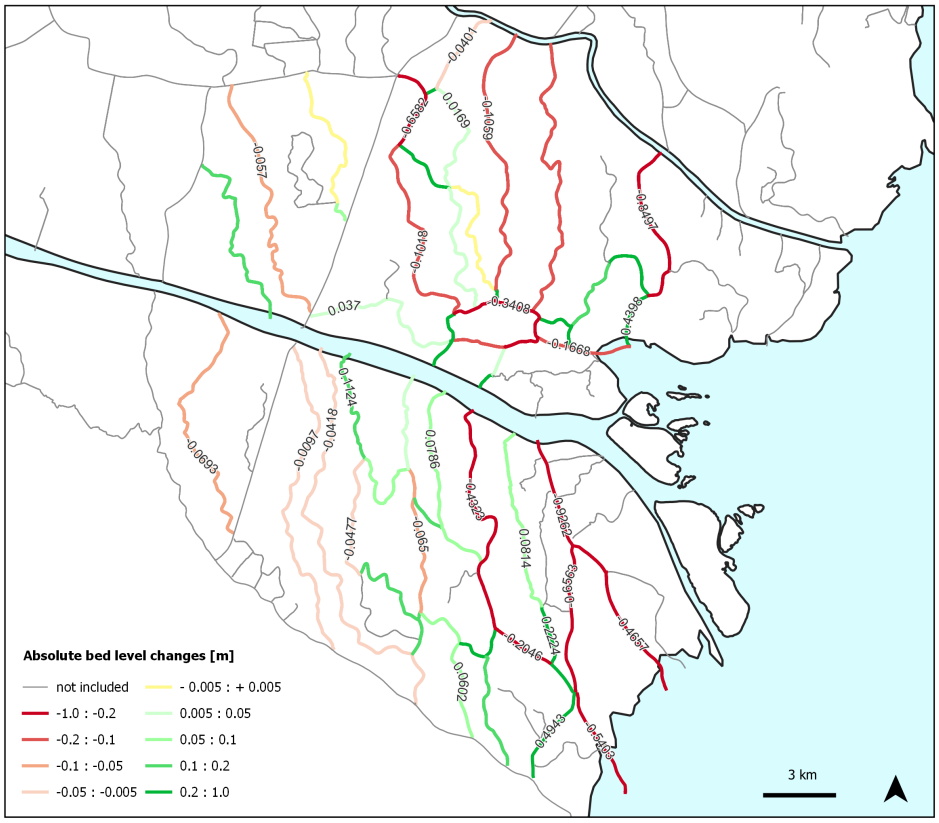
Absolute bed level changes [m]
not included
- 0.005 : + 0.005
-1.0 : -0.2
0.005 : 0.05
-0.2 : -0.1
0.05 : 0.1
-0.1 : -0.05
0.1 : 0.2
-0.05 : -0.005
0.2 : 1.0
3 km

K.2.2. A1

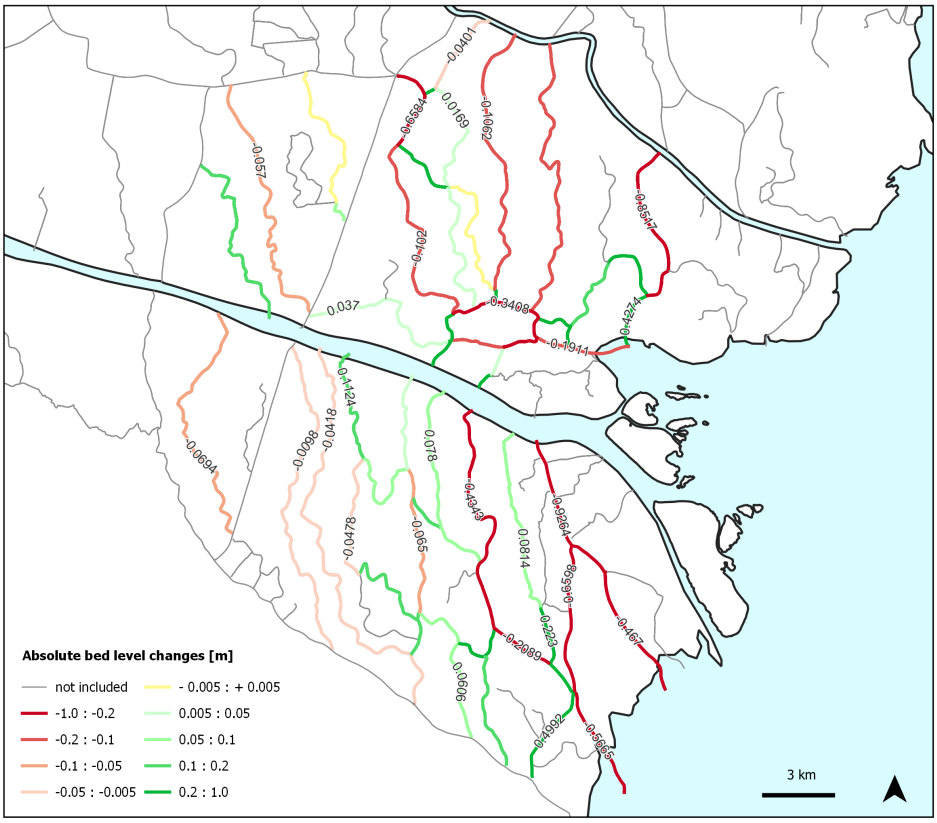
Absolute bed level changes [m]
not included
-1.0 : -0.2
-0.2 : -0.1
-0.1 : -0.05
-0.05 : -0.005
- 0.005 : + 0.005
0.005 : 0.05
0.05 : 0.1
0.1 : 0.2
0.2 : 1.0
3 km

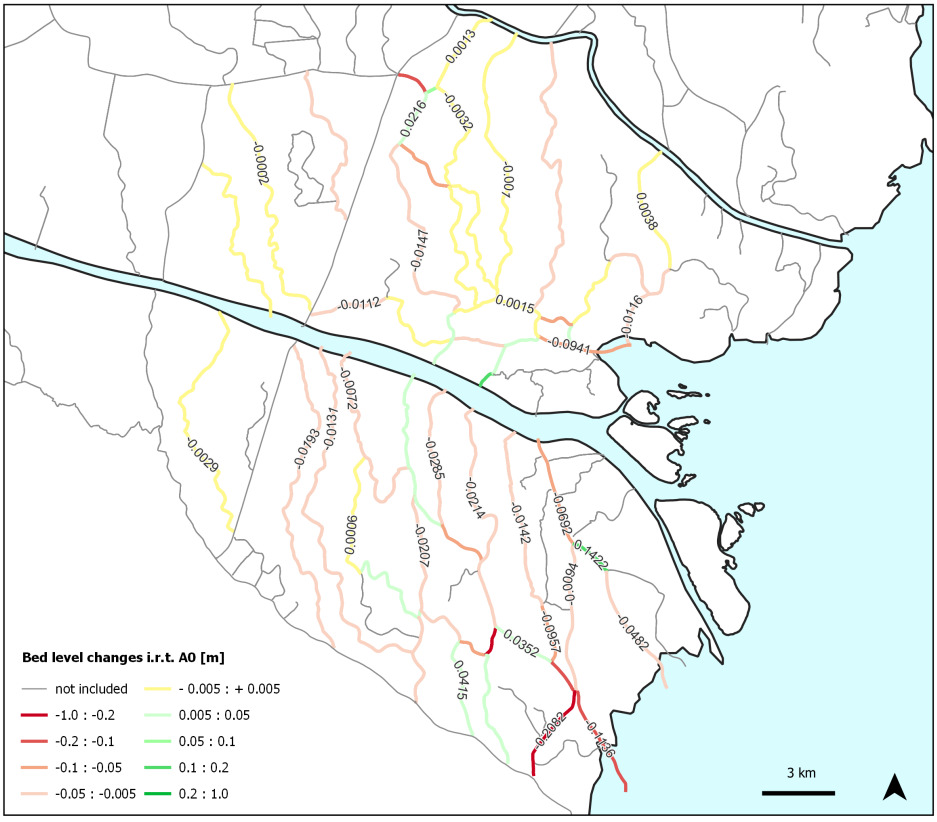
Bed level changes i.r.t. A0 [m]
not included
-1.0 : -0.2
-0.2 : -0.1
-0.1 : -0.05
-0.05 : -0.005
- 0.005 : + 0.005
0.005 : 0.05
0.05 : 0.1
0.1 : 0.2
0.2 : 1.0
3 km

K.2.3. A2

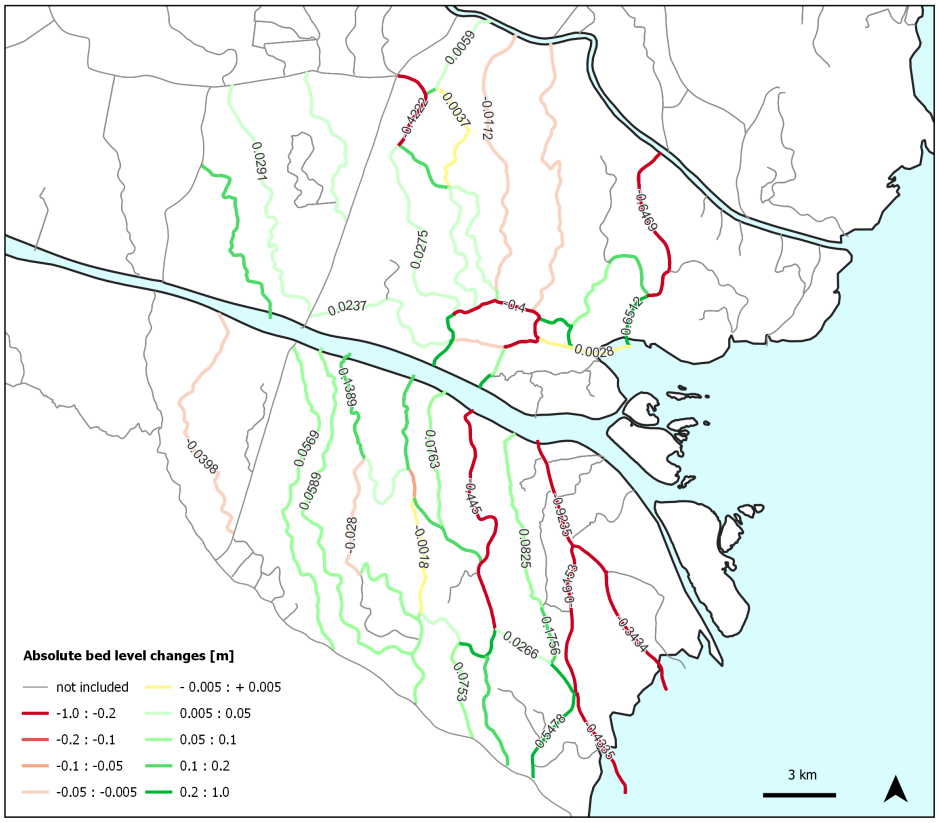
Absolute bed level changes [m]
not included
-1.0 : -0.2
-0.2 : -0.1
-0.1 : -0.05
-0.05 : -0.005
- 0.005 : + 0.005
0.005 : 0.05
0.05 : 0.1
0.1 : 0.2
0.2 : 1.0
3 km

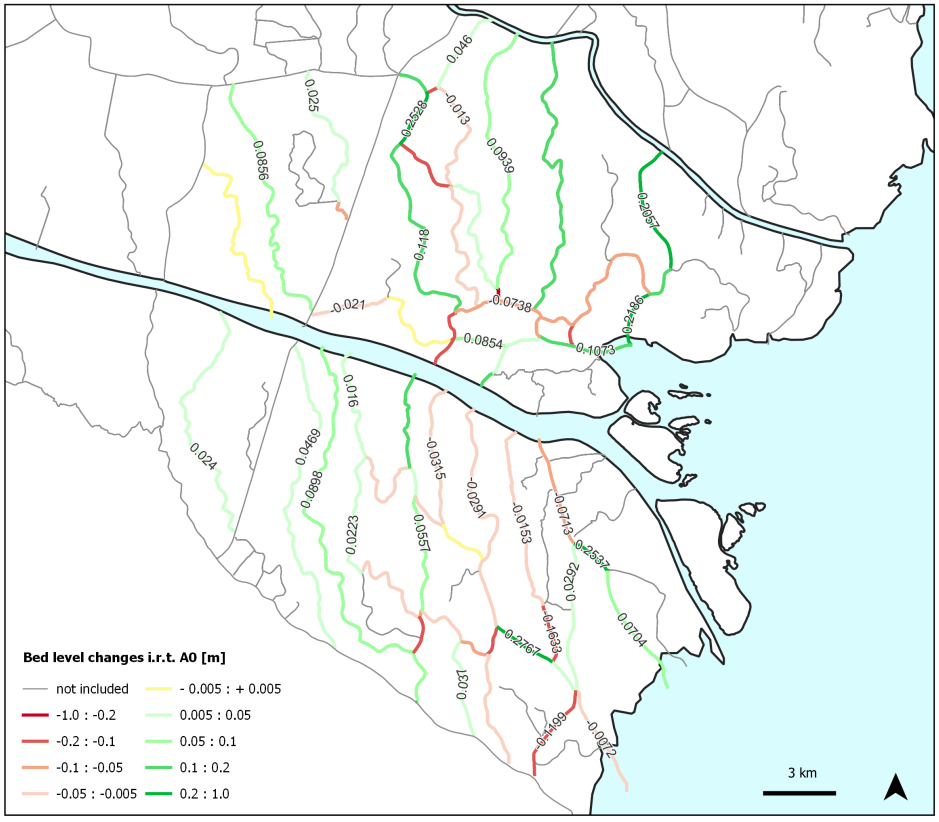
Bed level changes i.r.t. A0 [m]
not included
-1.0 : -0.2
-0.2 : -0.1
-0.1 : -0.05
-0.05 : -0.005
- 0.005 : + 0.005
0.005 : 0.05
0.05 : 0.1
0.1 : 0.2
0.2 : 1.0
3 km

K.2.4. A3 (no lateral discharge functionality)

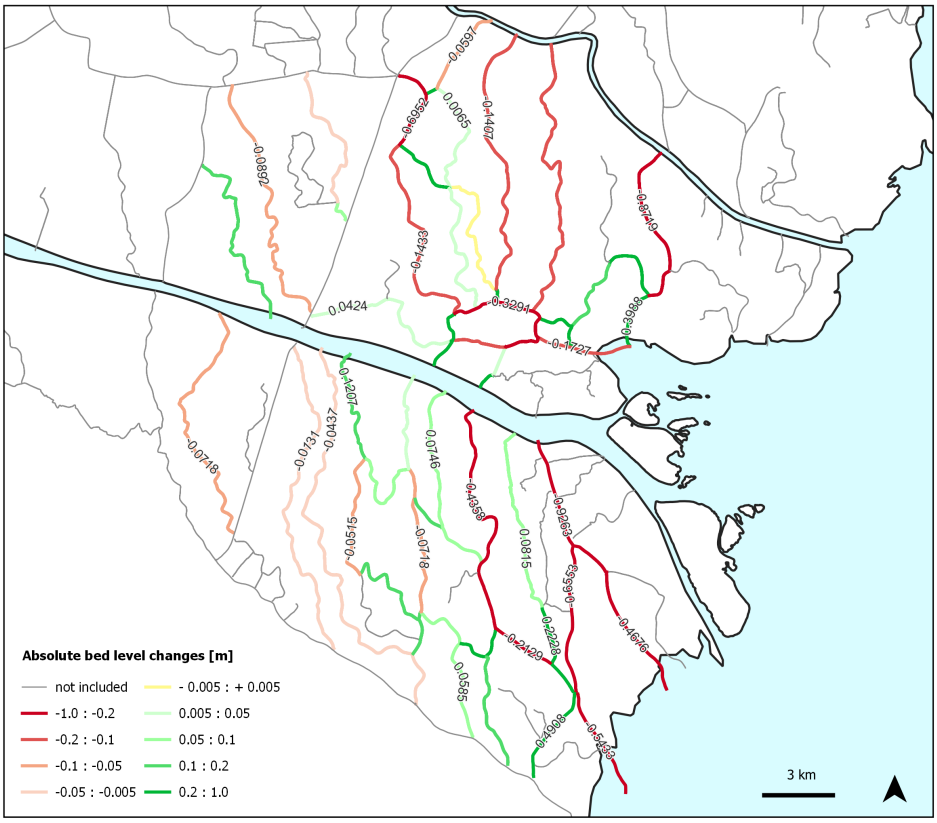

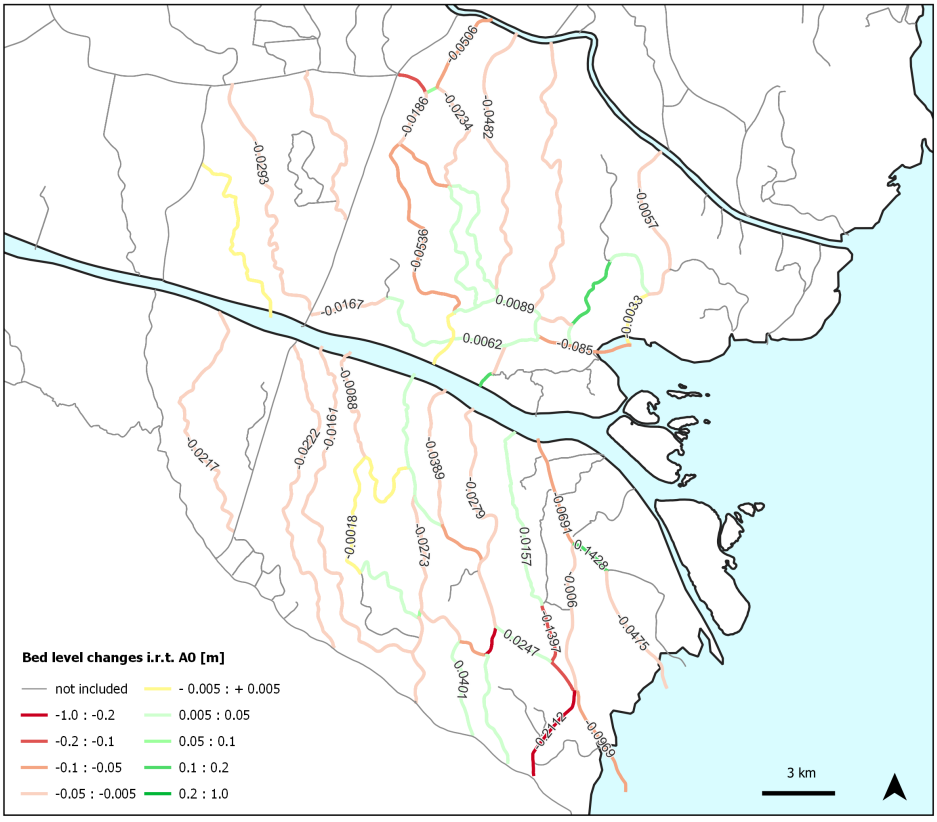

K.2.5. A4

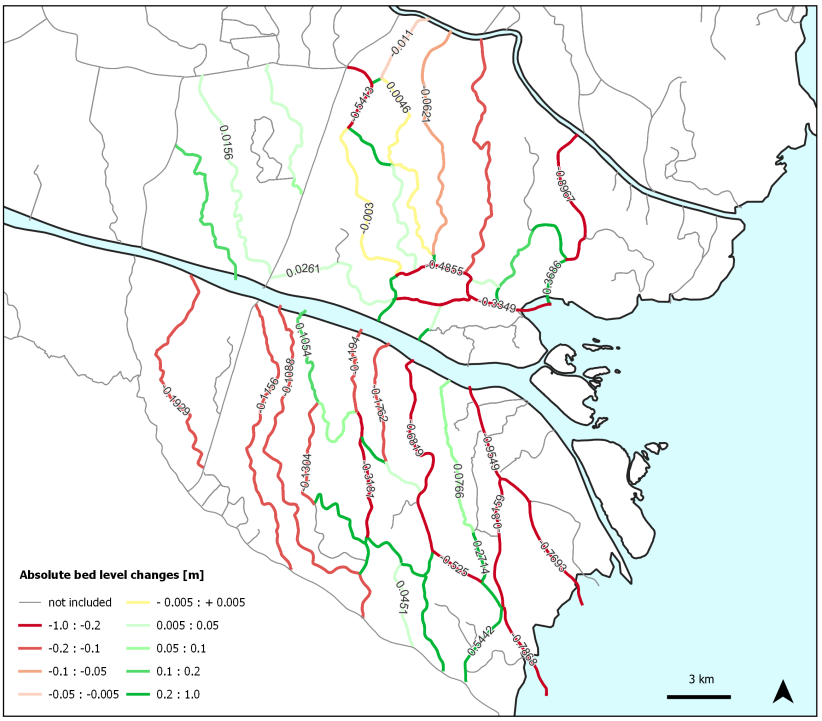
Absolute bed level changes [m]
not included
-1.0 : -0.2
-0.2 : -0.1
-0.1 : -0.05
-0.05 : -0.005
- 0.005 : + 0.005
0.005 : 0.05
0.05 : 0.1
0.1 : 0.2
0.2 : 1.0
3 km

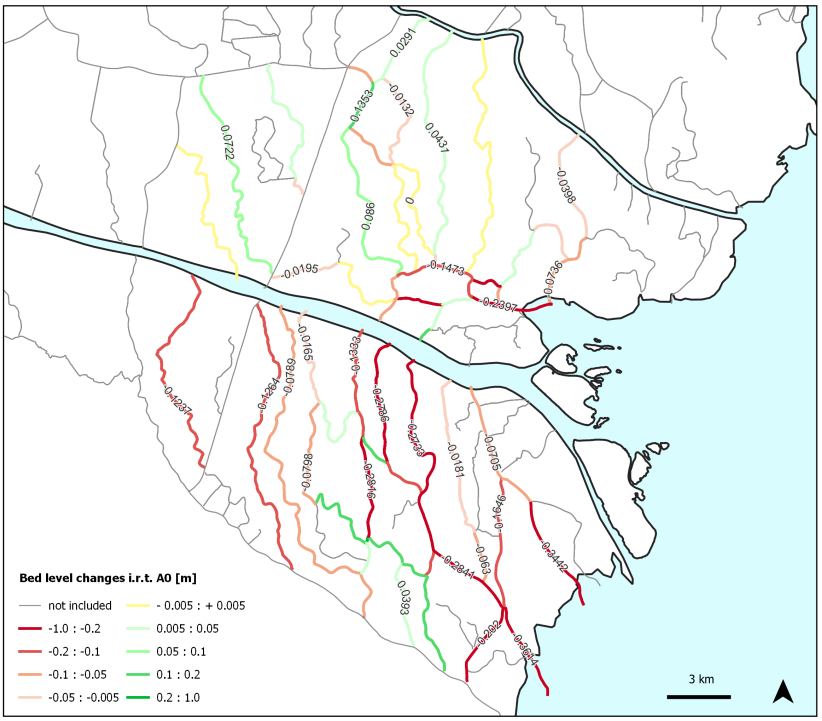
Bed level changes i.r.t. A0 [m]
not included
-1.0 : -0.2
-0.2 : -0.1
-0.1 : -0.05
-0.05 : -0.005
- 0.005 : + 0.005
0.005 : 0.05
0.05 : 0.1
0.1 : 0.2
0.2 : 1.0
3 km

K.2.6. A5

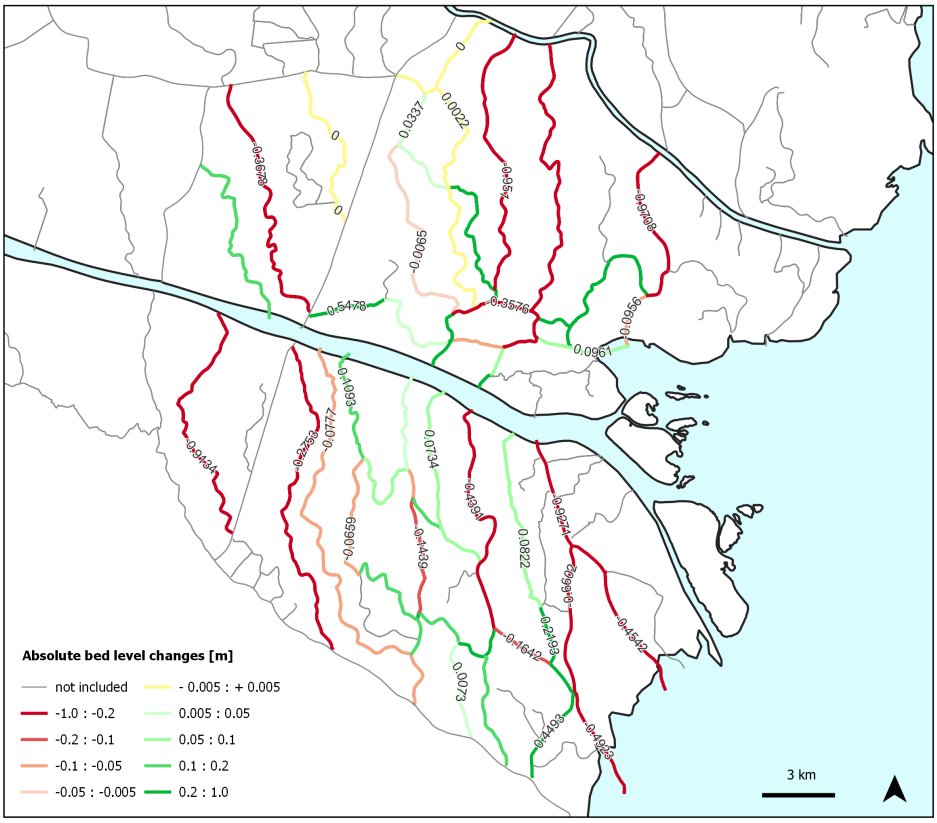
Absolute bed level changes [m]
not included
-1.0 : -0.2
-0.2 : -0.1
-0.1 : -0.05
-0.05 : -0.005
- 0.005 : + 0.005
0.005 : 0.05
0.05 : 0.1
0.1 : 0.2
0.2 : 1.0
3 km

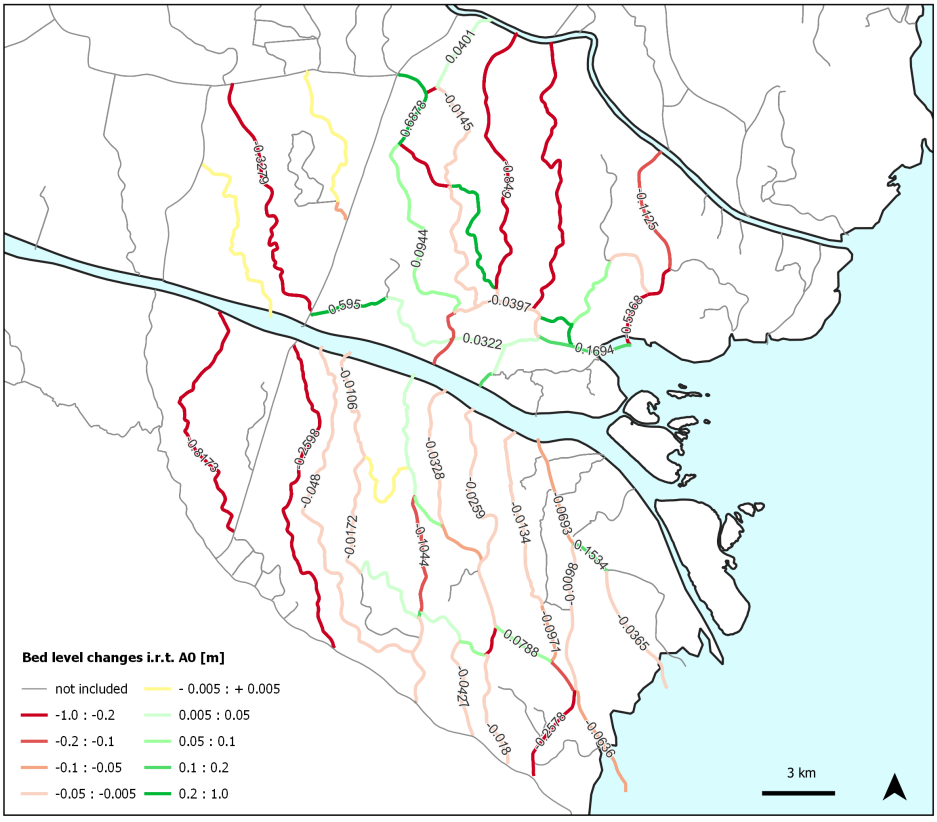
Bed level changes i.r.t. A0 [m]
not included
-1.0 : -0.2
-0.2 : -0.1
-0.1 : -0.05
-0.05 : -0.005
- 0.005 : + 0.005
0.005 : 0.05
0.05 : 0.1
0.1 : 0.2
0.2 : 1.0
3 km

K.2.7. B0

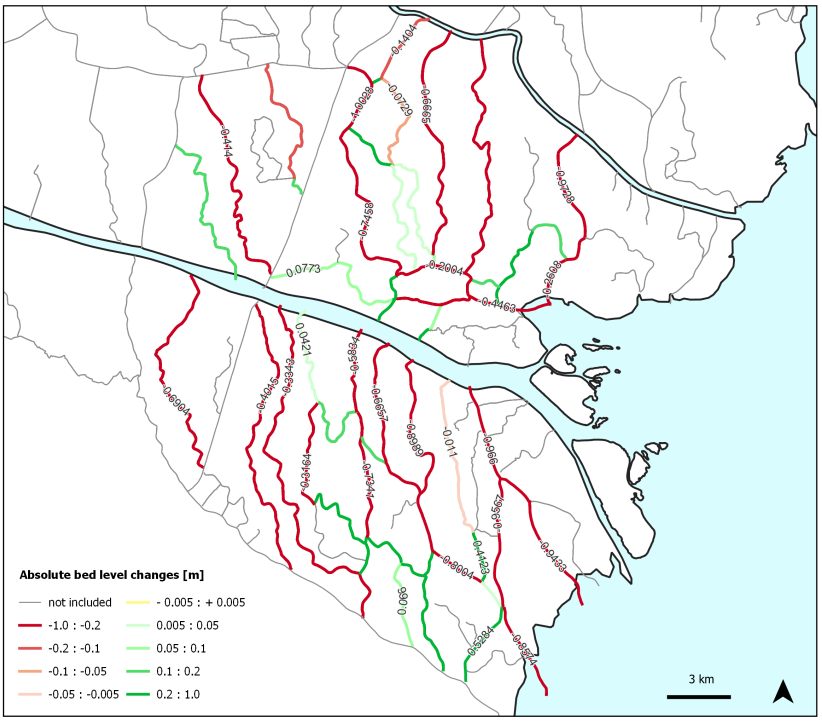
Absolute bed level changes [m]
not included
-1.0 : -0.2
-0.2 : -0.1
-0.1 : -0.05
-0.05 : -0.005
- 0.005 : + 0.005
0.005 : 0.05
0.05 : 0.1
0.1 : 0.2
0.2 : 1.0
3 km

K.2.8. B1

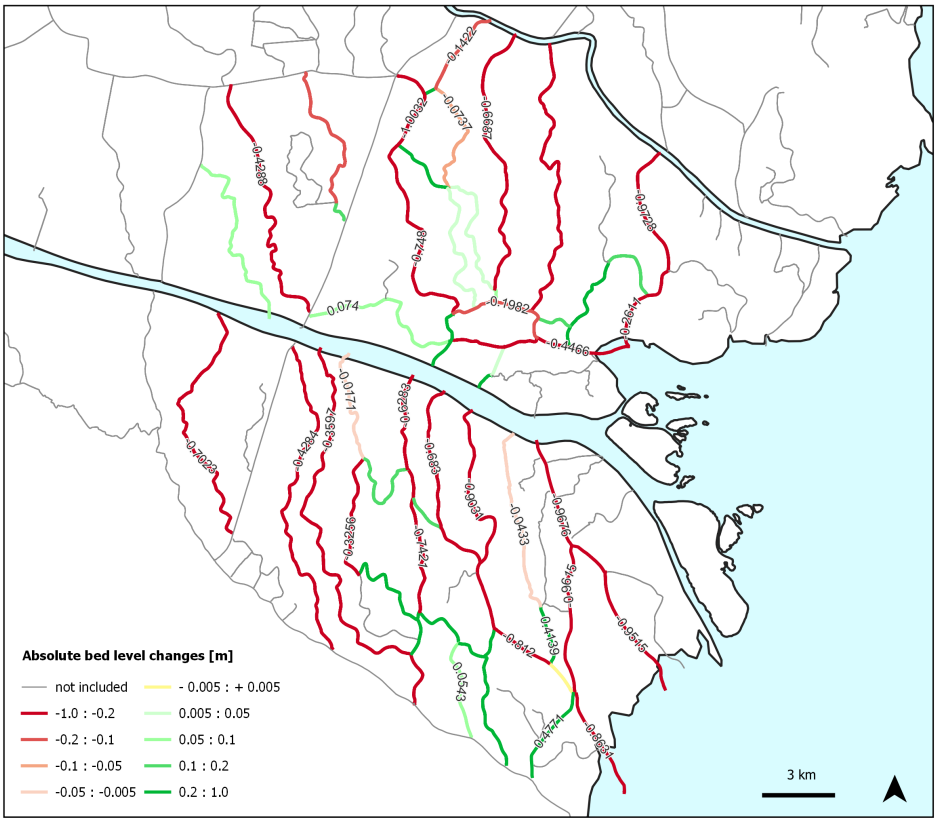
Absolute bed level changes [m]
not included
- 0.005 : + 0.005
-1.0 : -0.2
0.005 : 0.05
-0.2 : -0.1
0.05 : 0.1
-0.1 : -0.05
0.1 : 0.2
-0.05 : -0.005
0.2 : 1.0
3 km

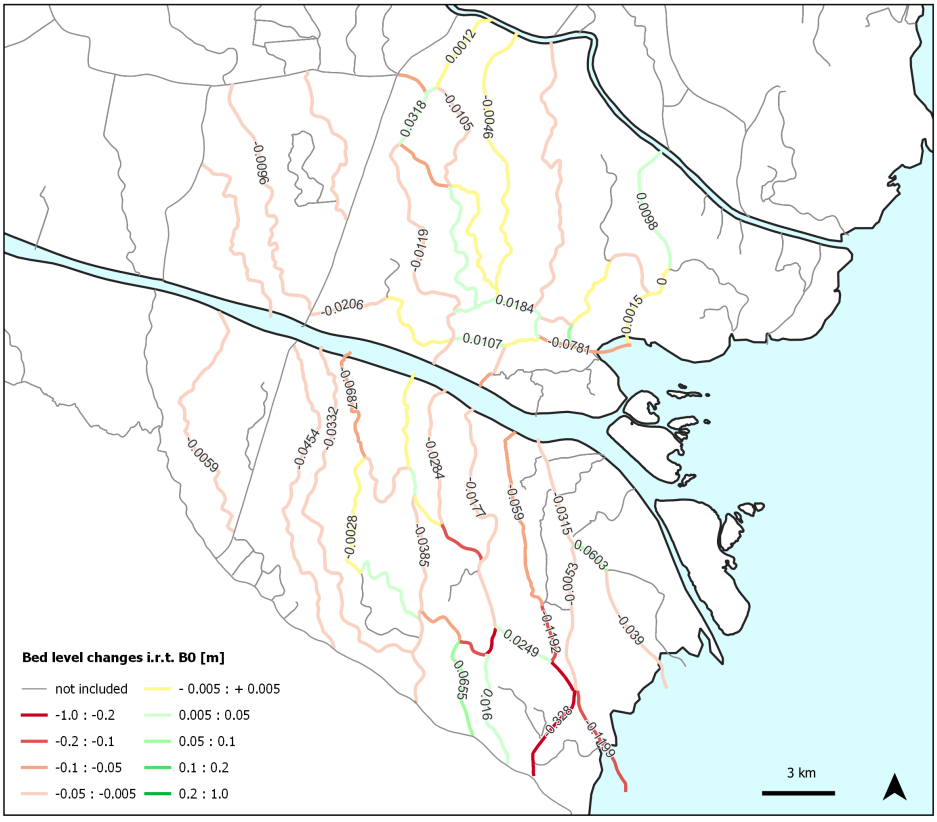
Bed level changes i.r.t. B0 [m]
not included
- 0.005 : + 0.005
-1.0 : -0.2
0.005 : 0.05
-0.2 : -0.1
0.05 : 0.1
-0.1 : -0.05
0.1 : 0.2
-0.05 : -0.005
0.2 : 1.0
3 km

K.2.9. B2

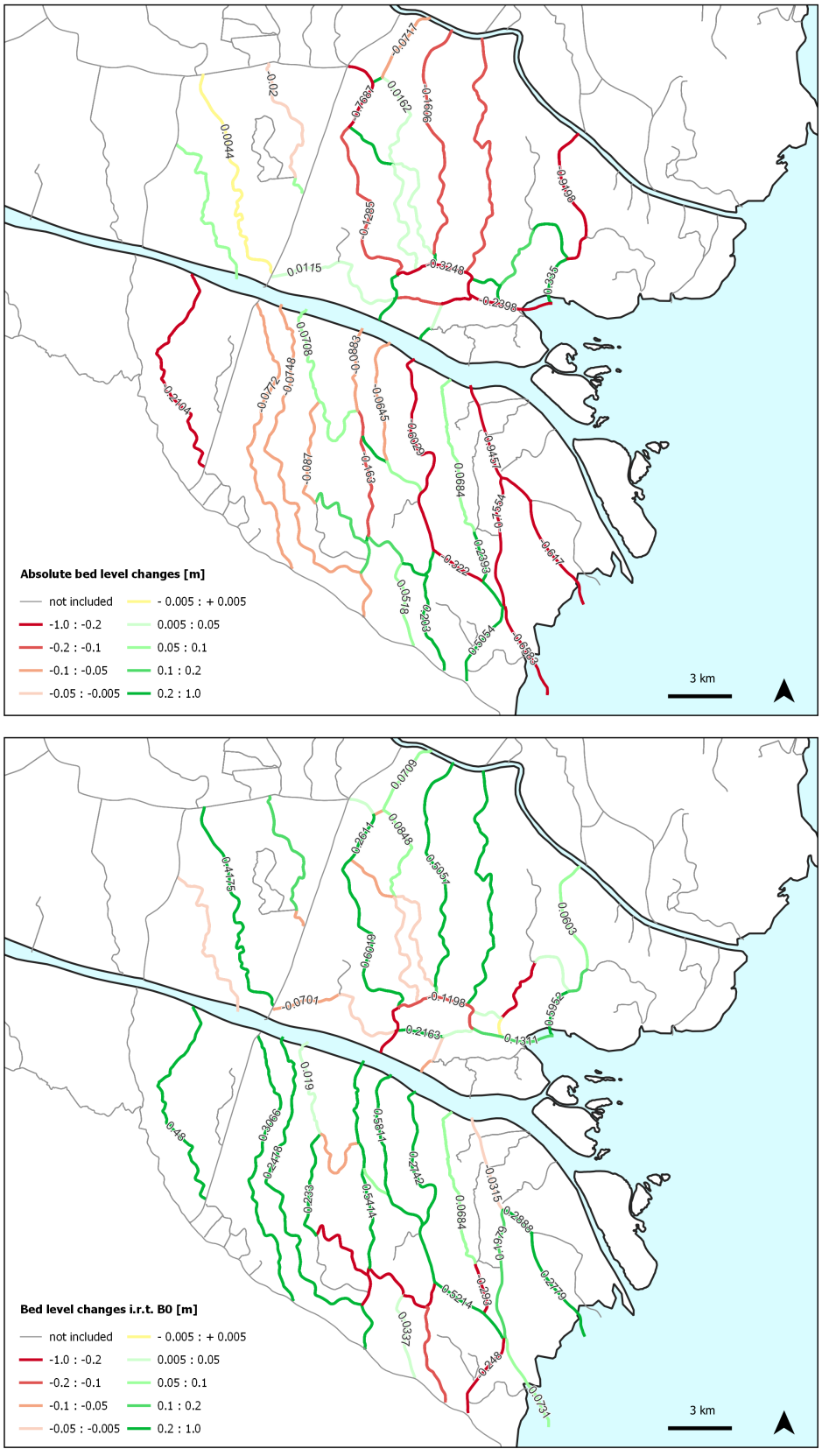
Absolute bed level changes [m]
not included
-1.0 : -0.2
-0.2 : -0.1
-0.1 : -0.05
-0.05 : -0.005
- 0.005 : + 0.005
0.005 : 0.05
0.05 : 0.1
0.1 : 0.2
0.2 : 1.0
3 km
Bed level changes i.r.t. B0 [m]
not included
-1.0 : -0.2
-0.2 : -0.1
-0.1 : -0.05
-0.05 : -0.005
- 0.005 : + 0.005
0.005 : 0.05
0.05 : 0.1
0.1 : 0.2
0.2 : 1.0
3 km

K.2.10. B3

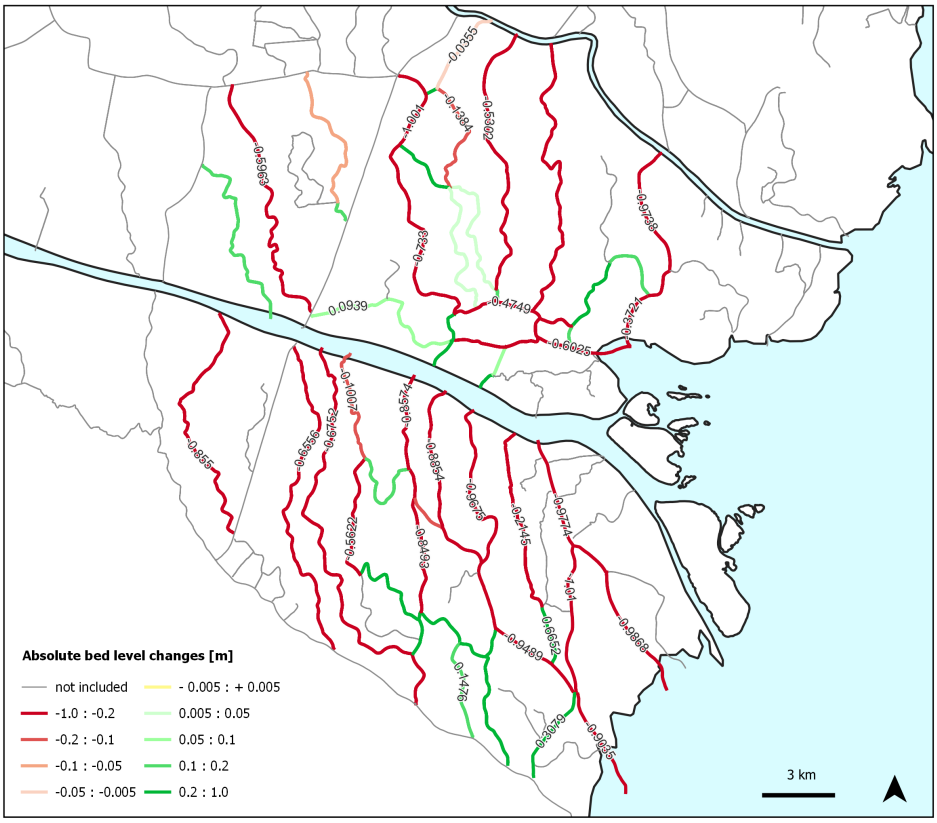
Absolute bed level changes [m]
not included
- 0.005 : + 0.005
-1.0 : -0.2
0.005 : 0.05
-0.2 : -0.1
0.05 : 0.1
-0.1 : -0.05
0.1 : 0.2
-0.05 : -0.005
0.2 : 1.0
3 km

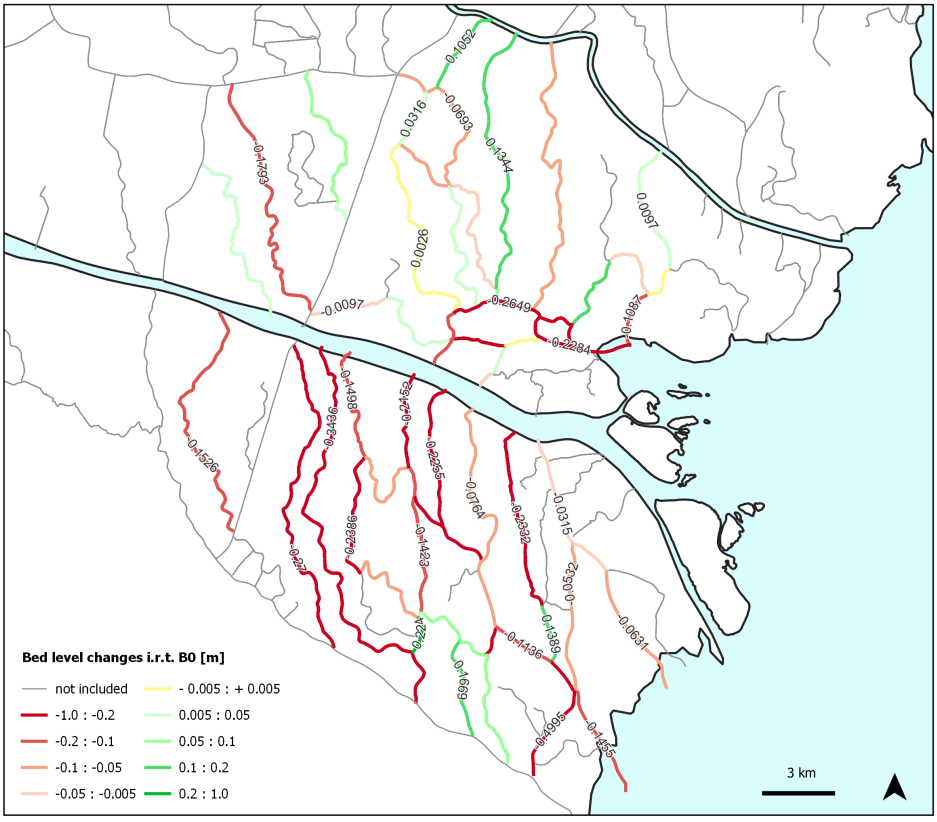
Bed level changes i.r.t. B0 [m]
not included
- 0.005 : + 0.005
-1.0 : -0.2
0.005 : 0.05
-0.2 : -0.1
0.05 : 0.1
-0.1 : -0.05
0.1 : 0.2
-0.05 : -0.005
0.2 : 1.0
3 km

K.2.11. B4

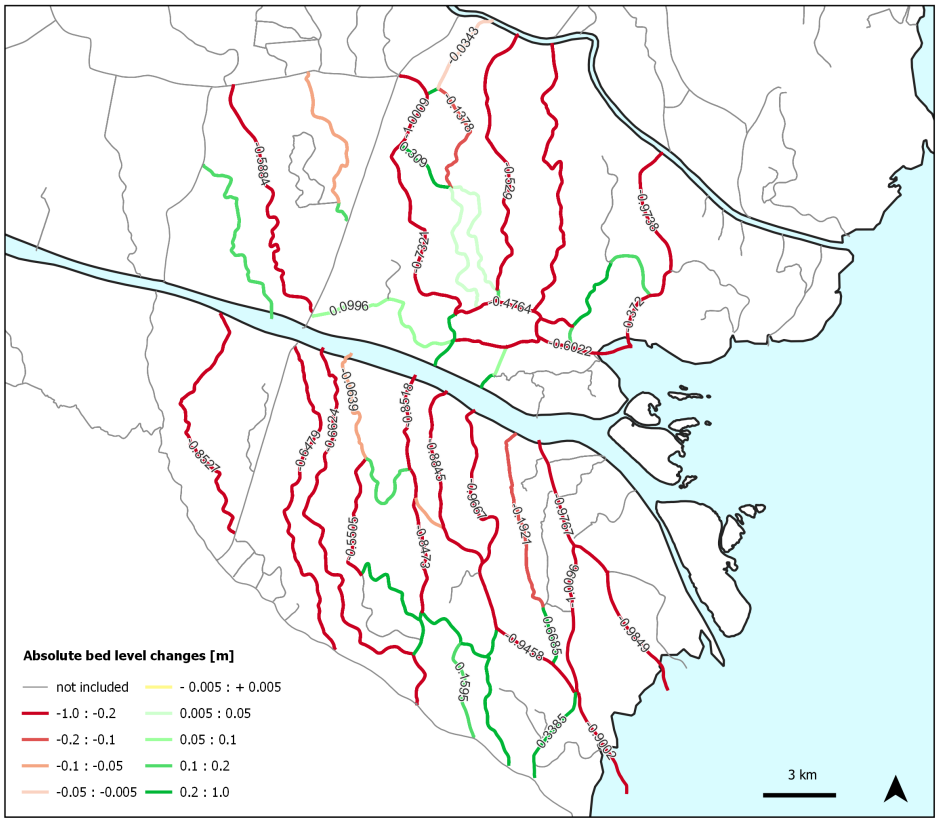
Absolute bed level changes [m]
not included
- 0.005 : + 0.005
-1.0 : -0.2
0.005 : 0.05
-0.2 : -0.1
0.05 : 0.1
-0.1 : -0.05
0.1 : 0.2
-0.05 : -0.005
0.2 : 1.0
3 km

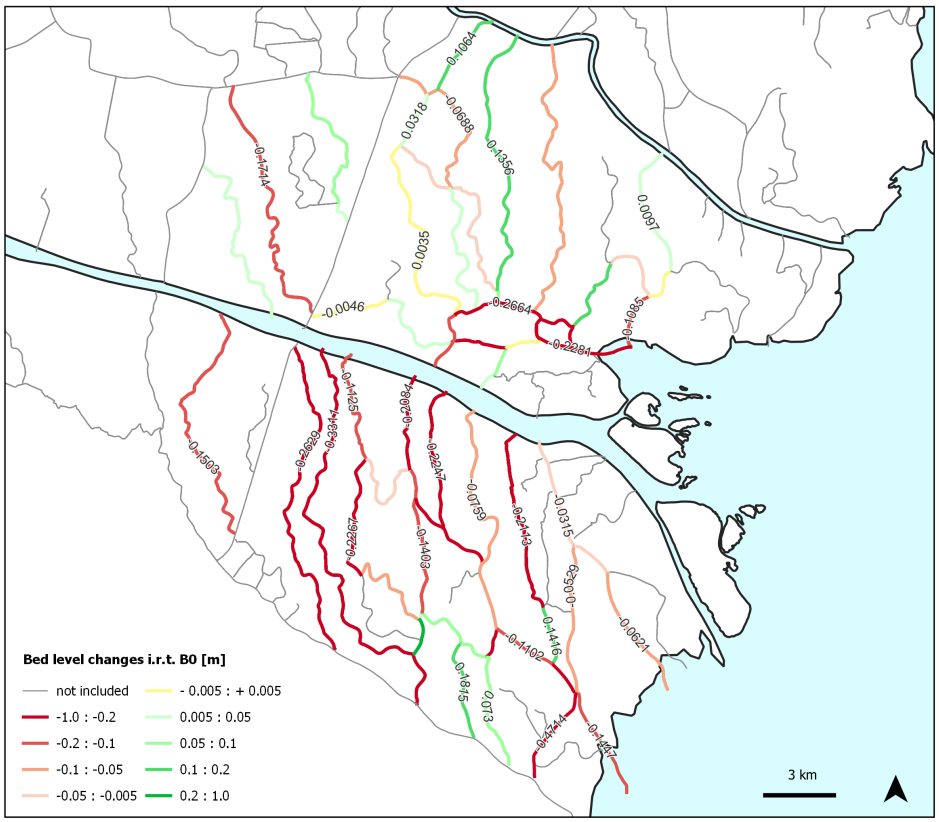
Bed level changes i.r.t. B0 [m]
not included
- 0.005 : + 0.005
-1.0 : -0.2
0.005 : 0.05
-0.2 : -0.1
0.05 : 0.1
-0.1 : -0.05
0.1 : 0.2
-0.05 : -0.005
0.2 : 1.0
3 km

Bibliography

M. Amsler and Edmundo Drago. A review of the suspended sediment budget at the confluence of the paraná and paraguay rivers. *Hydrological Processes*, 23:3230–3235, October 2009. doi: 10.1002/hyp.7390.

M. Amsler, Edmundo Drago, and Aldo Paira. Fluvial sediments: Main channel and floodplain interrelationships. In *The Middle Paraná River: Limnology of a Subtropical Wetland*, pages 123–142. Springer-Verlag Berlin Heidelberg, January 2007. doi: 10.1007/978-3-540-70624-3_5.

Santiago Baeza and José Paruelo. Land use/land cover change (2000-2014) in the rio de la plata grasslands: An analysis based on modis ndvi time series. *Remote Sensing*, 12:381, January 2020. doi: 10.3390/rs12030381.

Marciano A. Balay. Cause and periodicity of large floods in rio de la plata (flood of 27 and 28 july 1958). Technical report, Argentine Navy Hydrogrpahic Office, 1958.

Agustín Barletti. *Canal Martín Irigoyen*. Globalports, 2021.

Vicente Barros. Global climate change and the coastal areas of the río de la plata. Technical report, Assessments of Impacts andAdaptations to Climate Change (AIACC), 2005. Project No. LA 26.

Jurjen A. Battjes and Robert Jan Labeur. *Unsteady Flow in Open Channels*. Cambridge University Press, Cambridge, 2017. doi: 10.1017/9781316576878. URL https://www.cambridge.org/core/books/unsteady-flow-in-open-channels/5CCE099F37BCC5AF4E67B35F15666E7B.

E. H. Berbery and C. R. Mechoso. Climatology and hydrology of the la plata basin, a document of the vamos scientific study group on la plata basin, 2001.

Ernesto Hugo Berbery and Vicente R. Barros. The hydrologic cycle of the la plata basin in south america. *Journal of Hydrometeorology*, 3(6):630–645, 2002. doi: 10.1175/1525-7541(2002)003<0630:THCOTL>2.0.CO;2. URL https://journals.ametsoc.org/view/journals/hydr/3/6/1525-7541_2002_003_0630_thcotl_2_0_co_2.xml.

A Blom. Bedforms and bed load transport, 2019.

Judith Bosboom and M.J.F. Stive. *Coastal Dynamics 1*. Delft Academic Press / VSSD, 2015.

J.D. Brea and L. Spalletti. Generación y transporte de sedimentosen la cuenca binacional del río bermejo: Generación y transporte de sedimentosen la cuenca binacional del río bermejo. Technical report, Comisión Binacional para el Desarrollo de la Alta Cuenca del Río Bermejo y el Río Grande de Tarija, 2010.

P. Bronstein and AN Menéndez. Plan de protección hídrica de las islas del delta (provincia de buenos aires). Technical report, SUCCE (Sub-Unidad Central de Coordinación para la Emergencia) Ministerio del Interior, 1995.

Maria Fernanda Cabré, S.A Solman, and M.N. Nuñez. Creating regional climate change scenarios over southern south america for the 2020's and 2050's using the pattern scaling technique: validity and limitations. *Climate change*, 2010.

Ines Camilloni and Vicente Barros. Extreme discharge events in paraná river and their climate forcing. *Journal of Hydrology - J HYDROL*, 278, January 2004. doi: 10.1016/S0022-1694(03)00133-1.

C.A. Cathcart. The structure and dynamics of a river delta are related through its nourishment area, suggesting optimality. Master's thesis, University of Arkansas, 2019. URL https://scholarworks.uark.edu/etd/3408.

Juan Colombo, Carlos Skorupka, Claudio Bilos, Leandro Tatone, Natalia Cappelletti, M. Carolina Migoya, Malena Astoviza, and Eric Speranza. Seasonal and inter-annual variability of water quality in the uruguay river, argentina. *Hydrological Sciences Journal/Journal des Sciences Hydrologiques*, 60, March 2014. doi: 10.1080/02626667.2014.905690.

Maurício Cordeiro. Water detection in high resolution satellite images using the waterdetect python package, November 2020. URL https://towardsdatascience.com/water-detection-in-high-resolution-satellite-images-using-the-waterdetect-python-p

Piedra Cueva, Ismael, Rodriguez, and Hugo. Finite element modeling of the rio de la plata. *International Conference on Estuaries and Coasts, 2003, Hangzhou, China*, November 2003.

David J. Dean and John C. Schmidt. The role of feedback mechanism in histori channel changes of the lower río grande in the big bend region. *Geomorphology*, 126.3-4:333–349, 2011. URL https://doi.org/10.1016/J.GEOMORPH.2010.03.009.

Deltares. *D-Flow Flexible Mesh*, February 2022.

Pedro J. Depetris. The paraná river under extreme flooding: A hydrological and hydro-geochemical insight. *Interciencia*, 32(10):656–662, October 2007. ISSN 03781844.

Moira Doyle, Vicente Barros, and Ines Camilloni. Potential impacts of climate change in the plata basin. *International Association of Hydrological Sciences*, 2005.

Moira E. Doyle and Vicente R. Barros. Attribution of the river flow growth in the plata basin. *Int. J. Climatol.*, 31(15):2234–2248, December 2011. ISSN 0899-8418. doi: 10.1002/joc.2228. URL https://doi.org/10.1002/joc.2228.

E.C. Drago and M.L. Amsler. Suspended sediment at a cross section of the middle paraná river: concentration, granulometry and influence of the main tributaries. In *Sediment Budgets (Proceedings of the Porto Alergre Symoposium, December 1988)*, 1988.

Edmundo C. Drago and Mario L. Amsler. Bed sediment characteristics in the paraná and paraguay rivers. *null*, 23(3):174–183, September 1998. ISSN 0250-8060. doi: 10.1080/02508069808686764. URL https://doi.org/10.1080/02508069808686764.

M. Fossati and I. Piedra-Cueva. A 3d hydrodynamic numerical model of the río de la plata and montevideo's coastal zone. *Applied Mathematical Modelling*, 37(3):1310–1332, 2013. ISSN 0307-904X. doi: 10.1016/j.apm.2012.04.010. URL https://www.sciencedirect.com/science/article/pii/S0307904X12002351.

Monica Fossati, Florence Cayocca, and Ismael piedra cueva. Fine sediment dynamics in the río de la plata. *Advances in Geosciences*, 39, March 2014. doi: 10.5194/adgeo-39-75-2014.

Mónica Fossati and Ismael Piedra-Cueva. Numerical modelling of residual flow and salinity in the río de la plata. *Applied Mathematical Modelling*, 32(6):1066–1086, 2008. ISSN 0307-904X. doi: 10.1016/j.apm.2007.02.034. URL https://www.sciencedirect.com/science/article/pii/S0307904X07000716.

Carlos Galperín, Veronica Fossati, and María Lottici. *Socio-economic valuation of the goods and services of the Paraná Delta wetland*. Fundación para la Conservación y el Uso Sustentable de los Humedales / Wetlands International Argentina, August 2013.

Norberto O. García and Carlos R. Mechoso. Variability in the discharge of south american rivers and in climate / variabilité des débits de rivières d'amérique du sud et du climat. *null*, 50(3):null–478, June 2005. ISSN 0262-6667. doi: 10.1623/hysj.50.3.459.65030. URL https://doi.org/10.1623/hysj.50.3.459.65030.

Garmin. echomap™ chirp 42cv, 2016. URL https://www.garmin.com/en-CA/p/577144#inTheBox.

Vincenzo Marco Gatto, Bram Christiaan van Prooijen, and Zheng Bing Wang. Net sediment transport in tidal basins. *Ocean dynamics*, 67(11):1385–1406, November 2017. ISSN 1616-7341. doi: 10.1007/s10236-017-1099-3.

Marcela González, Eugenia Garbarini, María Skansi, and Alfredo Rolla. Enso influence over precipitation in argentina. In *Advances in Environmental Research*, pages 223–246. Nova Science Publishers, June 2016.

Google. Water occurance (1984-2015), 2021. URL https://developers.google.com/earth-engine/tutorials/tutorial_global_surface_water_02.

Marcello Gugliotta, Yoshiki Saito, Thi Kim Oanh Ta, Van Lap Nguyen, Toru Tamura, Zhanghua Wang, Andrew D. La Croix, and Rei Nakashima. Abandonment and rapid infilling of a tide-dominated distributary channel at 0.7 ka in the mekong river delta. *Scientific Reports*, 11(1), 2021. doi: 10.1038/s41598-021-90268-6. URL https://hdl.handle.net/10289/14343.

Kate Happee. Modelling the influence of variability on the sediment dynamics in canal emilio mitre. Master's thesis, University of Technology Delft, 2019.

Peter T. Harris, Peter T. Harris, and Elaine K. Baker. Ch. 6 - seafloor geomorphology - coast, shelf, and abyss. In *Seafloor Geomorphology as Benthic Habitat*, pages 109–155. Elsevier, London, 2012. doi: 10.1016/B978-0-12-385140-6.00006-2. URL https://www.sciencedirect.com/science/article/pii/B9780123851406000062.

A. J. F. Hoitink and D. A. Jay. Tidal river dynamics: Implications for deltas. *Rev. Geophys.*, 54(1): 240–272, March 2016. ISSN 8755-1209. doi: 10.1002/2015RG000507. URL https://doi.org/10.1002/2015RG000507.

A. J. F. Hoitink, Z. B. Wang, B. Vermeulen, Y. Huismans, and K. Kästner. Tidal controls on river delta morphology. *Nature Geoscience*, 10(9):637–645, 2017. ISSN 1752-0908. doi: 10.1038/ngeo3000. URL https://doi.org/10.1038/ngeo3000.

Martín Iriondo. The littoral complex at the paraná mouth. *Quaternary International*, 114:143–154, December 2004. doi: 10.1016/S1040-6182(03)00049-1.

M. V. Isupova and V. N. Mikhailov. Long-term variations of water runoff and suspended sediment yield in the parana and uruguay rivers. *Water Resources*, 45(6):846–860, 2018. ISSN 1608-344X. doi: 10.1134/S0097807818060088. URL https://doi.org/10.1134/S0097807818060088.

P Ph Jansen. *Principles of River Engineering: The non-tidal allluvial river*. VSSD, 1979.

K. Kästner, A. J. F. Hoitink, B. Vermeulen, T. J. Geertsema, and N. S. Ningsih. Distributary channels in the fluvial to tidal transition zone. *J. Geophys. Res. Earth Surf.*, 122(3):696–710, March 2017. ISSN 2169-9003. doi: 10.1002/2016JF004075. URL https://doi.org/10.1002/2016JF004075.

Eunjee Lee, Angela Livino, Shin-Chan Han, John Briscoe, Jerson Kelman, and Paul Moorcroft. Land cover change explains the increasing discharge of the paraná river. *Regional Environmental Change*, 18:1–11, August 2018. doi: 10.1007/s10113-018-1321-y.

J. Lelievre and E. Navntoft. Measuring sediment load in the paraná river. In *Water Power & Dam Construction*, 1980.

G.O. Magrin, J.A. Marengo, J.P. Boulanger, M.S. Buckeridge, E. Castellanos, G. Poveda, F.R. Scarano, and S. Vicuña. *Climate Change 2014: Impacts, Adaptation, and Vulnerability. Part B: Regional Aspects. Contribution of Working Group II to the Fifth Assessment Report of the Intergovernmental Panelon Climate Change*. Cambridge University Press, 2014. Chapter 27. 2014: Central and South America.

S. Marcomini, Alfonsina Tripaldi, Pablo Leal, R. A. López, M. S. Alonso, Patricia Ciccioli, Agustín Quesada, and P. Bunicontro. Morfodynamics and sedimentation of a sector of parana delta front between 1933 and 2016, province of buenos aires, argentina. *Revista de la Asociacion Geologica Argentina*, 75:1–16, January 2018.

Jose Marengo, Sin Chan Chou, Gillian Kay, Lincoln Alves, José Pesquero, Wagner Soares, Daniel Santos, Andre Lyra, Gustavo Medeiros, Richard Betts, Diego Chagas, Jorge Gomes, Josiane Bustamante, and Priscila Tavares. Development of regional future climate change scenarios in south america using the eta cptec/hadcm3 climate change projections: Climatology and regional analyses for the amazon, são francisco and the paraná river basins. *Climate Dynamics*, 38:1829–1848, May 2011. doi: 10.1007/s00382-011-1155-5.

Rubén Medina and J. O. Codignotto. Evolución del delta del río paraná y su posible vinculación con el calentamiento global. *Revista del Museo Argentino de Ciencias Naturales, Nueva Serie*, 15:191–200, December 2013. doi: 10.22179/REVMACN.15.181.

Baptiste Mengual, Pierre L. Hir, Florence Cayocca, and Thierry Garlan. Modelling fine sediment dynamics: Towards a common erosion law for fine sand, mud and mixtures, 2017. ISSN 2073-4441.

Angel Menéndez, Mariano Re, Alejo Sarubbi, and Pablo Garcia. *A Conceptual Model for Sediment Transport in the Inner Plata River*. September 2009.

V. N. Mikhailov. Hydrology and formation of river mouth bars. *Problems of the Humid Tropical Zone Deltas*, 1:59–64, 1966.

Mayra Morale, Martin Sabartos Gerbect, Mariano Re, Nicolás Ortiz, and Julieta Bernal. Delta del paraná: del territorio hacia la modelación hidrodinámica. Technical report, Instituto Nacional del Agua, Laboratorio de Hidráulica, Programa de Hidráulica Computacional, 2018.

Fekadu Moreda, Ben Lord, Pedro Coli Valdes Daussa, and Juliana Corrales Corrales. Hydro-bid case study no. 4: Application of hydro-bid in bermejo river basin to quantify sediment loads, argentina. 2016.

E. Mosselman. River bifurcations part 1. Lecture slides River Dynamics 2:, 2020.

Tosiyuki Nakaegawa, Akio Kitoh, and Masahiro Hosaka. Discharge of major global rivers in the late 21st century climate projected with the high horizontal resolution mri-agcms. *Hydrol. Process.*, 27 (23):3301–3318, November 2013. ISSN 0885-6087. doi: 10.1002/hyp.9831. URL https://doi.org/10.1002/hyp.9831.

NOAA. El nino related global temperature and precipitation patterns, December 2005. URL https://www.cpc.ncep.noaa.gov/products/analysis_monitoring/ensocycle/elninosfc.shtml.

Jan Null. El niño and la niña years and intensities, 2022. URL https://ggweather.com/enso/oni.htm.

OAS. Bermejo river basin: Implementation of the strategic action program for the binational basin of the bermejo river. In *Water Project Series*. Organization of American States, Office for Sustainable Development & Environment, 2005.

Ismael Piedra-Cueva and Mónica Fossati. Residual currents and corridor of flow in the rio de la plata. *Applied Mathematical Modelling*, 31(3):564–577, 2007. ISSN 0307-904X. doi: 10.1016/j.apm.2005.11.033. URL https://www.sciencedirect.com/science/article/pii/S0307904X05002544.

Carlos Ramonell. *GEOMORFOLOGÍA Y MORFODINÁMICA DE LA PLANICIE ALUVIAL DEL RÍO PARANÁ EN SU TRAMO MEDIO*. PhD thesis, April 2021.

Carlos Ramonell, M. Amsler, and H. A. Toniolo. Shifting modes of the paraná river thalweg in its middle/lower reach. *Zeitschrift fur Geomorphologie, Supplementband*, 129:129–142, January 2002. doi: 10.5216/bgg.v19i1.15356.

Mariano Re, Angel N. Menéndez, and Mario L. Amsler. MetodologÍa para la generaciÓn de series temporales de descargasÓlida de los rÍos paranÁ de las palmas y paranÁ guazÚ. In *Rios 2009*. Instituto Nacional del Agua (INA) and Facultad de Ingeniería (FIUBA) –Instituto Nacional de Limnología (INALI), 2009.

Mariano Re, Martin Sabarots Gerbec, and Lucas Storto. *Estadística de Niveles en el Delta del río Paraná mediante Modelación Hidrodinámica*. -, November 2015.

Van Rijn and Barth. Settling and consolidation of soft mud-sand layers. In *Journal of Waterway, Port, Coastal and Ocean Engineering*, 2018.

M.. Sabarots Gerbec and Mayra Morale Pablo E. Garcia. Modelación bidimesional del delta de paraná en delft3d fm. Insituto Nacional Del Agua, Deltares, 2018.

Martin Sabarots Gerbec. *Estudio de la dinámica superficial de la red de canales del Delta Medio del río Paraná*. October 2014. doi: 10.13140/RG.2.1.1212.3044.

Martin Sabarots Gerbec, Borús J.A., Irigoyen M., Gonzalez A., and Álvarez J. Abordaje interinstitucional en el estudio delta del río paraná. In *XXVI Congreso Nacional del Agua*, 2017a.

Martin Sabarots Gerbec, Lucas Storto, and Mariano Re. *Modelo Digital de Elevación del Delta del río Paraná DELTA PARANA*. March 2017b. doi: 10.13140/RG.2.2.20459.59688.

Romina Sanci and Héctor Osvaldo Panarello. Distribution and isotopic signature of deep gases in submerged soils in an island of the lower delta of the paraná river, argentina. *Environmental Monitoring and Assessment*, 190(11):647, 2018. ISSN 1573-2959. doi: 10.1007/s10661-018-7026-3. URL https://doi.org/10.1007/s10661-018-7026-3.

Sara Santamaria-Aguilar, Mark Schuerch, Athanasios T. Vafeidis, and Silvina C. Carretero. Long-term trends and variability of water levels and tides in buenos aires and mar del plata, argentina. *Frontiers in Marine Science*, 4:380, 2017. ISSN 2296-7745. doi: 10.3389/fmars.2017.00380. URL https://www.frontiersin.org/article/10.3389/fmars.2017.00380.

Pablo E. Santoro, Mónica Fossati, and Ismael Piedra-Cueva. Study of the meteorological tide in the río de la plata. *Continental Shelf Research*, 60:51–63, 2013. ISSN 0278-4343. doi: 10.1016/j.csr.2013.04.018. URL https://www.sciencedirect.com/science/article/pii/S0278434313001180.

A. Sarubbi and A. Menendez. Un modelo numérico para representar el avance dei frente dei delta del rio parana a escala secular. *Mecánica Computacional*, 26:2203–2216, 2007.

Alejo Sarubbi, Marcos G. Pittau, and Ángel N. Menéndez. Delta del paraná: Balance de sedimentos. Technical report, INA, 2004.

Hubert H. G. Savenije. 2 - tide and estuary shape. In *Salinity and Tides in Alluvial Estuaries*, pages 23–68. Elsevier Science Ltd, Amsterdam, 2005. doi: 10.1016/B978-044452107-1/50003-4. URL https://www.sciencedirect.com/science/article/pii/B9780444521071500034.

EM Shaw. *Hydrology in practice, Third Edition*. Stanley Thornes Ltd, 1999.

Servicia de Hidrografía Naval SHN. Tablas de marea - separata zona del río de la plata. *H-610*, 2021. ISSN 0329-1375. H-610.

Claudia Simionato, Diego Moreira, Francis Gohin, Florence Cayocca, and Moira Luz Clara. Suspended matters mean distribution and seasonal cycle in the río de la plata estuary and the adjacent shelf from modis and in situ observations. page 1394, April 2013.

J. Smagorinsky. General circulation experiments with the primitive equations. *Monthly Weather Review*, 1963.

SSPYVN. Dredging data 1995 - 2019, September 2019. URL viaOnedrive.

Esther Stouthamer, Kim M. Cohen, and Marc J. P. Gouw. Avulsion and its implications for fluvial-deltaic architecture: Insights from the holocene rhine–meuse delta. 2011.

V. Teles, Benoit Chauveau, Philippe Joseph, Pierre Weill, and Fakher Maktouf. Cats - a process-based model for turbulent turbidite systems at the reservoir scale. *Comptes Rendus Geoscience*, June 2016. doi: 10.1016/j.crte.2016.03.002.

Sophia Turcot. The prolonged drought of the paraná river, January 2022. URL https://latinarepublic.com/2022/01/13/the-prolonged-drought-of-the-parana-river/.

US-FISP. *SAMPLING WITH THE US DH-48 DEPTH-INTEGRATING SUSPENDED-SEDIMENT SAMPLER*. Federal Interagency Sedimentation Project, Halls Ferry Road 3909, 1999.

Hydrographic Surveying. USACE, em 1110-2-1003 edition, November 2013.

D. S. van Maren, T. van Kessel, K. Cronin, and L. Sittoni. The impact of channel deepening and dredging on estuarine sediment concentration. *Continental Shelf Research*, 95:1–14, 2015a. ISSN 0278-4343. doi: 10.1016/j.csr.2014.12.010. URL https://www.sciencedirect.com/science/article/pii/S0278434314003720.

Dirk S. van Maren, Johan C. Winterwerp, and Julia Vroom. Fine sediment transport into the hyper-turbid lower ems river: the role of channel deepening and sediment-induced drag reduction. *Ocean Dynamics*, 65(4):589–605, 2015b. ISSN 1616-7228. doi: 10.1007/s10236-015-0821-2. URL https://doi.org/10.1007/s10236-015-0821-2.

Leo van Rijn. Siltation study of euroamerica terminalat campana, argentina. Client: Euroamerica, July 2017.

Leo C. van Rijn. Literature review of critical bed-shear stresses for mud-sand mixtures. Critical bed-shear stress for mud-sand beds, August 2020.

Andrés Vargas-Luna, Alessandra Crosato, and Wim S. J. Uijttewaal. Effects of vegetation on flow and sediment transport: comparative analyses and validation of predicting models. *Earth Surf. Process. Landforms*, 40(2):157–176, February 2015. ISSN 0197-9337. doi: 10.1002/esp.3633. URL https://doi.org/10.1002/esp.3633.

José Rodriques Vieira and Néstor W. Lanfredi. A hydrodynamic model for the río de la plata, argentina. *Journal of Coastal Research*, 12(2):430–446, 1996. ISSN 07490208, 15515036. URL http://www.jstor.org/stable/4298495.

J. Vroom. Tidal divides: A study on a simplified case and the dutch wadden sea. Master's thesis, TU Delft, 2011. URL http://resolver.tudelft.nl/uuid:7c28338b-7a43-489f-8b57-98af6a00561c.

J. C. Winterwerp, W. G. M. van Kesteren, B. van Prooijen, and W. Jacobs. A conceptual framework for shear flow-induced erosion of soft cohesive sediment beds. *J. Geophys. Res.*, 117(C10), October 2012. ISSN 0148-0227. doi: 10.1029/2012JC008072. URL https://doi.org/10.1029/2012JC008072.

E. Wolanski. *Estuarine Ecohydrology*. Elsevier, 2007. ISBN 978-0-444-53066-0.

Veronica Zagare. Dichotomous delta: Between the natural and the metropolitan: The case of the parana delta, argentina. *Built Environment (1978-)*, 40(2):213–229, 2014. ISSN 02637960. URL http://www.jstor.org/stable/43296888.